Universitat Politècnica de Catalunya
Electrical Engineering Department

Institut de Recerca en Energia de Catalunya
Catalonia Institute for Energy Research

PhD Thesis

Contributions of Flywheel Systems in Wind Power Plants

Author: **Francisco Díaz-González**

Advisors: **Andreas Sumper**
Oriol Gomis-Bellmunt

Barcelona, July 2013

Catalonia Institute for Energy Research (IREC)
Electrical Engineering Research Area
Jardins de les Dones de Negre 1 2nd floor,
08930 Sant Adrià de Besòs, Barcelona, Spain

Printed in Barcelona by Fotocòpies Diagonal
First Print, July 2013

UNIVERSITAT POLITÈCNICA DE CATALUNYA
BARCELONATECH
Escola de Doctorat

Curs acadèmic:

Acta de qualificació de tesi doctoral

Nom i cognoms

DNI / NIE / Passaport

Programa de doctorat

Unitat estructural responsable del programa

Resolució del Tribunal

Reunit el Tribunal designat a l'efecte, el doctorand / la doctoranda exposa el tema de la seva tesi doctoral titulada

_____

_____.

Acabada la lectura i després de donar resposta a les qüestions formulades pels membres titulars del tribunal, aquest atorga la qualificació:

☐ APTA/E ☐ NO APTA/E

(Nom, cognoms i signatura) President/a		(Nom, cognoms i signatura) Secretari/ària
(Nom, cognoms i signatura) Vocal	(Nom, cognoms i signatura) Vocal	(Nom, cognoms i signatura) Vocal

_____, _____ d'/de _____ de _____

El resultat de l'escrutini dels vots emesos pels membres titulars del tribunal, efectuat per l'Escola de Doctorat, a instància de la Comissió de Doctorat de la UPC, atorga la MENCIÓ CUM LAUDE:

☐ SÍ ☐ NO

(Nom, cognoms i signatura) Presidenta de la Comissió de Doctorat	(Nom, cognoms i signatura) Secretària de la Comissió de Doctorat

Barcelona, _____ d'/de _____ de _____

To Rocío

Abstract

The stepwise replacement of conventional power plants by renewable-based ones such as wind power plants could affect the system behaviour and planning. First, the network stability may be compromised as it becomes less resilient against sudden changes in the loads or generator trips. This is because wind turbines are not synchronized with network frequency but they are usually connected to the grid through fast controllable electronic power converters. And second, due to the stochastic nature of wind, the electrical power generated by wind power plants is neither constant non controllable. This affects the network planning as the expected generation level depends on non reliable wind forecasts. Also it affects the power quality as the fast fluctuations of wind power can cause harmonics and flicker emissions.

For these reasons, network operators gradually set up more stringent requirements for the grid integration of wind power. These regulations require wind power plants to behave in several aspects as conventional synchronized generating units. Among other requirements, it is set the provision of some ancillary services to the grid as frequency and voltage control, the capability of withstanding short-circuits and faults, and to respect some threshold level with regard to the quality of the power generated.

Accordingly, energy storage systems may play an important role in wind power applications by enhancing the controllability of the output of wind power plants and providing ancillary services to the power system and thus, enabling an increased penetration of wind power in the system.

This thesis focuses on the potential uses of flywheel energy storage systems in wind power. The thesis introduces the basis of several energy storage

systems as well as identifies their applications in wind power based on an extensive literature review. It follows with the presentation of the design and setting up of a scale-lab flywheel-based energy storage system. From this work, research concentrates on the application of flywheel devices for power smoothing of wind power plants. The developed concepts are proved by simulations but also experimentally using the above mentioned scale-lab test bench. In particular, research focuses on the definition of an optimization criteria for the operation of flywheel devices while smoothing the wind power, and the design and experimental validation of the proposed control algorithms of the storage device.

The last chapters of the thesis research on the role of wind power plants in system frequency control support. In this sense, an extensive literature review on the network operator's requirements for the participation of wind power plants in system frequency control related-tasks is offered. Also, this review covers the proposed control methods in the literature for enabling wind turbines to participate in system frequency control. The results of this work open the door to the design of control systems of wind turbines and wind power plants for primary frequency control. The contribution of flywheel devices is also considered.

Results highlight the tremendous potential of energy storage systems in general for facilitating the grid integration of wind power plants. Regarding the uses of flywheel devices, it is worth noting that some of their characteristics as the high-ramp power rates can be exploited for reducing the variability of the power generated by wind turbines, and thus for improving the quality of the power injected to the grid by wind power plants. Also, they can support wind power plants to fulfil the requirements for their participation in system frequency control support related tasks.

Resum

El progressiu desplaçament de plantes de generació convencionals per part de plantes de generació de tipus renovable, com els parcs eòlics, pot afectar el comportament i la planificació del sistema elèctric. Primer, l'estabilitat pot ser compromesa ja que el sistema elèctric resulta més vulnerable davant canvis abruptes provocats per les càrregues del sistema o desconnexions no programades de generadors. Això es degut a que les turbines eòliques no estan sincronitzades amb la freqüència elèctrica del sistema ja que la seva connexió és a través de convertidors electrònics de potència. Segon, degut a la gran variabilitat del vent, la potència elèctrica generada per les turbines eòliques no és constant ni controlable. En aquest sentit, la qualitat de la potència del parc eòlic es pot veure compromesa, ja que es poden detectar nivells apreciables d'harmònics i emissions de "flicker" degudes a les ràpides variacions de la potència generada pel parc eòlic.

Per aquests motius, els operadors dels sistemes elèctrics fan gradualment més restrictius els requeriments de connexió dels parcs eòlics al sistema elèctric. Aquestes regulacions requereixen als parcs eòlics que es comportin en molts aspectes com plantes de generació convencional. Entre d'altres requeriments, els parcs eòlics han de proveir serveis auxiliars per a la operació del sistema elèctric com també el suport en el control dels nivells de tensió i freqüència de la xarxa; oferir suport durant curtcircuits; i mantenir uns nivells mínims en la qualitat de la potència generada.

Els sistemes d'emmagatzematge d'energia poden millorar la controlabilitat de la potència generada pels parcs eòlics i ajudar a aquests a proveir serveis auxiliars al sistema elèctric, afavorint així la seva integració a la xarxa. Aque-

sta tesi tracta l'aplicació en parcs eòlics dels sistemes d'emmagatzematge d'energia basats en volants d'inèrcia. La tesi introdueix les bases de diversos sistemes d'emmagatzematge i identifica les seves potencials aplicacions en parcs eòlics en base a una extensa revisió bibliogràfica. El treball continua amb la posta a punt d'un equipament de laboratori, que configura un sistema d'emmagatzematge d'energia basat en un volant d'inèrcia.

Següents capítols de la tesi estudien l'aplicació dels volants d'inèrcia per a esmorteir el perfil fluctuant de la potència generada pels parcs eòlics. Els treballs es focalitzen en la definició dels criteris per a la operació òptima dels volants d'inèrcia per la seva aplicació d'esmorteir el perfil fluctuant de potencia eòlica, i també en el disseny i validació experimental dels algoritmes de control desenvolupats per governar el sistema d'emmagatzematge.

Els capítols finals de la tesi tracten sobre el suport al control de freqüència per part dels parcs eòlics. S'ofereix una extensa revisió bibliogràfica respecte els requeriments indicats pels operadors del sistema elèctric en aquest sentit. A més, aquesta revisió cobreix els mètodes de control dels parcs eòlics i turbines eòliques per la seva participació en el suport al control de freqüència. Les conclusions extretes serveixen per proposar sistemes de control de parcs eòlics i de turbines eòliques per proveir el servei de control de freqüència. Aquest treball, també contempla la inclusió de volants d'inèrcia en els parcs eòlics.

Dels resultats de la tesi se'n dedueix l'important potencial dels sistemes d'emmagatzematge d'energia per a afavorir la integració a la xarxa dels parcs eòlics. La controlabilitat de la potència dels volants d'inèrcia, afavoreix el seu ús per reduir la variabilitat de la potència generada pels parcs eòlics, millorant així la qualitat de potència del mateix. A més, els volants d'inèrcia poder ajudar als parcs eòlics a complir amb els requeriments per a la seva integració a xarxa, com la participació en el control de freqüència del sistema elèctric.

Acknowledgements

Doing this thesis has involved a tremendous and continuous learning effort at all levels. Overcoming all phases of the thesis requires a continuous improvement of working methods and scientific knowledge. But it also requires work on personal skills such as the spirit of self-improvement and the capacity of learning from the people you had the opportunity to work with, among others.

I would like to acknowledge the support received during the last four years from my advisers Andreas Sumper and Oriol Gomis-Bellmunt. Thanks for giving me the opportunity to undertake a PhD with all it means: learning, writing papers, collaborate in research projects, travelling to other countries, among others, and for the invaluable scientific support you gave to me.

I would like to also acknowledge the support from my colleagues from IREC. Thanks for giving me your fellowship. Specially, I acknowledge the help and the friendship received from Albert, David B., David L., Fernando, José Luis, Jordi, Lázaro and Mikel. Thanks to make all the challenges during the thesis a little more easy, and amusing!

I could not forget to thank also the support received from Melanie Hau in IWES. Your invaluable advice has become fundamental for improving the work we have done during the predoctoral stay.

The support I received from family has been fundamental, vital. I would like to acknowledge to my parents Vicenta and Manuel, my sister Rosa and my brothers Jose, Carlos and Manuel and their families for all their support throughout this adventure and during all of my life.

I will never forget also the support I received from my girlfriend Rocío. You encouraged me for doing this thesis and helped me when I was stuck. I thank God for being sharing our life together. And because I consider to be also my family, I acknowledge the support and all cares from Rocio's family, her parents Araceli and Manuel, and Dolores. Thank you for having me as a son.

Thank you everyone, without any doubt there is a little bit of all of you in the words of this thesis.

Finally, I would like to acknowledge the economic support for the development of the thesis by Catalonia Institute for Energy Research (IREC) through the call number 09/09 for predoctoral research grants. I would like to also acknowledge the economic support received from Fraunhofer IWES for the predoctoral stay.

Contents

List of Tables

List of Figures

Acronyms

BESS	Battery Energy Storage System
C-PCS	Control and Power Conditioning System
CAES	Compressed Air Energy Storage
CAN	Controller Area Network
DoD	Depth of Discharge
DFIG	Doubly Fed Induction Generator
DSP	Digital Signal Processor
ENTSO-E	European Network of Transmission System Operators for Electricity
ESS	Energy Storage Systems
FBESS	Flow Battery Energy Storage System
FESS	Flywheel Energy Storage System
HESS	Hydrogen-based Energy Storage System
Li-ion	Lithium-ion
LVRT	Low Voltage Ride Through
NaS	Sodium-Sulphur
Ni-Cd	Nickel-Cadmium
PCC	Point of Common Coupling
PHS	Pumped Hydro Storage
PMSM	Permanent Magnet Synchronous Machine

PSB	Polysulphide-Bromide flow Battery
RFC	Regenerative Fuel Cell
ROCOF	Rate of Change of Frequency
SCESS	Supercapacitor Energy Storage System
SMES	Superconducting Magnetic Energy Storage
SoC	State of Charge
SVPWM	Space Vector Pulse Width Modulation
TSO	Transmission System Operators
VRB	Vanadium Redox Battery
WPP	Wind power plants
ZBB	Zinc-Bromine flow Battery

Preface

This thesis was framed in the doctorate program of the Department of Electrical Engineering of the Polytechnical University of Catalonia (UPC). It was developed between September 2009 and July 2013, in the Electrical Engineering Research Area (EERA) of Catalonia Institute for Energy Research (IREC), in Barcelona. IREC is framed in the Catalan, Spanish and global economic systems. It was created in 2007 with the objective of the creation of value through scientific knowledge and technological development in the energy sector. The EERA focuses its activities in the field of wind power, microgrids and electric vehicles. As a PhD fellowship in EERA, the author had the opportunity of participating in projects with industry collaboration in the field of grid integration of wind power. This facilitated the identification of the interests of the industry with respect to the grid integration of wind power and the energy sector in general. The proximity to industry enriched the scientific development of the contents of the thesis with respect to wind power and ESSs. Moreover, it is worth highlighting that the thesis has been enriched with the availability of laboratory equipments which become fundamental for the proper development of the research.

Much of the thesis has been developed in IREC. However, the thesis also comprised a predoctoral stay in the Fraunhofer Institute for Wind Energy and Energy System Technology (IWES), Kassel, Germany. The stay lasted for a period of six months, comprising the months of July to December 2012. From this stay, the author gained experience on working theme and methods of an international research center. The work done during this stay focused on the frequency control support by WPPs.

1 Introduction

Wind energy is one of the fastest growing sources of electricity nowadays. In fact, the cumulative wind power installation in the EU at the end of 2012 was 931.9 GW. This installed capacity would be enough to cover up to 7% of European electricity consumption in a normal wind year. The penetration of wind power in some European countries has reached values close to 20%, as in the case of Denmark (27%), Portugal (17%) and Spain (16%) [289]. Due to the stochastic nature of wind, the electric power generated by wind turbines is highly erratic, and therefore the wind power penetration in power systems and may affect both the power quality and the planning of power systems [4]. These problems may be especially important in weak or islanded grids. As a consequence, the electrical system operators are gradually developing more stringent requirements for the grid integration of wind generation facilities. These requirements define the so-called grid codes and among others, they require wind generation facilities to present special control capabilities with output power and voltage, to withstand disturbances and short circuits in the network during defined periods of time, as well as to provide some ancillary services for the proper operation of the electrical network as conventional generating units do. In this way, wind generation facilities are known as wind power plants.

In this scenario, energy storage systems (ESS) may play an important role in wind power applications by controlling wind power plant output and providing ancillary services to the power system and thus, enabling an increased penetration of wind power in the system. Among the broad catalogue of energy storage systems, this thesis focuses on the potential uses of flywheel energy storage systems in wind power.

Flywheels are electromechanical systems that store energy in form of kinetic energy. Its operation principle is based on the rotating movement of a disk, which is coupled with an electric machine. Energy is transferred to the flywheel when the machine operates as a motor (the flywheel accelerates), charging the energy storage device. The flywheel is discharged when the electric machine regenerates through the drive (slowing the flywheel). The energy capacity of flywheels is so that the system can exchange power continuously at its ratings during no more than a few minutes at most. This way, flywheels are classified as short-term energy storage devices. The major advantages of the system are high efficiency, high cyclability, high ramp power rates and short time responses. On the other hand, flywheels present relatively high standing losses, so they are not adequate devices for long-term energy storage.

The thesis has three different parts. The first part comprises Chapters 2 and 3. These chapters provides an extensive state of the art on energy storage systems as well as the setting up of laboratory equipments for the experimental validation of the concepts developed throughout the thesis. The second part comprises the Chapters 4 and 5, which deal with wind power smoothing related studies. The last part of the thesis comprises Chapters 6 and 7, which deal with the topic of frequency control support by wind power plants (considering also the support of flywheel systems).

As previously noted, in Chapter 2 a literature review on the potential applications of energy storage systems in wind power plants is presented. This section introduces the basis of several storage systems such as those with extremely high energy and power capacities (e.g. pumped-hydro installations or hydrogen-based energy storage systems); those with medium energy and power capacities (e.g. batteries and flow batteries); and those with low energy and power capacities (e.g. supercapacitors and flywheels). Following this introduction, a literature review on studies concerning the uses of the above mentioned energy storage systems in wind power is offered. The storage devices are thus classified according to their suitability in different tasks that comes in different time frames from the fast power smoothing of wind turbines to the long seasonal storage of wind power. This Chapter provides a general idea of the state of the art of energy storage systems, and in the views of the purposes of the thesis, it helps to identify the interest of the scientific community in the uses of flywheel systems.

To carry out the experimental validation of some of the concepts developed throughout the thesis, it has been necessary the design and setting up of a scale-lab flywheel-based energy storage test bench. The results of this work are presented in Chapter 3. The resultant is not a high-tech de-

vice, but a proof of concept system instead. The setting up of the system comprises several tasks such as the modeling of the system in a simulation software, the design and the tuning of the control algorithms, as well as the implementation of these algorithms in the Digital Signal Processors (DSPs) of the control boards of the electronic power converters of the system.

Chapters 4 and 5 focus on wind power smoothing related studies. These studies propose the inclusion of a flywheel storage device to the point of connection of a wind turbine (or a wind power plant). The flywheel is in charge of fastly inject or absorb power so that the net power injected into the grid by the wind generation facility and the storage device becomes smoothed as much as possible. The high controllability and the high ramp power rates of the flywheel define this system as well suited for this application. To maximize the smoothing of wind power, it has been detected the necessity of including a high-level energy management algorithm for the flywheel. In particular, this is motivated from the need of maintaining a determined average State of Charge (SoC) of the flywheel function of the expected energy to be exchanged so as to ensure the availability of the storage device at all times and to improve the wind power smoothing. The definition of the optimization criteria for the operation of the flywheel is the main object of Chapter 4. The work presented in Chapter 5 deeps on the design of the high-level energy management algorithm and presents also the experimental validation of the developed concepts.

Finally, Chapters 6 and 7 address the topic of system frequency control support by wind power plants. This is one of the mandatory ancillary services required by system operators to wind power plants for their grid integration. Chapter 6 presents an extensive literature review on the requirements set by some European grid codes in this regard, as well as on control methods for operating wind turbines so that they can maintain a determined level of power reserves to be able to participate in frequency control related tasks. Chapter 7, based on the previous literature review, proposes a control method for variable speed wind turbines to maintain the required power reserves by the network operator. Also, it proposes the inclusion of a flywheel-based energy storage system to the wind power plant to provide part of the required power reserves by the network operator. This way, the need of deloading the wind turbines to provide the required power reserves is alleviated. The inclusion of the storage system in the wind power plant involves the design of a wind power plant central controller to coordinate the power reserves maintained by the wind turbines and the storage system.

2

A review of energy storage technologies for wind power applications

Summary.- Energy Storage Systems (ESS) may play an important role in wind power applications by controlling WPP output and providing ancillary services to the power system and therefore, enabling an increased penetration of wind power in the system. This chapter deals with the review of several energy storage technologies for wind power applications. The main objectives of the chapter are the introduction of the operating principles, as well as the presentation of the main characteristics of energy storage technologies suitable for stationary applications, and the definition and discussion of potential ESS applications in wind power, according to an extensive literature review.

2.1 Introduction

Numerous publications regarding the review of suitable storage technologies for stationary applications are found in literature [35, 145, 231]. In [145, 231], a summary of ESS main features is provided. In addition, a revision of specific, worldwide ESS examples for renewable energy applications is detailed in [35].

This chapter focuses on two main objectives; firstly, the introduction of operating principles and the main characteristics of several storage technologies suitable for stationary applications; and, secondly, the definition and discussion of potential ESS applications in wind power. The classification of potential ESS applications has been performed under full power duration of the storage criteria in each case. Thus, applications where ESS are required to inject or absorb power for less than a minute, as in power smoothing of wind turbines; or long-term storage applications, such as those related to load following or seasonal storage, have been considered.

2.2 Energy storage technologies

Electrical energy can be converted to many different forms for storage [231]:

- as gravitational potential energy with water reservoirs,
- as compressed air,
- as electrochemical energy in batteries and flow batteries,
- as chemical energy in fuel cells,
- as kinetic energy in flywheels,
- as magnetic field in inductors,
- as electric field in capacitors.

In this section, a review of several available technologies of energy storage that can be used for wind power applications is evaluated. Among other aspects, the operating principles, the main components and the most relevant characteristics of each technology are detailed. In order to obtain an overview of the main characteristics of the energy storage technologies presented in this chapter, and the differences between them in a comprehensive way, some tables and graphics, based on the data collected from several publications and manufacturers, are shown.

2.2.1 Pumped Hydro Storage (PHS)

PHS is a large scale ESS. Its operating principle is based on managing the gravitational potential energy of water, by pumping it from a lower reservoir to an upper reservoir during periods of low power demand. When the power demand is high, water flows from the upper reservoir to the lower reservoir, activating the turbines to generate electricity. The energy stored is proportional to the water volume in the upper reservoir and the height of the waterfall. According to [92], the use of PHS can be divided into 24 hours time-scale applications, and applications involving a more prolonged energy storage in time, including several days. Actually, there is a tremendous potential for hydro-storage capacity in many areas globally. In type-one applications, the potential is around 1675 GW, and for type-two, 1454 GW. This technology is the most used for high-power applications [145].

An illustrative example of a PHS installation, is in operation by First Hydro Company [112]. This installation was commissioned in 1984. It can inject 1728 MW for 5 hours, including high power ramp rates. The system is capable of moving from 0 to 1320 MW power injection in 12 seconds by means of managing 6 motor-generators of 330 MW activated by reversible Francis water turbines, installed in Europe's largest man-made cavern.

In general, the life time of PHS installations is around 30-50 years, with an acceptable round trip efficiency of 65-75% and power capital costs of 500-1500 €/kW and 10-20 €/kWh [160]. Despite the large power volumes and energy management in PHS installations, it is remarkable that a fast response time (less than 1 minute [112]) enables the PHS systems as important components to control electrical network frequency and in provision of reserve generation.

2.2.2 Compressed Air Energy Storage (CAES)

CAES systems are based on conventional gas turbine technology. In this type of system, the energy is stored in form of compressed air in an underground storage cavern. When energy is required to be injected into the grid, the compressed air is drawn from the storage cavern, heated and then expanded in a set of high and low pressure turbines which convert most of the energy of the compressed air into rotational kinetic energy. The air is additionally mixed with natural gas and combusted. While the turbines are connected to electrical generators in order to obtain electrical energy, the turbine exhaust is used to heat the cavern air. The topology of the whole system is shown in Figure 2.1.

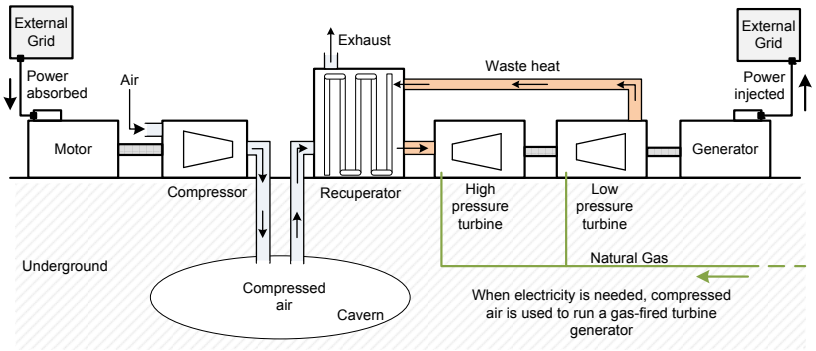

Figure 2.1: System description of Compressed Air Energy Storage

Currently, the use of CAES systems is not widespread. Only two plants have been constructed in the world so far; one in Germany (290 MW) and the other in the USA (110 MW) [145]. Nevertheless, this technology is currently attracting much interest. One of the biggest projects that is being carried out is the Iowa Stored Energy Park, with 2,700 MW of turbine power. This is being developed in conjunction with a large wind farm. The aim of CAES is to store the excess of wind energy generation [290].

Advances in this technology have led to the development of Advanced-Adiabatic CAES (AA-CAES). As its name suggests, the air is adiabatically compressed and then pumped into an underground cavern. The key parts of this system are the heat exchangers, which are quite expensive. The effectiveness and the economics of these heat exchangers, and the compressor and expander trains are the main concerns for the success of AA-CAES [231].

The life time of CAES installations is approximately 40 years, with an energy efficiency of 71% [80]. Since the self-discharge of the system is very low, CAES systems are considered long-term time scale storage installations which can compete with PHS.

2.2.3 Battery Energy Storage System (BESS)

Batteries are one of the most used energy storage technologies available on the market. The energy is stored in the form of electrochemical energy, in a set of multiple cells, connected in series or in parallel or both, in order to obtain the desired voltage and capacity. Each cell consists of two conductor electrodes and an electrolyte, placed together in a special, sealed container and connected to an external source or load [287]. The electrolyte enables the exchange of ions between the two electrodes; while the electrons flow

through the external circuit. BESS is a solution based on low-voltage power battery modules, connected in series / parallel in order to achieve the desired electrical characteristics. According to [85], BESS comprises batteries, the Control and Power Conditioning System (C-PCS) and the rest of the plant, which is in charge of providing good protection for the entire system (see Figure 2.2).

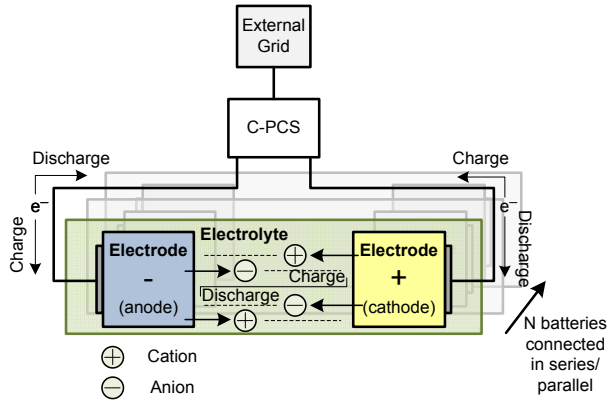

Figure 2.2: Operation principle of Battery Energy Storage System

Many types of batteries are now mature technologies. In fact, research activities involving Lead-Acid batteries have been conducted for over 140 years. Notwithstanding, a tremendous effort is being carried out to turn technologies like Nickel-Cadmium and Lithium-Ion batteries into cost effective options for higher power applications. In the following sections, a description of some of the most important typologies of batteries is presented.

Lead-Acid battery

The Lead-Acid battery is the most mature type of battery. It is made up of stacked cells, immersed in a dilute solution of sulfuric acid (H_2SO_4) as an electrolyte. The positive electrode of each cell is composed of lead dioxide (PbO_2), while the negative electrode is sponge lead (Pb). During discharge, both electrodes are converted into lead sulphate ($PbSO_4$). During the charge cycle, both electrodes return to their initial state. There are two major types of Lead-Acid batteries: flooded batteries, which is the most common topology, and valve-regulated batteries, which are the subject of extensive research and development [228].

The reversible redox reactions deteriorate the battery electrodes, giving them a cycle life of 1200-1800 cycles (depending on the Depth of Discharge, DoD), with a round trip efficiency of 75-80%. The life time of the system is approximately 5-15 years [126] and depends on the operating temperature of the system. In fact, high operating temperatures (up to 45°C [128]) can improve the battery performance in terms of higher capacity, but reduce the life time of the system. Due to their low daily self-discharge, <0.1% [126], Lead-Acid batteries are suitable for storing energy for long periods of time [146].

In addition to the relatively poor performance of the battery at low and high ambient temperatures, and its relatively short life time, the main disadvantages of the Lead-Acid battery are the necessity for periodic water maintenance (in the case of a flooded battery) and its low specific energy and power, 30 Wh/kg and 180 W/kg respectively. In addition, Lead-Acid batteries present difficulties in providing frequent power cycling, often at a partial state of charge, which can lead to premature failure due to sulphation [198].

Nickel-Cadmium battery (Ni-Cd)

Development of this type of alkaline rechargeable batteries has been carried out since 1950. This has helped to make them a well-established technology in the market place. The main components of Ni-Cd batteries are nickel species and cadmium species as the positive and negative electrodes' active materials respectively, and aqueous alkali solution as the electrolyte [203]. During the discharge cycle, $Ni(OH)_2$ is the active material of the positive electrode, and $Cd(OH)_2$ is the active material of the negative electrode. During the charge cycle, NiOOH is the active material of the positive electrode, and metallic Cd the active material of the negative electrode. The alkaline solution KOH acts as the electrolyte [46].

This type of battery can be commonly found in two different forms, depending on the application: in its sealed form in portable equipment, and in its flooded form in general industrial applications. In order to obtain a full-charge flooded Ni-Cd battery, it is necessary to apply a certain level of overcharging, with a very quick charge cycle. The discharge cycle is also very quick, due to significant lower internal resistance [203]. Ni-Cd batteries can inject their rated power during 2 hours [46].

The Ni-Cd battery has good characteristics with respect to its long cycle life (more than 3500 cycles [46]), combined with low maintenance requirements [198]. Nevertheless, its cycle life is highly dependent on the DoD. It

can reach more than 50000 cycles at 10% of DoD.

Although the Ni-Cd battery presents some good technical characteristics, it has not had a major commercial success, mainly due to its considerable costs at more than 10 times of Lead-Acid [79]. However, Ni-Cd production gross is increasing, despite having a strong competitor such as NiMH in the field of alkaline batteries. Thus, the alkaline rechargeable battery market should rapidly expand [46].

Two major drawbacks of Ni-Cd batteries are their toxicity and the fact that they suffer from the memory effect. Actually, cadmium and nickel are toxic heavy metals which can cause health risk in humans [313, 176]. For this reason, in November 2003, the European Commission drew up a proposal for new directives including recycling targets of 75% for this type of battery. With this new legal framework, energy storage in Ni-Cd batteries has an uncertain future.

Sodium-Sulphur battery (NaS)

Besides being a relatively recent technology, NaS batteries are one of the most promising options for high power energy storage applications. The anode of this type of battery is made of sodium (Na), while the cathode is made of sulphur (S). Ceramic Beta-Al_2O_3 acts as both the electrolyte and the separator simultaneously [309]. During the discharge cycle, the metallic anodic material (sodium) is oxidized, releasing Na^+ ions, while the cathodic material is reduced, releasing S^{-2} sulphur anions. The electrolyte enables the transfer of sodium ions to the cathode where they combine with sulphur anions and produce sodium polysulphide NaS_x. During the charge cycle, the opposite reaction occurs; sodium polysulphide is decomposed into sodium and sulphur.

NaS battery cells are usually designed in a tubular manner where the sodium is normally contained in an interior cavity formed by the electrolyte. An important feature of this type of battery is its high temperature operation, around 350°C [46]. At this temperature, sodium, sulphur and the product of the electrochemical reaction, NaS_x, are in liquid state, which allows a high reactivity of the electrodes. There are many concerns regarding the high temperature operation of the battery. To summarize: as the cell reactions are exothermic, the energy input required to maintain a proper operating temperature is low and therefore, the efficiency of the battery is not substantially reduced [221]. According to [309], the lower the electrolytic resistance of the battery, the better the performance due to the minimization of the energy lost in form of heat in the electrolyte.

One of the largest manufacturers of NaS batteries is the Japanese company NGK insulators [216]. One of its models can inject 50 kW of rated power for 7 hours [41]. The energy density and the energy efficiency of this type of batteries are very high, 151 kWh/m^3 and 85% respectively, [151].

Additional important features of NaS batteries are no self-discharge, low maintenance and their 99% recyclability.

Lithium-ion battery (Li-ion)

Li-ion batteries are widely used in small applications, such as mobile phones and portable electronic devices; therefore the annual production gross is around 2 billion cells [48]. In addition, this type of batteries attracts much interest in the field of material technology and others, in order to obtain high power devices for applications like electric vehicles and stationary energy storage.

The operation of Li-ion batteries is based on the electrochemical reactions between positive lithium ions (Li^+) with anolytic and catholytic active materials [304]. The cells of Li-ion batteries are made of anolytic and catholytic plates, filled with liquid electrolyte material. The electrode areas are delimited by a porous separator of polyethylene or polypropylene, which allows the transit of lithium ions. The catholytic material is usually based on lithium metal oxide, as lithium cobalate ($LiCoO_2$), while the anolytic material is graphite (C). The electrolyte is usually a non-aqueous organic liquid, such as PC, EC or DMC, which contains dissolved lithium salts such as $LiClO_4$.

The charging and discharging cycles of the battery are detailed as follows. During the charge cycle, Li^+ flows from the positive electrode, made of $LiCoO_2$, to the graphite sheets of the negative electrode [48, 304]. The discharge cycle consists of the reverse process.

Since the performance and the range size of the battery are strongly related to the active materials of the electrodes and the electrolyte, there is a tremendous amount of research in the field of material technology nowadays [48, 111, 195, 304].

As important features of Li-ion batteries, it is appropriate to mention their high energy density and specific energy, 170-300 Wh/l and 75-125 Wh/kg respectively [304]. Another major feature is their fast charge and discharge capability [317]. In fact, time constants (understood here as the time to reach 90% of the rated power of the battery) around 200 ms, with a relatively high round trip efficiency of 78% within 3500 cycles, have been reported [6]. These characteristics make Li-ion batteries good candidates for applications where the response time and weight are important. In addition, Li-ion batteries

are mainly an option in short time scale applications, due to their relatively high daily self-discharge, between 1-5% [128, 231, 317].

Referring to the drawbacks of Li-ion batteries, it can be mentioned that, since their life time is dependent on cycle DoD, this technology is not adequate for the use in back-up applications where they may become fully discharged. In addition, maintaining a safe voltage and temperature operation ranges are essential aspects for this technology, due to its fragility. Indeed, protection circuits are required [128]. In addition, the use of flammable organic electrolytes raises issues about security and greenness.

2.2.4 Flow Battery Energy Storage System (FBESS)

Flow batteries are a relatively young technology. Their operating principle is based on reversible electrochemical reactions that occur in a set of cells connected in series, parallel or both, in order to achieve the desired voltage level. Unlike conventional batteries, two different aqueous electrolytic solutions are contained in separate tanks. During the normal operation of the battery, these aqueous solutions are pumped through the electrochemical cell where the reactions occur [130, 260]. Three types of commercially available flow batteries are considered in this chapter: Vanadium Redox Battery (VRB), Zinc Bromine Battery (ZBB) and Polysulphide Bromide Battery (PSB). Since their operation is based on reduction and oxidation reactions of the electrolyte solutions, these types of batteries are also called redox flow batteries. Their operating principle is presented in Figure 2.3. As shown, during the charge process, the electrolyte A is oxidized at the anode, while the electrolyte B is reduced at the cathode. The discharge cycle consists of the reverse process.

One of the major advantages of flow batteries is that their energy capacity is easily scalable, since it depends on the volume of the stored electrolyte. This leads to lower installation costs the larger the system is [313]. As a result, energy and power capacity of flow batteries are independent characteristics: the power capacity of the system depends on the cell number and the size of the electrodes. But operating costs are not negligible, due to the control of electrolytic flows and pumps [130]. In this sense, the ZBB presents worse performance than a PSB and VRB, since a third pump is required for the recirculation of bromine complexes.

Other interesting features of flow batteries are their ability to become fully discharged without any damage, and their very low self-discharge, since the electrolytes are stored in separate sealed tanks. Therefore, redox flow batteries result as systems with a long life and low maintenance, able to

store energy over long periods of time.

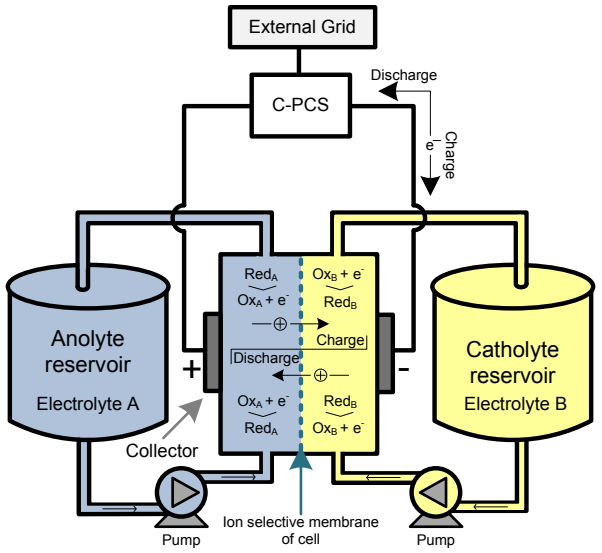

Figure 2.3: Operation principle of Flow Battery Energy Storage System

Vanadium Redox flow Battery (VRB)

The VRB stores energy in two tanks, an anolytic and catholytic reservoir, containing sulphuric acid solutions. In the anolytic reservoir, V^{2+}/V^{3+} are used as electrolytes, while the electrolytes V^{4+}/V^{5+} are used in the catholytic reservoir [233, 256]. When an electrochemical reaction occurs, carbon electrodes enable the electron flow through the load, while the electrical balance is achieved by means of the migration of a hydrogen ion through the membrane which separates the two electrolytes. Since the products of chemical reactions remain dissolved in the electrolytes, the reverse process leads solutions to their initial state. Moreover, there is no danger of cross-contamination of the electrolytes, as they both contain the same type of metal ion.

The system life is about 15-20 years [255], with more than 1000 charge and discharge cycles at 100% of DoD [36]. However, while electrolytes do not require special maintenance, it is recommended to replace the separator membrane every 5 years [256]. The system can achieve an energy efficiency of 78% [144], and it results in relatively low cost to store large amounts of energy for long times. According to [291], the cost per kWh decreases as

energy storage capacity increases, achieving costs as low as 150 $/kWh for 8 or more hours of storage devices.

Referring to the drawbacks of the system, it is remarkable that its low specific energy and energy density, around 25-35 Wh/kg and 20-33 Wh/l respectively [292] reduce the potential uses of the battery in non-stationary applications.

Zinc-Bromine flow Battery (ZBB)

In ZBBs, two aqueous solutions, based on Zn and Br and stored in separate tanks, flow through electrolytic cells where the reversible electrochemical reactions are produced. During the discharge process, bromide ions Br^- are converted to bromine Br_3^-, in the positive electrode, which reacts with other organic amines and creates thick bromine oil that sinks to the bottom of the tank. Meanwhile, in the negative electrode, positive zinc ions Zn^{2+} are converted to metallic Zn. Reverse reactions to those described are carried out during the charge process of the battery. Cell electrodes are composed of carbon-plastic composite and are separated by means of a micro-porous polyolefin membrane [97, 233].

Since the invention of ZBBs in 1970 by Exxon, this technology has evolved to the point that it is now commercially available in sizes of 1 MW / 3 MWh for utility-scale applications [97], with the ability to provide its rated power for 2-10 hours [183]. Indeed, large amounts of energy can be stored for long periods of time due to virtually no self-discharge of the battery [247]. Other important features of this technology are its relatively high specific energy of 75-85 Wh/kg [318] (between 2 or 3 times that of Lead-Acid batteries), a high energy efficiency of 75-85% [130] and a longer cycle life than 2000 charge and discharge cycles at 100% of DoD without any damage [108]. In terms of greenness, these products are basically made of recycled plastics, allowing low cost production and high recyclability [247].

Polysulphide-Bromide flow Battery (PSB)

The operation of PSBs, also called regenerative fuel cells or Regenesys, are based on the electrochemical reactions between two salt-based electrolytes: sodium bromide (NaBr) and sodium plysulphide (Na_2S_x). The electrolytes are separated by a polymer membrane which only allows the interchange of positive sodium ions [85, 313, 233, 260]. During the charge cycle, bromide ions (Br^-) are transformed into tribromide ions (Br_3^-) in the positive electrode of the cell. In the negative electrode, dissolved sodium particles

(S_4^{2-}) in the polysulphide electrolyte are reduced to sulphide ions (S_2^{2-}). The discharge cycle consists of the reverse process.

Regenesys Technologies built the larger system based on this battery type in 2003. The rated power and energy capacity of this system are 15 MW and 120 MWh respectively, which provide a duty cycle of 10 hours [233, 235]. The system has a modular design. Each module has 100 kW of rated power. The energy efficiency of the system is 75%, with a relatively long life, more than 15 years. The project budget was around 250 million dollars.

Since a PSB has practically no self-discharge, it is suitable for storing energy during long periods of time. Moreover, the chemical elements present in the battery are abundant in nature, and their costs are reasonable [233]. On the other hand, a tank failure would expel toxic bromine gas [313].

2.2.5 Hydrogen-based Energy Storage System (HESS)

Hydrogen can be obtained in various ways: by means of water electrolysis, from renewable energies such as solar or wind installations, gasifying biomass, coal or fuel (which is the most common option) [68, 310]. When hydrogen is produced from WPPs, it can be stored in order to be used directly in fuel cells, or transported to users through pipelines to produce electricity [267].

When hydrogen is stored, the technology used is known as Regenerative Fuel Cell (RFC) [57, 274]. As shown in Figure 2.4, it is composed of the following components: a water electrolyzer system, a fuel cell system, a hydrogen storage and a power conversion system. This technology is responsible for carrying out the electrochemical transformations in order to store energy in the form of hydrogen and inject it as electricity into the grid, when required.

As presented, electrolyzers are key parts of RFCs. By means of these devices, water is electrolytically decomposed into hydrogen and oxygen. There are many types of electrolyzers, from common technologies such as Alkaline electrolyzers [267], to more modern types like Polymer Electrolyte Membrane (PEM) electrolyzers. PEM electrolyzers were invented in 1970, but hydrogen production by means of this type of technology is currently considerable, reporting production volumes up to 10 Nm^3/h [236]. The electrolyzers are classified by their type of electrolyte, liquid or solid. The use of solid electrolytes allows PEM electrolyzers to generate hydrogen at suitable pressures (200-6000 psi [274]) in order to store it in tanks or in metal hydrides.

In fact, hydrogen can be stored in many forms [68, 128, 299]: as gas in metal tanks (or other composite materials like carbon fiber or polymer) at

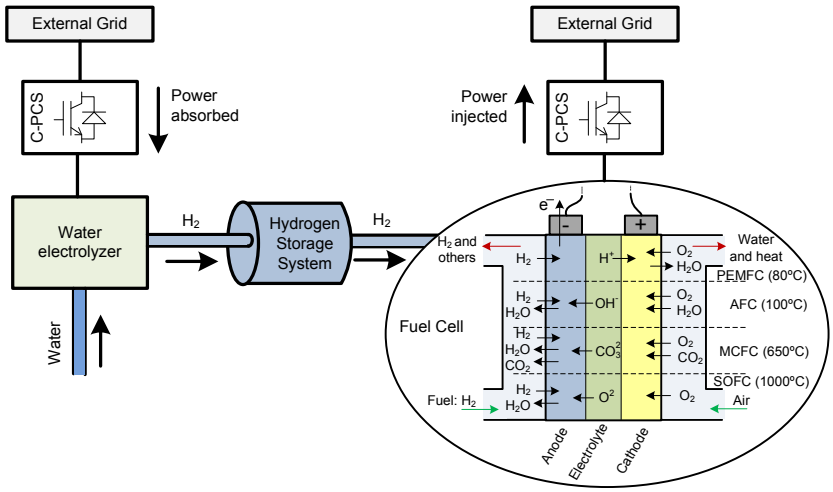

Figure 2.4: Topology of Regenerative Fuel Cell

pressures up to 350 bar, or in metal hydrides. Storing hydrogen in metal tanks may be suitable for large volume applications for long term storage (more than 30 hours), while storing hydrogen in metal hydrides is suitable for storage periods longer than 3 hours [310]. Other less developed storage technologies include the liquefaction of hydrogen and the storage in carbon nanofibers.

Similarly to the electrolyzers, there are many types of fuel cells for stationary and distributed generation purposes [214, 296], depending on their electrolytic material. In Figure 2.4, the Polymer Electrolyte Membrane Fuel Cell (PEMFC), Alkaline Fuel Cell (AFC), Molten Carbonate Fuel Cell (MCFC) and Solid Oxide Fuel Cell (SOFC) are detailed. The PEMFC is the most used technology. Its low operation temperature (between 50-100°C), maintenance and corrosion, as its electrolyte is solid, are important characteristics of this type of fuel cell. On the other hand, since the catalytic material is platinum, the cost of the device increases significantly. In addition, this technology is affected by hydrogen impurities, which affect its life.

The sizing of the stack depends on the type of technology used, leading to 100 kW PEMFC stacks or 2 MW SOFC stacks. Fuel cells are noted for their good dynamic behavior, allowing a quick start-up, even at partial load. No acoustic emissions are noted during their operation and they only discharge water as a product [57].

As they are flow batteries, RFC power and energy capacity are not related characteristics. In addition, since they are designed in a modular manner,

high energy systems with more than 100 MWh and with high peak power, more than 10 MW, can be achieved. Their practically zero self-discharge (depending on the type of hydrogen storage) allows these systems to store energy for long periods of time. In terms of their useful life and cycle life, they are estimated at more than 15 years and 20000 charge and discharge cycles (at 100% of DoD) respectively [145, 274, 310]. Finally, notice that one of the major drawbacks of a RFC is its low energy efficiency, about 42%, due to the relatively low energy efficiencies of the fuel cell and the electrolyzer, about 60% and 70% respectively [184].

2.2.6 Flywheel Energy Storage System (FESS)

A FESS is an electromechanical system that stores energy in form of kinetic energy. A mass rotates on two magnetic bearings in order to decrease friction at high speed, coupled with an electric machine. The entire structure is placed in a vacuum to reduce wind shear [42, 313, 189, 321]. The scheme of the system is presented in Figure 2.5.

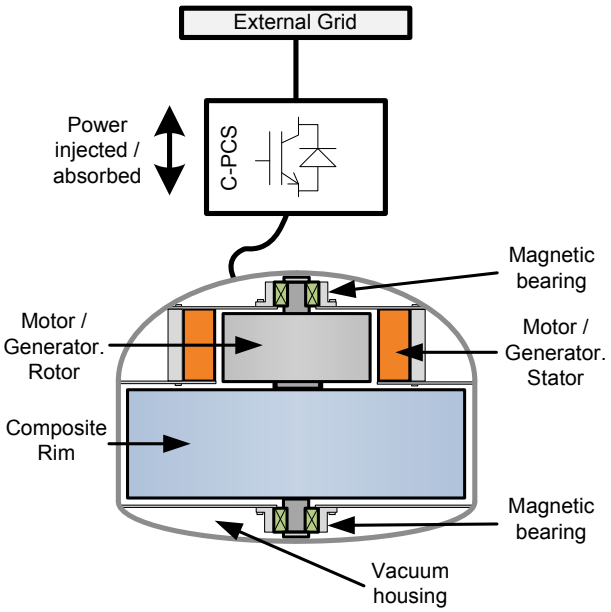

Figure 2.5: Topology of Flywheel Energy Storage System

Energy is transferred to the flywheel when the machine operates as a motor (the flywheel accelerates), charging the energy storage device. The FESS is discharged when the electric machine regenerates through the drive (slowing

the flywheel). In fact, the energy stored by the flywheel is dependent on the square of the rotating speed and its inertia. Commercially, the two major types of machines used for flywheels systems are the axial-flux and the radial-flux permanent magnet machines. Apart from the permanent magnet machine used in almost all flywheels, there is also the possibility of using synchronous reluctance or induction machines. In general, flywheels can be classified as low speed or high speed devices. The first operates at revolutions per minute (rpm), measured in thousands (this class of flywheel uses steel as the main structural material in the rotor), while the latter operates at rpm measured in tens of thousands (this class of flywheel uses a rotor made of an advanced composite material, such as carbon-fiber or graphite [141, 189]). The energy density of the flywheel depends on the product of a shape factor, taking the inertia of the rotating disk into account, and the permissible tangential strength of the disk, which depends on its material. Moreover, the maximum specific energy of the system is determined by the ratio of the energy density and the density of the material of the rotating disk [21, 141]. Thus, the choice of the material is a key point in the system performance, since high-strength but lightweight materials are required. Moreover, the rated power of the system is limited by its C-PCS.

On the one hand, a FESS presents good features regarding high efficiency (around 90% at rated power), long cycling life, wide operating temperature range, freedom from depth-of-discharge effects, higher power and higher energy density [42, 313, 154, 249]. On the other hand, flywheels present relatively high standing losses. Self-discharge rates for complete flywheel systems are about 20% of the stored capacity per hour [128]. This is the reason why flywheels are not adequate devices for long-term energy storage. The largest available kinetic energy storage device is manufactured by Piller Power Systems [232]. This system is designed to operate within a speed range of 3600 rpm to 1500 rpm. Its energy capacity is about 19 MWs and can deliver 10 seconds of ride-through at 1.65 MW load and proportionately a longer ride-through at lesser loads.

2.2.7 Superconducting Magnetic Energy Storage (SMES)

The SMES system is a relatively recent technology. The first system based on this technology was built in 1970 [249]. Its operation is based on storing energy in a magnetic field, which is created by a DC current through a large superconducting coil at a cryogenic temperature.

The energy stored is calculated as the product of the self-inductance of the coil and the square of the current flowing through it [218]. Thus, the

Table 2.1: Capital cost, energy and power ratings of ESSs

Technology	Capital cost	Energy rating (MWh)	Power rating (MW)
PHS	10-20 €/kWh [160], 35-70 €/kWh [110]	500-8000 [151]	10-1000 [151]
HESS	2-15 €/kWh [160]	120 [145]	0.1-15 [145], 0.3-50 [113]
CAES	3-5 €/kWh [160], 10-70 €/kWh [110]	2860 [250], 580 [250]	110 [250], 290 [250], 50-300 [128]
VRB	600 $/kWh [25]	2 [198], 6 [11], 1.2-60 [237], 120 [298]	0.25 [198], 6 [11], 0.2-10 [237], 12 [298]
ZBB	500 $/kWh [293]	0.1-3 [97], 0.15 [234], 0.4 [70], 2 [106], 2.8 [11], 4 [35]	0.1-1 [97], 0.1 [234], 0.2 [70], 2 [106], 0.5 [11], 1 [35]
PSB	125-150 €/kWh [160], 450 $/kWh [25], 360-1000 €/kWh [85]	0.005-120 [233]	0.1-15 [233]
NaS	210-250 €/kWh [160], 450 $/kWh [293]	0.4 [309], 0.4-244.8 [162]	0.05 [309], 0.05-34 [162]
Lead-Acid	50-100 $/kWh [128], 210-270 €/kWh [160], 185 €/kWh [198]	0.001-40 [198]	0.05-10 [198]
Ni-Cd	400-2400 $/kWh [128]	6.75 [11]	45 [11]
Li-ion	900-1300 $/kWh [128]	0.0016 [65], 0.5 [1], 0.0015-50 [257]	0.1 [65], 2 [1], 0.015-50 [257]
SMES	-	0.001 [258], 0.00083 [35], 0.015 [132]	1 [258], 3 [35], 100 [132], 1-10 [130, 249]
FESS	400-800 $/kWh [128]	0.0052 [232], 0.025-5 [34]	1.65 [232], 0.1-20 [34]
SCESS	20000 $/kWh [128], 6800 €/kWh [175]	0.01 [77]	0.05-0.1 [145], 0.25 [77]

Table 2.2: Specific energy and power, as well as cycling capability and life in years of ESSs

Technology	Specific energy (Wh/kg)	Spec. power (W/kg)	Cycling capability	Life (years)
PHS	-	-	$2{\cdot}10^4$-$5{\cdot}10^4$ [97]	30-50 [160], 50 [151]
HESS	100-150 [274], 400-1000 [274]	-	$2{\cdot}10^4$ [274]	15 [274]
CAES	3.2-5.5 [128]	-	10^4-$3{\cdot}10^4$ [97]	30 [193], 40 [80]
VRB	20 [80], 25-35 [233]	166 [28]	1000 [36], 13000 [144]	10 [237], 15-20 [255], 20 [80, 233]
ZBB	60 [36], 70-90 [274], 75-85 [130]	45 [99]	2000 [108], 2500 [144]	8-10 [255]
PSB	-	-	-	15 [233]
NaS	100 [36], 175 [292]	115 [99], 90-230 [93]	2500 [309]	12-20 [151], 10-15 [160]
Lead-Acid	30 [128], 35-50 [22]	180 [128], 200 [99]	200-300 [85], 500 [79], 1200-1800 [128], 1800 [256]	5-15 [128]
Ni-Cd	30-40 [131], 50 [128, 36], 45-80 [22]	100-150 [131], 160 [99]	3500 [198][46]	13-16 [255], 20 [22, 46]
Li-ion	80-150 [128], 100-150 [36], 160 [22], 120-200 [90]	245-430 [131], 400-500 [292], 500-2000 [128]	1500 [128], 3500 [6]	14-16 [255]
SMES	10-75 [249]	-	10^4-10^5 [218]	20 [99]
FESS	20 [274], 5-80 [251], 5-100 [128]	11900 [189]	10^5-10^7 [128]	20 [34]
SCESS	2-5 [90], 5.69 [273], 1-10 [239], 10 [251], 5-15 [145], 30 [190]	800-2000 [145], 2000-5000 [90], 10000 [128, 239], 13800 [273], 23600 [60]	$5{\cdot}10^5$ [128], 10^6 [239]	8-10 [145], 12 [128], 17 [197]

Table 2.3: Energy efficiency, daily self-discharge and manufacturers of ESSs

Technology	Energy efficiency (%)	Daily self-discharge (%)	Manufacturers
PHS	65-75 [160], 67 [151], 75-80 [128][80]	No [151]	First Hydro Company [112], MWH [210]
HESS	35 [145], 40 [193], 35-40 [37], 42 [184]	No [113]	Fuel Cell Energy Inc. [113]
CAES	70 [145], 71 [80], 73 [128]	No [151]	Enis Windgen [100], Dresser-Rand [88]
VRB	65-75 [237], 76 [80], 75-85 [130], 78 [144], 72-88 [256]	Very low [237]	Prudent Energy Corp. [237]
ZBB	65-75 [77], 68 [144], 70 [168], 80 [233], 75-85 [130]	No [247]	Redflow [247], ZBB Energy Corp. [318], Premium Power Corp. [234]
PSB	60-65 [255], 75 [233]	No [233]	Regenesys Technologies [248]
NaS	75-85 [160], 80 [46], 85 [151], 84-87 [128]	No [309]	NGK [41]
Lead-Acid	75-80 [160], 70-80 [256]	<0.1 [128], 0.1 [9, 231], 0.2 [168]	Alcad [12], Exide Technologies [109]
Ni-Cd	72 [31]	0.2 [9], 0.3 [128]	Saft [257], Alcad [12], Harding Energy Inc. [131]
Li-ion	78 [6], 88 [65]	1 [231], 5 [128]	A123 Systems [1], Li-Tec Battery GmbH. [185], Harding Energy Inc. [131]
SMES	80 [231], 90 [218], 95 [15]	10-15 [35]	Superconductor Technologies Inc. [281], American Superconductor Corp. [16]
FESS	85 [145]	100 [128]	Beacon Power [34], Active Power [5], Piller [232]
SCESS	65 [168], 80 [231, 136], 90 [26, 170]	5 [145], 10-20 [231]	Maxwell [197], EPCOS [105], ESMA [157], NEC-Tokin [213]

characterization of the coil has a central role in the system design. Depending on the system operating temperatures, superconducting coils can be classified as: High Temperature Coils (HTS), which work at temperatures around 70 K, and Low Temperature Coils (LTS), a more mature technology, with working temperatures around 5 K. A balance between cost and system requirements determines the technology used.

The maximum current that can flow through the superconductor is temperature dependent. Indeed, the lower the operating temperatures, the higher the operating currents that can be achieved. According to [231], flux densities around 10 T at 4.2 K have been experimentally reported, allowing energy densities of 40 MJ/m^3. Therefore, higher energy densities than those of flywheels and conventional batteries can be obtained.

The cooling system must be considered as a core element of the system, since it is fundamental to obtain a superconductor coil in its cryogenic state [270]. In this sense, the system has two cryocoolers, the first is responsible for cooling the superconductor coil by means of liquid helium or nitrogen bath, and the second is required to cool shields outside the bath [265]. Fortunately, the energy required for these cooling systems is much smaller than the energy stored in the system. Therefore, and taking into account other energy losses such as those due to the C-PCS, SMES systems have very high energy efficiencies up to 90% [218]. Indeed, a cryocooler can keep the system operating temperature at 20 K with a lower power consumption than 20 W/s [165].

Concerning the C-PCS, two different types of power converters are considered, the VSC and the CSC [15, 218]. Even though the active and reactive power can be properly controlled with both power electronics-based converters, a reactive power management with a very low or even zero current in the coil is only possible with VSC. On the other hand, CSCs are able to inject higher reactive currents. In addition, VSC control is usually more complicated than a CSC one, due to the presence of a DC/DC chopper.

Finally, it is appropriate to highlight some important features of SMES systems. Undoubtedly, a defining feature of these systems is their ability to inject or absorb large amounts of energy in a very short time. According to [258], the power injection of a 1 MW / 1 kWh SMES can be increased in 200 kW in only 20 ms. Other experimental studies show similar results [133]. The energy capacity of these systems ranges from 100 kW to 10 MW, and it is possible to inject their rated power only for a few minutes before being discharged [218, 249]. In addition, SMES systems have a very long cycle life of tens of thousands of cycles [218]. Despite their good technological features, there are actually very few SMES systems built, mainly due to

their high cost [231]. According to [35], the capital power cost may vary between 1000-10000 $/kW.

2.2.8 Supercapacitor Energy Storage System

Supercapacitors are also known as ultracapacitors or double-layer capacitors. Like batteries, supercapacitors are based on electrochemical cells which contain two conductor electrodes, an electrolyte and a porous membrane whereby ion transit between the two electrodes is permitted. However, no redox reactions occur in the cells, because the operating voltage is lower, in order to electrostatically store charge on the interface between the surfaces of the electrolyte and the two conductor electrodes [127, 239, 266]. In fact, this structure creates two capacitors (due to both interfaces, electrolyte - negative electrode and electrolyte - positive electrode), and for this reason, they are called double-layer capacitors.

The energy stored in the capacitors is directly proportional to their capacity and the square of the voltage between the terminals of the electrochemical cell, while the capacity is proportional to the electrode-surface area and inversely proportional to the distance between the electrodes. Therefore, the main difference between capacitors and supercapacitors is the use of porous electrodes with high surface-areas by the latter ones, providing higher energy densities to the system [87, 266].

Due to their low-cell voltage (about 3V), the desired voltage and capacity of the supercapacitor are achieved by the series and parallel connection of a set of cells [231]. The topology of a system based on a supercapacitor is shown in Figure 2.6.

There are two types of supercapacitors depending on the design of the electrodes [23, 26, 266]: symmetrical and asymmetrical supercapacitors. Unlike unsymmetrical ones, symmetrical supercapacitors utilize the same material for their positive and negative electrodes. Moreover, further classification can be made for electrodes based upon their materials [24]. In this sense, it can be distinguished between activated carbon electrodes, metal-oxide electrodes and electronically conducting polymer electrodes. Activated carbon electrodes are commonly used in commercial systems due to their low cost and high capacity (up to 5000F [197, 239]). In fact, activated carbon electrodes provide capacities from 100 to 1000 times per unit volume over conventional electrolytic capacitors [207]. Concerning the electrolyte, since its breakdown voltage limits the voltage of the supercapacitor cell, the proper choice of its material is very important. There are several types of electrolytes. To summarize, they can be classified into aqueous electrolytes

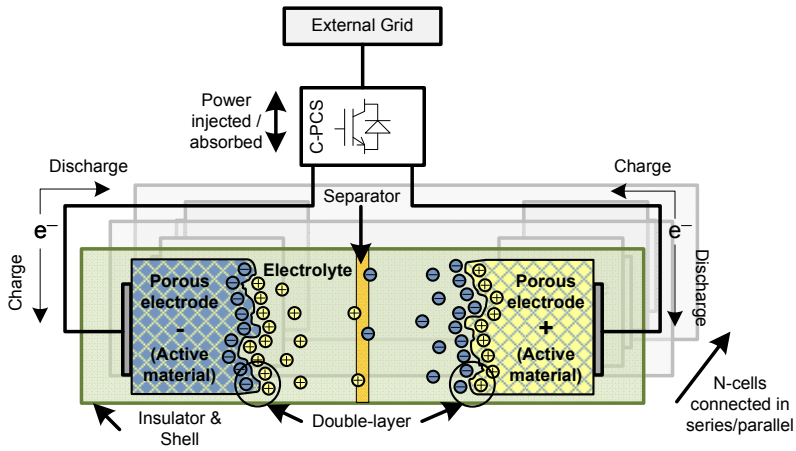

Figure 2.6: ESS based on a supercapacitor

and organic electrolytes, which are most common [266].

As mentioned, electrolyte and electrode materials have a fundamental influence on the energy and power capacity of the supercapacitor, as well as its dynamic behavior. Actually, the product of the equivalent resistance of the electrolyte and the capacity of the supercapacitor determine its charge and discharge time constants. This equivalent resistance is very small (less than 1 miliohm [229]), therefore short time constants can be achieved. In addition, power densities 10 times higher than batteries can be achieved. These features, combined with the high self-discharge of the system (which can be 20% of its rated capacity in 12 hours, due to the non negligible equivalent resistance of the contact between the electrolyte and the electrodes [168, 223]), define the system as a candidate for short time scale applications with short time responses.

Other important features of supercapacitors are their long life, more than $5{\cdot}10^4$-10^5 cycles with virtually no maintenance and energy efficiency of about 75-80% [136]. Charge and discharge cycle times of the system are about 1-30 seconds at rated power, while the specific power and energy power of the system are very high, 2000-5000 W/kg and 20000-30000 W/m^3 respectively. However, its specific energy and energy density are low, 2-5 Wh/kg and 10000 Wh/m^3, due to the difficult access to the porous surface of the electrode by ions [90, 60]. Finally, it can be noted that the most important drawback of supercapacitors is their high cost, estimated at 5 times that of Lead-Acid battery cost, 9500 $/kWh [175].

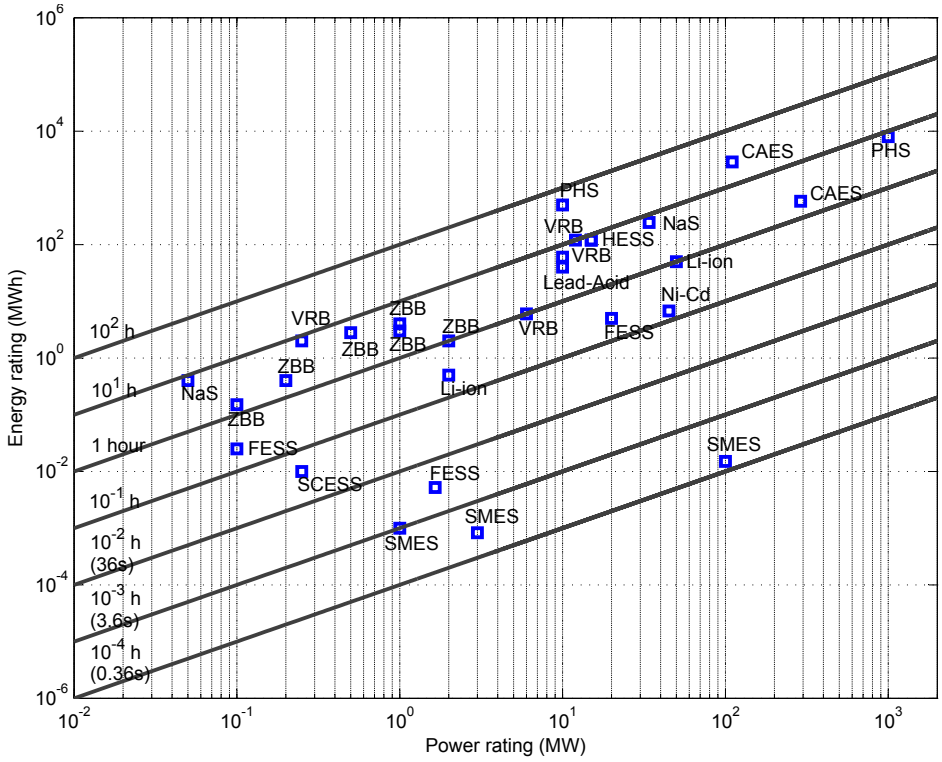

Figure 2.7: Discharge time at rated power of ESS, according to the data collected in Table 2.1

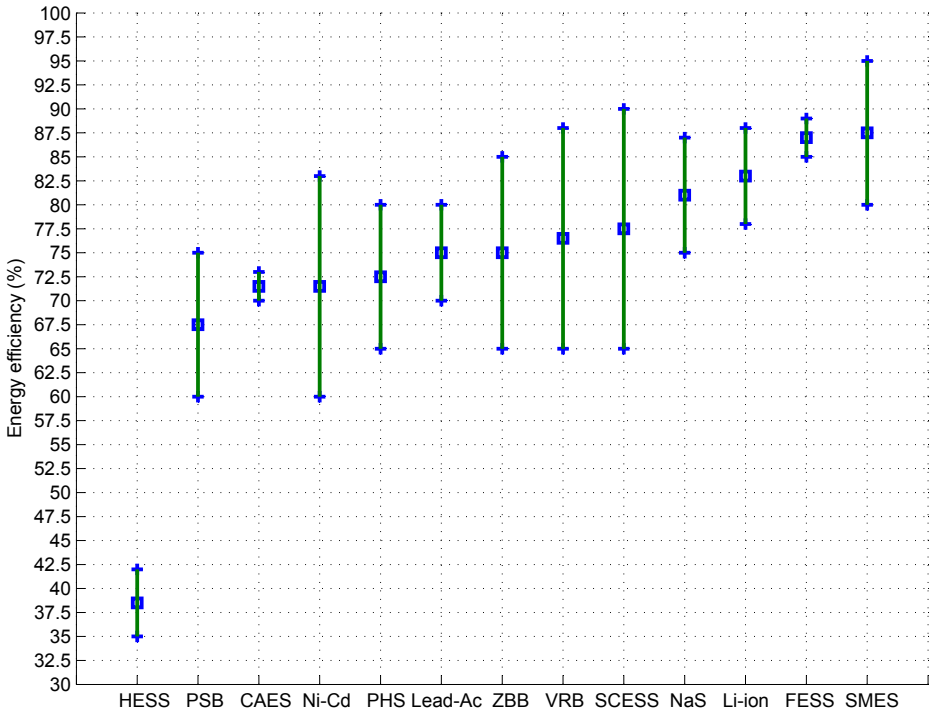

Figure 2.8: Energy efficiency of ESS's, according to the data collected in Table 2.2

2.3 Applications of the storage technologies in wind power

This section details the potential applications of ESS in wind power. Each technical issue, concerning different aspects related with the management of WPPs and their integration into the electrical network, has been identified and defined according to [31, 33, 35, 79, 106, 115, 284]. In addition, the definition of these aspects is complemented by a brief discussion on the ESS role in each case. Finally, a review of several publications concerning the ESS applications in wind power is summarized in Table 2.4 and Table 2.5.

2.3.1 Fluctuation suppression

Fast output fluctuations (in the time range up to a minute) of the power of wind generators can cause network frequency and voltage variations, especially in isolated power systems, and thus impairing the power quality [208]. In order to mitigate the effects of power fluctuations, an ESS can be used. Storage technologies suitable for this application present high ramp power rates and high cycling capability, since fast power modulation and continuous operation are required. Thus, batteries (excluding conventional Lead-Acid batteries), flow batteries, and especially short time scale energy storage like supercapacitors, flywheels and SMES are well suited for this service.

A widely accepted solution to mitigate the power fluctuations of a wind turbine driving a DFIG is to include an ESS in the dc-link of the back-to-back converters of the machine. This storage device is equipped with a control which interacts with the turbine's and other controls in order to optimize the net power delivered to the external grid by the entire system. This is the case presented in [238]: a supercapacitor connected to the dc-link of a wind generator through a two-quadrant dc-dc converter. Two levels of control are defined, the high level (wind farm supervisory controller), which is in charge of coordinating the set points of each wind generator, and the low level, which details the vector controllers of the converters of each wind generator. As a wind turbine controller, the C-PCS of each storage device receives the set point calculated by the high level controller, and manages the power injection or absorption by means of computing the difference between this signal and the actual active power of the wind generator.

Flywheels are also under study for complementation of the dc-link of DFIG wind turbines. Since the operating principle of this technology is highly related to the power management of a motor / generator, the control theory

Table 2.4: Overview of publications regarding the uses of ESS in wind power (part I)

	Full power duration of storage	PHS	HESS	CAES	VRB	ZBB	PSB
Fluctuation suppresion	$\leq$ 1min				[8, 200, 306, 314]	[8, 108]	[8]
LVRT	$\leq$ 1 min				[200, 308]	$\surd$ [1]	$\surd$ [1]
Voltage control support	$\leq$ 1min				[8, 200, 298, 306]	[8]	[8]
Oscillation damping	$\leq$ 1 min		[149]		[8]	[8]	[8]
Spinning reserve	1 min - 30 min	[92]	[32]	[72]	[8, 259, 298, 306, 314]	[8, 108, 259, 298]	[8, 259, 298]
Load following	min - $\leq$ 10h	[47, 49, 62, 118, 125]	[7, 32, 122, 148, 182, 186, 211, 222]	[59, 194, 283]	[27, 28, 91, 298]	[44, 91, 183, 298]	[298]
Peak shaving	1-10 h	[17, 37, 47, 53, 161, 227]	[38, 122, 148, 267]	[298, 316]	[91, 156, 142]	[11, 91, 183]	[142]
Trans. curtailment	5-12 h	[17, 58, 92, 191]	[57, 122, 169]	[81, 191, 316]	[135]	$\surd$ [1]	$\surd$ [1]
Time shifting	5-12 h	[58]	[145, 148, 267]	[220]	[106]	[11]	$\surd$ [1]
Unit commitment	hours - days	[47]	$\surd$ [1]	[72]			
Seasonal storage	$\geq$ 4 months	[76]	[169, 186]				

[1] Although the storage technology is suitable for this application, dedicated studies are not listed here.

Table 2.5: Overview of publications regarding the uses of ESS in wind power (part II)

	Full power duration of storage	NaS	Lead acid	Ni-Cd	Li-ion	SMES	FESS	SCESS
Fluc. suppresion	≤ 1min	[268]		[264, 262]	[65, 174]	[133, 150, 134, 165, 167, 219, 269]	[43, 117, 180, 242, 243, 282, 54, 55, 56]	[2, 136, 238, 243]
LVRT	≤ 1 min	[39, 41, 307]	[39, 307]	[39, 307]	[39, 307]	[2, 13, 20, 166, 167, 188, 225, 249, 269]	[249]	[2, 26]
Voltage control support	≤ 1min	[30, 39]	[30, 228, 294, 302]	[30, 264, 262]	[30, 39]	[133, 188, 249, 305]	[249, 282]	[266]
Oscillation damping	≤ 1 min	[89, 139, 307, 209]	[89, 209, 307]	[89, 209, 307]	[89, 209, 307]	[14, 89, 188, 215, 225, 305]	[187, 323]	[207]
Spinning reserve	1 min - 30 min	[182, 199, 309]	[182, 199, 228, 303]	[11, 182, 199]	[182, 199]	[218]	[178, 298]	
Load following	min - ≤ 10h	[91, 138, 147, 181, 309]	[61, 181, 91, 228, 303]	[91, 181, 264]	[181]			
Peak shaving	1-10 h	[168, 91, 181, 252]	[50, 91, 181, 228]	[91, 181]	[181]			
Trans. curtailment	5-12 h	√ [1]						
Time shifting	5-12 h	[91]						
Unit commitment	hours - days							
Seasonal storage	≥ 4 months							

[1] Although the storage technology is suitable for this application, dedicated studies are not listed here.

of electrical drives plays a key role in these studies. In [43], three techniques of sensor-less vector-controlled induction motors driving a flywheel are compared. In addition, control theories based on the Model Reference Adaptative System (MRAS) for the design of speed estimation algorithms, as well as flux weakening aspects, motivated by the high speed of the flywheel are taken into account [54, 55]. In addition to the use of induction machines, permanent magnet and switched reluctance machines are studied for flywheel storage devices [56].

As noted at the beginning of this section, the effects of power fluctuations of wind turbines regarding power quality issues, are remarkable, especially in isolated systems. Related to this problem, the combination of storage systems, like flywheels, supercapacitors or batteries in hybrid systems with offshore wind generation, diesel and photovoltaic generation, is proposed by [243].

Other studies [134, 165] propose the use of SMES in order to perform the task of fluctuation suppression, providing storage at the PCC of the wind farm to the network. In this configuration, the rated power of SMES reaches several MW. For instance, a 15 MWh - 60 seconds SMES is proposed in [219], in order to smooth the power fluctuations of a 100 MW wind power installation. In this case, the WPP is connected to the external grid through a back-to-back DC link. To conclude, it is noted that by means of the management of charge and discharge rates of SMES, the capacity of the power converters of the WPP can be reduced by 60%. Issues such as SMES capital costs, as well as power losses, due to maintaining low temperature of operation and leakage magnetic fields, have to be taken into account.

2.3.2 Low Voltage Ride Through (LVRT)

The voltage control of WPPs at the point of connection with the external grid during voltage dips, is carried out in order to prevent the WPP from being disconnected, which could cause the collapse of the network. For this reason, Grid Codes require WPPs to withstand voltage dips up to 0% of the rated voltage and for a specified duration. These requirements are known as LVRT requirements. Since many technologies of wind generators include power converters, it is possible to adjust the reactive power injected into the grid during these situations [120, 121, 159]. Therefore, energy storage is not necessary in these situations, but may protect the dc-link of the converters from over-voltage.

As in the case of fluctuation suppression service, the suitable storage systems for this application present high ramp-up rates enabling a fast power

modulation. Therefore, batteries, flow batteries, and short time scale energy storage like supercapacitors, flywheels and SMES are well suited for this application.

In [2], the dc-link of the set of back-to-back converters of a wind turbine driving a DFIG is complemented by supercapacitors. Numerous simulation results show the improved ride-through capability of the system with energy storage support. Fuzzy logic control techniques are suggested to manage the interaction between the C-PCS of the supercapacitors and the wind generator converter controllers, dumping the voltage variations of the dc-link during these disturbances.

The use of these control theories is also proposed in [13]. This article deals with the SMES implementation in a system with fixed speed wind turbines equipped with pitch control. The SMES is connected to an ac cable through a six pulse PWM rectifier/inverter, using IGBTs and two quadrant dc-dc choppers. Both converters are linked by a dc-link capacitor. The effectiveness of pitch control and the SMES in the voltage stability of the system under persistent fault situations, caused by the inability of reclosure the circuits breakers of the system, is studied. The improvement of the voltage stability with SMES under LVRT situations is discussed also in [269].

Another C-PCS of SMES is presented in [167]. In this case results as a combination of series and parallel inverters. Their dc-links are connected to a two-quadrant dc-dc converter with a dc-link capacitor and a superconducting coil. While the series converter is responsible for regulating the voltage oscillations of the wind generator, the parallel converter simultaneously controls active and reactive power in order to damp the oscillations of the tie-line power flow. The dc bus voltage is properly maintained by controlling the superconducting coil.

As well as SMES and supercapacitors, batteries and flow batteries are also proposed for LVRT applications. For instance, in [308], a VRB is connected to a dc-link of a direct drive wind turbine driving a permanent magnet synchronous generator. The control of the dc-dc converter of the VRB enables an improved capability of the generator under LVRT situations.

2.3.3 Voltage control support

Wind generators, and especially squirrel cage induction generators, consume large amounts of reactive power. The control of the reactive power flow in an electrical network is crucial for maintaining proper levels of voltage in the system. Therefore, various technologies of wind generators have been

developed so far [29]. Wind turbines driving a DFIG or full power converters synchronous generators are ways to transfer all or a part of power generated to the network via power converters. With these topologies, the reactive power control of wind generators and hence the voltage control at their connection point is feasible. Also, with the inclusion of energy storage support, the dynamics of the voltage control can be improved.

Batteries, flow batteries, and short time scale energy storage like supercapacitors, flywheels and SMES, are well suited for this application, mainly because of their high enough ramp rates. Since the storage device must be able to manage both active and reactive power, the C-PCS of the storage device becomes essential. In this sense, FACTS/ESS systems are proposed to carry out this task properly, e.g. [282] proposes a Distribution Static Synchronous Compensator (DSTATCOM), coupled with a flywheel in order to mitigate voltage stability problems due to the introduction of wind generation in the electric system. Since the dc-link of the STATCOM is strengthened by the energy storage support, it can exchange both active and reactive power.

In [30], a STATCOM/BESS is connected to a wind self-excited induction generator, not only to manage reactive power, but also to compensate harmonic currents and load changes of an isolated system. As a result, the efficiency and the availability of the system are enhanced.

It is important to note that active power control features depend on the storage technology. In this sense, a SMES system presents very good characteristics for a fast injection or absorption of active power; e.g. [133] shows field test results of SMES, where a 16.6 ms response time in the step input of both active and reactive power can be seen.

2.3.4 Oscillation damping

The system stability against disturbances may be compromised with high penetration levels of wind power to the grid. For this reason, WPPs will be required in future Grid Codes for helping generators of an interconnected network not to lose synchronism against perturbations. Thus, WPPs will be required to mitigate these power oscillations of the system by absorbing or injecting active power at frequencies of 0.5 to 1 Hz [106].

Many storage technologies are suitable for this service. The time of injection / absorption of active power by the storage device is about one minute, therefore high ramp-up rates and response time are preferable. Thus, HESS, flow batteries, batteries, and short time scale energy storage like supercapacitors, flywheels and SMES are well suited for this application. System

stability aspects are usually dealt with by modal and frequency domain analysis. Flywheels are proposed to be included in the network in favor of better dynamic performance under disturbances [187, 323]. For instance, in [187], a general multimachine system is considered a study case in which a method for an optimal installing location of flywheel devices is performed in order to damp the low frequency power oscillations of the system.

The SMES system capacity to quickly manage large quantities of active and reactive power simultaneously is investigated in [188, 215, 225, 305]. WPPs with SMES are required to provide oscillation damping of power flows in an interconnected system in these studies. A frequency domain analysis, based on linearized system models using eigenvalue techniques, as well as time domain analysis, based on a more detailed non-linear system models under disturbance conditions, are proposed. These system disturbances may be caused by the disruption of local loads, wind gusts, fast wind fluctuations or short-circuits. Control techniques are a key aspect here. Since system uncertainties must be taken into account, e.g. various generating and loading conditions, parameter variations and non-linearities, the application of linear controllers is not always appropriate.

In this regard it is interesting to note the methods described in [215]. Here, a robust non-linear control of SMES is proposed, which bases its operation on the addition of a power disturbance in a wind-based network with oscillating power flow in order to reach a net constant power flow in the system. The consideration of uncertainties of the system in SMES control provides a much adequate behavior of its response.

Not only theoretical studies have been done, but also experimental tests, [89]. Here, the benefits of the inclusion of storage devices for improving the system stability are discussed. It is concluded that power oscillation damping control is more robust against variations of power system conditions in the case of managing active and reactive power by means of SMES and batteries actuation.

2.3.5 Spinning reserve

According to [244], spinning reserve is defined as the unused capacity that can be activated by the system operator's decision, and which is provided by synchronizing with the network devices capable of affecting the active power of the system. Since a secondary and tertiary reserve can be activated by the system operator's decision, they are regarded as spinning reserves. Therefore, according to the definition, WPPs are required to regulate their active power for up to 30 minutes, in order to provide a frequency support

to the system.

There are many storage technologies which are suitable for this application: flywheels, SMES, batteries, flow batteries, HESS, CAES or PHS installations. Batteries and flow batteries have been the subject of study in numerous publications for providing spinning reserve capability in WPPs.

The provision of spinning reserves plays a key role, especially in isolated systems [182, 199]. In this sense, BESS is proposed to be included in an isolated wind - hydro - gas system in [199]. The management, as well as the optimal size of batteries, are the main concerns of study in order to obtain the maximum economical benefit by the owner of the storage device while fulfilling the spinning reserve function. A numerical optimization problem is proposed in order to optimize the economical benefit, given by the difference between the revenues, due to the frequency control reserves availability and the storage energy sales income, and costs, due to maintenance and investments in storage technologies. The experience results of providing spinning reserve by a 6 MW - 6 MWh VRB in a 30.6 MW WPP are reported in [314]. In conclusion, it is important to remark that wind generator power oscillations for a period of 30 minutes are reduced by a factor of 3. The estimation of the battery charge state by means of cell voltage measurement favors the VRB operation.

Flow batteries in spinning reserve applications have been extensively reported in literature. In fact, short response times and the capacity of being overloaded make these system superbly well suited for this application, even having advantages over other conventional facilities, like fossil fuel power stations [259].

2.3.6 Load following

In this service, storage technologies are required to provide energy in the time frame of minutes to 10 hours [31]. Due to the stochastic nature of wind, the WPP output would not match the power demand. This leads to various technical and economic problems regarding the operation of the electrical system. Technical issues, like voltage and frequency variations due to imbalances between electricity generation and demand, limit the renewable technologies' penetration into the electrical network. Regarding economic issues, it should be remarked that some regulatory frameworks specify economic penalties to WPPs for not meeting generation bids, on account of wind forecasting errors. In this sense, the ESS can be used to store and inject electrical power for hours. Batteries, flow batteries, as well as HESS, CAES or PHS installations are well suited for this application.

Probably, a glaring example of the feasibility of combining wind with battery solutions is a wind power installation case in Futumata (Japan), where a 34 MW NaS battery bank is used to level the production of a 51 MW WPP [147]. Proper management of the energy of the battery is essential, not only regarding technical issues (e.g. shortage/surplus of the battery), but also from an economic point of view. In this sense, in [138], a control algorithm that optimizes the economic benefit of the system, minimizing the storage in peak-demand hours when the market price of the energy is high, is developed.

In this case, control and dimensioning aspects of flow batteries are discussed in [27, 28, 44]. As a conclusion of these works, it can be said that many techno-economic benefits for the electrical system derives from a proper solution of these aspects. Proper control of the batteries improves the predictability of WPPs and therefore, the associated costs for their grid integration regarding reserve requirements can be decreased, since great precision in matching their output with their forecast power is achieved. According to [44], 34 MW and 40 MWh of storage capacity are required to improve the forecast power output of a 100 MW wind plant (34% of the rated power of the plant) with a tolerance of 4%/pu, 90% of the time.

Techno-economic analyses are addressed in [59, 193, 283], regarding CAES use in load following applications. As an example, [283] presents a stochastic electricity market model in order to study the effects of high penetration of wind power in the electrical systems, as well as the economical viability of including CAES solutions. With system minimization costs as criteria, there is an optimization problem which takes into account aspects, such as transmission capabilities of the system, energy prices, technical characteristics of the generating plants, electricity demand profiles, investments costs and power reserve requirements. Important conclusions (taking into account the German electricity market), include an economic advantage of CAES to conventional peak thermal plants in a scenario with high penetration of wind power.

Finally, it is important to remark that hydrogen-based storage technologies are considered as one of the most promising technologies in load following applications. Actually, several demo projects have been developed as a proof of concept concerning stand-alone systems with wind, photovoltaic generation and hydrogen storage [7, 148, 186]. These projects focus on developing power management algorithms, using the excess of energy for creating hydrogen in an electrolyser and using it in a fuel cell in order to inject power to the system when required. The evaluation of the system operation shows the technical feasibility of such isolated schemes with hydrogen support.

2.3.7 Peak shaving

This service falls within the time frame of 1 hour to 10 hours. The operating strategy for the storage devices is to store cheap energy at off-peak demand periods (overnight), and to inject it into the network during periods of high electricity demand, and hence soften the typical mountain and valley shape of the load curve.

Well suited ESSs for peak shaving applications are batteries, flow batteries, CAES, HESS and PHS. Regarding the batteries, numerous techno-economic studies display the feasibility to store energy during off-peak demand hours and sell it at peak demand periods.

In [91, 252], the use of NaS batteries for this application is discussed. While technical benefits for the electrical system in a real case, as well as details referring to the design of the C-PCS of the battery, are presented in [252], an interesting techno-economic analysis of BESS is discussed in [91]. In conclusion, in order to define an available economic operation of BESS in the Spanish energy market, the sale price of the battery energy is fixed at 0.22 - 0.31 €/kWh (actually, the energy price is around 0.04 - 0.05 €/kWh). Therefore, it is concluded that BESS operators should receive subsidies, due to the emissions that would imply the use of conventional fuel plants for peak shaving applications, in order to make its use economically profitable.

The selling price of BESS energy is substantially lower than that of a RFC system. According to [38], in order to make a RFC economically viable to operate with a WPP, it would imply fixing its energy selling price at 1.71 €/kWh in the Spanish case, due to the low energy efficiency of the storage technology and the high cost of its components. Therefore, compared with the selling price of the energy injected by batteries, the selling price of the energy injected by hydrogen-based technology is around 5-8 times higher. This is one of the main challenges regarding the inclusion of hydrogen-based storage systems in the network.

Without a doubt, PHS is considered to be one of the most well suited storage systems in order to achieve high penetration levels of wind power in isolated systems. Indeed, wind-hydro systems have been studied, amongst other publications, in [47, 161, 227]. A techno-economic study of the viability of wind-hydro systems in providing power during peak load demand periods is performed in [161]. The results show an excellent technical and economic performance. It can be concluded that the integration of WPPs in the isolated study case can be increased by 9%, allowing to a penetration level of 20%. In addition, a significant reduction of CO_2 emissions through the use of PHS installations instead of using fuel peak power plants is highlighted in

[37]. However, regarding dynamic security issues of the system operation, it can be concluded that it may be appropriate to add some more technologies in order to provide spinning reserve to the system [47].

2.3.8 Transmission curtailment

In this application, storage technologies are required to provide energy in the time frame of 5 hours to 12 hours. Due to several reasons, such as the need for ensuring the stability of the electrical system or technical limitations in power transmission lines, WPPs have to be disconnected. In this sense, an ESS can store energy for hours and inject it in a controlled manner according to the capacity of transmission lines and stability issues, and thus, avoiding the disconnection of wind turbines. Well suited ESS for this application are flow batteries, CAES, hydrogen-based systems and PHS installations.

Studies regarding wind-hydro systems and CAES installations for transmission curtailment applications are considered by [17, 81, 92, 316]. In general, wind-based isolated systems or systems connected to weak grids are considered to display the most interesting scenarios. Findings agree with the idea of including ESS in highly renewable penetration systems with the aim of reducing wind curtailments, backup power, transmission losses, ensuring security of supply, saving update costs and avoiding the building of new transmission lines.

Finally, since hydrogen can be created by means of rejected wind power, hydrogen-based storage systems are considered a promising technology to be included in wind power applications. Once the hydrogen is stored, it can be used in different ways: either to generate electricity in fuel cells and inject it into the network during periods of peak power demand or for other uses, such as the field of mobility. As introduced to the previous section, the main challenges for the inclusion of hydrogen-based storage systems are related to the uncertainty of their economic viability (owing to the high system costs and its low energy efficiency) and the dependence of high hydrogen market prices [57, 122, 169, 191].

2.3.9 Time shifting

In time shifting services, storage technologies are required to provide energy in the time frame of 5 hours to 12 hours. In this case, ESS is required to absorb all the energy from WPPs during off-peak demand periods, supplemented with cheap power bought from the network if necessary, and selling it during peak-power demand periods, thus avoiding the activation or update

of other conventional peak power generation plants.

Flow batteries, CAES, PHS installations and hydrogen-based storage technologies are well suited for this application.

In [220], the effects on the operation of electrical networks considering bulk energy storage capacity and WPPs are discussed. In this sense, many operating strategies for wind-ESS are considered. One of the most interesting study cases is based on charging the storage device continuously for 12 hours period (low demand period) and injecting its power in a controlled manner during the following 12 hours (high demand period). As a conclusion, the fact is highlighted that time shifting services by means of ESS inclusion into the network are not economically viable without any kind of subsidy, due to high investments costs of the technologies (in this case, CAES systems is the most favorable technology) and relatively low energy efficiencies (depending on the technology). Regarding environmental aspects, ESS should be able to inject power during the entire high peak demand period, otherwise the operation of base load plants would be increased, with a consequent increase of CO_2 emissions.

2.3.10 Unit commitment

In unit commitment services, storage technologies are required to provide energy in the time-frame of hours to days. Due to the uncertainties regarding mesoscale variations of the wind, it is hard to manage the commitment of wind turbines in order to meet the estimated demand at all times. Also, the introduction of WPPs into electrical systems motivates the need to maintain a certain level of energy reserves in order to compensate forecast errors. Therefore, the introduction of high capability ESS into the network may be useful to fight the effects of uncertainties in wind forecasting and to reduce system energy reserves during its normal operation. Large scale ESSs are suitable for this application: CAES and PHS installations, as well as hydrogen-based storage technologies.

This topic is addressed as a numerical optimization problem, in which the objective function is to minimize the operation costs of the electrical network, so as to maximize the return of the investments in including ESS [47, 72]. For instance, in [72], the unit commitment problem is formulated in a power system with wind generation and CAES. The benefits of including CAES solutions, in order to reduce the operation costs of the electrical network by means of allowing the use of wind energy in charging this storage technology when the energy is not required by the system, and thus avoiding the disconnection of the wind turbines, are discussed.

2.3.11 Seasonal storage

In this application, ESSs capable of storing and injecting energy during periods in the time frame of months are well suited. Storing energy for long periods of time can be useful in systems with large seasonal variations in the level of generation or consumption. Clearly, only those storage technologies with a very large energy capacity and no self-discharge are eligible, such as large PHS installations or hydrogen-based solutions.

In cases where it can be technically interesting to include seasonal storage, and taking into account the investment costs regarding the installation of wind turbines and storage systems based on hydrogen, it may look favorable to oversize WPPs in order to reduce the size of the storage reserves [169]. However, this would increase the non-utilized wind power capacity range and hence decrease the efficiency of the system. On the other hand, the energy costs of the system would be reduced.

A demo project regarding seasonal storage by means of hydrogen-based storage technologies in a stand-alone system is described in [186]. It must be noted, that although storing energy during long periods of time is technically feasible due to no leaks in the hydrogen storage tank, the use of the RFC must be limited, in order just to store the excess productions of wind power, in favor of minimizing the losses of the system, since the energy efficiency of RFCs is very low.

2.4 Chapter remarks

In this chapter, the operating principles as well as the main characteristics of several storage technologies suitable for stationary applications have been described. In addition, a summary of potential ESS applications in wind power have been defined and discussed according to an extensive literature review. In conclusion, it is worth pointing out that several benefits for the operation of the power system considering WPPs as well as some considerations can be achieved:

- High power ramp rates of some systems such as SMES, flywheels or supercapacitors allow their use for power smoothing of wind turbines, favoring the mitigation of the voltage and frequency variations at the connection point of the WPP.

- Regarding the use of short time-scale storage technologies, their optimal location in the wind plant and sizing have to be addressed in

order to ensure their proper operation. In addition, since the C-PCS of the ESS have to interact with the power converters of wind turbines in most of the cases, the topology of the wind plant, as well as the wind turbine types and control strategies play a key role in the system operation and design.

- Other aspects related with the system stability under perturbations, like oscillation damping issues and LVRT capability, become clearly improved with energy storage support. These capabilities take on a key role from their incorporation into Grid Codes. Once more, energy technologies with high ramp rates are required.

- The technical feasibility of isolated and hybrid systems with high penetration rates of wind power becomes significantly improved since the predictability of WPPs with ESS is increased. Also, a continuous power supply for the loads of such systems can be ensured.

- The predictability improvement of the output of WPPs with an ESS not only involves technical benefits that favor the incorporation of wind power in the network, but also economic benefits owing to penalty reductions in forecasting errors. In addition, operation costs of the power system can be reduced due to the reduced power reserve requirements of the system.

- The installation of ESS strongly depends on the economic viability of the project. In this sense, although hydrogen-based storage technologies have a great potential for long term storage applications, the main challenges for their inclusion are related to the uncertainty of their economic viability (due to high system costs and low energy efficiency) and the dependence on high hydrogen market prices.

- A proper control strategy by the system operator is necessary in order to ensure the correctness in the utilization of long term storage technologies. In addition, it is found that ESS operators should receive subsidies according to the emissions that would imply the use of conventional fuel plants for peak shaving applications, in order to make their use economically profitable.

- Nowadays, there is a tremendous effort in improving the capabilities and efficiencies of the available storage technologies, as well as reducing their capital costs. The aim of this research is to make ESS

economically suitable for the use in stationary applications and, therefore, allow higher penetration ratios of renewable energies in the power system.

3

Modeling, control and experimental validation of the flywheel test bench

Summary.- This chapter deals with the modeling, control and experimental validation of a flywheel test bench which is part of IREC's lab-scale microgrid. The system is based on a low-speed rotating disk mechanically coupled to a Permanent Magnet Synchronous Machine (PMSM). The electrical power is exchanged with the external grid by means of a set of back-to-back power converters. These power electronics control the speed of the machine, and thus the active power absorbed or injected by the device, and also regulate the reactive power at the point of common coupling with the external grid. Vector control techniques are used for designing the converter controllers: a field oriented vector control algorithm is implemented for governing the servomotor while an instantaneous power theory-based algorithm is used to manage the active and reactive currents flowing from the grid side converter. The control implementation in the experimental setup has been carried out by means of programming Digital Signal Processors (DSP's). The modeling and control system design has been validated after executing several experiments. Other characteristics such as the torque losses of the system as well as the system performance concerning energy rating, power rating and energy efficiency characteristics are determined experimentally.

3.1 Introduction

The most used technologies for flywheel systems are permanent magnet, induction and synchronous reluctance machine types. Control theory of electrical drives plays a key role in flywheel-related studies. Some examples are found in the literature mainly concerning flywheel-based induction machines, i.e. field oriented vector control [63], V/f control [279], and sensorless vector control [43, 54, 55], where results were experimentally validated.

In the present chapter, a field oriented vector control algorithm [171, 288, 19] is implemented for governing, in this case, a flywheel-based Permanent Magnet Synchronous Machine (PMSM). The study is focused on the modeling of the storage device, its control design and its experimental validation with field data. This is the main contribution of the chapter. Also, the performance of the storage device regarding power and energy capacity as well as energy efficiency is experimentally determined.

The storage device is based on a rotating disk mechanically coupled to a PMSM. It is a low-speed system type since the rated speed is 3000 rpm. Electrical power is exchanged with the external grid by means of a set of a back-to-back power converters. Figure 3.1 presents the topology of the ESS.

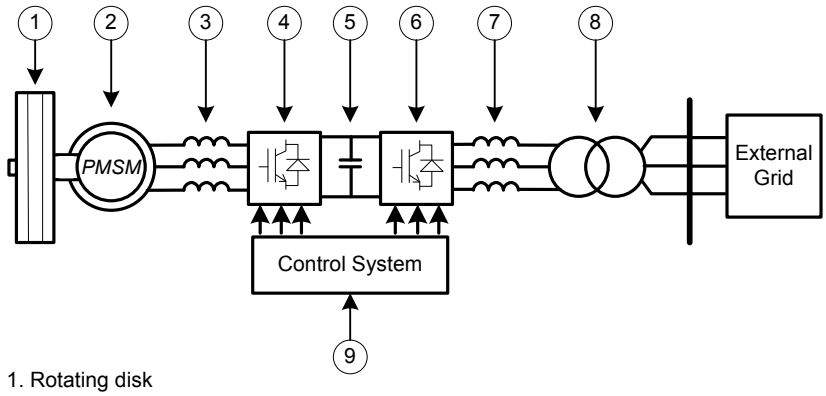

Figure 3.1: System topology

This chapter has been structured as follows: in Section 3.2, the IREC's

microgrid is shortly presented; in Section 3.3, the system modeling is introduced; in Section 3.4, the control methods description and design are explained; Section 3.5 presents detailed data of the experimental setup, the determination procedures of the torque losses of the system as well as experimental results for the modeling of the system and its control validation; Section 3.6 deals with the determination of the energy rating, power rating and energy efficiency characteristics of the system; finally, in Section 3.7, the conclusions of the chapter are presented.

3.2 IREC's microgrid and flywheel device

The flywheel-based storage device is integrated in IREC's microgrid. As shown in Figure 3.2, IREC's microgrid is a flexible system that includes emulated devices, semi-emulated devices, real power systems, electric vehicle fast chargers and header elements. Emulated devices comprise several cabinets that emulate generators, loads or storage devices by adjusting the consumption or absorption time-dependent reference curves of their power electronic converters. The units are managed and controlled by energy efficient algorithms, and measurement systems provide real time supervision and regulation. Test benches that emulate wind turbine generators of different technologies comprise semi-emulated devices. These test benches emulate wind turbines driving a permanent magnet synchronous generator, a doubly feed induction generator and a squirrel cage induction generator. Each test bench comprises an electric motor driven by a frequency regulator, mechanically coupled to the shaft of the generator. This motor acts as a wind turbine, i.e., its velocity is regulated to emulate the effect of the power captured by the blades of the turbine on the shaft of the generator. The setting up of some of these test benches are still in progress.

The real power systems comprise a micro wind turbine, a solar panel and storage devices as ultracapacitors, a lithium battery and a flywheel. Controllable power electronics and measured systems are included. Finally, the microgrid includes three electric vehicle fast chargers and the so-called headers elements, which permits us to emulate different grid characteristics, faults, disturbances and so on. Rated power of the microgrid is 200 kW. The energy management of the microgrid is carried out by communication systems with IEC 61850 standard. All these equipments permits us to study different aspects related to the management, design and integration into the grid of microgrids, wind power installations and ESSs. More details about IREC's microgrid can be found in [66, 254, 98, 121].

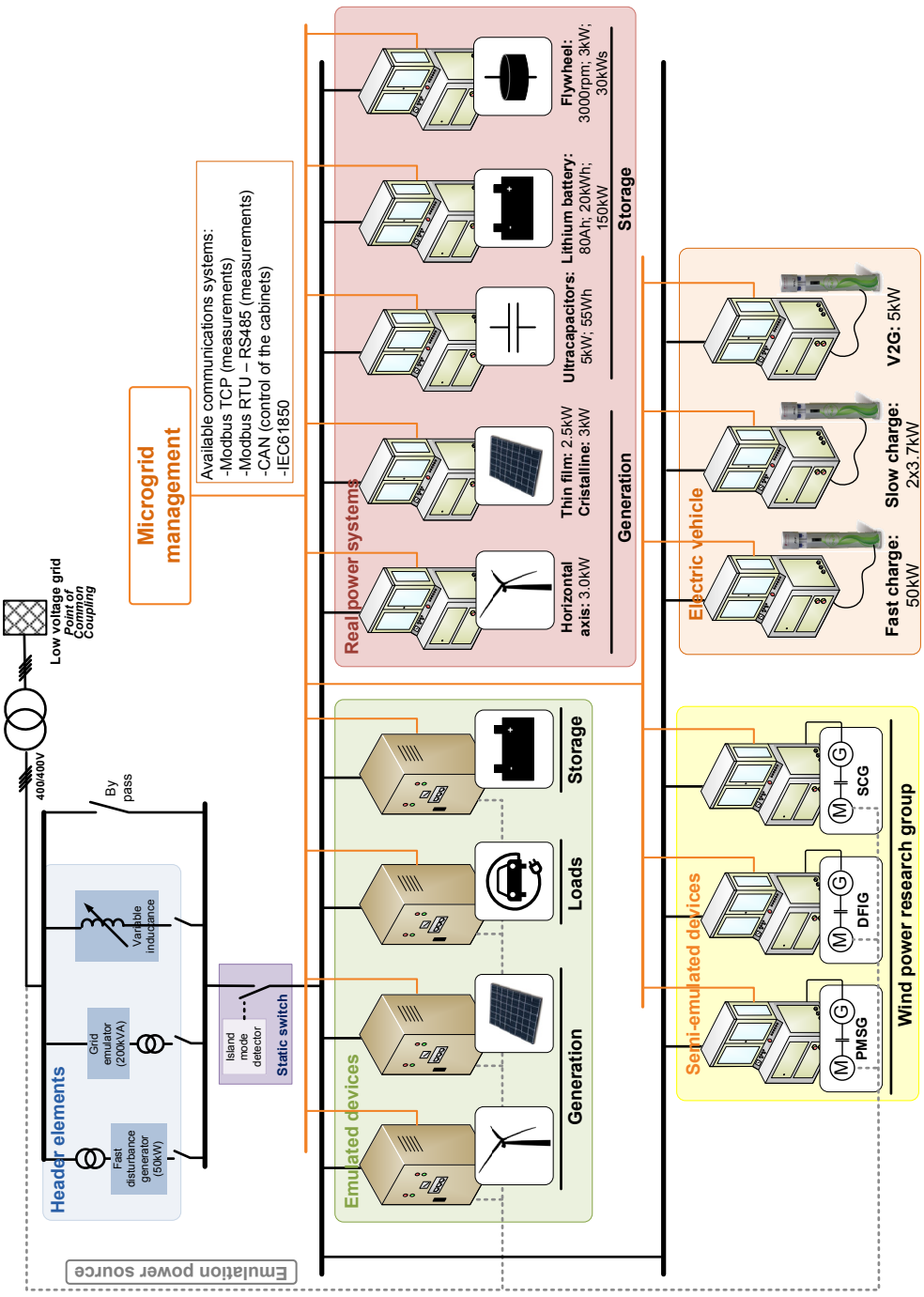

Figure 3.2: IREC's microgrid

3.3 System modeling

The following Sections deal with the modeling of both the electrical machine and the power electronics of the flywheel.

3.3.1 PMSM and rotating disk modeling

Since the mechanical coupling between the electrical machine and the rotating disk does not include a gear box, the whole system can be modelled as a single mass system.

To describe the machine equations it is common practice not to use instantaneous values leading to a three-dimensional problem in the *abc* coordinate system, but to transform all value into a rotating reference frame. This transformation is called $qd0$ or Park's transformation [171]. Accordingly, voltage equations of the PM machine in the rotor reference frame are presented as follows (stator currents are shown in motor orientation, and all magnitudes are expressed in SI units,)

$$u_{sq} = R_s i_{sq} + L_q \frac{d}{dt} i_{sq} + \omega_r L_d i_{sd} + \omega_r \psi_{PM} \tag{3.1}$$

$$u_{sd} = R_s i_{sd} + L_d \frac{d}{dt} i_{sd} - \omega_r L_q i_{sq} \tag{3.2}$$

$$u_{0s} = R_s i_{0s} + L_{ls} \frac{d}{dt} i_{s0} \tag{3.3}$$

where u_{sqd0} and i_{sqd0} are the stator voltages and currents; $L_q = L_{ls} + L_{mq}$, $L_d = L_{ls} + L_{md}$ and ψ_{PM} is the flux generated by the permanent magnets; R_s is the stator resistance and ω_r is the electrical frequency (the mechanical speed ω_m results dividing ω_r by the pole pairs of the machine).

Since a surface mounted permanent magnet machine is considered, and according to the data provided by the manufacturer of the permanent magnet machine object of study in this chapter [69], there is no significant internal asymmetry in the iron parts of the rotor, so direct-axis and quadrature-axis inductances of the machine are approximately equal, $L_d \approx L_q$. Accordingly, the electrical torque can be expressed as follows,

$$T_e = \left(\frac{3}{2}\right)\left(\frac{p}{2}\right)\psi_{PM} i_{sq} \tag{3.4}$$

The modeling is completed by means of including the equation of motion of the electromechanical system composed by the electrical machine and the rotating disk.

$$\frac{d\omega_r}{dt} = \frac{p}{2}\frac{T_e - T_l}{J} \tag{3.5}$$

where T_l is the torque losses of the system, which is mainly due to the friction in the bearings, and presents a speed-dependent profile,

$$T_l = k_1 \cdot \omega_m + k_2 \tag{3.6}$$

3.3.2 Power converters modeling

The FESS power converters are in a back-to-back configuration. These electronic power converters are modeled as six force-commutated IGBT power switches connected in a bridge configuration. In addition, series inductances are included at the AC terminals of both the grid side converter and the rotor side converter. The topology of the system is detailed in Figure 3.3.

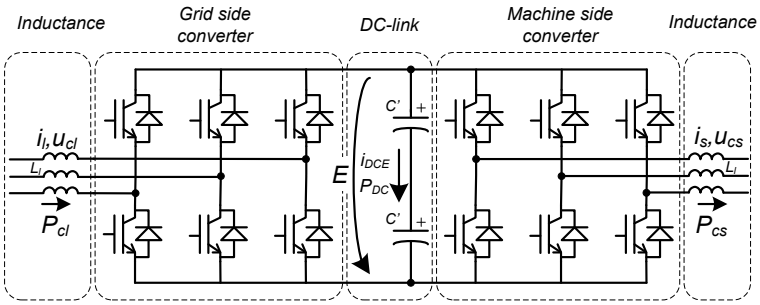

Figure 3.3: Set of back-to-back power converters

The mathematical modeling of the grid side converter circuit, the dc-link, and the machine side converter circuit are presented in the following sections.

Grid side converter circuit

Figure 3.4 shows the electrical connection between the grid side converter and the coupling transformer. As illustrated, an inductive filter is included between these two elements.

Voltage equations of the electrical circuit presented in Figure 3.4, expressed in a synchronous $qd0$ reference with the grid frequency, take the form of,

$$u_{lq} - u_{clq} = r_l i_{lq} + L_l \frac{d}{dt} i_{lq} + \omega_l L_l i_{ld} \tag{3.7}$$

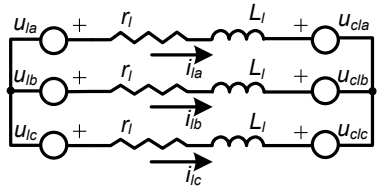

Figure 3.4: Grid side converter circuit modeling

$$u_{ld} - u_{cld} = r_l i_{ld} + L_l \frac{d}{dt} i_{ld} - \omega_l L_l i_{lq} \tag{3.8}$$

DC-link modeling

According to Figure 3.3, the DC-link power balance gives the following expression,

$$P_{cl} - P_{cs} = P_{DC} \tag{3.9}$$

where P_{cl} is the power extracted from the network, P_{cs} is the power consumed by the electrical machine, and therefore, P_{DC} is the power consumed by the DC-link capacitors. These magnitudes, as shown by the following equations, can be expressed in terms of the AC currents and voltages, and the DC-link voltage,

$$P_{cl} = \left(\frac{3}{2}\right)(u_{cld} i_{cld} + u_{clq} i_{clq}) \tag{3.10}$$

$$P_{cs} = \left(\frac{3}{2}\right)(u_{csd} i_{csd} + u_{csq} i_{csq}) \tag{3.11}$$

$$P_{DC} = \frac{1}{2} C \frac{d}{dt} E^2 \tag{3.12}$$

The time dependent value of the DC bus voltage $E(t)$ is computed as,

$$E(t) = E_0 + \frac{1}{C} \int_0^t (i_{DCcl} - i_{DCm}) \mathrm{d}t \tag{3.13}$$

where E_0 is the DC bus voltage at time $t = 0$; C is the total capacitance value; i_{DCcl} is the injected current from the grid side converter; and i_{DCm} is the injected current to the machine side converter circuit.

Machine side converter circuit

As in the case of the grid side converter, an inductive filter is included in the machine side converter output. Its aim is to filter the harmonic components of the currents flowing into the servomotor. Considering the converter as three ideal voltage sources, the equivalent electric circuit of the machine side converter circuit is presented in Figure 3.5.

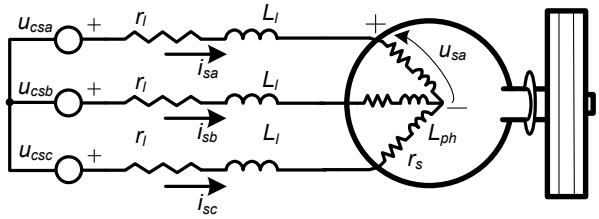

Figure 3.5: Machine side converter circuit

In a synchronous $qd0$ reference with the electrical frequency of the servomotor, the mathematical modeling of the system presented in Figure 3.5, take the form of,

$$u_{csq} - u_{sq} = r_l i_{sq} + L_l \frac{d}{dt} i_{sq} + \omega_r L_l i_{sd} \tag{3.14}$$

$$u_{csd} - u_{sd} = r_l i_{sd} + L_l \frac{d}{dt} i_{sd} - \omega_r L_l i_{sq} \tag{3.15}$$

Substituting (3.1)-(3.2) in (3.14)-(3.15), results,

$$u_{csq} = (r_l + r_s) i_{sq} + (L_l + L_q) \frac{d}{dt} i_{sq} + \omega_r (L_l + L_d) i_{sd} + \omega_r \psi_{PM} \tag{3.16}$$

$$u_{csd} = (r_l + r_s) i_{sd} + (L_l + L_d) \frac{d}{dt} i_{sd} - \omega_r (L_l + L_q) i_{sq} \tag{3.17}$$

3.4 Control system design

3.4.1 Machine side converter controller

Figure 3.6 shows the control system scheme. This section presents the methods used for designing the machine side converter controller.

The machine side converter controller is based on the current vector control algorithm of the PM machine [171, 288, 277]. Its main objective is to

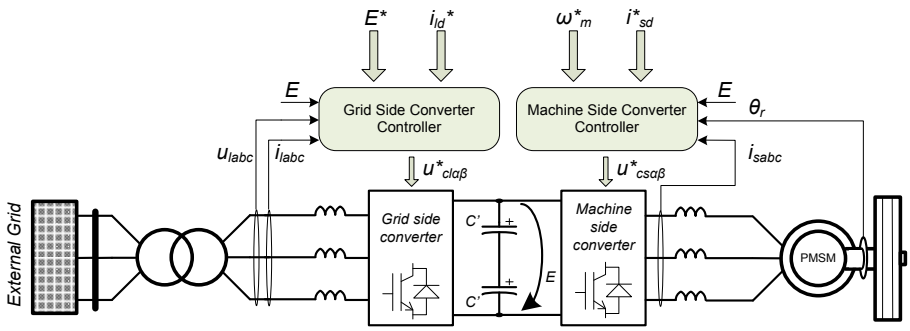

Figure 3.6: Control scheme of the energy storage system

control the speed of the servomotor and the reactive currents flowing from the stator of the machine. According to equation (3.4), the electromagnetic torque produced by the machine is only dependent on the quadrature-axis stator current. Thus, the direct-axis current i_{sd}, i.e. reactive current, does not have any effect on the torque.

Usually, for speeds below the rated speed of the machine, i^*_{sd} is set to zero. This type of control is possible for machines where inductances present relatively small values and the armature reaction is almost insignificant. However, when speed exceeds its rated value, it is necessary to set $i^*_{sd} \neq 0$: it is necessary to apply the principle of flux weakening control in order not to exceed the rated voltage of the machine [55, 172].

In summary, the control scheme of the machine side converter is presented in Figure 3.7.

As shown, the measured signals needed for the control algorithm are the alternating currents flowing from the converter i_{sabc}, the rotor angle θ_r, and the dc-link voltage E. Setpoint signals are the speed of the servomotor ω^*_m and the direct-axis stator current component i^*_{sd}. The outputs of the algorithm are the voltage setpoints for the converter expressed in a stationary frame $u^*_{cs\alpha\beta}$.

The three-phase alternating voltages of the voltage source converter that drives the machine are obtained by means of Space Vector Pulse Width Modulation (SVPWM) techniques [171] from the mentioned voltage setpoints $u^*_{cs\alpha\beta}$. It is a common practice in back-to-back VSC-based power converters to use this modulation technique. The main advantages of SVPWM technique are the low harmonic content of the output voltage waveform of the converter (much lower than in other modulation techniques such as PWM and histeresis modulation [171]), and the ease of implementation in DSPs.

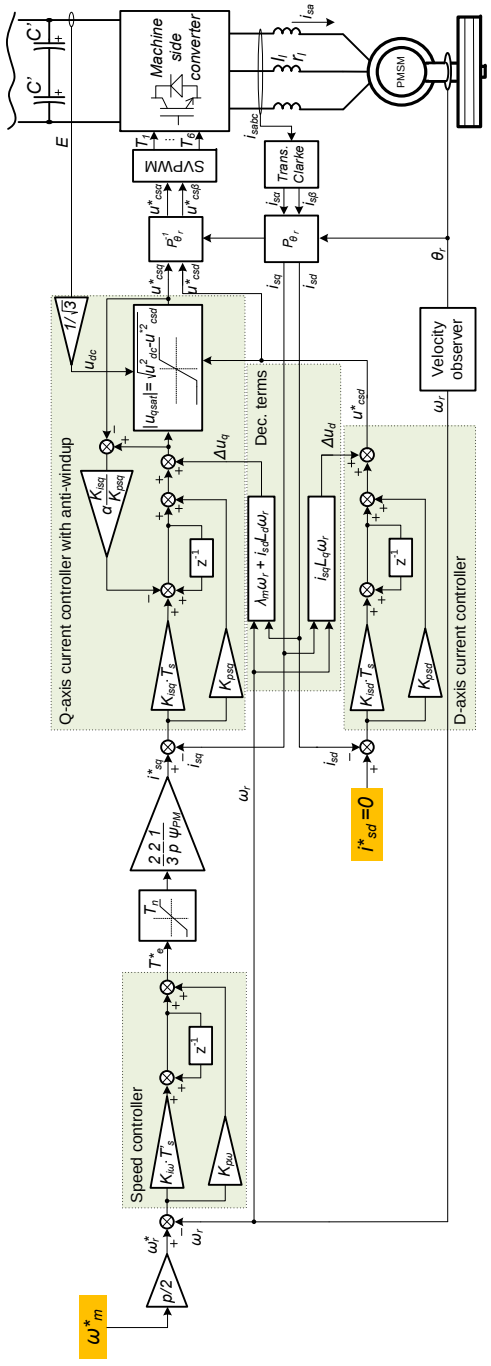

Figure 3.7: Machine side converter control scheme

The voltage references $u^*_{cs\alpha\beta}$ for the converter, are obtained by applying current control loops using linear controllers. Following sections deal with the tuning of these linear controllers.

Current control of the PMSM

According to the equations (3.16) and (3.17), the quadrature-axis component of the stator voltage u_{sq} depends on the direct-axis component of the stator current i_{sd}. In like manner, the direct-axis component of the voltage u_{sd} depends on the quadrature-axis current component i_{sq}. In order to obtain a decoupled linear system, the following restructuring is proposed,

$$u_{csq} = \hat{u}_{csq} + \underbrace{\omega_r(L_l + L_d)i_{sd} + \omega_r\psi_{PM}}_{\Delta u_q} \tag{3.18}$$

$$u_{csd} = \hat{u}_{csd} - \underbrace{\omega_r(L_l + L_q)i_{sq}}_{\Delta u_d} \tag{3.19}$$

where $\hat{u}_{csq}$ and $\hat{u}_{csd}$ describe a decoupled linear system, $G(s)$, in which, applying the Laplace transformation, takes the following form,

$$i_{sqd} = \underbrace{\begin{pmatrix} \frac{1}{(r_l+r_s)+(L_l+L_q)s} & 0 \\ 0 & \frac{1}{(r_l+r_s)+(L_l+L_d)s} \end{pmatrix}}_{G(s)} \hat{u}_{csqd} \tag{3.20}$$

Now, the addition of the decoupling terms Δu_q and Δu_d to $\hat{u}_{csq}$ and $\hat{u}_{csd}$ respectively complete the computation of u_{csq} and u_{csd}. Since $G(s)$ describes a linear system, a PI controller is proposed in order to control the stator currents of the servomotor.

The direct synthesis method is used for designing this controller [18]. This method consists on defining a controler $C(s)$, which transfer function is specified according to the desired closed-loop transfer function of the system, $M(s)$. Figure 3.8 shows the block diagram control methodology.

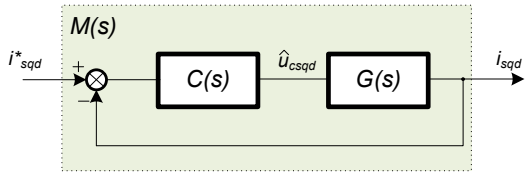

Figure 3.8: Block diagram control methodology for the stator currents

The desired closed-loop transfer function of the system $M(s)$ is a first-order type dependent on a parameter λ_s,

$$M(s) = \frac{1}{1 + \lambda_s s} \tag{3.21}$$

Then, for instance, the quadrature-axis current controller $C(s)$, results as a PI controller as derived in the following expression,

$$C(s) = \frac{M(s)}{G_{11}(s)(1 - M(s))} = \frac{(L_l + L_q)}{\lambda_s} + \frac{(r_l + r_s)}{\lambda_s s} = K_{psq} + \frac{K_{isq}}{s} \tag{3.22}$$

where $G_{11}(s)$ is the one-one component of the matrix $G(s)$. Thus, the proportional and integral parameters of the controller are,

$$K_{psq} = \frac{(L_l + L_q)}{\lambda_s} \tag{3.23}$$

$$K_{isq} = \frac{(r_l + r_s)}{\lambda_s} \tag{3.24}$$

As shown, the direct synthesis method is based on the exact cancellation of the poles of the transfer function of the plant $G(s)$ by the proper location of the zero of the PI controller for both the q and d axis. For the knowledge of the poles of the plant it is required to know the inductances and resistances of the system. The uncertainty in these magnitudes reduces the robustness of the designed controller. Therefore, the response of the system would be affected according to the magnitude of the error made in the determination of the system parameters. However, it is important to note that if the location of the zero of the PI controller of, for instance, the q-axis, do not exactly matches the pole of the plant $G_{11}(s)$, the resultant of the product of the transfer functions of the PI and $G_{11}(s)$ would lead a second order function. Thus, the stability of the system would be ensured as far as the gain of the controller is not excessive. Moreover, it is worth noting that the effects of these slightly incorrect location of the zeros of the controller are mitigated by the considered feed-forward decoupling terms Δu_q and Δu_d.

According to Figure 3.7, the q-axis current controller is equipped with an anti-windup scheme. The following lines describe the aim of this component. Although the peak value of the stator voltage is limited by the converter itself, a variable dc-link voltage can lead to instabilities in the machine side converter controller. For instance, in the event of dramatic dc-link voltage drop, the voltage obtained from the converter could be not high enough

for maintaining the desired speed of the machine and, thus, the controller integrator could fall into an over-saturated state. After a sudden recovery of the dc-link voltage, and due to the over-saturated state of the controller, the servomotor will accelerate uncontrollably. In order to avoid this over-saturation of the integrator and thus maintain the system in a controlled state during these situations, the q-axis PI current controller is equipped with an anti-windup.

Considering SVPWM techniques, the peak value for the alternating voltages that can be obtained in a range of linear modulation is achieved with a modulus equal to the radius of the largest circle that can be circumscribed within the boundaries of the hexagon built by the 6 possible states for the transistors of the power converter. Thus, the peak value of the fundamental component of the line-to-neutral voltage that can be produced is $|u_{ref}| \leq E/\sqrt{3}$. The outer circle to the hexagon can be achieved by over-modulation.

Accordingly, the saturation value for the q-axis voltage reference u^*_{csq} results as,

$$|u^{sat}_{csq}| = \sqrt{\left(\frac{E}{\sqrt{3}}\right)^2 - (u^*_{csd})^2} \tag{3.25}$$

When u^*_{csq} reaches the value of u^{sat}_{csq}, the controller output u^*_{csq} is saturated and the integrator input is computed by the error signal e multiplied by a gain, where $e = u^*_{csq} - u^{sat}_{csq}$. The gain is determined by the expression $\alpha K_{psq}/K_{isq}$.

Speed control of the PMSM

The speed control is accomplished by adjusting the torque of the servomotor. Thus, the speed controller provides the torque reference, which is proportional to the q-axis stator current i_{sq}, according to the equation (3.4). In this way, the speed control output feeds a cascaded current regulated field oriented drive, creating electromagnetic torque of the motor (see Figure 3.7). An ideal orientation of the $qd0$ reference with the magnetic flux created by the magnets of the rotor, and a current controller bandwidth much beyond required motion control bandwidth are assumed.

The accelerating torque of the servomotor is related with the torque losses and the rotating speed, as explained in equation (3.5). The expression of this equation in the Laplace domain yields to,

$$T_e^* - T_l = \frac{2Js}{p}\omega_r \tag{3.26}$$

Accordingly, the block diagram control loop for the rotating speed is presented in Figure 3.9.

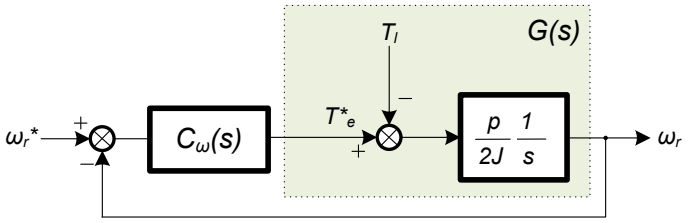

Figure 3.9: Rotating speed control scheme

If T_l equals to zero, the controller $C_\omega(s)$ could be made simply by a gain proportional to the error $e = \omega_r^* - \omega_r$, in order not to obtain a steady state error in response to a step-profiled speed reference ω_r^* since the open loop transmittance $C_\omega(s)G(s)$ contains a pure integrator,

$$C_\omega(s)G(s) = K_{p\omega}\frac{p}{2Js} \tag{3.27}$$

However, since T_l is not negligible, the speed regulator should contain an integral part in order to obtain a zero steady state error. Notwithstanding that, in the current study case a proportional controller is considered. Although, the controller output, i.e. the torque reference, is limited.

The closed loop transfer function of ω_r/ω_r^* results as follows,

$$\frac{\omega_r}{\omega_r^*} = \frac{C_\omega(s)G(s)}{C_\omega(s)G(s)+1} = \frac{\frac{K_{p\omega}p}{2Js}}{\frac{K_{p\omega}p}{2Js}+1} = \frac{1}{\frac{2J}{K_{p\omega}p}s+1} \tag{3.28}$$

which is a first-order transfer function,

$$\frac{\omega_r}{\omega_r^*} = \frac{1}{\lambda_\omega s+1} \tag{3.29}$$

Thus, the proportional parameter of the controller results as,

$$K_{p\omega} = \frac{2J}{p\lambda_\omega} \tag{3.30}$$

where λ_ω is a time constant response.

3.4.2 Grid side converter controller

The grid side converter controller is responsible for maintaining the DC bus voltage to a constant referenced value. In addition, this controller is in charge of regulating the injected or absorbed reactive power to or from the external grid. An instantaneous power theory-based algorithm [10, 159, 86, 119] is used to control these magnitudes. The control scheme of the grid side converter is presented in Figure 3.10.

As shown, the measured signals needed for the control algorithm are the alternating currents flowing from the converter i_{labc}, the alternating voltages at low-voltage side of the coupling transformer, u_{labc}, and the dc-link voltage E. Setpoint signals are the desired dc-link voltage E^* and the direct-axis current component flowing from the converter i_{ld}^*. The outputs of the algorithm are the voltage setpoints for the converter expressed in a stationary frame $u_{cl\alpha\beta}^*$.

Current control loop

According to the equations (3.7) and (3.8), the quadrature-axis component of the grid side converter voltage u_{clq} depends on the direct-axis component of the current flowing to the grid i_{ld}. In like manner, the direct-axis component of the voltage u_{cld} depends on the quadrature-axis current component i_{lq}. In order to obtain a decoupled linear system, the following restructuring (analogue to the case of the machine side converter controller) is proposed,

$$u_{clq} = -\hat{u}_{clq} + \underbrace{u_{lq} - \omega_l L_l i_{ld}}_{\Delta u_q} \tag{3.31}$$

$$u_{cld} = -\hat{u}_{cld} + \underbrace{\omega_l L_l i_{lq}}_{\Delta u_d} \tag{3.32}$$

where $\hat{u}_{clq}$ and $\hat{u}_{cld}$ perform a decoupled first-order type system $G(s)$, which expressed in Laplace domain takes the following form,

$$i_{lqd} = \underbrace{\begin{pmatrix} \frac{1}{r_l + L_l s} & 0 \\ 0 & \frac{1}{r_l + L_l s} \end{pmatrix}}_{G(s)} \hat{u}_{clqd} \tag{3.33}$$

The addition of the decoupling terms Δu_q and Δu_d to $\hat{u}_{clq}$ and $\hat{u}_{cld}$ respectively completes the computation of u_{clq} and u_{cld}. Since $G(s)$ describes

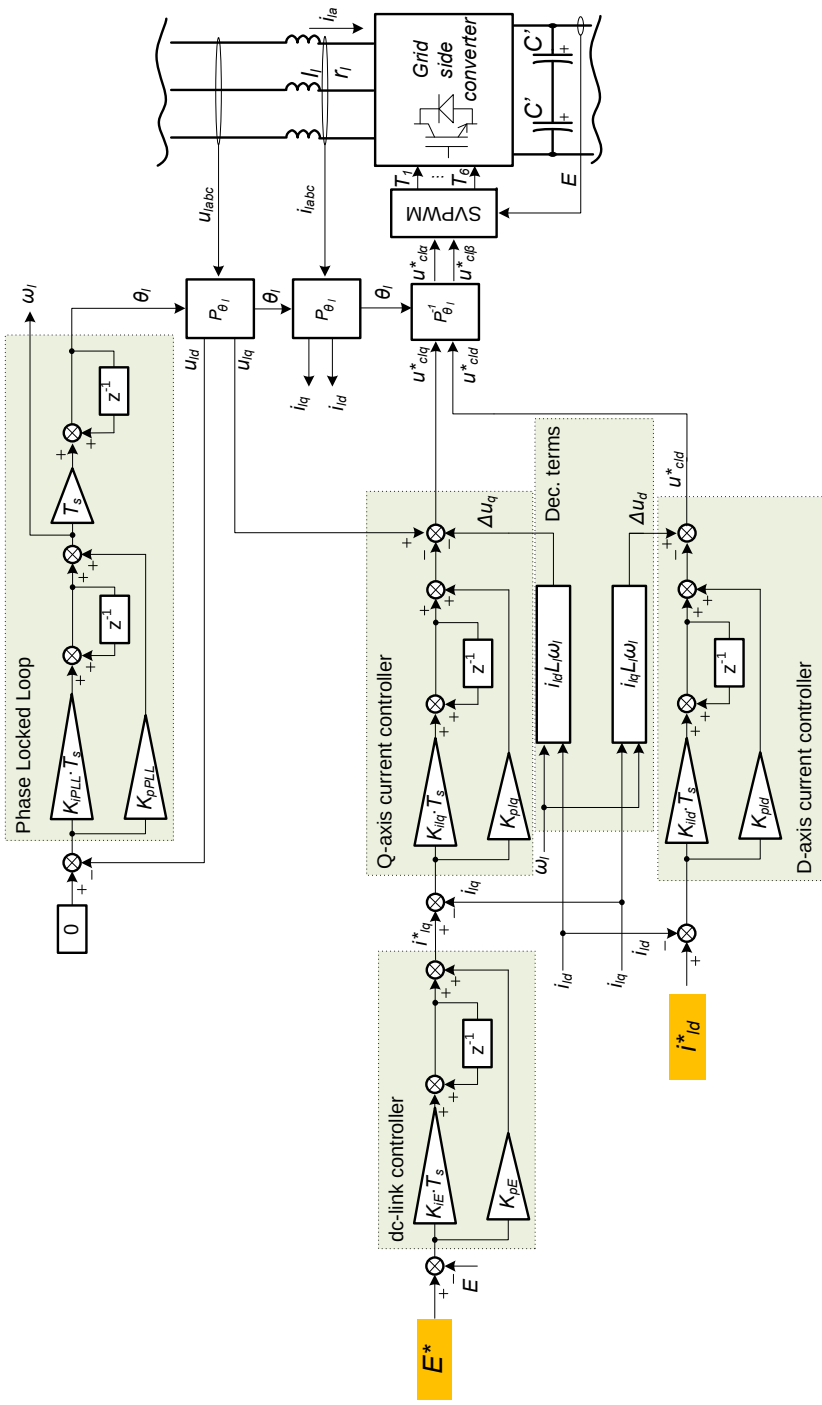

Figure 3.10: Grid side converter controller

a first-order type system, a linear controller is proposed in order to regulate the currents flowing from the grid side converter. By means of using the direct synthesis method [18], the linear controller $C(s)$ is designed in the following lines. Its transfer function is determined so that the desired closed-loop transfer function of the system, $M(s)$, is accomplished. The desired closed-loop transfer function of the system $M(s)$ is a first-order type dependent on a parameter λ_l,

$$M(s) = \frac{1}{1 + \lambda_l s} \tag{3.34}$$

The parameters for the q-axis current controller are determined using an analogous procedure to that detailed in equation (3.22),

$$K_{plq} = \frac{L_l}{\lambda_l} \tag{3.35}$$

$$K_{ilq} = \frac{r_l}{\lambda_l} \tag{3.36}$$

DC-link voltage controller

The input of this controller is the desired DC voltage level E^*. The output provides the q-axis current reference i_{lq}^* for the inner current control loop. The dc-link voltage controller design is carried out with the following hypothesis: i) a large enough dc-link capacitor is considered so that the dynamics of the dc voltage are much more slower than the dynamics of the inner current control loop; ii) the inner current control loop is considered fast enough so that the converter can be seen as an ideal three-phase current source; iii) the power converter performs a perfect ac-dc voltage conversion, with no power losses.

According to Figure 3.3, and taking into account both the above-named assumption iii) and a $qd0$ reference orientation in such a way the direct-axis component of the grid side converter voltage u_{cld} is set to zero, the dc current coming from the grid can be expressed as,

$$i_{DCcl} = \frac{3}{2}\frac{u_{clq} i_{lq}}{E} \tag{3.37}$$

where, considering $k = E/u_{clq}$ as a constant value, results,

$$i_{DCcl} = \frac{3k}{2} i_{lq} \tag{3.38}$$

Therefore, a linear relationship between the dc-bus current i_{DCcl} and the q-axis component of the grid side converter current i_{lq} is derived. In turn, the dc-link voltage is related to dc bus currents i_{DCcl} and i_{DCm} by means of the equation (3.13). That is how the control scheme of Figure 3.11 is obtained.

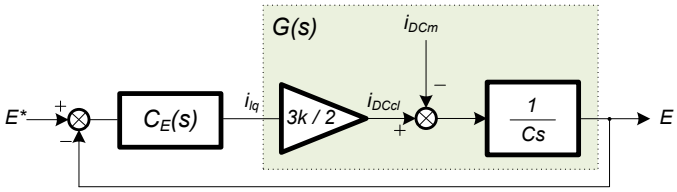

Figure 3.11: DC-link voltage control scheme

Since i_{DCm} is normally different to zero, a proportional integral type controller is required in order to obtain a zero steady state error. Accordingly, the closed loop transfer function E/E^* results as follows,

$$\frac{E}{E^*} = \frac{C_E(s)G(s)}{1 + C_E(s)G(s)} = \frac{\frac{3kK_{pE}}{2C}s + \frac{3kK_{iE}}{2C}}{s^2 + \frac{3kK_{pE}}{2C}s + \frac{3kK_{iE}}{2C}} \tag{3.39}$$

which is equivalent to the following expression,

$$\frac{E}{E^*} = \frac{2\xi_E\omega_E s + \omega_E^2}{s^2 + 2\xi_E\omega_E s + \omega_E^2} \tag{3.40}$$

Lastly, the parameters of the linear controller are,

$$K_{pE} = \frac{4C\xi_E\omega_E}{3k} \tag{3.41}$$

$$K_{iE} = \frac{2C\omega_E^2}{3k} \tag{3.42}$$

3.5 Testing of the experimental setup and model validation

This section deals with the testing of the experimental setup and the validation of its modeling in the software Matlab Simulink. The chapter is divided in three main sections. In Section 3.5.1 the characteristic parameters as well as the torque losses of the system are detailed. In Section 3.5.2 the performance of the current vector control algorithm and the speed regulator

of the PM machine are introduced. Finally, in Section 3.5.3 the dynamics of the alternating currents flowing from the grid side converter in response to step-profiled reactive current references as well as the dc-link controller performance are presented.

3.5.1 Description of the experimental setup

In Table 3.1, detailed data of the servomotor, the dc-link and the inductive filters of the system are offered. Parameters of PMSM and the cabinet are obtained from manufacturer's catalogues [69, 64]. In addition, Figure 3.12 pictures the experimental setup.

Table 3.1: Characteristic parameters of the system

Element	Parameter	Symbol	Value
PMSM	Rated power	P_n	5.5 kW
	Rated voltage	U_n	400 V
	Resistance (ph-ph)	R_s	0.44 Ω
	Inductance on qd axis	$L_q = L_d$	$2.88{\cdot}10^{-3}$ mH
	Flux created by the magnets	ψ_{PM}	0.2465 Wb
Rotating disk	Inertia	J	0.868 kg·m^2
Power converters	Over current protection	-	16 A
Inductive filters	Inductance	L_l	4.6 mH
	Resistance	R_l	0.3 Ω
DC-link	Capacitance	C	0.0050 μF

In order to quantify the torque losses of the system, an experiment has been carried out. As a result, Figure 3.13 presents the power losses of the system versus its mechanical speed.

As shown, the relationship between these two magnitudes can be accurately modeled by a second order function P_l. Since T_l can be expressed as the power losses divided by the mechanical speed, its speed dependency results as,

$$T_l = \frac{P_l}{\omega_m} = 0.0019\omega_m + 1.4606 \tag{3.43}$$

Ergo, T_l is linearly dependent with the mechanical speed and the static friction level of the system is modeled as a constant torque equals to 1.4606 Nm.

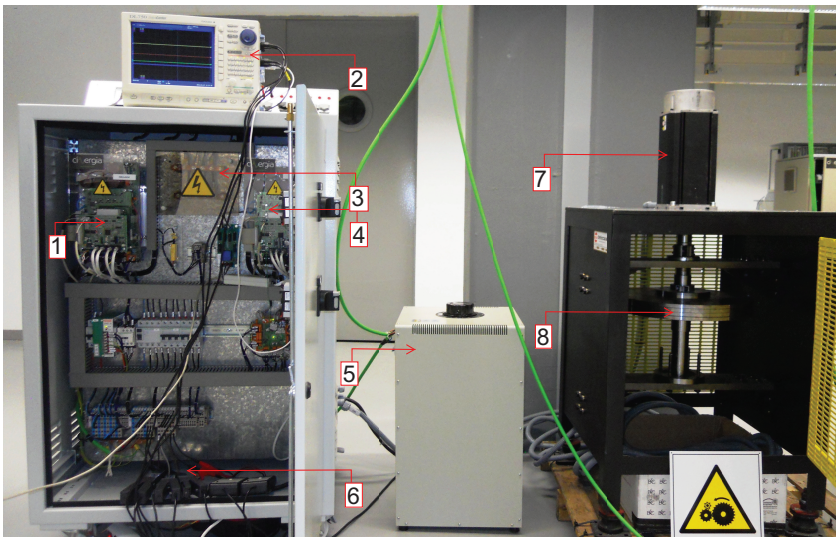

Figure 3.12: Experimental setup. From left to right: item 1) Grid side converter; item 2) Oscilloscope; item 3) Dc-link; item 4) Machine side converter; item 5) Autotransformer; item 6) Measurement devices; item 7) PMSM; item 8) Rotating disk

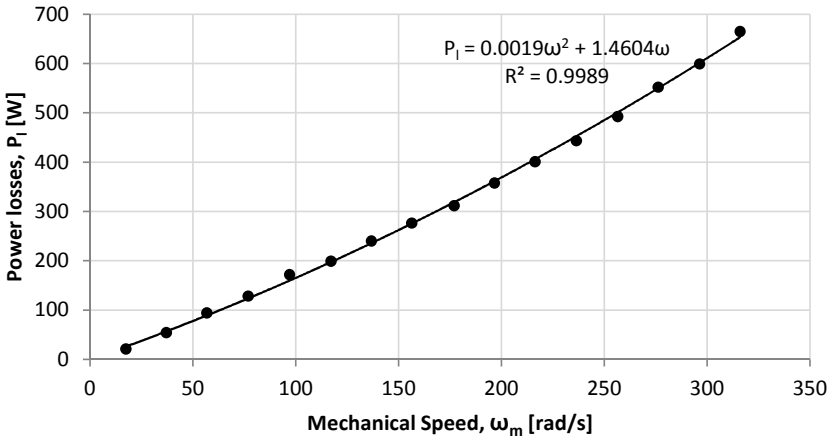

Figure 3.13: Power losses versus mechanical speed profile

3.5.2 Machine side converter controller testing and validation

Bearing in mind the computation expressions for the parameters of the linear controllers presented in Section 3.4.1, i.e. equations (3.23)-(3.24) and (3.30), the particular values of proportional and integral parts of these linear controllers used in the current study case are introduced in Table 3.2.

For calculating the above-mentioned parameters, the desired closed loop time constants for the PI current contollers are selected as one hundred times the sample time of the DSP. In that case, $\lambda_s = \frac{100T_s}{2\pi}$, where sample time T_s is 12 kHz^{-1}.

Moreover, the selected time constant value of the speed regulator is $\lambda_\omega = 0.5$ s. This time constant value allows the controller to support instantaneous gradients of the mechanical speed reference up to 20 rad/s without saturating the q-axis current reference.

Table 3.2: Machine side converter controller parameters

Controller	Proportional gain		Integral gain	
	Symbol	Value	Symbol	Value
Q-axis current controller	K_{psq}	5.74	K_{isq}	567.57
D-axis current controller	K_{psd}	5.74	K_{isd}	567.57
Speed regulator	$K_{p\omega}$	0.193	$K_{i\omega}$	-

A phase-to-phase RMS value of grid voltage ($V_{ph-ph_{RMS}}$) approximately equals 305 V is fixed in all experiments in this Section. The dc-link voltage value is set to $E = 650V$. In Figures 3.14 and 3.15 the dynamics of the *abc* currents flowing to the servomotor while changes in q-axis or d-axis current references are presented.

Figure 3.16 shows a temporal response to step-profiled mechanical speed reference. As previously noted, a steady state error in the response can be observed.

Figure 3.17 presents the performance of the anti-windup algorithm of the i_{sq} current controller. The rotating speed of the machine is approximately 170 rad/s when a dc-link voltage drop occurs. That makes the converter unable to maintain the speed of the machine above approximately 140 rad/s since the dc-link voltage drops to 400 V and a peak value of the fundamental component of the line-to-neutral voltage that can be produced by the converter is set to 115 V. Thus, in order to prevent the current controller integrator from falling into an over-saturated state, the anti-windup algorithm comes into play reducing the currents of the machine and facilitating its normal operation when the dc-link voltage shoot up to a higher value.

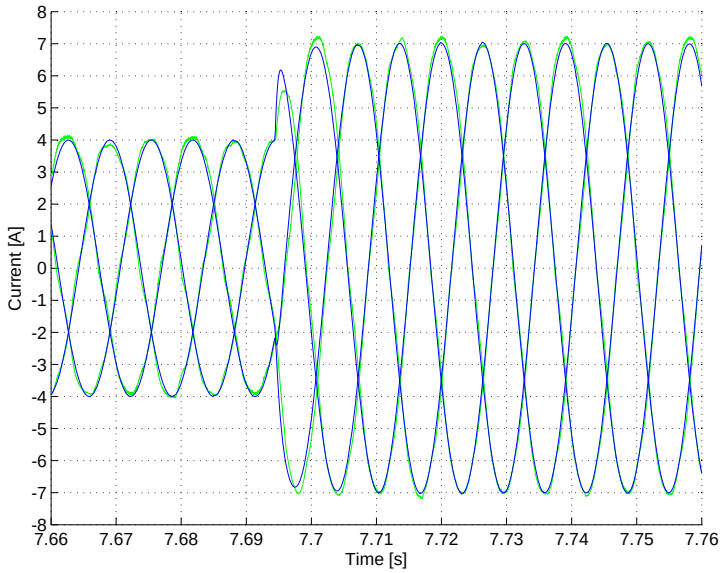

Figure 3.14: Temporal response to a step-profiled q-axis current reference from 4 A to 7 A. Green lines plot measured values while blue lines plot simulation results

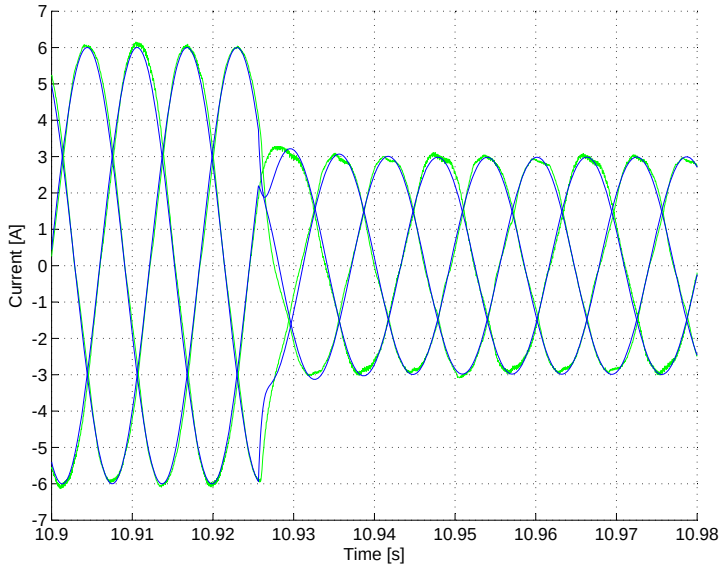

Figure 3.15: Temporal response to a step-profiled d-axis current reference from 6 A to 3 A. Green lines plot measured values while blue lines plot simulation results

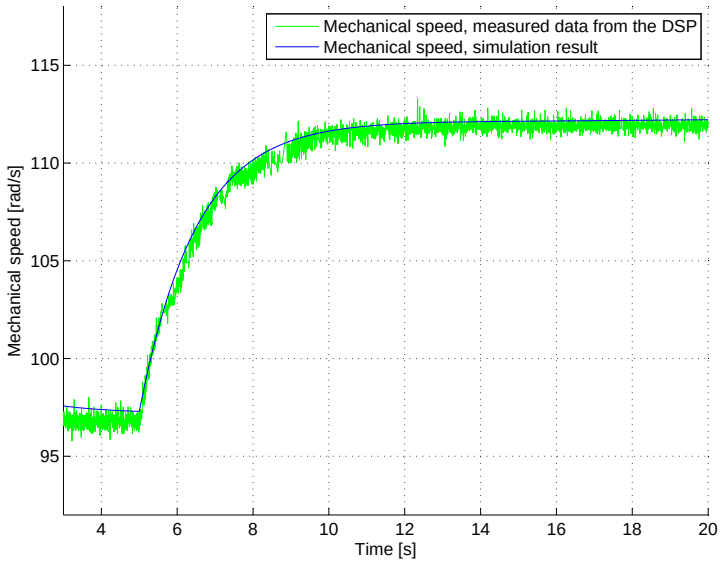

Figure 3.16: Temporal response to a step-profiled speed reference from 100 rad/s to 115 rad/s. Green line plot measured values while blue line plot simulation results

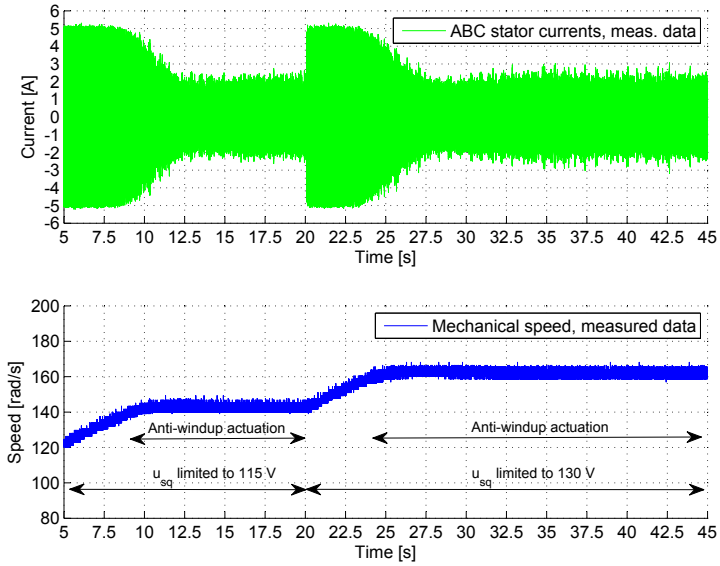

Figure 3.17: Alternating stator currents of the machine while using the q-axis current controller anti-windup. The q-axis current reference is equal to $i_{sq}^{*} = 5$ A throughout

3.5.3 Grid side converter controller testing and validation

The design process to calculate the electrical current control loops of the grid side converter and also the dc-link voltage regulator have been presented in Section 3.4.2. Bearing in mind the computational expressions for the proportional and integral parameters of these linear controllers, i.e. equations (3.35)-(3.36) and (3.41)-(3.42), the particular values of proportional and integral parts of these linear controllers used in the actual study case are introduced in Table 3.3.

For calculating the above-mentioned parameters, the desired closed loop time constants for the PI current controllers are selected as thirty times the sample time of the DSP. In that case, $\lambda_l = \frac{30T_s}{2\pi}$, where sample time T_s is 24 kHz^{-1}. Moreover, the selected natural frequency ω_E and the damping factor ξ_E of the closed loop transfer function E/E^* (see equation (3.40)) are equals to $\omega_E = 2 \cdot \pi \cdot 1.8\text{Hz} = 11.31$ rad/s and $\xi_E = 0.98$. Finally, the control parameters of the Phase-Locked-Loop (PLL) for obtaining the angle of the grid voltage are depicted, (see Figure 3.10). It is worth noting that the tuning of a PLL can be a challenging task, in fact it is subject of extensive research activities, and it is thickened, for instance, from considering stability issues under network disturbances. However, these aspects have not been considered in the present study as being out of the scope. This work considers a classical design for the PLL structure [18] and the value of its control parameters are also shown in Table 3.3.

Table 3.3: Grid side converter controller parameters

Controller	Proportional gain		Integral gain	
	Symbol	Value	Symbol	Value
Q-axis current controller	K_{plq}	23.51	K_{ilq}	1533.1
D-axis current controller	K_{pld}	23.51	K_{ild}	1533.1
Dc-voltage regulator	K_{pE}	0.1929	K_{iE}	1.113
PLL parameters	K_{pPLL}	1.1	K_{iPLL}	1.5

A phase-to-phase RMS value of grid voltage $V_{ph-ph_{RMS}}$ approximately of 305 V is fixed in all experiments in this Section. For the proper operation of SVPWM techniques, the dc-link voltage must remain within a suitable operational range. Specifically, the lower operating value for the dc-link voltage is noted as follows,

$$E_{min} = \frac{2\sqrt{2}V_{ph-ph_{RMS}}}{\sqrt{3}} \approx 500V \tag{3.44}$$

Thus, in the following experiments the dc-link voltage will be regulated within a range represented by $E = [550, 750]V$.

Figure 3.18 shows the dynamics of the dc-link regulator in response to a step-profiled voltage reference E^*. In Figure 3.19, the dynamics of the direct-axis current while a change in the dc-link voltage level occurs is presented.

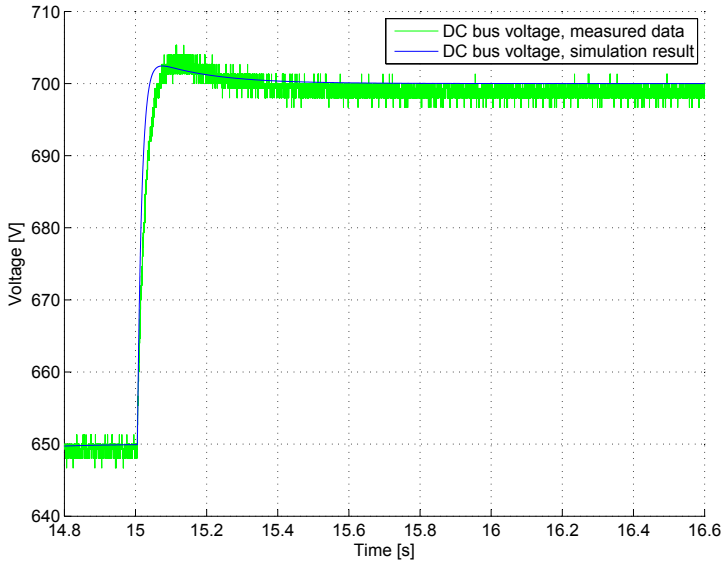

Figure 3.18: Temporal response to a step-profiled voltage reference from E^* equals to 650 V to 700 V. Green line plots the measured dc-link voltage while blue line plots the simulation result

As previously noted, dc-link allows the power transmission between the servomotor and the external grid. Since the speed of the electrical machine is continuously changing, the dc-link voltage controller have to face several disturbances in the dc-voltage level due to these transient states. Figure 3.20 plots the dc-voltage level during a step-profiled reference of q-axis stator current component i^*_{sq} from 9 A to -9 A. As can be observed, the dc-link voltage controller keeps the dc-voltage level within the operating limits, which are set to $E_{min} = 550$V and $E_{max} = 750$V.

Figure 3.21 plots the dynamics of the *abc* grid currents in response to a step-profiled current reference i^*_{ld}.

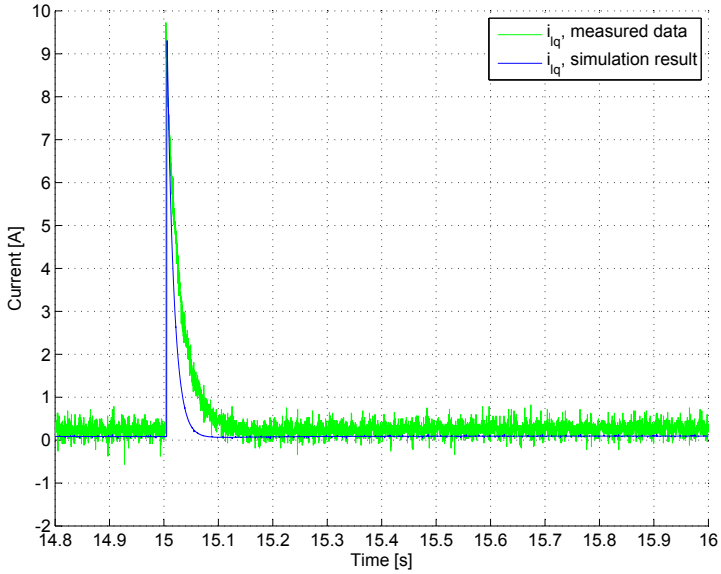

Figure 3.19: Direct-axis current component in response to a step-profiled voltage reference from E^* equals to 650 V to 700 V. Green line plots the measured data from the DSP while blue line plots the simulation result

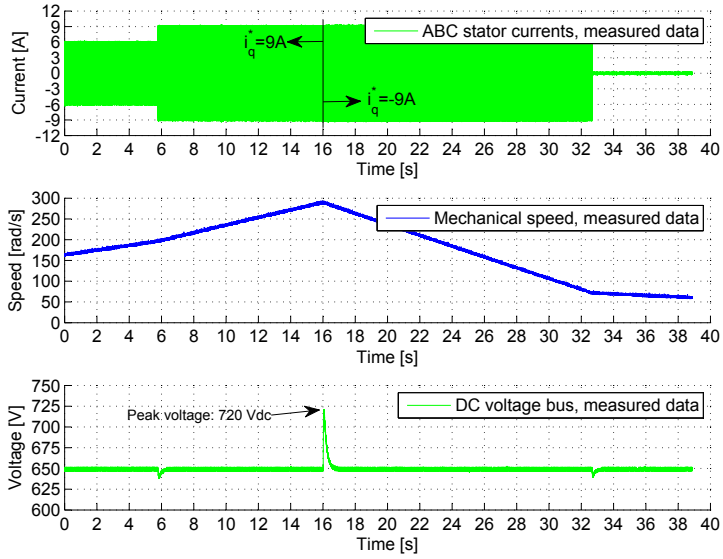

Figure 3.20: Dc-link voltage level while the servomotor is being accelerated and suddenly decelerated near its rated speed

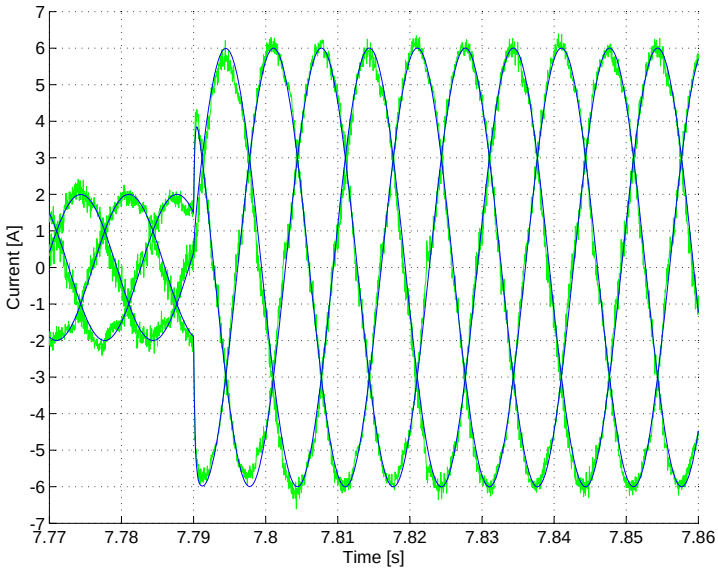

Figure 3.21: Temporal response to a step-profiled d-axis current reference from 2 A to 6 A. Green lines plot measured values while blue lines plot simulation results

3.6 Characterization of the energy storage system

This section deals with the determination of some of the main characteristics of the storage system such as energy rating, power rating and energy efficiency. Experimental data has been obtained from an acceleration of the system from its operational minimum speed, set at 50 rad/s to maximum operating speed, set at 314 rad/s. Since active power generated or absorbed by the PMSM results from the product of electrical torque and rotating speed of the machine, at low speeds the ability to inject or absorb power of the storage device is very limited. This is why a non zero minimum operating speed is indicated. In fact, it is a common practice not to operate commercial flywheels below 50% of their maximum rotating speed [34].

Figures 3.22 and 3.23 show the instantaneous injected or absorbed power of the storage system at its Point of Common Coupling (PCC) with the external grid and the alternating currents respectively. The acceleration and deceleration of the system is controlled by the speed regulator presented and described in Section 3.5.2. As explained, the output of this controller provides a servomotor torque reference. In order to limit the maximum currents flowing through the system the torque reference has been limited

to 10 Nm. Thus, the currents of the servomotor results saturated at 9 A maximum during the acceleration of the machine to 300 rad/s. Similarly, the currents becomes saturated at -9 A during the deceleration of the machine to 65 rad/s.

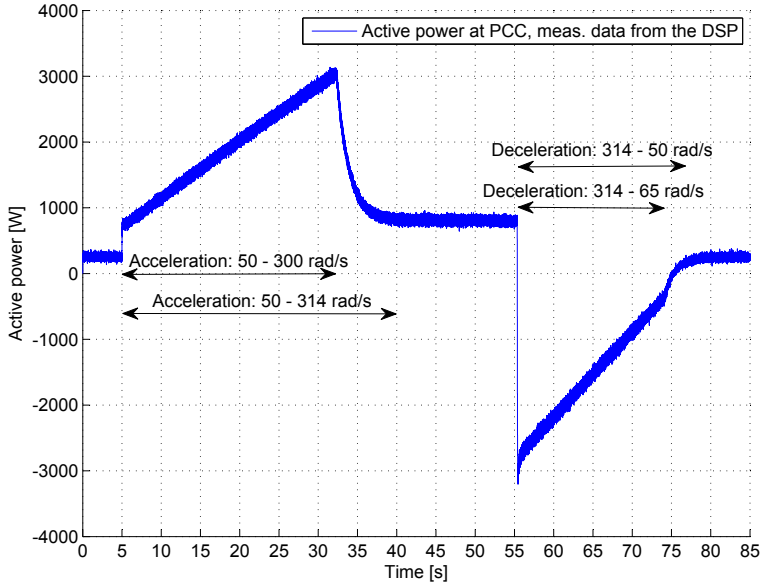

Figure 3.22: Active power at PCC during an acceleration from 50 rad/s to 314 rad/s and a following deceleration to 50 rad/s

According to IEEE Std 1679-2010, which is a recommended practice for the characterization and evaluation of energy storage technologies in stationary applications [146], the energy rating is defined as the usable energy storage capacity of the system at a defined discharge rate. Therefore, and according to Figure 3.22, the energy rating E_{rating} of the system at a constant stator currents discharge rate of -9 A, while the mechanical speed decreases from 314 rad/s to 65 rad/s is computed as follows,

$$E_{rating} = \int_{t=55.4s}^{t=74.4s} P(t) \cdot \mathrm{dt} \approx 30\,\mathrm{kW} \cdot \mathrm{s} \tag{3.45}$$

Considering the system fully charged while running at its rated speed, the power rating is determined as 3 kW for a State of Charge (SoC) equals 100%, during a discharge rate defined by the constant value of the stator currents of the PMSM equals -9A.

Finally, energy efficiency is defined as the usable energy output divided

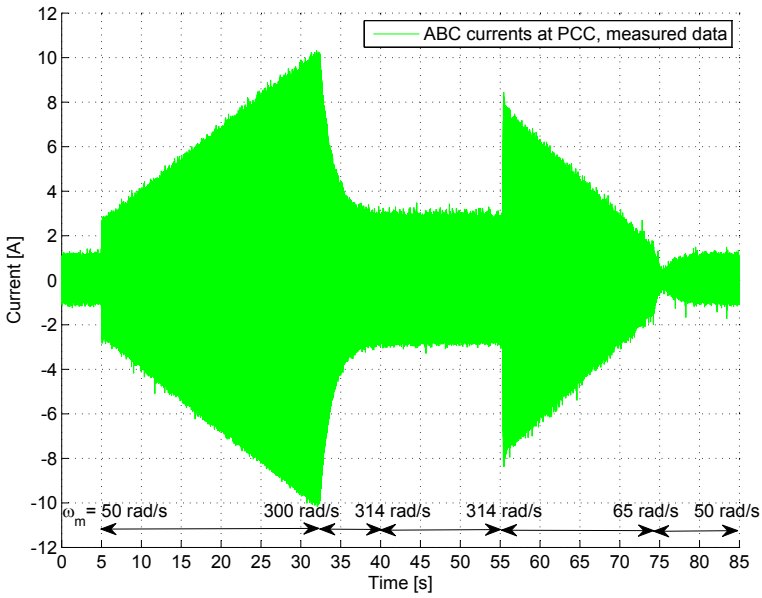

Figure 3.23: Alternating currents at PCC during an acceleration from 50 rad/s to 314 rad/s and a following deceleration to 50 rad/s

by the energy input to the system. Taking into account the energy rating value previously defined, and understanding the energy input to the system as the kinetic energy of the rotating disk E_k, the energy efficiency during the discharge process presented in Figure 3.22 is computed as,

$$E_{eff} = \frac{E_{rating}}{E_{k|_{\omega_m=314\text{rad/s}}} - E_{k|_{\omega_m=65\text{rad/s}}}} \cdot 100 = 73\% \tag{3.46}$$

It is clear that the system performance is far from usual features of commercial systems. However, the goal of the project is not to develop a high-tech flywheel. The system has been designed as a proof of concept instead. However, is worth noticing that in the views of improve the utility of the system in terms of power, energy capacity and efficiency some modifications of the system topology and control strategy could be set out. For instance, since the power exchanged by the PMSM is proportional to the i_q current and the rotating speed, increasing the maximum allowable currents through the system would improve the power capacity of the storage device. Also, field weakening control strategies of the PMSM would permit the system to achieve rotating speeds above rated value, and then improve the stored energy in the rotating disk. And finally, it is clear from Figure 3.13 that the

power losses are very important in the system, limiting in great extent the energy efficiency of the system. In this regard, the use of magnetic bearings would dramatically reduce the mechanical losses of the system.

3.7 Chapter remarks

In this chapter, the modeling, control and experimental validation of a flywheel-based energy storage device have been presented. A field oriented vector control algorithm has been implemented for governing the servomotor while the instantaneous power theory-based algorithm has been used to manage the active and reactive currents flowing from the grid side converter. The modeling, which has been carried out in software Matlab Simulink, and control system design have been validated executing several experiments. Moreover, other characteristics like the torque losses of the system have been determined experimentally. The energy capacity of the system has been determined to be 30 kWs while decreasing the speed of the machine from its rated value to 65 rad/s at constant stator current rated discharge equals 9 A. The energy efficiency of this process has been quantified to 73%. Moreover, the power capacity of the system has been limited to 3 kW in order to operate the system within secure operating limits of the power converters.

4

Energy management of a flywheel for wind power smoothing

Summary.- Power fluctuations of wind generators may affect power quality especially in weak or isolated grids. This chapter proposes an energy management strategy for a flywheel-based energy storage device. The aim of the flywheel is to smooth the net power flow injected to the grid by a variable speed wind turbine. The design of the energy management strategy is conducted through several phases. First, a definition and determination of the optimal operation of the storage device is carried out through the formulation and deterministic solution of an optimization problem in GAMS. Based on this solution, an online energy management algorithm is proposed to achieve a close to optimal operation of the flywheel. This algorithm determines the set points of the torque control of the flywheel electrical machine. The proposed methodology is illustrated by simulations.

4.1 Introduction

Power fluctuations (in the time range up to a minute) of wind turbines may cause fast voltage variations, especially in weak or isolated grids [208, 143]. In fact, and according to [276, 40, 286], fast power fluctuations of wind turbines could markedly affect power quality levels. In particular, high flicker levels can be noted due to cyclic perturbations to the rotational torque as well as other stochastic factors related to the randomness of wind. The flicker is a voltage fluctuation that is clearly observed in lighting levels. In order to mitigate the effects of power fluctuations, an ESS can be used [83, 249, 202, 285, 137, 315]. Storage technologies with high ramp power rates and high cycling capability are required for this purpose. Short time scale ESSs such as supercapacitors, superconducting magnetic energy storage devices and flywheel systems are well suited.

The application of flywheel systems has been proved to be effective for wind power smoothing. The related studies address two control levels: the energy management algorithm and the control scheme of the electrical machine. The latter control level includes sensorless control and field weakening strategies to maximize the energy capacity of the system. For instance, three techniques of sensorless vector-controlled induction motors driving a flywheel are compared in [43]. In [56] flywheel system is activated by a Switched Reluctance Machine (SRM) and is connected to a DC bus of back-to-back power converters of a wind turbine. The aim of the flywheel control is to regulate the dc-link voltage against fluctuations in the generated current by the wind turbine. Cardenas et al. [55] has proposed the same scheme as in [56], but in this case the flywheel is impulsed by an induction machine. This machine is controlled to operate in a wide speed range by using flux weakening above its rated speed. In [116] an induction machine-based flywheel device is driven by a direct AC-AC matrix converter system as an alternative to the conventional set of back-to-back power converters. Field weakening capability is also added to this control.

Within the high-level energy management algorithms, several schemes based on fuzzy-logic ideas have been proposed. For instance, a coordinated control algorithm is presented for regulating the dc-link voltage in a variable speed wind turbine with flywheel [54]. The aim of the control of induction machine-based flywheel is to smooth the net dc-link current disturbances using a feedforward compensation scheme augmented by a fuzzy-implemented nonlinear controller. Dc-link stability of a variable speed wind turbine with flywheel is also regarded in [63] and [153]. In these articles, a fuzzy-logic based algorithm is also used to manage the current injection or absorption

to the dc-link by the flywheel. The fuzzy-logic algorithm is established to generate the adequate regulation of the power injected to the grid by means of the flywheel speed and the filtered power of the wind turbine. A fuzzy-logic structure is implemented also in [180] to manage the power exchanged between the flywheel energy storage and the ac grid taking into account the filtered value of wind turbine power and the State of Charge (SoC) of the storage device.

This chapter proposes a methodology to design the high-level energy management algorithm of the storage device. This methodology consists of several stages. First, a definition and determination of the optimal operation of the storage device is carried out through the formulation and deterministic resolution of an optimization problem in GAMS. From the solution of this optimization problem, it is possible to determine the optimal mean flywheel speed to achieve the better energy management of the storage device. This optimal mean flywheel speed along with the wind power is used to determine the power that the flywheel must store in order to smooth the power delivered to the grid. Modeling and control system implementation as well as the performance of the obtained results are analysed using Matlab Simulink.

4.2 Flywheel systems for wind power smoothing

Figure 4.1 depicts a conceptual diagram of the system. It comprises a variable speed wind turbine and a flywheel-based storage device. Only partial load operation of the wind turbine is considered in this chapter. The wind turbine provides highly variable power to the grid. To smooth this power, the storage device exchanges power with an external network in order to smooth the power flow. For high wind power values, part of the energy is stored in the flywheel. This energy is delivered to the grid during low wind power levels. Thus, the variability of power injected into grid is smoother than the power that would be injected by the wind turbine without flywheel support. Since the energy storage capability of the flywheel is limited it is necessary an energy management strategy to operate the system within its SoC limits. The flywheel need to maintain some energy stored to be able to supply power when the grid requires it. Without an adequate energy management strategy, the storage device could frequently be fully discharged, thus limiting its operability. Figure 4.2 shows the block diagram of wind and wind turbine model. Detailed explanation of each part of the wind model can be found in [40, 217] and [230]. However, appropriate approach to the wind model is offered in the following.

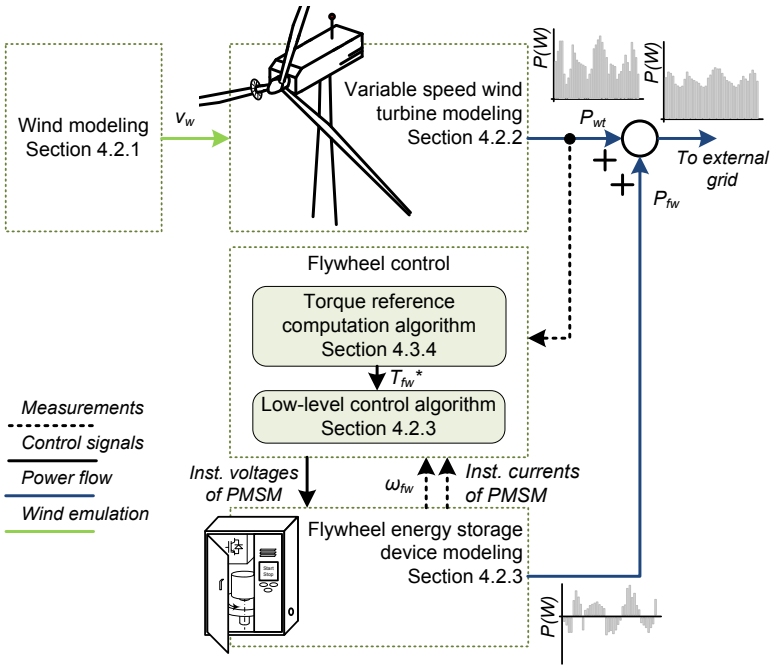

Figure 4.1: Conceptual diagram of the FESS for wind power smoothing

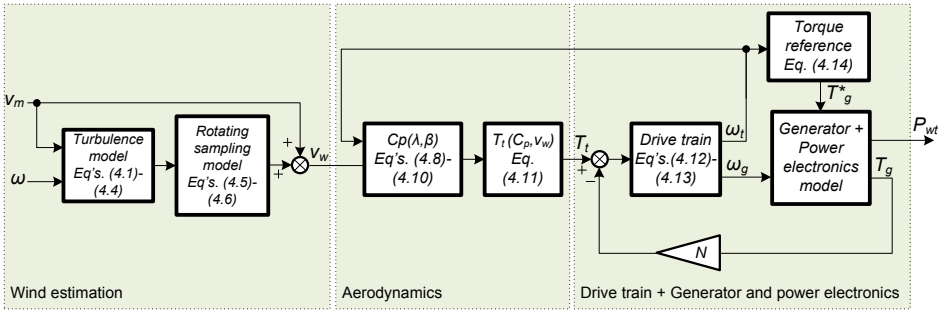

Figure 4.2: Wind and wind turbine model

4.2.1 Wind speed model

Wind speed experienced by a particular point of a blade can be modeled as a quasi-constant average component, evaluated in the range of minutes, and a changing wind speed component depending on both deterministic and stochastic factors. Deterministic factors are primarily wind shear, tower shadow, and the presence of other wind turbines and near obstacles. Stochastic components are derived from the spatial and temporal distribution of the turbulence [40, 75].

This chapter adopts the so-called "Effective wind model" (see e.g. [40]). By means of this model, an equivalent scalar wind speed to the three-dimensional wind field that experiences the blades of the rotor is computed. Mean wind speed component, turbulence as well as rotating sampling effect are considered in this model.

As it can be noted in Figure 4.2, the wind turbulence is obtained from affecting a white noise $\omega(t)$ through a low-pass filter [40]. This can be computed as

$$H_{turb} = K_V \frac{(T_V a_1 s + 1)}{(T_V s + 1)(T_V a_2 + 1)}, \tag{4.1}$$

where the parameters a_1 and a_2 depends on the location of the wind turbine. T_V depends the mean wind speed V_m and the heigh of the hub of the turbine L_V and is computed by

$$T_V = L_V / V_m. \tag{4.2}$$

The parameter K_V normalizes the variance of the turbulence by

$$K_V = \sqrt{2T_V(1 - a_2^2)\left(\frac{a_1^2}{a_2} - a_2 + 1 - a_1^2\right)^{-1}}. \tag{4.3}$$

The output of this filter is multiplied by the estimated standard deviation of the turbulence σ_v, which is computed as

$$\sigma_V = V_m \sigma_v, \tag{4.4}$$

where σ_v is obtained experimentally and depends also on the location of the wind turbine. The particular values of all parameters of the wind model are presented in Table B.1 in Appendix.

The above presented operations build the model of the wind turbulence. Then, its output is affected by the rotating sampling effect. This effect denotes in some extent the cycling torque perturbations due to the airflow deviation through the tower section. The frequency of this perturbation is

established by the mean rotational frequency of the turbine P corresponding to the considered mean wind speed multiplied by the number of blades N. Mathematically, this model can be built up by two filters. The aim of the first one H_{rot_1} is to smooth the high-frequency components of the turbulence

$$H_{rot_1} = \frac{\omega_{sf}}{s + \omega_{sf}}, \tag{4.5}$$

where ω_{sf} is the cut-off frequency. The second filter H_{rot_2} represents the effect of the rotating sampling

$$H_{rot_2} = \frac{(NP)^2 + d^2}{(NP)^2} \cdot \frac{(s + NP)^2}{(s^2 + 2ds + d^2 + (NP)^2)}, \tag{4.6}$$

where d depends on the mean wind speed, the speed of the turbine and the turbulence intensity [40]. The above presented procedures complete the wind model. Wind shear effects have not been modeled since summation torque from the blades removes most of these effects [276]. Since the time range considered for the analysis under study in this chapter is chosen as 10 minutes, mean wind speed component is defined constant. Figure 4.3 presents a wind profile obtained with this model for mean wind speed of 7.5 m/s and 0.05 p.u. turbulence. The wind turbulence can be defined as the division between its standard deviation and its mean value during a given time period.

4.2.2 Wind turbine model

Power captured by a wind turbine P_{wt} is given by

$$P_{wt} = \frac{1}{2}\rho A C_p(\lambda, \beta) v_w^3, \tag{4.7}$$

where A is the area swept by the blades, ρ is the air density, v_w is the wind speed, and $C_p(\cdot)$ is the power coefficient that depends on the pitch angle β and tip-speed-ratio

$$\lambda = \frac{\omega_t R}{v_w}, \tag{4.8}$$

where ω_t is the rotational speed of the turbine and R is the rotor radius. The power coefficient can be given by the following expression

$$C_p(\lambda, \beta) = c_1(c_2 \frac{1}{\wedge} - c_3\beta - c_4\beta^{c_5} - c_6)e^{-c_7 \frac{1}{\wedge}}, \tag{4.9}$$

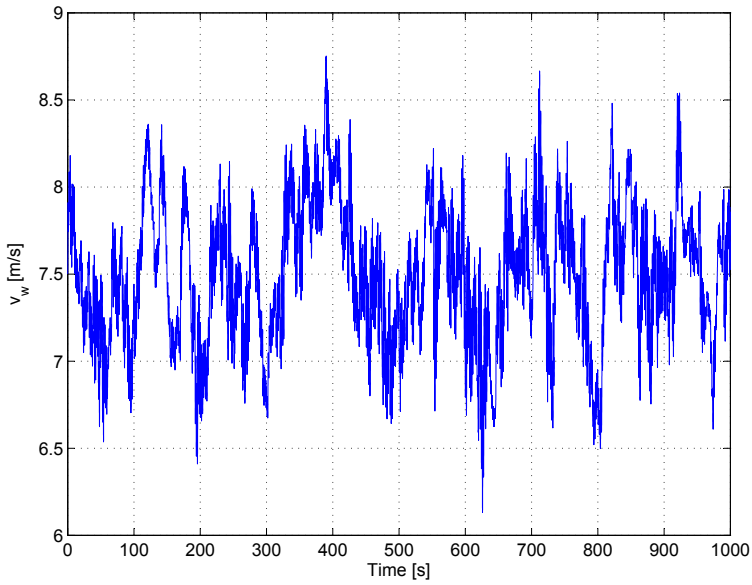

Figure 4.3: Wind profile corresponding to a mean wind speed of 7.5 m/s and 0.05 p.u. turbulence

where

$$\frac{1}{\wedge} = \frac{1}{\lambda + c_8\beta} - \frac{c_9}{1+\beta^3}, \tag{4.10}$$

and c_1 to c_9 depend on the particular wind turbine [4]. The mechanical torque developed by the turbine is given by

$$T_t = \frac{1}{2}\frac{\rho A R C_p(\lambda,\beta) v_w^2}{\lambda}. \tag{4.11}$$

The drive-train of the wind turbine is modeled as a two mass system. Thus, the mechanical dynamics is governed by

$$T_t^{'} = J_t^{'}\frac{d\omega_t^{'}}{dt} + D^{'}(\omega_t^{'} - \omega_g) + k^{'}(\theta_t^{'} - \theta_g) \tag{4.12}$$

$$-T_g = J_g\frac{d\omega_g}{dt} + D^{'}(\omega_g - \omega_t^{'}) + k^{'}(\theta_g - \theta_t^{'}) \tag{4.13}$$

where T_g is the generator torque, J_g is the inertia of the generator, θ_g is the angle of the generator, J_t is the inertia of the blades, θ_t is the angle of the turbine, D is the damping of the shaft and k represents its stiffness. The superscript indicates that the quantities and parameters are referred

to the high speed end of the gearbox. As presented, this model inputs the mechanical torque at the turbine shaft $T_t^{'}$ and the electrical torque T_g obtained from the electrical model of the generator. From these magnitudes, the differential equations in the model can be solved, which provide the speed at both the generator and the turbine shaft. In steady-state, the torque of the turbine $T_t^{'}$ is equal to the torque at generator shaft T_g times the gear-box ratio N. The generator torque T_g follows the electrical torque reference T_g^*, which corresponds to the output of a maximum power tracking algorithm. At partial load operation region, the torque reference signal is calculated as

$$T_g^* = K_{Cp}\omega_t^2, \tag{4.14}$$

where K_{Cp} is a parameter that depends on the wind turbine [159], [119]. The electrical dynamics of the generator are much faster than the mechanical dynamics, and can be approximated to a first order type system with a time constant in the range of milliseconds [275], since the generator is controlled by fast power converters. Figure 4.4 shows the frequency power spectrum corresponding to a three-blade wind turbine of 1.5 MW exposed to the wind profile in Figure 4.3.

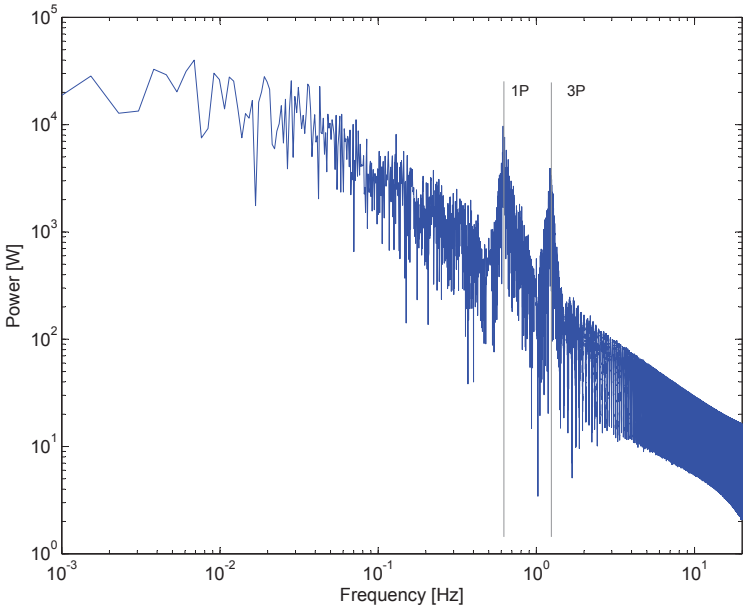

Figure 4.4: Frequency power spectrum of a three blade wind turbine of 1.5 MW exposed to the wind profile in Figure 4.3

Detailed data of the wind turbine can be found in Table B.1 in Appendix.

As can be seen, the concentration of energy around the rotational frequency of the turbine P times its number of blades. The $1P$ component and its second harmonic $3P$ are clearly identified.

4.2.3 Flywheel modeling and control

The ESS comprises a 100 kW high-speed Permanent Magnet Synchronous Machine (PMSM) coupled with a rotating disk. The storage device exchanges electrical power by means of regulating the electrical torque of the servomotor.

In practice, the flywheel could be directly connected to the point of common coupling of the wind turbine with the grid. In this case, the storage device would exchange power with the grid through a set of back-to-back power converters. Another possibility is to connect the storage device to the dc-link of a variable speed wind turbine (DFIG or full power converter-based). Considering the latter option, the grid side converter of the set of back-to-back power converters of the flywheel is not required. However, the grid side converter of the wind turbine should be oversized as it manages the power from the rotor side converter of the turbine and also the power of the flywheel. From a literature review [83], it is worth noting that power smoothing of wind turbines do not commonly require storage devices with power capacities higher than 10% of the rated power of the turbine. This figure bounds the oversizing of the rotor side converter of the wind turbine.

In this chapter, the FESS includes a ac-dc power converter for its connection to the dc-link of a variable speed wind turbine. The machine side converter controls the rotational speed of the flywheel. The grid side converter of the wind turbine is in charge of transferring the sum of the power generated by the wind turbine and also the power from the FESS to the grid. The main characteristics of the system are presented in Table B.1 in Appendix, with the data adopted from [282].

The modeling of the electrical machine and the low level control algorithms of the power converters of the flywheel are deeply explained in Chapter 3, Section 3.3. For the purposes of the present chapter, the modeling of the grid side converter of the storage device is omitted, and the machine side power converter is modeled as three-phase ideal controlled voltage sources.

Figure 4.5 presents the control system of the storage device. As it can be noted, a multilevel controller has been implemented. The setpoints of the low-level control algorithm of the machine side converter of the flywheel (i.e. the field oriented vector control of the PMSM [171, 288, 277]), are obtained from the high-level control algorithm. The parameters of the PI current

controllers of the field oriented vector control can be set as

$$K_{psqd} = \frac{L_q}{\lambda_s}, \tag{4.15}$$

$$K_{isqd} = \frac{R_s}{\lambda_s}, \tag{4.16}$$

where λ_s is a time constant value [18]. The particular values of the above parameters used in this chapter are presented in Table B.1 in Appendix.

As shown in Figure 4.5, the high-level control algorithm is in charge of determining the torque reference of the servomotor. This algorithm inputs the instantaneous speed of the flywheel ω_{fw} as well as the instantaneous power generated by the wind turbine P_{wt}. Since the operation of the flywheel is bounded by the synchronous speed of the PMSM, direct-axis current reference is always zero. The following section introduces the motivation of this algorithm as well as details its design.

4.3 Optimal operation of the storage device

The storage device exchanges power at the dc-link of the wind turbine so as to the net power flow injected together with the wind turbine becomes smoothed as much as possible.

The variability of the power generated by the wind turbine increases in high wind speeds (considering the partial load operation of the wind turbine). Thus, the wind energy that the storage unit has to compensate depends on the power generated by the wind turbine. Also, the capability of the flywheel to inject or absorb energy depends on its SoC, i.e. on its rotational speed. This is because the power of the flywheel is bounded by the product of its current rotational speed and its rated torque. Therefore, it is proposed to manage the average SoC of the flywheel with respect to the average generation level of the wind turbine to adequate the capability of the flywheel to inject or absorb energy to the expected wind energy to be compensated.

The inclusion of an energy management strategy of the flywheel is also motivated from further considerations.

First, it is worth noting that without a proper control of the SoC of the storage unit, the flywheel would overcome its maximum and minimum charge levels during its operation.

Second, the flywheel is characterized by its high-standing losses. Therefore, despite the fact that the flywheel is required to balance the wind power

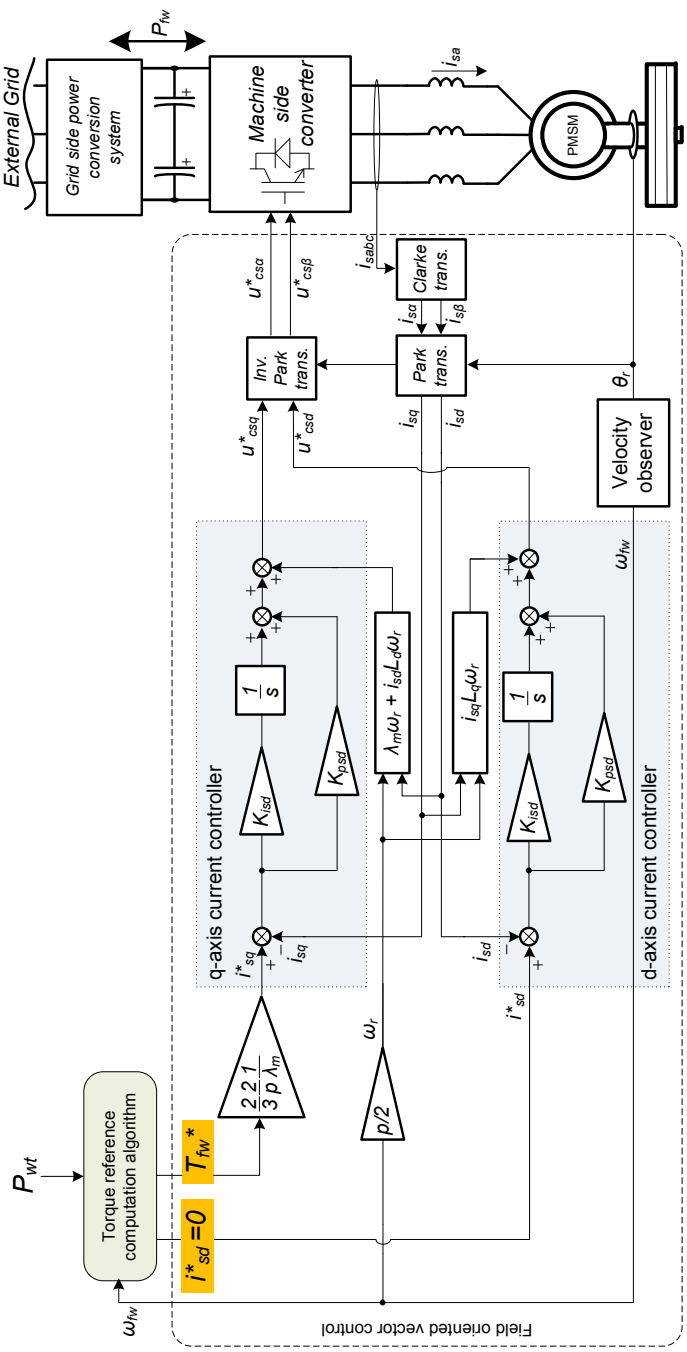

Figure 4.5: Control scheme of the machine side converter with low-level control structure presented in detail

fluctuations with average value close to zero, the flywheel would become fully discharged without the maintenance of a proper mean SoC, thus limiting its operability.

And third, since the losses in the flywheel depend on the rotational speed, it is interesting to search the optimum mean SoC so that it can ensure a proper performance of the storage unit taking also into account its power losses. For instance, there is no reason to maintain a high level of SoC if the flywheel is required to exchange low levels of power.

In practice, the management of the mean SoC of the flywheel is achieved by controlling the accelerations of its machine, i.e. the electrical torque. Accordingly, the energy management algorithm of the flywheel is represented as the torque reference computation algorithm block in Figure 4.5. The details of the design of this block are given in this section.

Several tasks relating the definition and determination of the optimal operation of the system as well as the definition of the control algorithm itself have to be addressed to design the torque reference computation algorithm. As presented in Figure 4.6, the first stage of the proposed methodology is the definition of the so-called optimal operation of the storage device as well as the general and specific objectives of the torque reference computation algorithm. A second stage deals with the mathematical formulation of the optimal operation and its resolution by means of a deterministic procedure in GAMS [114]. GAMS is a software for mathematical programming and optimization. Then, a third stage provides a function based on the solution of the previous optimization procedure to compute online the close to optimal mean SoC reference of the flywheel, i.e. the angular mean speed reference. The optimization problem in online operation would require the knowledge of future data for its resolution. Moreover, solving the optimization problem is too time consuming. For these reasons implementing online the optimization problem is not possible making necessary the implementation of the mentioned function instead. The fourth stage consist in the design of the torque reference computation algorithm that drives the low-level control scheme of the PMSM based on the results obtained in the previous stages. The following subsections detail all these stages.

4.3.1 Stage 1: Operational strategy objectives

The general objective of the high-level control algorithm of the storage device, i.e., of the torque reference computation algorithm, is to fulfil a close to optimal operation of the storage system. Optimal operation of the system is defined as one that minimizes the difference between the energy to be

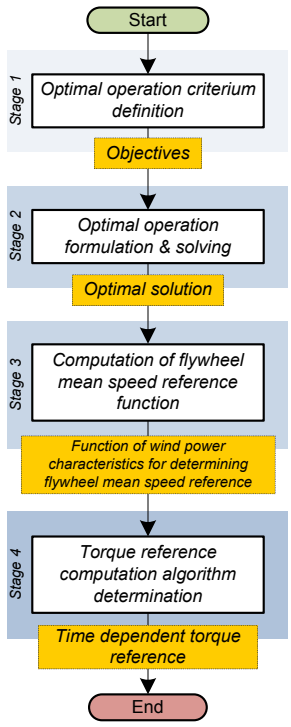

Figure 4.6: Methodology for the design of the energy management algorithm

injected or absorbed by the storage system, and the energy that is finally injected or absorbed by it during a given time interval. This general objective is translated into the determination of the torque reference of the field oriented vector control of the PMSM, which ensures that the mean value of SoC of the storage device remains close to the optimal operation.

4.3.2 Stage 2: Optimal operation of the storage device formulation and solving

The energy absorbed or injected into the grid by the flywheel during a certain time interval depends on two terms:

- The power due to the acceleration of the storage device, which is expressed as a function of its rotating speed $\omega^*_{fw_t}$ and the electrical torque T_{acc_t}

$$P_{acc_t} = T_{acc_t}\omega^*_{fw_t}. \tag{4.17}$$

- The power losses of the storage device, which are expressed as a second order function of its rotating speed

$$P_{loss_t} = c_1 \omega_{fw_t}^{*2} + c_2 \omega_{fw_t}^{*}. \tag{4.18}$$

To smooth the power delivery to the grid, the flywheel has to compensate the power reference P_{ref_t} corresponding to the turbulent components of wind power. Therefore, the difference ΔP between the power absorbed or injected by the flywheel and the power reference has to be minimized at all times. In terms of energy, this corresponds to minimize the following function

$$J = \sum_{t=1}^{N} \{u_t [\underbrace{P_{ref_t} - (P_{acc_t} + P_{loss_t})}_{\Delta P}] \Delta t - (1 - u_t) [\underbrace{P_{ref_t} - (P_{acc_t} + P_{loss_t})}_{\Delta P}] \Delta t\}, \tag{4.19}$$

where the binary variable u_t depends on the sign of P_{ref_t}.

Notice that the difference ΔP, and J, would be zero only if the flywheel could be able to compensate all turbulent components of the wind power represented by P_{ref_t}. However, the energy and power the storage unit is capable of injecting or absorbing are limited and depend on its SoC. As previously noted, the power of the flywheel is bounded by the SoC as it depends on the product of its rotational speed and its rated torque. Also, the energy the storage device is capable of storing is bounded by the maximum rotational speed of the system, i.e. by the maximum SoC.

As a consequence, ΔP would not be zero in practice and the optimal rotational speed of the flywheel $\omega_{fw_t}^{*}$ and the electrical torque T_{acc_t} must be obtained from solving the following optimization problem

$$\min_{(T_{acc_t}, \omega_{fw_t}^{*})} J, \tag{4.20}$$

subject to:

- The storage device must remain within its speed operating limits,

$$\omega_{fw_{min}} \leq \omega_{fw_t}^{*} \leq \omega_{fw_{max}} \tag{4.21}$$

- Maximum electrical torque of the servomotor due to the acceleration of the system cannot be exceeded,

$$T_{acc_{min}} \leq T_{acc_t} \leq T_{acc_{max}} \tag{4.22}$$

- The speed profile must accomplish the equation of motion of the system,

$$\frac{\omega^*_{fw_t} - \omega^*_{fw_{(t-1)}}}{\Delta t} k_2 = T_{acc_t} \tag{4.23}$$

- The binary parameter u_t is set to 1 while positive values of P_{ref_t} are considered,

$$u_t P_{ref_t} \geq 0 \tag{4.24}$$

- The binary parameter u_t is set to 0 while negative values of P_{ref_t} are considered,

$$(1 - u_t) P_{ref_t} \leq 0 \tag{4.25}$$

- The power injected by the storage device should not exceed the power referenced,

$$u_t P_{ref_t} \geq u_t (P_{acc_t} + P_{loss_t}) \tag{4.26}$$

- The power absorbed by the storage device should not exceed the power referenced,

$$(1 - u_t) P_{ref_t} \leq (1 - u_t)(P_{acc_t} + P_{loss_t}) \tag{4.27}$$

- The operating state of the storage device i.e., to inject or absorb power, must agree with the sign of the power referenced.

$$P_{ref_t}(P_{acc_t} + P_{loss_t}) \geq 0 \tag{4.28}$$

The variables to be determined are

- T_{acc_t} is the electrical current consumed or injected by the flywheel due to an acceleration or deceleration at time t,
- $\omega^*_{fw_t}$ is the angular speed reference of the flywheel at time t,

and the input data are

- P_{ref_t} is the series of the power reference of the flywheel, obtained by computing the difference between the output power of the wind turbine and its filtered value at a given cutoff frequency. This power reference is also limited by the rated power of the flywheel. This series depends on the particular mean wind speed and its turbulence,
- u_t is a binary parameter which depends on the signal of P_{ref_t}.

The optimization problem parameters are

- ω_{min} and ω_{max}, (rad/s), are the operational speed limits of the flywheel,
- $T_{acc_{min}}$ and $T_{acc_{max}}$, (A), are the maximum positive and negative values for the electrical torque of the flywheel servomotor, due to the acceleration or deceleration of the system,
- k_2, (kgm^2), is a flywheel characteristic computed by $2J/p$,
- c_1, (Ws^2/rad^2), is a flywheel power losses characteristic,
- c_2, (Ws/rad), is a flywheel power losses characteristic,
- Δt, (s), is the time interval unit.

Given a time series of P_{ref_t}, the solution of the optimization problem determines the optimum instantaneous rotational speed and torque developed by the flywheel for the considered period of time. Thus, it provides the time series of the power exchanged by the flywheel so as to the net energy injected and absorbed matches as much as possible to the requirements, taking into account the limitations of the storage unit. This formulation results in a mixed integer non linear problem, which is solved using GAMS.

4.3.3 Stage 3: Computation of flywheel mean speed reference function

The energy management algorithm needs the optimal angular speed reference ω^*_{fw} to achieve an optimal operation of the FESS. However, the solution of the optimization problem (4.20) cannot be included in the energy management algorithm because it is too time consuming and requires the knowledge of future data. To circumvent this problem, the optimization problem is solved for sufficient representative cases (two hundred cases) in order to be able to express the flywheel mean speed reference $\bar{\omega}^*_{fw}$ as a function of the wind power characteristics during a given time interval. Thus, this function can be used in the energy management algorithm to compute the speed reference instead of obtaining the optimal instantaneous speed by solving the optimization problem (4.20).

To obtain the function of the wind power characteristics, several wind profiles are generated for a given mean wind speed and turbulence. Then, the power reference P_{ref} is computed for each wind profile. As noted in Figure 4.9, the wind power for the computation of P_{ref} is passed through a fourth order Butterworth filter with 0.4 Hz as cutoff frequency. This

filter permits to separate the power associated to the turbulence, which are desired to be attenuated. The corresponding angular speed reference ω_{fw}^* are obtained by solving the optimization problem (4.20). From this procedure the speed reference for each time step are obtained. Then, the function provides the mean value of these angular speeds for each mean wind power. Repeating this procedure for different wind power profiles, i.e., different values of mean wind speed and turbulence, permits to generate a look-up-table, which provides the angular mean speed reference $\bar{\omega}_{fw}^*$.

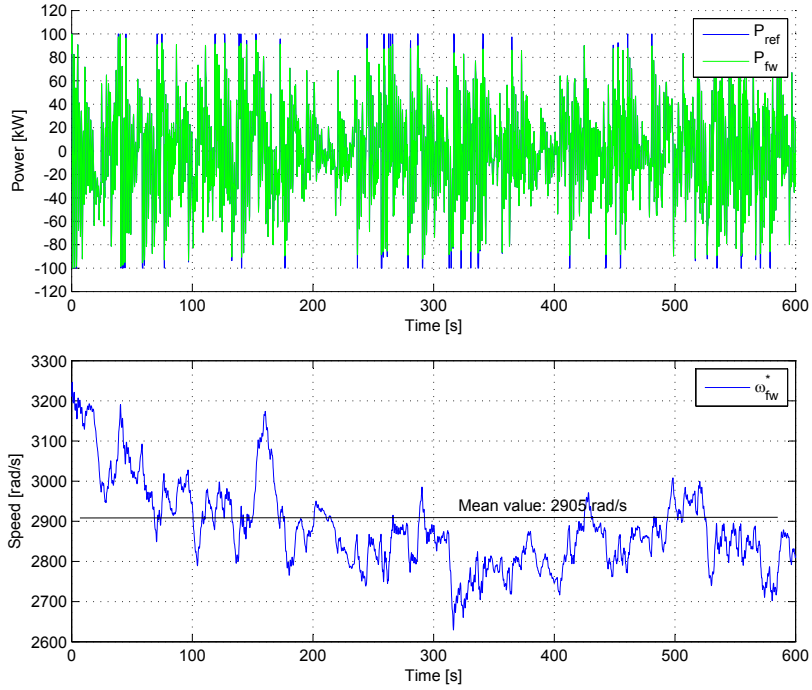

Figure 4.7: Power reference, actual power delivered by the flywheel and the optimal angular speed reference ω_{fw}^* corresponding to a wind profile of 7.5 m/s mean wind speed and 0.05 p.u. of turbulence

In Figure 4.7, the time series of the power reference P_{ref}, and the actual power delivered by the flywheel P_{fw} for a particular wind profile are shown. The corresponding solution of the optimization problem (4.20) is also presented in this figure. The considered mean wind speed is 7.5 m/s and the turbulence is 0.05 p.u, which corresponds to 0.15 p.u of wind power turbulence. A 600 s time interval is considered for each wind profile. It can be observed that 99% of the energy required by the optimal solution can be

provided by the flywheel. Remind that the power reference P_{ref} indicates the power that ideally must be provided by the flywheel to smooth the wind power and taking into account the power limitations of the storage device. The difference between P_{ref} and P_{fw} is a consequence of the SoC of the flywheel in a particular moment.

Figure 4.8 presents the angular mean speed reference function of the mean wind power for a flywheel of 100 kW and a wind turbine of 1.5 MW (see Appendix for more details). This function was obtained following the procedure previously described. Only partial load operation of the wind turbine has been considered. Results indicate that the higher mean wind power, the higher mean rotating speed.

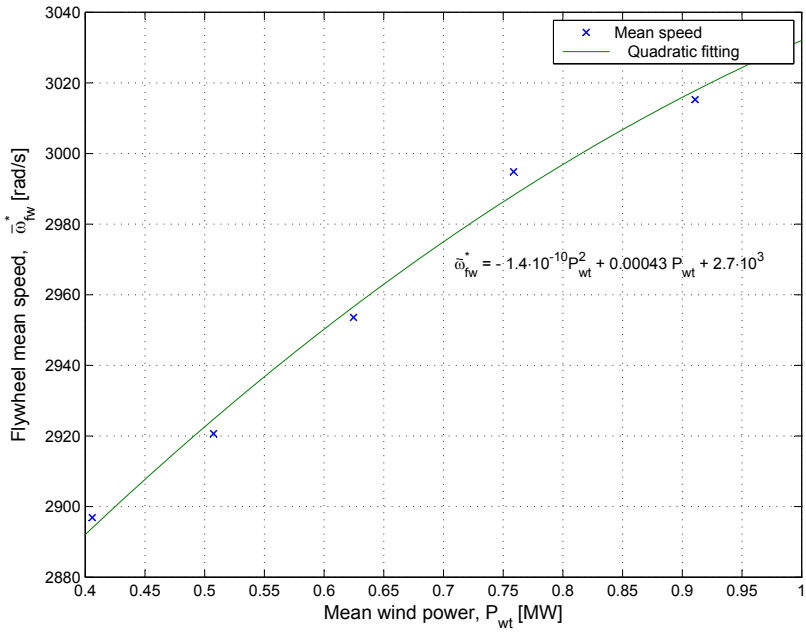

Figure 4.8: Relationship between flywheel mean speed reference $\bar{\omega}^*_{fw}$ and mean wind power obtained by analysing optimal results. Each cross corresponds to the mean value of $\bar{\omega}^*_{fw}$ for all cases evaluated for each mean wind power

Given a wind turbulence, the wind power that the storage device has to compensate is higher considering high mean generation levels of the wind turbine than considering low generation levels (referring to the partial load operation of the wind turbine), as most wind power is injected into the grid. The energy the flywheel is able to exchange is proportional to the square of

its rotating speed. Thus, seems to be reasonable to consider different mean rotating speeds of the flywheel dependent on the mean expected energy levels to inject or absorb.

As shown in Figure 4.8, this trend can be fitted by a second order function. The mean speed reference are in the range of 2900 to 3020 rad/s approximately, this represent a 89 to 93% of SoC. The mean energy delivered by the storage device is approximately 99% of the energy required in all cases considered in the present study.

4.3.4 Stage 4: Torque reference computation algorithm

As previously noted, the results of the optimization problem determine the optimum values of the flywheel angular speed reference depending on wind power profiles. However, these results obtained by GAMS cannot compute the torque reference during the operation of the flywheel. For this reason, a look-up-table from Figure 4.8 is used instead to compute the mean angular speed reference of the flywheel. In this section, the torque reference computation algorithm is presented. Figure 4.9 summarizes this algorithm. Two inputs can be noted: the instantaneous power of the wind turbine and the speed of the flywheel. The output of the control algorithm is the torque reference of the field oriented vector control of the PMSM.

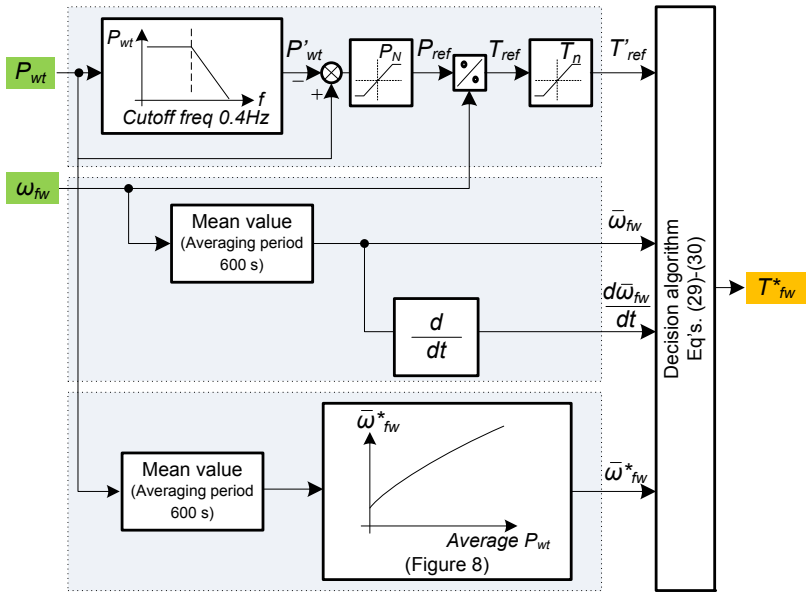

Figure 4.9: Torque reference computation algorithm

The algorithm consists in four main parts: the desirable optimal torque reference computation; the instantaneous flywheel speed signal treatment; the optimal mean flywheel speed acquisition; and the decision algorithm. Each procedure is explained in the following lines.

Desirable optimal torque reference computation The difference between the instantaneous power of the wind turbine and its filtered value provides the power reference. This power is limited by the power limits of the flywheel. This is the time dependent power reference profile used for the resolution of the optimization problem. The torque reference T_{ref} is obtained by dividing the power reference between the instantaneous value of the flywheel speed. This torque reference is saturated at the rated value of the PMSM in order to meet the operational restriction of the equation (4.22). This is the desirable optimal torque reference, $T_{ref}^{'}$.

Instantaneous flywheel speed signal treatment Two inputs to the so-called decision algorithm are derived from reading the flywheel speed: the mean flywheel speed value $\bar{\omega}_{fw}$, with an averaging period of 600 s, and its time derivative $\frac{d\bar{\omega}_{fw}}{dt}$.

Optimal mean flywheel speed acquisition Optimization problem solution provides a direct relationship between the wind power and the angular speed reference of the flywheel ω_{fw}^{*}. This relationship provides a function to determine the mean flywheel speed $\bar{\omega}_{fw}^{*}$ from mean wind power. This function is presented in Figure 4.8.

Decision algorithm Each of the above-detailed processes determines an input to the decision algorithm. This algorithm provides the torque reference of the storage device T_{fw}^{*} during its normal operation. Accordingly, flywheel average speed results as close as possible to its optimum value, while allowing a close to optimal operation of the storage device. The decision algorithm provides a reference torque of the PMSM T_{fw}^{*} equals the desirable optimal torque reference $T_{ref}^{'}$ when any of the following conditions occur.

- Given a non-negative desirable optimal torque reference $T_{ref}^{'} \geq 0$ the decision algorithm gives a torque reference T_{fw}^{*} equals zero when instantaneous flywheel speed reaches its maximum value. The torque reference T_{fw}^{*} is also set to zero when the mean flywheel speed is higher than its optimum level $\bar{\omega}_{fw}^{*}$ minus a given interval $\Delta\omega$, and

also its time derivative is strongly increasing with maximum growth rate of $\Delta\alpha$. These conditions are imposed to maintain a close to optimal mean SoC of the storage device. This can be summarized as

$$T_{fw}^{*} = \begin{cases} 0 & \text{if} \quad \omega_{fw} \geq \omega_{max} \\ 0 & \text{if} \quad (\bar{\omega}_{fw} \geq \bar{\omega}_{fw}^{*} - \Delta\omega)\& \\ & \quad \frac{d\bar{\omega}_{fw}}{dt} \geq \Delta\alpha \geq 0 \\ T_{ref}^{'} \geq 0 & \text{otherwise} \end{cases} \tag{4.29}$$

- Analogously to the previous case, given a non-positive desirable optimal torque reference $T_{ref}^{'} \leq 0$ the decision algorithm gives a torque reference T_{fw}^{*} equals zero when instantaneous flywheel speed reaches its minimum value. The torque reference T_{fw}^{*} is also set to zero when the mean flywheel speed is lower than its optimum level plus a given interval $\Delta\omega$ and also its time derivative is strongly decreasing with maximum growth rate of $\Delta\alpha$. This is summarized as

$$T_{fw}^{*} = \begin{cases} 0 & \text{if} \quad \omega_{fw} \leq \omega_{min} \\ 0 & \text{if} \quad (\bar{\omega}_{fw} \leq \bar{\omega}_{fw}^{*} + \Delta\omega)\& \\ & \quad \frac{d\bar{\omega}_{fw}}{dt} \leq \Delta\alpha \leq 0 \\ T_{ref}^{'} \leq 0 & \text{otherwise} \end{cases} \tag{4.30}$$

4.4 Application example of the dynamic performance

This section presents the results of the simulation of the system. The particular study case imposes an average wind speed of 7 m/s, and wind turbulence of 0.05 p.u., which results in wind turbine power turbulence of 0.14 p.u. The data used for the simulations are given in Table B.1 in Appendix. The aim of the storage device is to smooth power of the wind turbine from a cutoff frequency of 0.4 Hz. The operation of the storage device is defined according to the torque reference control algorithm designed in previous sections. A close to optimal operation of the storage device is achieved by applying the proposed energy management algorithm.

Previously defined intervals $\Delta\omega$ and $\Delta\alpha$ are used in the formulation of the so-called decision algorithm (see Section 4.3.4) in order to limit the flywheel reference torque T_{fw}^{*} starting from its average speed. Particular values of these indices are dependent on the study case regarding the size of the storage device, the wind turbine dimension as well as the mean flywheel speed reference. Particular values $\Delta\omega = 10$ rad/s and $\Delta\alpha = 0.1$ rad/s^2 have been chosen as most well suited to the current study case.

Figure 4.10 shows the spectrum of the power injected to the grid, with and without including the storage device support, according to above detailed study case definition. As presented, rotating sampling effect of the wind turbine is clearly smoothed through the flywheel support.

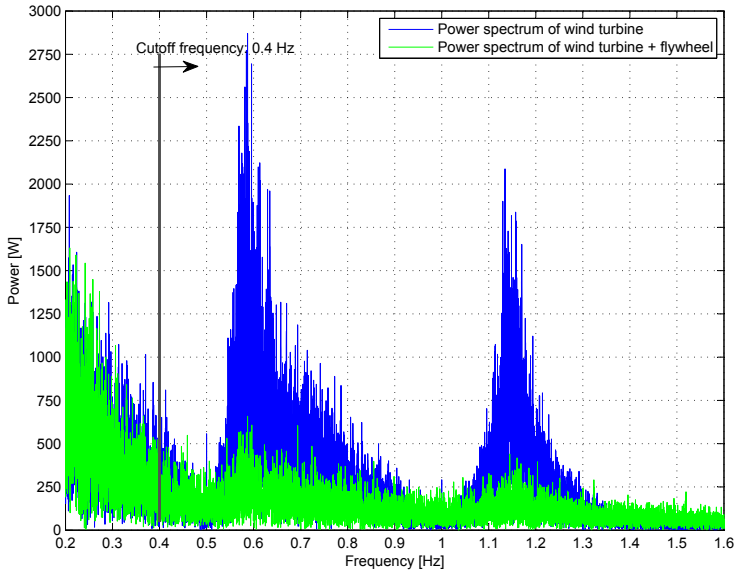

Figure 4.10: Spectrum of the power injected to the grid, with and without including storage support. The mean wind speed is 7 m/s, and wind turbulence is 0.05 p.u.

In order to better quantify the improvement achieved by the storage device controlled by the proposed algorithm, an index is introduced. This index is defined as the quotient of the turbulent energy component reduction of the wind turbine output from the indicated cutoff filtering frequency 0.4 Hz after the application of the storage device and the turbulent energy component without the flywheel support. This turbulent energy component is computed by the time integral of the power output above the indicated cutoff filtering frequency. The proposed improvement index ν is mathematically expressed by

$$\%\nu = \frac{E_f}{E_0}100 = \frac{\int |(P_{wt} + P_{fw}) - P_{Filt\_wt}|dt}{\int |P_{wt} - P_{Filt\_wt}|dt}100, \tag{4.31}$$

where E_0 is the turbulent energy component of the wind turbine from the indicated cutoff filtering frequency, and therefore depends on the wind turbine power profile, P_{wt}, and its time dependent filtered characteristic P_{Filt_wt}.

Similarly, E_f is defined as the turbulent energy component of the total power injected to the grid by both wind turbine and storage device form the indicated cutoff filtering frequency. This magnitude depends on the wind turbine power profile, its time dependent filtered characteristic and the storage device power profile P_{fw}. Figure 4.11 draws on the definition of the previous concepts. For the data presented in Figure 4.10, the improvement index results in $\%\,\nu = 91.9\%$.

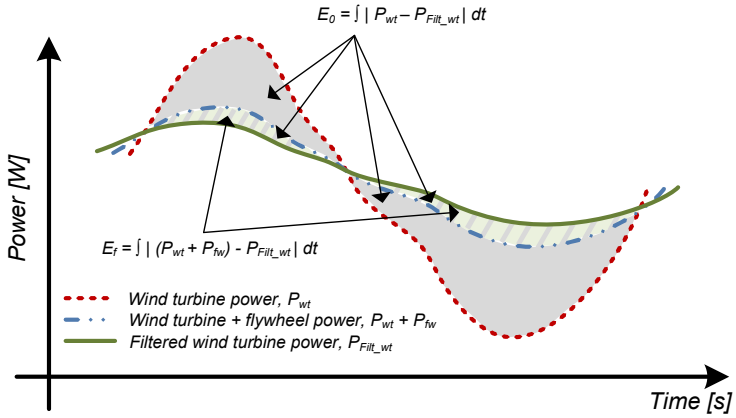

Figure 4.11: Instantaneous wind power profile, its filtered profile and the resulted power injected to the grid with the storage device support

A close to optimal operation of the storage device provides the results presented in Figure 4.10. Figure 4.12 plots the instantaneous flywheel speed, its time dependent average value, and the flywheel mean speed reference during the simulation of the study case. As shown, average speed of the flywheel is close to flywheel mean speed reference at all times. A close to optimal SoC of the system is achieved therefore validating the torque reference computation algorithm design. As a result, 92.7% of total energy demanded to the storage device is provided by means of continuously regulating the acceleration and deceleration of the flywheel. Recall that 99% of total energy demanded is satisfied by means of an optimal operation.

Additional simulation results are presented in Figure 4.13 and Figure 4.14. Figure 4.13 shows the total power injected into the grid by the system and its comparison with the power generated by the wind turbine. Also, it is shown the variability of the mechanical speed of the turbine due to the randomness of the wind.

Figure 4.14 presents the power of the flywheel, which corresponds to the difference between the net power injected to the grid and the power of the

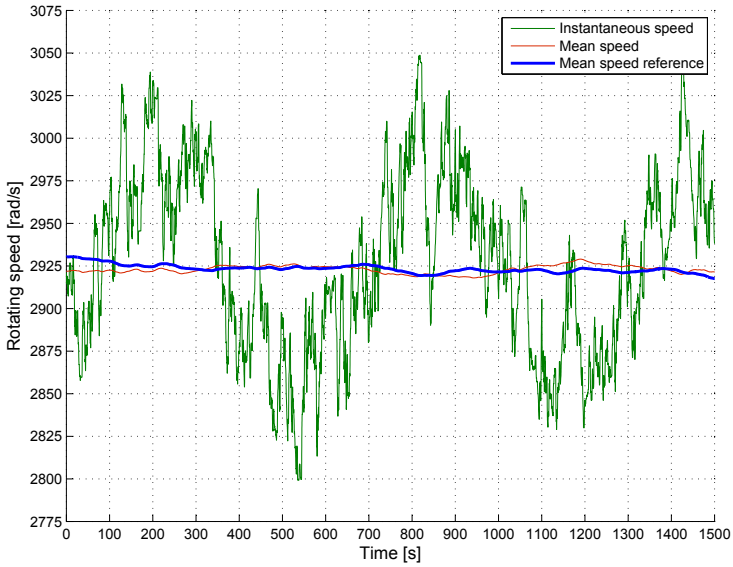

Figure 4.12: Instantaneous flywheel speed, its average value and the flywheel angular speed reference obtained by the simulation of the current study case

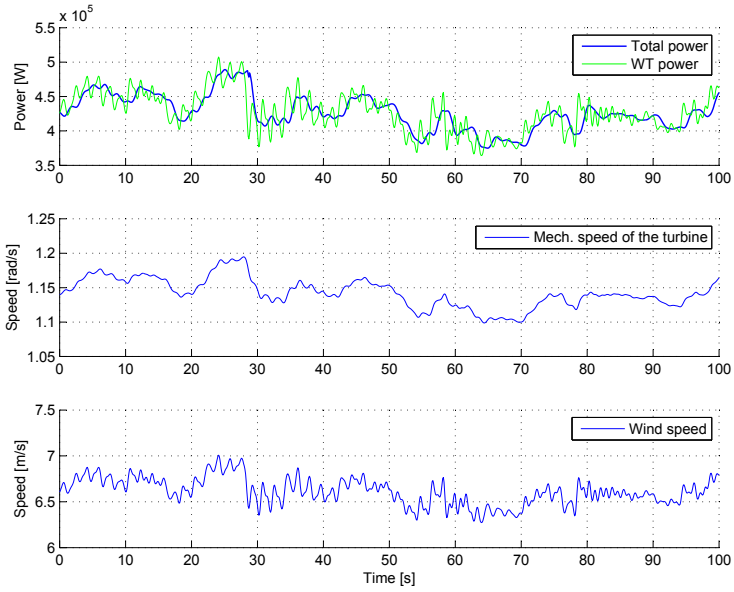

Figure 4.13: Detail of the total power injected into the grid, the power generated by the turbine, its rotating speed and the wind speed (mean value 7 m/s)

wind turbine. Further magnitudes of the flywheel as the electrical currents and the instantaneous speed are shown. As it can be noted, the dynamics of the electrical currents are much faster than the rate of change of the speed due to the inertia of the flywheel.

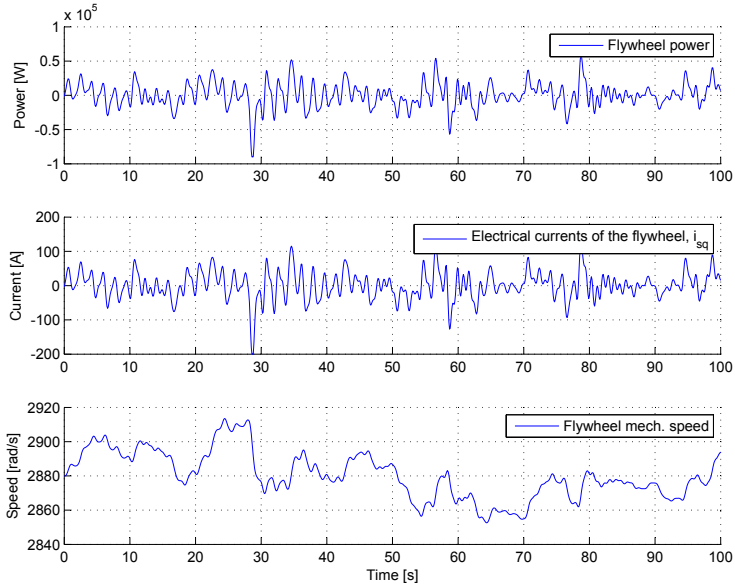

Figure 4.14: Detail of the power, current and speed of the flywheel for a reduced time frame of 100s

Table 4.1 presents some complementary results to compare different operational strategies of the storage device. Different mean operational SoC of the system, i.e., different mean operational rotating speeds are set instead of setting at all times the SoC defined by Figure 4.7. It also includes the optimal solution obtained by GAMS that cannot be implemented in online operation of the system (see Section 4.3.3). It can be observed that clearly the better improvement is obtained with the optimal solution. However, the proposed close to optimal strategy produces results close to the optimal. The sacrifice of not using the optimal reference is not significant in this case. Besides, the proposed algorithm provides better improvement than the use of other mean operational SoC of the flywheel.

Table 4.1: Evaluation of different operational strategies with mean wind speed 7 m/s and 0.05 turbulence.

Op. Strategy	ω_{fw} (rad/s)	$\%\nu$
Opt. Solution	2920 (90.0% SoC)	97.1
Close to opt. Op.	*2920 (90.0% SoC)*	*91.9*
With 95% mean SoC	3080	91.1
With 85% mean SoC	2761	89.6
With 80% mean SoC	2602	87.2
With 75% mean SoC	2425	85.7

4.5 Chapter remarks

This chapter proposes an energy management strategy of a FESS. The aim of the flywheel is to smooth the net power flow injected to the grid by a variable speed wind turbine. An optimal energy management of the storage device is defined as that which minimizes the difference between the energy to be injected or absorbed by the storage device and the energy that is finally exchanged by it during a given time interval.

The formulation and solution of an optimization problem in GAMS for a set of sufficient representative wind profiles provides the optimal mean SoC of the flywheel. From the solution of this optimization problem a function is produced to compute offline a close to optimal flywheel angular speed reference. This simplifies the implementation of the algorithm online. The optimization results also show that the higher mean wind power, the higher mean rotating speed of the flywheel. In all cases, the optimal operation of the storage device is in the range of 89 to 93% of its mean SoC.

Simulation results for an illustrative example show that the flywheel with the proposed energy management algorithm is able to achieve a 91.9% of turbulent energy component reduction in the high frequency components of the wind power. This is close to the 97.1% obtained by the optimal operation of the flywheel.

5

Design and experimental validation of a novel control strategy of a flywheel for power smoothing of wind power plants

Summary.- This chapter deals with the design and the experimental validation in scale-lab test benches of an energy management algorithm based on feedback control techniques for a flywheel energy storage device. The designed energy management algorithm is based on the results obtained in Chapter 4. The aim of the flywheel is to smooth the net power injected to the grid by a wind turbine or by a WPP. In particular, the objective is to compensate the power disturbances produced by the cycling torque disturbances of the wind turbines due to the airflow deviation through its tower section. The chapter describes the control design, its tuning, as well as the description of the experimental setup and the methods for the experimental validation of the proposed concepts. Results show that the fast wind power fluctuations can be mostly compensated through the flywheel support.

5.1 Introduction

As explained in previous Chapters, to minimize the effects of the variability of wind power, an ESS can be used [83, 249, 315]. Furthermore, the utilization of energy storage devices together with wind turbines have some additional functionalities, such as frequency support and matching of forecasted and real active power production. Flywheel systems are effective for wind power smoothing. As noted in Chapter 4, related studies address two control levels: the design of high level energy management algorithms of the storage device and the research in the low level control scheme of the electrical machine.

The inclusion of a high-level control algorithm is motivated from the need of maintaining the State of Charge (SoC) within certain operating limits so as to ensure the availability of the storage device to compensate the wind power fluctuations when required. Within the related studies, it can be found several proposals based on fuzzy-logic schemes [153, 63, 180]. These high-level energy management algorithms determine the set points to the low-level control scheme of the electrical machine of the flywheel, i.e. the instantaneous torque (or power) reference, from the measurement of the power of the wind turbine and the SoC of the storage device. Despite the fact that the SoC is maintained within certain operating limits in the previous works, its average value is not controlled. However, in [82] it has been concluded that an improvement in the power smoothing can be achieved if the average SoC is adjusted with respect to the expected energy to be exchanged between the network and the storage device.

This chapter complements previous works depicted in Chapter 4. It proposes a novel high-level control algorithm of a flywheel-based storage device using the expected energy exchanged to maintain an optimal SoC and thus to improve the smoothing of the power injected by a wind turbine or by a WPP. The high-level control algorithm is in charge of managing the energy stored in the flywheel so that it can compensate as much as possible the turbulent components of the wind power. The aim of the control algorithm is to maintain a determined average SoC, i.e. an average rotational speed of the flywheel, while also permitting the fast accelerations and decelerations of the machine for compensating the turbulent components of the wind power. Similarly to [54, 153, 63, 180], the high-level control algorithm determines the set points to the low-level one from the measurement of the rotational speed of the flywheel and the wind power. As a difference with the above mentioned works, the proposal of the present chapter is based on active power control through an I-P control structure [158, 201] instead of

fuzzy-logic-based control schemes. The proposed control scheme has been evaluated experimentally in laboratory. The main advantages with respect to previous works based on fuzzy-logic are design procedure, ensuring specific dynamic performance, and the simplicity of the proposed algorithm. The latter is an important point since the computation time in these schemes could be a constraint for their implementation in industrial computers [63].

5.2 Conceptual diagram of the proposed control scheme

The present chapter, as that depicted in Chapter 4, focuses on the smoothing of the turbulent components of the power which mainly correspond to the rotating sampling effect. Only partial load operation of the wind turbines is considered, as the variability of the power generated is alleviated from the action of the pitch actuator in the full load operating region of the turbines.

To smooth the net power injection to the grid, the flywheel is added to the point of connection of the wind turbine. The flywheel is in charge of fastly injecting and absorbing power so that it can compensate the wind power fluctuations. The turbulent components of the wind power to be compensated are obtained from filtering the wind power measurement P_{wt}. This power filtering is part of the flywheel control system which receives also the measurement of the flywheel speed ω_{fw}. From these signals the high-level control algorithm sets out the electrical torque reference T^*_{fw} for the machine side converter of the flywheel, so that the net power injection by the flywheel and the wind turbine becomes smoothed as much as possible. The proposed control scheme is detailed in Figure 5.1.

The electrical torque reference T^*_{fw} set by the energy management algorithm of the flywheel permits the storage device to accelerate and brake but also to maintain a determined average SoC within the specified operating limits.

In [82], it is found that in order to operate the flywheel in an optimal way, i.e. to smooth as much as possible the turbulent components of the wind turbine, the storage device has to maintain a determined average rotational speed function of the average power generated by the wind turbine. This is motivated from the dependence between the power capacity of the flywheel and its rotational speed. In fact, the power that the flywheel is capable of exchanging results from the product of its rotational speed and its rated torque. Moreover, the magnitude of the turbulent components of wind power to be compensated by the flywheel depends on the power generated by the

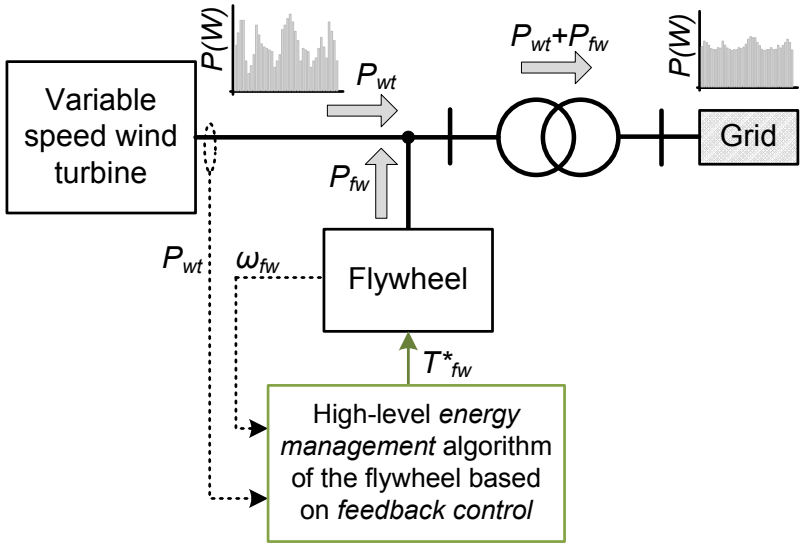

Figure 5.1: Conceptual diagram of the proposed control scheme

turbine which is greater in high wind speeds.

Accordingly, it is proposed to adjust the average SoC of the flywheel with the average power generated by the wind turbine to fit the power capacity of the flywheel to the expected wind power to be compensated.

Also, the inclusion of an energy management algorithm of the flywheel is motivated from the following reasons:

1. The limited energy capacity of the flywheel. Without an energy management strategy, the storage device would frequently become fully charged or discharged, thus limiting its operability.

2. The need of compensating the high-standing losses of the flywheel. Compensating the turbulent components of the wind power requires the flywheel to exchange a power series with average value close to zero. However, without a proper compensation of the standing losses, the storage device will become continuously discharged.

3. The possibility of reducing the losses of the flywheel in operation. The losses of the flywheel increase with the rotational speed. Thus, there is no reason to concern, for instance, high average rotational speeds if the flywheel is intended of just exchanging low levels of power.

Following sections describe the design of the energy management algorithm of the flywheel.

5.3 Design of the high-level energy management algorithm of the flywheel

The energy management algorithm of the flywheel is presented in Figure 5.2. As it can be noted, the algorithm consists of two main parts: the so-called inputs filtering and processing; and the feedback control. These two parts are described in the next subsections.

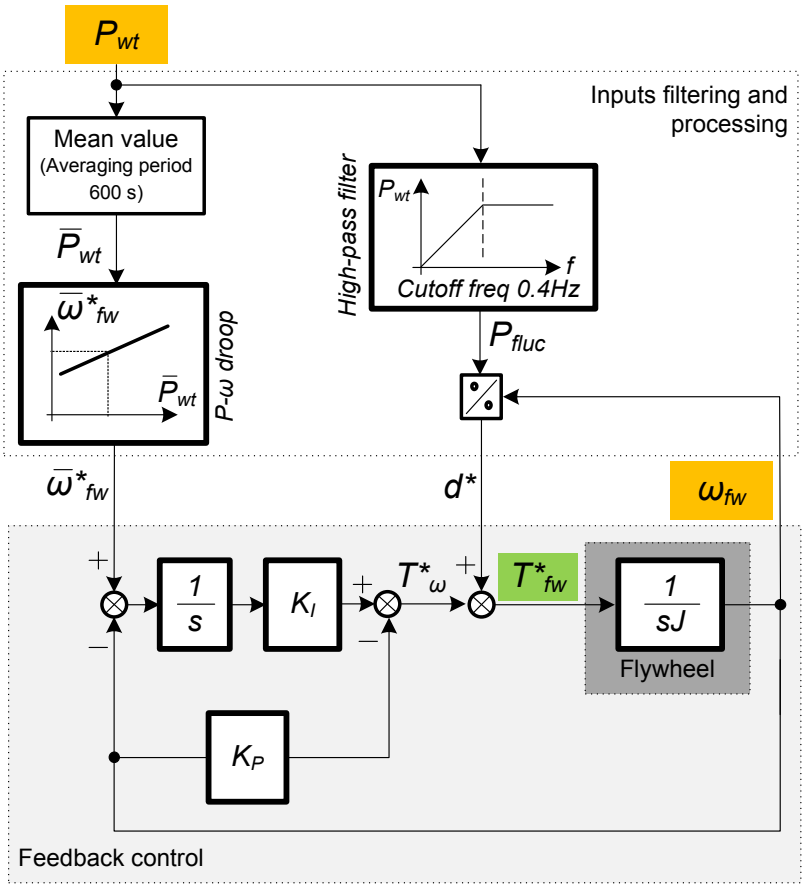

Figure 5.2: Energy management algorithm of the flywheel. The input signals of the algorithm (P_{wt} and ω_{fw}) are shaded in orange, while the output T^*_{fw} is shaded in green

5.3.1 Inputs filtering and processing

As noted in Section 5.2, the high-level energy management algorithm of the flywheel has two main objectives: to let the flywheel maintain an optimum average rotational speed while enabling the fast accelerations and decelerations of the system. Mathematically, achieving these two objectives means to track the average rotational speed reference $\bar{\omega}^*_{fw}$ and the high frequency torque reference d^*. These signals are the setpoints enter the feedback control in different point as can be seen in Figure 5.2. The block "inputs filtering and processing" in the energy management algorithm computes these setpoint signals from the input signals ω_{fw} and P_{wt}. The optimum average rotational speed $\bar{\omega}^*_{fw}$ depends on the mean wind power (with averaging period several minutes) and is obtained from solving an optimization problem presented in [82]. In the present chapter, the dependency between these two variables is represented by the $P - \omega$ droop characteristic (see Figure 5.2).

While the optimum average rotational speed $\bar{\omega}^*_{fw}$ is a slowly varying signal, the torque reference d^* contents high frequency components. The reference d^* is computed from

$$d^* = \frac{P_{fluc}}{\omega_{fw}}, \tag{5.1}$$

where P_{fluc} corresponds to the fast wind power fluctuations that must be attenuated. This signal is obtained from passing the wind power measures through a high pass filter. The cutoff frequency of this filter is chosen so that the power disturbances caused by the rotating sampling effect passes through the filter without significant distortion.

5.3.2 Feedback control

The aim of the feedback control is to ensure the tracking of the slowly varying reference $\bar{\omega}^*_{fw}$ and the fast varying reference d^*. To this end, an I-P controller acts on the torque reference T^*_ω to regulate the instantaneous rotational speed of the flywheel ω_{fw}. The I-P structure facilitates the development of a systematic procedure for the tuning of the controller. Also, it satisfies the two first motivations (or control requirements) for the energy management algorithm that are depicted in Section 5.2. As a reminder, the first and the second requirement refer to the need of not overcoming the operating limits of the storage device, and of compensating the standing losses of the flywheel. These requirements are satisfied by the proportional and integral parts of the controller. The third requirement of the energy management algorithm refers to the need of varying the average SoC with the average

wind power. This is satisfied by adding the previously presented $P-\omega$ droop characteristic (see Figure 5.2).

As can be seen in Figure 5.2, the torque reference T_{fw}^* is the sum of the torque d^* and the compensation term

$$T_w^* = K_I \int (\bar{\omega}_{fw}^* - \omega_{fw}) dt - K_P \omega_{fw}. \tag{5.2}$$

The parameters K_I and K_P of the I-P controller are tuned to shape the frequency responses of the transfer functions from $\bar{\omega}_{fw}^*$ to ω_{fw} and from d^* to ω_{fw}.

Note that the error between the reference signal and the feedback of the plant is affected by a pure integrator in both P-I and I-P controllers. However, as a difference with conventional P-I controllers, the proportional gain does not affect the error signal but the feedback of the plant instead in I-P controllers (Figure 5.2).

For the controller design purpose, the plant (the flywheel) is characterized by its mechanical dynamics imposed by the inertia J (see Figure 5.2). The fast electrical dynamics of the machine is omitted as being much faster than the mechanical one. Accordingly, the flywheel speed is given by

$$\omega_{fw}(s) = \frac{1}{Js + K_P} \left(d^*(s) + \frac{K_I}{s} (\bar{\omega}_{fw}^*(s) - \omega_{fw}(s)) \right). \tag{5.3}$$

Then, reorganizing terms

$$\omega_{fw}(s) = T_{d^*\omega}(s) d^*(s) + T(s) \bar{\omega}_{fw}^*, \tag{5.4}$$

where

$$T_{d^*\omega}(s) = \frac{s}{Js^2 + K_P s + K_I}, \tag{5.5}$$

$$T(s) = \frac{K_I}{Js^2 + K_P s + K_I}. \tag{5.6}$$

The reference d^* is not a completely exogenous signal since it depends on the flywheel speed according to (5.1). To consider this fact in the parameter tuning and guarantee stability in all possible values of power and flywheel speed, the reference is expressed as

$$d^* = \delta \cdot \omega_{fw}, \tag{5.7}$$

where $\delta = P_{fluc}/\omega_{fw}^2$ is a time varying parameter taking values in the interval $[-\delta_{max}, \delta_{max}]$ with

$$\delta_{max} = \frac{P_{max}^*}{\omega_{min}^2}. \tag{5.8}$$

With the previous definitions and using the small gain theorem [271], it is possible to state conditions to ensure stability of the close loop systems for all acceptable values of power and rotational speed. More precisely, the closed loop system is stable for all values of δ in $[-\delta_{max}, \delta_{max}]$ if the infinite norm of the transfer function from d^* to the output of the plant ω_{fw} ($T_{d^*\omega}$) does not exceed the upper limit δ_{max}, i.e.

$$||T_{d^*\omega}||_\infty = \max_\omega |T_{d^*\omega}(j\omega)| < \delta_{max}. \tag{5.9}$$

Assuming that the transfer function $T_{d^*\omega}$ has two real and different poles, i.e.

$$\begin{aligned} T_{d^*\omega} &= \frac{s/K_I}{(s/p_1+1)(s/p_2+1)} \\ &= \frac{s/K_I}{\frac{1}{p_1 p_2}s^2 + \left(\frac{1}{p_1}+\frac{1}{p_2}\right)s + 1}. \end{aligned} \tag{5.10}$$

If p_1 is the dominant pole ($p_1 \ll p_2$), then

$$||T_{d^*\omega}||_\infty < \frac{p_1}{K_I} < \frac{1}{\delta_{max}}. \tag{5.11}$$

Therefore, the integrator gain K_I should satisfy

$$K_I > p_1 \delta_{max} \tag{5.12}$$

to ensure closed loop stability for all possible values of power and speed. Further, the proportional gain can be obtained from comparing the denominators of (5.5) and (5.10),

$$K_P = K_I \left(\frac{1}{p_1} + \frac{1}{p_2}\right), \tag{5.13}$$

where $p_2 = K_I/Jp_1$.

In Figure 5.3, an asymptotic graph of the frequency responses of $T_{d^*\omega}$ and T can be observed. The pole p_1 defines the bandwidth of the speed tracking as well as the infinity norm of $T_{d^*\omega}$. Therefore, once the bandwidth of T, the parameters of the controller can be computed from (5.12) and (5.13).

5.4 Experimental validation

This section describes the flywheel test bench, the wind turbine emulator as well as the rest of the laboratory equipment used for configuring the system

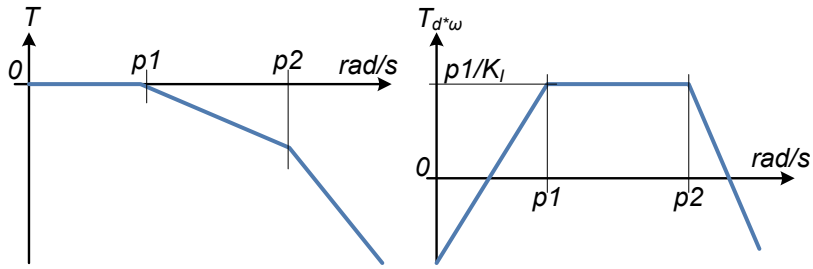

Figure 5.3: Asymptotic diagram of the frequency responses of the transfer functions $T_{d^*\omega}$ and T

for the purposes of the study. Emphasis is done in presenting those actions needed to emulate the variability of the power of the wind turbine in a lab-scaled equipment among other considerations. Then, experimental results are analysed with the aim of validating the proposed energy management algorithm of the flywheel.

5.4.1 Description of the experimental setup

Figure 5.4 presents an scheme of the experimental setup. As it can be noted, the system is composed by a flywheel test bench, a wind turbine emulator, a coupling transformer which connects the system to the grid, measurement devices and communication and control devices. Each of these main components of the system are detailed as follows.

Flywheel test bench

The flywheel test bench has been explained in detail in Chapter 3. The reader is referred to that chapter for further details. As a reminder, the system is composed by a rotating disk mechanically coupled to the shaft of a permanent magnet synchronous machine (PMSM). The electrical machine is controlled by a set of back-to-back power converters. These power converters are driven by digital signal processor (DSP)-based control boards.

As previously noted, the flywheel is added to the point of connection of the wind turbine emulator. The design and experimental validation of the low level algorithm of the power converters of the flywheel test bench are deeply explained in [84]. As a summary, the grid side converter of the system is in charge of regulating the voltage of the dc link of the back-to-back power converters and also the reactive currents exchanged with the network. The control of the machine side converter is the field oriented vector control

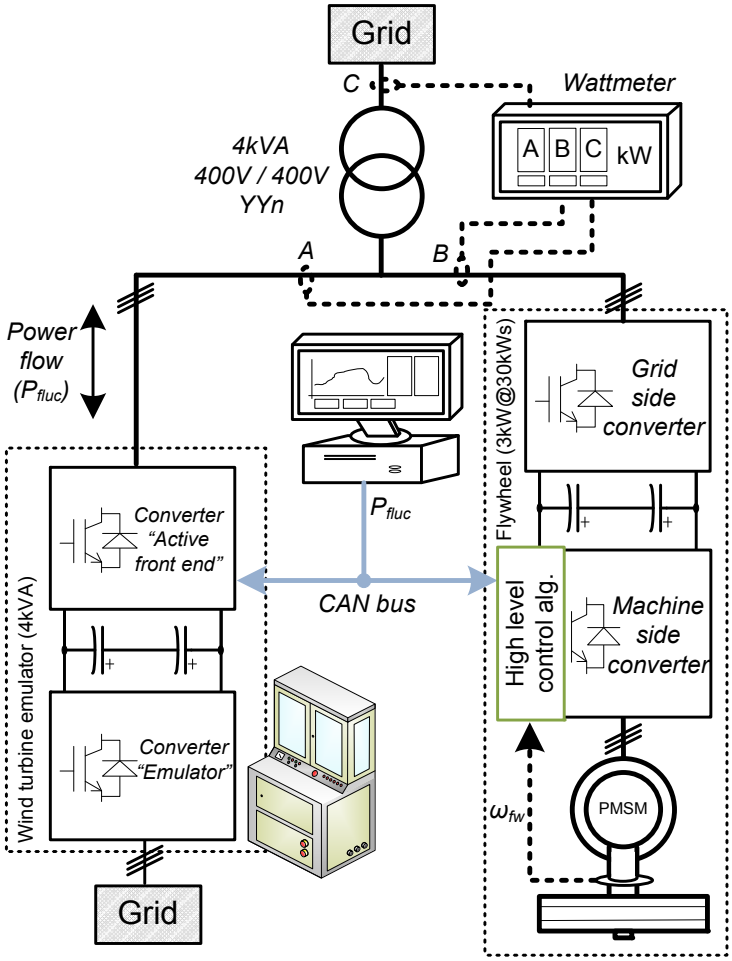

Figure 5.4: Scheme of the experimental setup

system of the PMSM [171, 288]. This control algorithm governs the PMSM so that it follows the instantaneous electrical torque T^*_{fw} referenced by the energy management algorithm.

The rated power capacity of the storage device is 3 kW, and the energy capacity is 30 kWs. Further parameters of the system are presented in Table B.2 in Appendix.

Wind turbine emulator

The wind turbine is emulated by a cabinet composed by two identical three phase voltage sources in back-to-back configuration [254] (see Figure 5.4).

A bidirectional power flow through the converters is possible since they can be operated as either active rectifiers or active inverters. According to Figure 5.4, power flows from the ac side of the converter "emulator" to the ac side of the converter "active front end" while representing the behaviour of a generator. The reverse process depicts the behaviour of a load. The low level control algorithms of the power converters of the cabinet receive the series of active and reactive power set points to represent the power profile of the wind turbine. The rated apparent power of the cabinet is bounded to 4 kVA. The relevant parameters of the cabinet for the purposes of the present chapter are presented in Table B.2 in Appendix. Further details of the cabinet are presented in [254].

Measurement devices

For the purposes of the chapter, it is needed to analyze the variability of the power injected by the emulator of the wind turbine, and its attenuation from the inclusion of the flywheel. Accordingly, a wattmeter registers simultaneously the power series in the points A, B and C depicted in Figure 5.4 for their post processing and analysis. These points corresponds to the terminals of the wind turbine emulator, the terminals of the flywheel test bench, and the point of connection of the system to the network respectively. Figure 5.5 depicts the wattmeter, the coupling transformer for the connection of the system to the network and the wind turbine emulator.

Communications

As presented in Figure 5.4, the wind turbine emulator represents the variability of the power of the wind turbine following the power set-points sent through a Controller Area Network (CAN) bus by a computer. CAN bus is also used to let the energy management algorithm of the flywheel know the

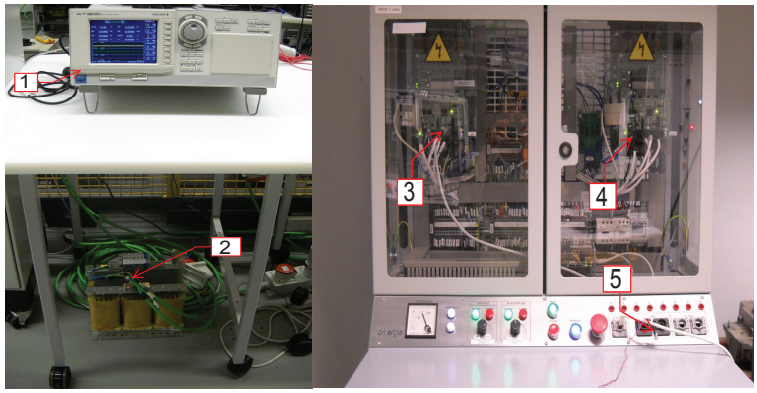

Figure 5.5: Experimental setup. From left to right: 1) wattmeter; 2) coupling transformer; 3) power converter of the wind turbine emulator "active front end"; 4) power converter "emulator"; 5) CAN bus port

above mentioned wind power. The precise clocking of the digital signal processor (DSP) of the control board the machine side power converter of the flywheel is used as a time basis to coordinate the exchange of signals between the computer, the wind turbine emulator and the flywheel. In particular, the signals are sent through the CAN bus each 20 milliseconds.

5.4.2 Assumptions for the emulation of the fluctuating components of wind power

According to Figure 5.2, the average optimum rotational speed of the flywheel $\bar{\omega}^*_{fw}$ and also the wind power fluctuations P_{fluc} have to be determined from filtering the generated power by a wind turbine P_{wt}. However, the presented experimental validation avoids the emulation of the power P_{wt} and consequently its filtering. Only the wind power fluctuation P_{fluc} is actually emulated instead by the wind turbine emulator. Thus, P_{fluc} is a power profile with average value close to zero that is obtained from the simulation of the system and the application of the high-pass filter to the output of the model of the wind turbine P_{wt}.

This is carried out with the aim of adjusting the magnitude of the wind power fluctuations P_{fluc} to the actual power ratings of the flywheel test bench and the wind turbine emulator. The present chapter considers a scaling factor of 20 for the power of a 1.5 MW wind turbine. The magnitude of the resultant profile P_{fluc} is similar to the ratings of the wind turbine emulator (4 kVA), and also to the ratings of the flywheel test bench (3 kW).

Therefore, the size of the flywheel test bench can be considered adequate to compensate the fluctuations of the power of a wind turbine with a rated power 1.5/20 MW.

Figure 5.6 plots the results of the simulation of a 1.5 MW wind turbine. Its power output profile P_{wt} has been scaled by a factor of 20. The subplot below shows the resultant P_{fluc}. As it can be noted, the magnitude of P_{fluc} is bounded to 3 kW approximately, which corresponds to the rated power of the flywheel test bench. The cutoff frequency of the high pass filter of P_{wt} is set to 0.4 Hz so that the rotating sampling effect can be represented. The details of this filter can be found in Appendix.

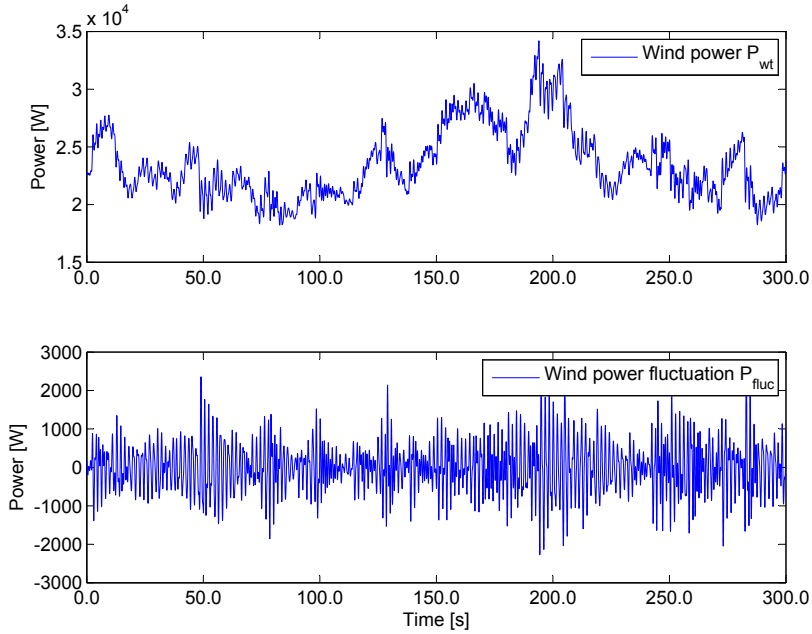

Figure 5.6: Scaled magnitude of the power output of a 1.5 MW wind turbine and the fluctuating components of it from a cutoff frequency of 0.4 Hz

As a consequence of the direct emulation of P_{fluc}, the $P-\omega$ droop characteristic (Figure 5.2) is not applied. Therefore, the optimum average rotational speed of the flywheel $\bar{\omega}^*_{fw}$ will be step-profiled in following sections for evaluating the performance of the designed feedback control.

5.4.3 Determination of the control parameters for the experimental system

Section 5.3.2 depicts the procedure for the tuning of the parameters of the I-P structure which builds up the feedback control. The present section presents the particular values of the controller determined for the study case.

As it can be noted in equations (5.12) and (5.13) the parameters of the I-P controller K_P and K_I depend on the location of the pole p_1, which in turn bounds the value of the pole p_2. The pole p_1 determines the time response of the control loop for the reference $\bar{\omega}^*_{fw}$. This time response can be very slow since the dynamics of $\bar{\omega}^*_{fw}$ depends on the average value of P_{wt} with an averaging period 600 seconds. Thus, the pole p_1 is set to $p_1 = 0.01$ rad/s. This implies a time response of the control loop system of 628 seconds approximately.

The value of K_I also depends on the parameter δ_{max} (see equation (5.8)). As a reminder, this parameters is given at maximum power developed by the flywheel P_{max} and at minimum operating rotational speed ω_{fw}. The maximum power is given by the maximum torque developed by the flywheel (12.2 Nm). Accordingly, the limit of the time varying parameter results $\delta_{max} = 0.122$ W/(rad/s)^2, assuming a minimum flywheel speed of 100 rad/s. Then, from equation (5.12), the parameter K_2 becomes

$$K_I = p_1 \delta_{max} = 0.0012 \text{ W/(rad/s)}. \tag{5.14}$$

Finally, applying equation (5.13), the value of the parameter K_P is set to

$$K_P = 0.1307 \text{ W/(rad/s)}^2 \tag{5.15}$$

provided that $p_2 = K_P/(J \cdot K_1)$ and J is 0.868 kg·m^2.

Figure 5.7 presents the frequency responses of T and $T_{d^*\omega}$ corresponding to the previous designed values of K_I and K_P. As it can be noted, the closed loop system will be able to track speed references until the cutoff frequency of 0.01 rad/s, which corresponds to the location of the pole p_1. The frequency response of $T_{d^*\omega}$ shows that the infinity norm is below the limit $(\delta_{max})^{-1} = 8.19$ Nm/(rad/s) (18.3 dB). The graph also shows that the system is able to track torque references in the ranging from 0.01 to 0.1 rad/s with the maximum gain allowed by the stability guarantee and the flywheel torque limits.

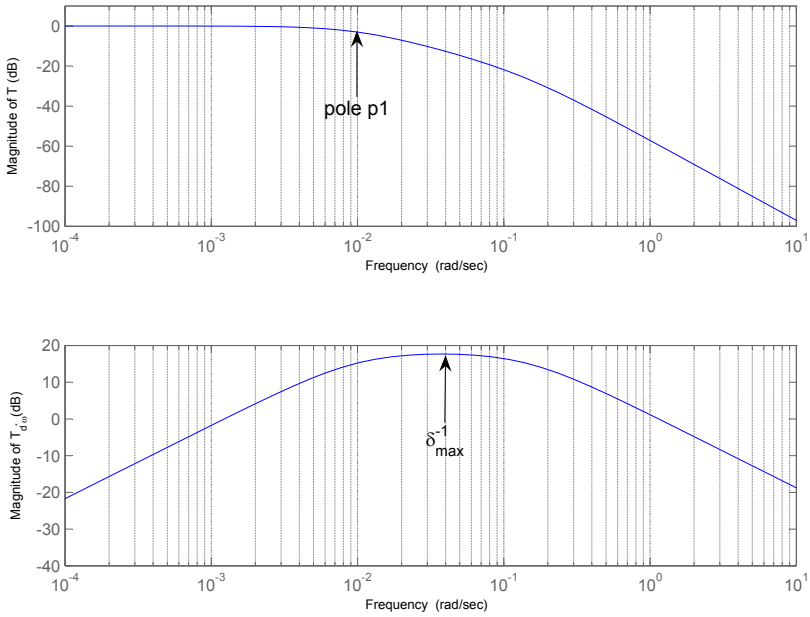

Figure 5.7: Bode diagrams of the closed loop transfer function T (from $\bar{\omega}^*_{fw}$ to ω_{fw}) and the transfer function $T_{d^*\omega}$ (from d^* to ω_{fw})

5.4.4 Analysis of the experimental results

Following content present the obtained experimental results to evaluate the performance of the proposed energy management algorithm of the flywheel. As noted in previous sections, the wind turbine emulator reproduces the fluctuating power components depicted in Figure 5.6, that the flywheel test bench is in charge of compensating. Accordingly, Figure 5.8 depicts the actual power developed by the wind turbine emulator, the flywheel and the net power exchanged with the network.

As it can be noted, the flywheel compensates the fluctuating components of wind power, leaving the net power profile almost constant. However, the average value of the power of the flywheel and thus of the net power exchanged with the network is not zero due to the necessity of compensating the power losses of the flywheel for maintaining the indicated average rotational speed $\bar{\omega}^*_{fw}$. The optimal average rotational speed is close to 220 rad/s in this case [82]. As this setup is meant to be a proof of concept system, the losses in the flywheel test bench are much higher than in a commercial flywheel storage device. In particular, the energy efficiency of the test bench is 73%, and the power losses depends on the rotational speed, reaching up

to 800 W at rated speed [84]. These figures are far from those corresponding to a high-tech flywheel, in which the energy efficiency is around 90% and the power losses level at rated speed represents just 2% of the rated power [179].

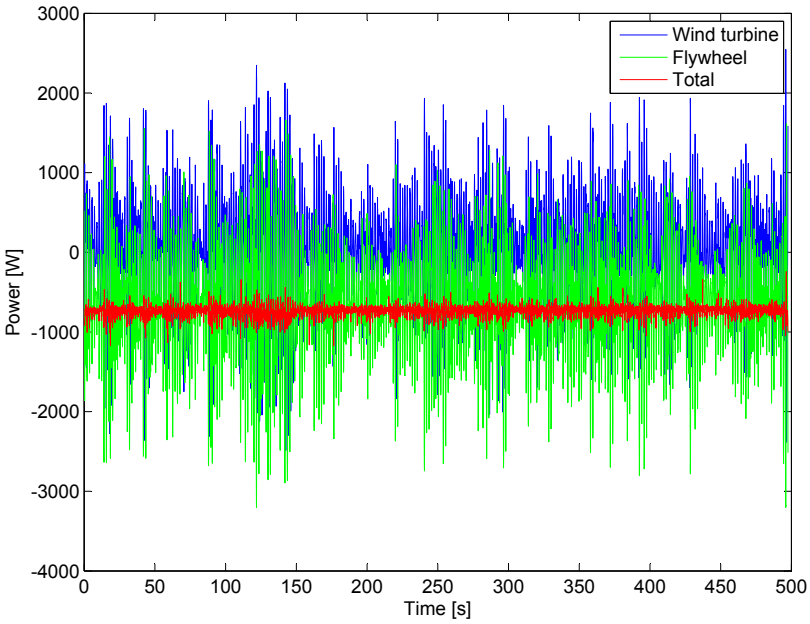

Figure 5.8: Power of the wind turbine emulator, the flywheel and the net power exchanged with the network. The average rotational speed of the flywheel is $\bar{\omega}_{fw} = 220$rad/s

Figure 5.9 examines more closely the previously presented power profiles in Figure 5.8. The power profile of the flywheel and the profile of the net power exchanged with the network have been corrected by subtracting the standing losses of the flywheel at the constant speed of $\bar{\omega}_{fw} = 220$ rad/s. This way, the average value of the power exchanged with the network and the average power profile of the flywheel are zero. As a result, in this Figure 5.9 it can be better observed that the instantaneous power of the flywheel (green line) compensates to a great extent the fluctuating components of the power of the wind turbine (blue line). This instantaneous regulation of the power of the flywheel is governed by the torque reference d^* (see Figure 5.2).

The RMS currents of the flywheel, the wind turbine emulator and the network are depicted in Figure 5.10. As shown, the magnitude of the cur-

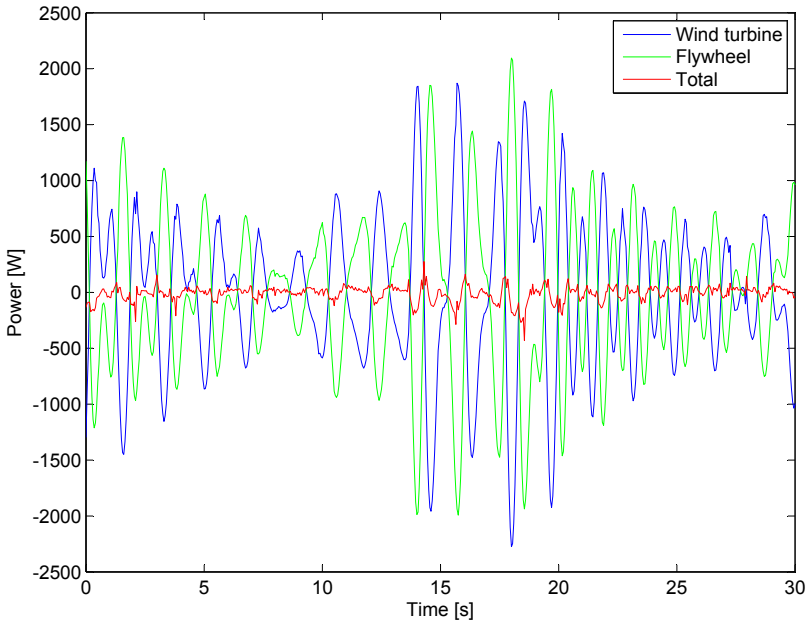

Figure 5.9: Instantaneous power of the wind turbine emulator (blue line), as well as the power profiles of the flywheel and at the network terminals subtracting the standing losses of the flywheel. The average rotational speed of the flywheel is 220 rad/s

rents of the flywheel are much higher than the currents of the wind turbine emulator, due to the necessity of compensating the losses of the system, as previously discussed. Without the proper losses compensation, the storage device will become completely discharged.

Apart from compensating the fast fluctuations of the power of the wind turbine, the second objective of the feedback controller of the flywheel is to maintain a determined average rotational speed $\bar{\omega}^*_{fw}$. The performance of this control loop is depicted in Figure 5.11. As it can be observed, the flywheel is steadily rotating at 220 rad/s in average and the time response to a step-profiled average speed reference $\bar{\omega}^*_{fw}$ from 220 rad/s to 270 rad/s is around 600 seconds, as imposed by the design of the controller presented in Section 5.4.3. Moreover, in the subplot below it can be observed that the voltage of the dc-link of the flywheel test bench keeps stable at 750 V in average, while regulating the rotational speed of the flywheel and compensating the fast wind power fluctuations.

The spectrum of the power of the wind turbine emulator, as well as the

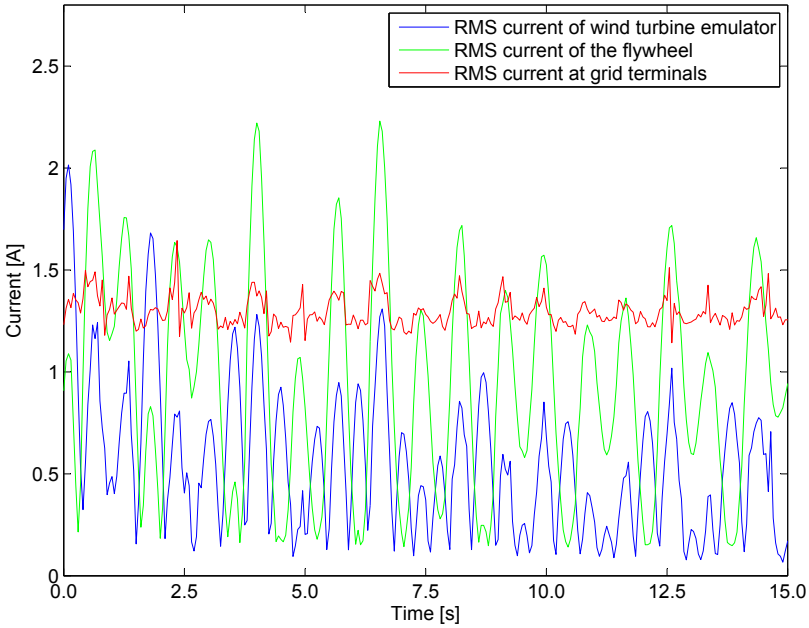

Figure 5.10: RMS electrical currents of the wind turbine emulator, the flywheel and the network. The average rotational speed of the flywheel is $\bar{\omega}^*_{fw} = 220\text{rad/s}$

total power exchanged with the network in case of considering the support of the flywheel are depicted in Figure 5.12. The average rotational speeds of the flywheel are 120 rad/s and 220 rad/s. As it can be noted, the wind turbine emulator clearly represents the rotational sampling effect of the turbine at 0.6 and 1.2 Hz approximately. The rotating sampling effect is mostly compensated with the flywheel support. The constant component of the power spectrum of the flywheel due to its losses has been subtracted so that it can be better observed the performance of the system. This figure depicts the support of the flywheel considering different average SoC. It is worth noting that the support that the flywheel can provide is better while rotating at 220 rad/s in average (close to the optimum) than while rotating at 120 rad/s. This is because the power capability of the flywheel is bounded by the product of the speed and the rated torque of the electrical machine and thus, as discussed in [82], there is an average optimal speed of the flywheel $\bar{\omega}^*_{fw}$ dependent on the magnitude of the fluctuating components of wind power to be compensated.

The performance of the system considering different flywheel average oper-

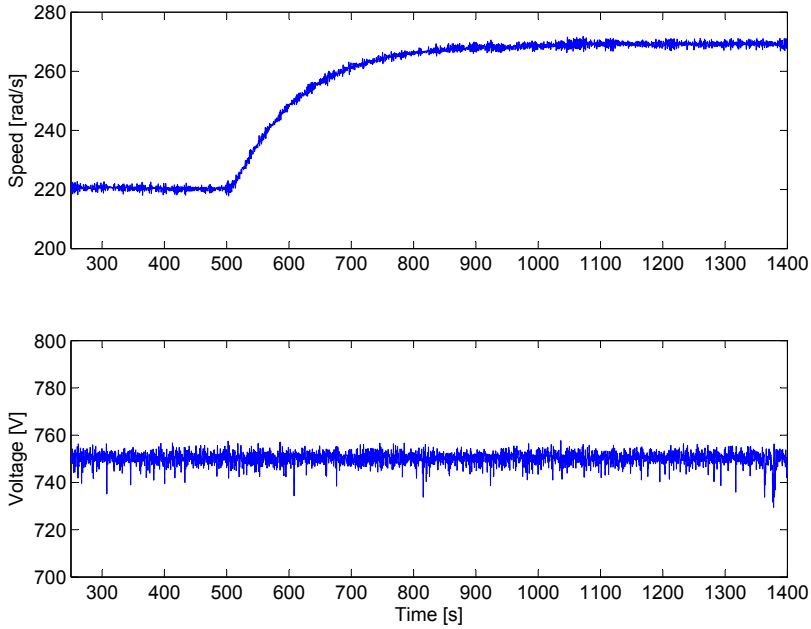

Figure 5.11: Rotational speed of the flywheel in response to a step-profiled average speed reference $\bar{\omega}^*_{fw}$ from 220 rad/s to 270 rad/s. The dc-link voltage of the flywheel test bench is presented in the bottom subplot

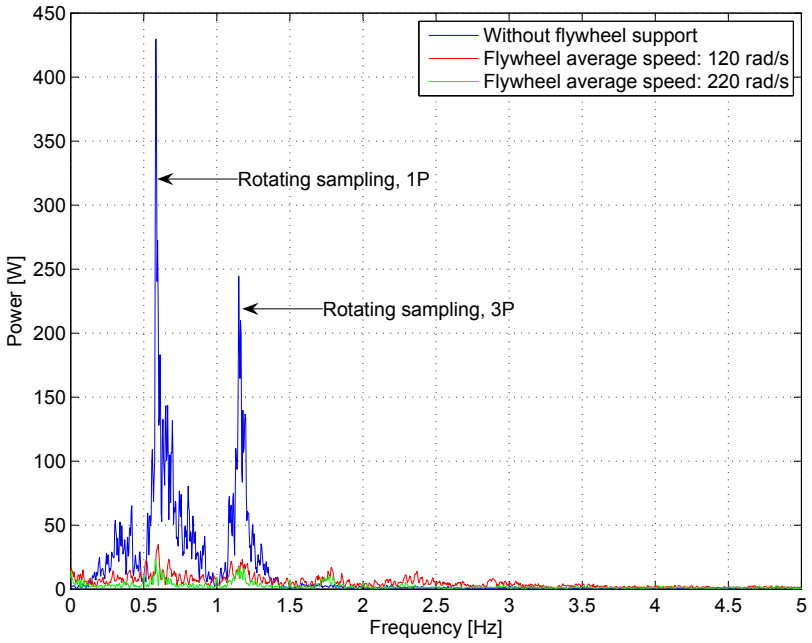

Figure 5.12: Spectrum of the net power exchanged with the network without flywheel support, as well as with flywheel at different average SoC. The average power losses of the flywheel have been subtracted

ating rotational speeds, is quantified from the attenuation of the fluctuating components of the net power exchanged with the network. This magnitude is computed from the data shown in Figure 5.12. The ratio between the energy of the fluctuating components of the net power exchanged with the network considering the flywheel support (red and green lines in Figure 5.12), and the fluctuating components of the wind turbine emulator (blue line in Figure 5.12), gives the attenuation. It is found an attenuation of 85% while the flywheel is rotating at 120 rad/s in average. The attenuation reaches the 92% with 220 rad/s as the average rotational speed of the flywheel.

5.5 Chapter remarks

A high-level energy management algorithm of a flywheel for power smoothing in wind generation systems has been designed. The algorithm is based on feedback control techniques. The controller has been conveniently formulated and tuned so that the desired time response of the storage device

can be ensured. The algorithm successes in letting the flywheel maintain an optimum average rotational speed while enabling the fast accelerations and decelerations of the storage device for smoothing the fast fluctuating components of the power of the wind turbine. The maintenance of the indicated average rotational speed of the flywheel avoids the progressive discharge of the storage device in its operation. Also, the control capability of the average rotational speed of the flywheel, permits to adjust the average SoC of the storage device to the magnitude of the power and energy to exchange. The controller has been validated experimentally in scale-lab equipments. Results show that most of the fluctuating components of the power of the wind turbine due to the rotating sampling effect can be compensated through the flywheel support.

This chapter proves that the short time response and high controllability define flywheel systems as well suited devices to compensate the variability of the power generated by wind turbines and thus, to promote their integration into the network. The quality of the power injected into the grid by a wind turbine or by a WPP, can be improved by adding a flywheel-based ESS to the generating facility.

6

Participation of wind power plants in system frequency control: review of Grid Code requirements and control methods

Summary.- Active power reserves are needed for a proper operation of the electrical system. These reserves are continuously regulated in order to match the generation and consumption in the system and thus, to maintain a constant electrical frequency. These reserves are usually provided by synchronized conventional generating units like hydraulic or thermal power plants. With the progressive displacement of these generating plants by non-synchronized renewable-based power plants (e.g. wind and solar) the net level of synchronous power reserves in the system becomes reduced. Therefore WPPs are required, according to some European Grid Codes, to provide also power reserves as conventional generating units do. This chapter focuses in the review of the requirements set by Grid Codes, but also in control methods of wind turbines for their participation in primary frequency control and inertial response.

6.1 Introduction

For a stable operation of the electrical network, system frequency control is decisive. It ensures a continuous adaptation of power generation to power consumption. The power balance in the electrical network is interrelated to the network frequency via all synchronous generators connected to it. E.g. an increase in the load decelerates the synchronous generators and thus leads to a frequency drop. As frequency is uniform throughout the interconnected network, it is convenient to use it as a control variable for a decentralized control system: the network frequency control. It makes use of the power plants in the network, which - according to their abilities and agreements - adapt their active power feed-in in according to the current system requirements. Thus, the power plants involved require a certain level of active power reserves. Traditionally and still typically, it is conventional generation plants, like hydroelectric and thermal power plants, which are used for frequency control. The ability of a system to maintain its frequency into a certain tolerance band is called frequency stability.

Another important function of conventional power plants for frequency control is the passively provided so-called instantaneous power reserve. Any imbalance between power generation and consumption is instantaneously balanced due to the physical principle of the synchronous generator. The large inertia of the rotating generator set works as a buffer storage, leading to the mentioned change in rotational speed and thus system frequency. The larger the synchronised inertia in the system, the slower the change of frequency [163].

The stepwise replacement of conventional generating units by WPPs will have a significant impact on the system frequency behaviour. First, the grid looses the active power reserves of conventional plants. And second, it looses instantaneous power reserves, because wind turbine generator sets are operated decoupled from system frequency, which allows for aerodynamically efficient operation. In detail, the turbine's synchronous or asynchronous generators are connected to the grid via fast controlled power electronics [312, 177, 83].

The contribution of the system inertia to limit the rate of change of frequency against active power disturbances may be insufficient for systems with high penetration of renewables. The studies by the Irish regulator set out that system frequency stability could be compromised with 60-70% of the total instantaneous power generated from WPPs [94].

In order to maintain system frequency stability in a network with an increasing share of wind power, wind turbines will have to take more and

more tasks of conventional power plants related to frequency control. This is reflected by a gradual development of more stringent requirements by system operators in regard of the integration of WPPs into network frequency control [101]. According to some system operators, e.g. the Irish operator [95], WPPs are already required to provide power reserves. Also, future regulations will appear with the development of new requirements regarding inertial response by WPPs [101].

Even though the power output of wind turbines depends on the non-reliable and difficultly predictable wind speed, and even though the generator set is not providing passive instantaneous power reserve, there are methods for WPPs to actually provide power reserves and thus to participate in system frequency control. Such abilities will be crucial for a sucessful integration of WPPs into the grid.

This chapter presents a review of some European Grid Codes and future trends regarding the tasks of WPPs related to participation in frequency control. Also, it covers a literature review about the proposed methods for enabling wind turbines to provide primary reserves and the aspects related to the inertial response of wind turbines.

6.2 Review of European Grid Codes regarding frequency control support

Due to the island situation of Ireland and UK, frequency control is a particularly challenging task in these electrical networks since they do not have access to the large power reserves in the interconnected network of continental Europe. Thus, requirements for WPPs are significantly stricter in these networks than in the continental grid. However, since the share of wind power also in the continental European grid rises, requirements will become stricter.

Accordingly, this section firstly depicts the basis for understanding the deployment sequence of power reserves for frequency control. Secondly, particular requirements for WPPs regarding frequency control according to the Grid Codes of Ireland and UK are presented. Finally, future trends based on the latest draft of the ENTSO-E [101] are discussed.

6.2.1 Power reserves: Definition and deployment sequence for frequency control

Power reserves can be defined as the additional active power (positive or negative) that can be delivered by a generating unit in response of a power unbalance in the network between generation and consumption. Three different reserve levels can be defined: primary, secondary and tertiary reserve [140]. This terminology is widely accepted; however nomenclature can vary from one country to another. With the aim of harmonizing these concepts, on June 2012 the European Network of Transmission System Operators for Electricity ENTSO-E, which is the association of Transmission System Operators (TSOs) in continental Europe, defines primary reserves as frequency containment reserves [104]; secondary reserves as frequency restoration reserves; and tertiary reserves as replacement reserves. Previously to the publication of this document, in ENTSO-E's "Operational Handbook" [103], these reserve levels were set as primary, secondary and tertiary control reserves. The present document considers both above mentioned publications (due to their complementary and non-exclusive character) to depict the ENTSO-E's recommendations regarding system frequency control and reserve power levels.

Primary reserve is intended to be the additional capacity of the network that can be automatically and locally activated by the generator's governor after a few seconds at most of an imbalance between demand and supply of electricity in the network [103]. The aim of primary reserve is to fastly balance the consumed and generated power in the system and thus to stabilize frequency at a certain level. These primary reserves are activated by automatic active power output adjustments of generating units according to a droop controller. Primary reserves must be delivered until the power deviation is completely offset by secondary or tertiary reserves. The physical stabilizing effect of all connected rotating machines due to their inertia is not considered to be primary reserve.

Secondary reserves are activated to restore the rated frequency of the system, releasing primary reserves, and to restore active power interchanges between control areas to their set points [103]. They are activated by the TSOs, modifying the active power set points of the generating units within each respective control area.

Finally, the aim of tertiary reserves is to replace the secondary reserves and to restore frequency to its rated value if secondary reserves were not sufficient. Furthermore they are used for economic power dispatch [261], considering system constraints such as current limits of transmissions lines.

These reserves are activated manually and centrally at TSO's control centers in case of observed sustained activation of secondary reserves, and to anticipate a response to expected unbalances [103].

General rules and technical recommendations regarding reserve power levels and their associated control performance are set in the ENTSO-E's "Operational Handbook" [103]. Despite these general guidelines, the responsibility of the national TSOs must be determined in their own Grid Codes.

Figure 6.1 depicts the principle behaviour of system frequency after a sudden lack of power generation in the network with all mentioned power reserve levels being involved. Some annotations on their activation are included according to [103].

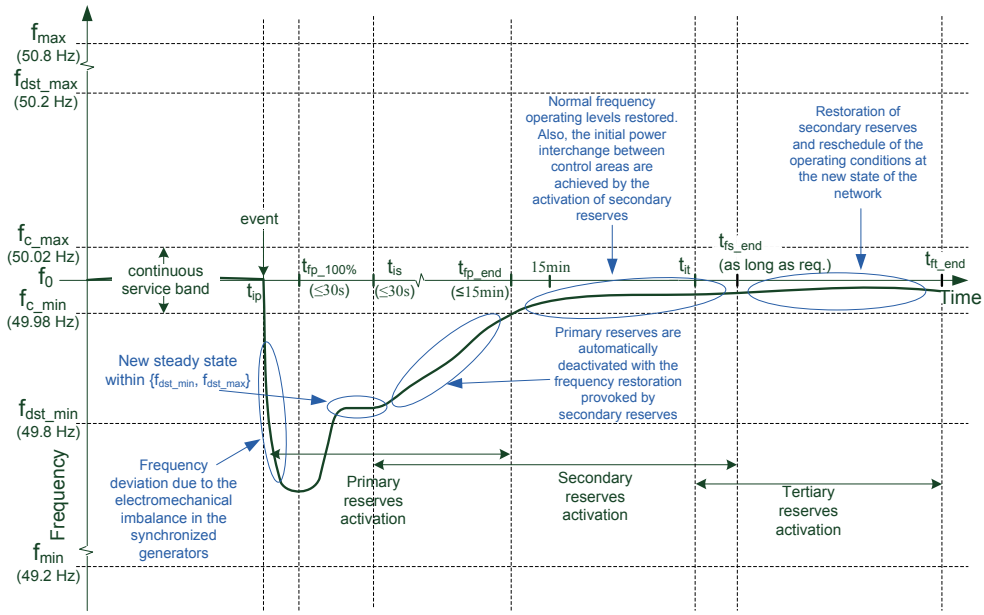

Figure 6.1: Concepts definition (particular values of time frames and frequencies are according to the recommendations of ENTSO-E [103])

In the event of a generation drop in the network, the instantaneous reserves of the synchronous generating units balance the power due to the mentioned passive effect. Their electrical power P_{elect} rapidly increases, which provokes an electromechanical unbalance in the generator set according to the following physical principle

$$P_{mech} - P_{elect} = J\omega_g \frac{d\omega_g}{dt}, \tag{6.1}$$

P_{mech} being the developed mechanical power by the generator, J is the moment of inertia referred to the generator shaft and ω_g the mechanical speed of the generator (the electrical rotational speed of the generator ω_r is deduced from the number of pairs p and ω_g as

$$\omega_r = \omega_g \frac{p}{2}. \tag{6.2}$$

The rate of change of system frequency depends on the amount of available instantaneous power reserves and thus on the inertia constant of the system H. The inertia constant, in seconds, determines the duration in which the generating unit theoretically may provide its rated power only using the kinetic energy stored in its rotating parts. It can be mathematically expressed as half of the mechanical acceleration time constant τ_{acc} (in seconds),

$$H = \frac{1}{2}\tau_{acc} = \frac{1}{2} J \frac{(\omega_{rot}^{nom})^2}{P_{nom}^{total}}, \tag{6.3}$$

where ω_{rot}^{nom} is the nominal rotor speed in rad/s, P_{nom}^{total} is the nominal power of the generating unit, and J is the moment of inertia in kgm^2, referred to the generator shaft. The reader is referred to [163] and [4] for further details regarding the definition of inertia constant. It is important to note that wind turbines have no inertia from a system point of view, since the rotor is not synchronized with the network but connected through power electronics.

At a certain frequency level, the primary power reserves are activated, the generators' driving mechanical power rises. As it reaches their electrical power, an equilibrium is achieved and the frequency stops dropping, i.e. the frequency nadir is achieved. A further increase of primary reserve power accelerates the generator sets, the system frequency rises. As the primary controller structure contains a droop, the frequency finally stabilizes at a new steady state below its rated value.

According to [163] and [280], the slope of the primary power - frequency droop characteristic has a major influence in the achieved frequency nadir and in the level of frequency in the following steady state after the network disturbance. Also, it can be noted that the slower the governor response of the wind turbine, the lower frequency nadir. However, it is neither noticed that droop characteristic, nor governor response speed influence the rate of change of frequency (ROCOF). This value is influenced by the system inertia instead [177]. Low levels of system inertia, i.e, high levels of ROCOF, can provoke the tripping of sensible loads, generating units and relays (implemented to avoid islanding [94]), thus affecting system frequency stability.

According to [177], ROCOF increases under system frequency disturbances as wind generation displaces conventional generation. This is due to the decoupling of the rotor of the generators by their fast controlled power electronics [163]. However, it does not happen with squirrel-cage asynchronous generators, since they provide naturally inertial response as being directly connected to the grid [278].

The activation of secondary reserves provokes the recuperation of the normal operating frequency levels and thus the deactivation of primary reserves. Secondary reserves are operated until being fully replaced by tertiary reserves. Proper explanations of the parameters presented in Figure 6.1 are listed as follows [103]:

- f_{min} and f_{max}: Minimum and maximum expected instantaneous frequency after a reference incident (loss of generation or loss of load) assuming predefined system conditions.

- f_{dst_min} and f_{dst_max}: Minimum and maximum steady state frequency. They define the tolerance band for the quasi-steady-state system frequency after the occurrence of a reference incident, assuming predefined system conditions. Outside this interval, all available primary reserves should be activated. This means that droop controllers of all units providing primary reserves should be set for deploying all their contracted or obligatory primary reserve capacity.

- f_{c_min} and f_{c_max}: Maximum allowed frequency dead-band for the activation of primary reserves. These limits define an interval in which primary reserves are not required to be activated. This allowed frequency deviation usually corresponds to the accuracy of the frequency measurement and the insensitivity of the controller. Notwithstanding that, a greater dead band is also permitted in accordance with TSO.

- t_{ip}, t_{is} and t_{it}: Maximum starting time for the activation of primary, secondary and tertiary reserves from the event detection time.

- $t_{fp\_50\%}$ and $t_{fp\_100\%}$: Maximum deployment time for 50% and 100% respectively of total primary reserves from the event detection time.

- $t_{fs\_100\%}$ and $t_{ft\_100\%}$: Maximum deployment time for 100% of total secondary and tertiary reserves from the event detection time.

- t_{fp_end}, t_{fs_end} and t_{ft_end}: Minimum capability of actuation of primary, secondary and tertiary reserves.

Accordingly, Table 6.1 presents specific values of the above listed frequency levels and time frames from ENTSO-E's recommendations in its Operational Handbook [103], as well as particular data from several European Grid Codes. It must be noted that the indicated values apply to conventional generating units participating in system frequency control. Particular values for WPPs are presented as well.

As can be noted in Table 6.1, the specified frequency levels in both German and Spanish Grid Codes mainly match with the recommendations of ENTSO-E [103]. Primary reserves are required to be fully activated 30s at most after the frequency deviation detection. In contrast to these continental Grid Codes, the Irish Grid Code requires a faster response time in full activation of power reserves. Despite the fact that the authors of this work were not able to find a particular value for the response time in full activation of primary reserves in the Irish Grid Code, the activation time of secondary reserves is set to 5s at most after the frequency deviation detection.

According to the analysed German Grid Code, it is mandatory for generator units with rated power greater than 100 MW to provide primary reserves to the system. Smaller generators may also be employed by agreement with the TSO [301]. The participation in this service is remunerated and also renewable power plants can participate. According to the Spanish Grid Code, all synchronized generators must provide primary reserves. This participation is not paid though. On the other hand, the provision of secondary and tertiary reserves is market regulated.

Neither the recommendations from ENTSO-E, nor the Grid Codes from Germany and Spain require renewable generating units to provide primary reserves. Notwithstanding that, and according to the German Grid Code, renewable generating units are required to reduce their output under system frequencies above 50.2 Hz and also they can provide primary reserves in agreement with the TSO [107]. On the other hand, Irish and UK Grid Codes, within the consulted regulations, set specific requirements for renewable generating units regarding primary reserve in both directions of frequency deviations. Frequency regulation-related tasks in Ireland and UK are particularly complicated since these countries are electrical islands. Generating units should be remunerated for their participation in this service according to Irish regulation.

According to this literature review, the following sections detail both Irish and UK regulations, emphasizing in the requirements regarding primary reserves for renewable generating units. A brief note about secondary reserves according to the Irish regulation is also included as being considered particularly interesting for the purpose of this chapter.

Table 6.1: Parameters extracted from ENTSO-E's recommendations and some European Grid Codes for conventional generating units participating in system frequency control

Param.	ENTSO-E (2009) [103]	Germany (2007) [301]	Spain (2009) [245, 246]	Ireland (2011) [95]	UK (2012) [212]
f_0	50 Hz	50 Hz	50 Hz	50 Hz	50 Hz
$\{f_{c\_min};f_{c\_max}\}$	±20 mHz	±20 mHz	±20 mHz	±15 mHz	±15 mHz
$\{f_{dst\_min};f_{dst\_max}\}$	±200 mHz	±200 mHz	±200 mHz	±500 mHz	±500 mHz
$\{f_{min};f_{max}\}$	±800 mHz	±800 mHz	±800 mHz	±1 Hz	±800 mHz
t_{ip}	A few sec. after detecting Δf of ±20 mHz[a][b]			with Δf of ±15 mHz[c]	
$t_{fp\_50\%}$	≤15 s	-	≤15 s[d]	-	-
$t_{fp\_100\%}$	≤30 s	≤30 s	≤30 s[e]	-	≤30 s[f]
t_{fp_end}	≥15 min	≥15 min	As long as req.	≥30 s	≥30 min[g]
t_{is}	≤30 s	≤30 s	-	≤5 s	-
$t_{fs\_100\%}$	≤15 min	≤15 min	300 s≤500 s[h]	≤15 s	-
t_{fs_end}	As long as required		≥15 min	10 min	-
t_{it}	In TSO's decision				
$t_{ft\_100\%}$	A short time		≤15 min	-	-
t_{ft_end}	-	-	≥2 h 15 min	-	-

[a] According to the corresponding document, section A-S2.3. "Physical deployment times".

[b] According to the German Grid Code, section 5.2.2, page 39 [301], and referring to the frequency control, "the TSO shall use primary control power in accordance with the rules of the UCTE-OH Policy 1", that is the document referred to the first column of the table ENTSO-E (2009) [103].

[c] According to the Grid Code of UK, section CC.A.3.4 [212], and referring to the activation of primary reserves, "the active power output should be released increasingly with time over the period 0 to 10 seconds from the time of the start of the frequency fall".

[d] The deployment time from 50% to 100% of total primary reserve rises linearly from $t_{fp\_50\%}$ to $t_{fp\_100\%}$.

[e] If network frequency variation is less than 100 mHz, $t_{fp\_100\%}$ =15 s.

[f] This value corresponds to the maximum deployment time of the so-called primary response capability of a generator unit operating in frequency sensitive mode. For more details please refer to Section 2.3

[g] This value corresponds to the minimum capability of actuation of the so-called secondary responses of a generating unit operating in frequency sensitive mode. For more details please refer to Section 2.3.

[h] Response time constant of 100 s of a 1st order type system.

6.2.2 Ireland

This section sets out the most relevant aspects regarding system frequency control support by WPPs according to the Irish Grid Code [95]. WPPs do not have the same characteristics as conventional synchronous generating units. Accordingly, the Irish regulation details, among other contents, a specific set of requirements for WPPs in regard of some aspects concerning their controllability and behaviour during grid disturbances and frequency and voltage control support.

There are some differences between the ENTSO-E [104] and the Irish terminology regarding power reserves. The Irish Grid Code adopts the term *operating margin*. It represents the power reserve to be sustained to meet the expected system demand for limiting and correcting system frequency deviations. The *operating margin* consists of *operating reserve*, *replacement reserve*, *substitute reserve* and *contingency reserve*. The *operating reserve* is defined as "the additional power output provided by generating units realizable in real time operation to limit and correct system frequency deviations to an acceptable level". This *operating reserve* consists, in turn, of *primary operating reserve*, *secondary operating reserve*, *tertiary operating reserve band 1* and *tertiary operating reserve band 2*. Each of these *operating reserves* applies over different time frames up to 20 minutes following an event.

Moreover, and continuing with the description of terminology differences, frequency control is carried out by means of using the *operating reserves* and occurs in two time scales: *primary frequency control*, and *secondary frequency control*. *Primary frequency control* takes place in the period of up to 30 seconds after the detection time of the frequency deviation. It is achieved by automatic corrective responses which include governor droop actions of generators and automatic load shedding. *Secondary frequency control* takes place in the time frame comprised between 5 seconds up to 10 minutes after a frequency deviation. It is carried out by a combination of automatic and manual actions (dispatch instructions from TSO).

Figure 6.2 sumarizes the Irish terminology regarding power reserves, and its equivalence with the ENTSO-E's terminology. WPPs are required to participate in system frequency control with the provision of *primary reserves* and *secondary reserves*.

As set in Table 6.1, primary reserves take place in the period of up to 30 seconds after the detection of a frequency deviation. In the case of WPPs, their activation is carried out by automatic local controllers. If frequency deviation is within the levels 49.8 Hz to 50.2 Hz, frequency control is intended

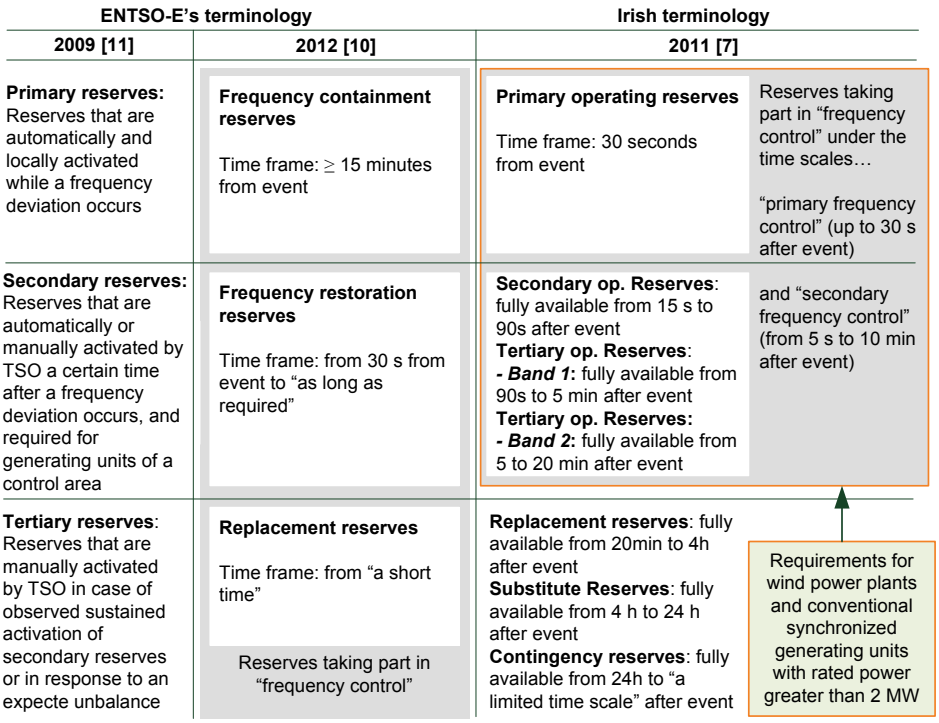

Figure 6.2: Equivalences between ENTSO-E (2009) [103], ENTSO-E (2012) [104] and Irish [95] regulations

as *frequency regulation* and should be carried out only by generating units with rated capacity greater than 60 MW and synchronized with the grid under the control of a governor control system. Therefore, WPPs are required to ramp up and down their power output only outside of these frequency limits. A wind farm control system shall present the capabilities according to Figure 6.3 regarding the activation of primary reserves, where P_A to P_E, and f_A to f_E are determined by the TSO before the start of operation of the unit. As can be noted from Figure 6.3, at rated system frequency, a WPP is required to feed in less than its available active power. This derated operation allows the WPP to provide both positive and negative power reserves, i.e. to ramp power both up and down in response to system frequency deviations. The *primary reserves* should be activated immediately after detecting a frequency deviation from the specified dead band without any control signal from the TSO.

Secondary reserves come into play in the time scale from 5 seconds up to

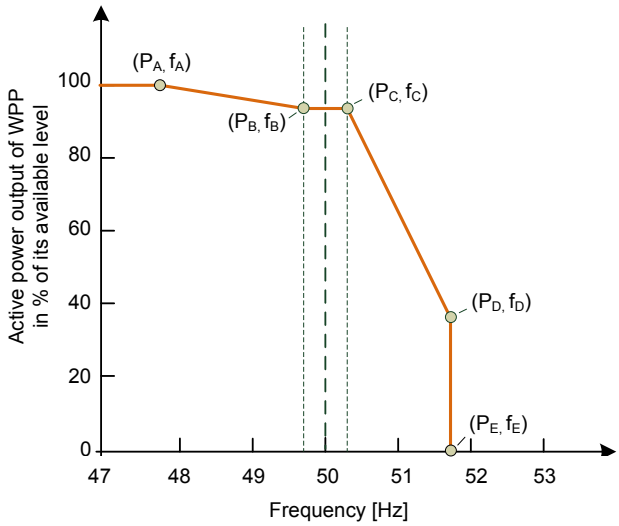

Figure 6.3: Droop characteristic for primary reserves activation according to requirements set by Irish regulation for WPPs [95]

10 minutes after detecting the frequency deviation. Its active power setpoint comes from the TSO. A time delay of up to 10 seconds from receiving this set point is allowed for their activation.

Regarding active power ramp rates for both *primary* and *secondary reserves* activation, the response rate of each available wind turbine shall be at least 1% of its rated capacity per second. Moreover, the TSO limits the active power ramp rate to the WPP as a global. In this sense, it shall be possible to vary the active power ramp rate between 1 MW/min to 30 MW/min.

6.2.3 United Kingdom

Each WPP (both onshore and offshore) with a registered capacity over 50 MW must be capable of participating in frequency control by continuously adjusting its active power output. This active power control can be performed applying two operating modes, the so-called *frequency sensitive mode* and *limited frequency sensitive mode*.

In the latter operational mode, the generating units must be capable of maintaining a constant level of active power output for system frequency changes within 49.5 Hz and 50.5 Hz. In the case of WPPs, the active power output shall be independent of the system frequency in this range. Moreover,

below 49.5 Hz to 47.0 Hz, the active power level of the WPPs shall not drop by more than 5% because of the decay in system frequency.

The participation in frequency control according to *frequency sensitive mode* is an ancillary service. There are two categories of ancillary services: the so-called system ancillary services and the commercial ancillary services. In the first category we find two types of ancillary services: types 1 and 2. Type 1 details mandatory capabilities in respect to reactive power and frequency control. This document focuses on this ancillary service type 1.

The term frequency sensitive mode is the generic description of an operation mode which includes the provision of *primary response*, and/or *secondary response* and/or *high frequency response*. The so-called *primary* and *secondary responses* refer to negative frequency deviation, while the *high frequency response* refers to positive frequency deviations. This frequency response capabilities are activated by automatic controllers in the generating unit. Therefore, and according to the used terminology in this document, *primary*, *secondary* and *high frequency response capability* can be intended as primary reserves. Each response capability must be tested inducing a ramp from 0 to 0.5 Hz change over a ten second period to the frequency control device. This frequency deviation must be sustained thereinafter.

Primary response capability of a generating unit is the minimum increase of active power between 10 and 30 seconds after the start of the induced frequency deviation ramp to the controller. *Secondary response capability* is the minimum increase of active power output between 30 seconds and 30 minutes after the activation of this ramp. Finally, *high frequency response capability* is the decrease in active power output 10 seconds after the induction of, in this case, a frequency ramp with positive slope. These concepts are depicted in Figure 6.4.

The minimum power output change required to a generating unit can be found in Figure 6.5. As shown, the change on the generation level depends on the actual loading of the unit. A generating unit must be capable of providing frequency response at least up to the indicated boundaries depending on its loading. Since the indicated power change levels correspond to a frequency deviation of 0.5 Hz, a directly proportional change of power level has to be determined for smaller frequency deviations. Also, two operational limits are highlighted: the *designed minimum operating level* and the *minimum generation level*. The latter defines the minimum stationary part-load level at which the generating unit must be capable to remain. This level should not exceed 65% of the rated power (see [212], page CC-68 for further explanations). For instance, a wind turbine, or a thermal power plant, must be capable of working at 65% or 60% of its rated capacity in steady

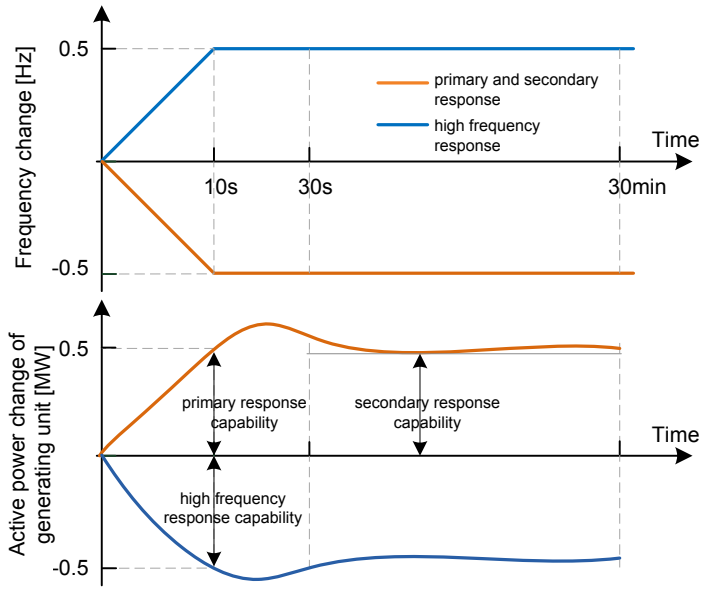

Figure 6.4: Representation of *primary*, *secondary* and *high frequency response capabilities* according to UK Grid Code [212]

state. The former concept, the *designed minimum operating level*, bounds the minimum generation level at which the generating unit must provide *high frequency response*, i.e., must activate negative primary reserves at grid frequencies above 50.0 Hz. The generating unit would have to provide also *high frequency response* under the *designed minimum operating level* but only under frequencies above 50.5 Hz.

From Figure 6.5, we can conclude that, similar to the Irish case, a continuous power derating should be applied to WPPs in order to be able to transiently increase their output according to the requirements of provision of primary reserve (provided that no energy storage devices are included in the WPP). Finally, it should be noted that the deadband of frequency control devices in *frequency sensitive mode* must be ± 0.015 Hz at most.

6.2.4 Future trends regarding the provision of primary reserves by WPPs and inertial response

In order to harmonize the connection requirements for generating units of the European power system, ENTSO-E presented its first network code [101] in June 2012. The network code applies to all grid connected generators.

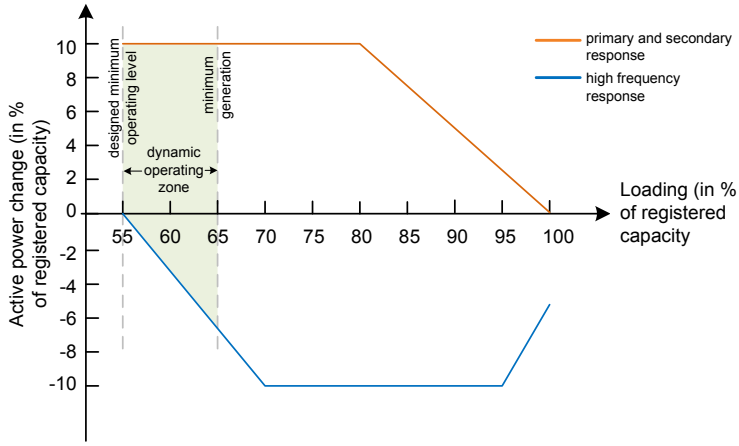

Figure 6.5: Minimum active power regulation levels for *primary, secondary* and *high frequency response capabilities* (i.e. primary reserves activation) for WPPs in the event of a system frequency deviation of 0.5 Hz according to UK Grid Code [212]

Generating units are classified in different types according to the voltage level at their grid connection point and their rated power. In spite of not explicitly referring to the terms primary, secondary and tertiary reserves, the network code details specific requirements for generating units regarding their participation in frequency control.

Most restrictive requirements regarding frequency control are borne by the so-called generating units type C. This category covers, for instance, WPPs with rated power above 50 MW in continental Europe, above 10 MW in UK and above 5 MW in Ireland. These WPPs must be equipped with a power control system for frequency response. There are two operation modes for this control system, i.e., the *limited frequency sensitive mode* and the *frequency sensitive mode*[1].

In the latter operating mode, the control system is in charge of ramping up and down the active power output of the generating unit in case of over and underfrequency, according to a power - frequency droop characteristic. The *limited frequency sensitive mode*, as a particular case, just requires the generating unit to increase its power output while while frequency lies between 49.5 and 49.8 Hz. These concepts are depicted in Figure 6.6.

As shown, in *frequency sensitive mode* the generating unit must be capable

[1]This terminology for defining the operation modes are clearly consistent with that defined in UK regulation.

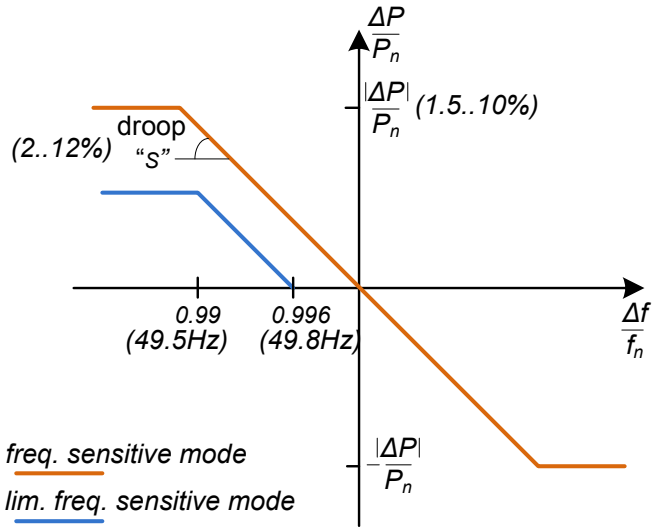

Figure 6.6: Active power frequency response droop characteristic according to ENTSO-E's network code [101]

of regulating its power output according to the system frequency within a given range around the currently available power. The required range can be defined between 1.5 and 10% of the nominal power of the unit. The droop characteristic is saturated at predefined frequency levels, which must be determined in accordance with the relevant TSO. The droop characteristic must present a slope comprised between 2 and 12% and could include a deadband up to 0.5 Hz (in accordance with the relevant TSO). Finally, taking into account inevitable frequency measurement errors, there is a tolerance for frequency measurement of 10-30 mHz. The maximum admissible time delay for the activation of primary reserves must be determined in accordance with the relevant TSO (for synchronized generators its value is 2 seconds at most), while the full activation time is 30 seconds at most. This active power surplus has to be provided for 15-30 minutes depending on the type of generating unit and the agreement achieved with the TSO.

Apart from the requirements regarding primary reserves, the network code introduces the concept of *synthetic inertia* (or inertial response thereinafter) [101].

With the aim of contributing to the frequency stability of the electrical system, TSOs are encouraged to set, in the future, requirements for WPPs (both onshore and offshore) for providing *inertial response* under low frequency events. *Inertial response* means to replicate the inertia of a synchro-

nized generating units by a non-synchronized generating unit, i.e. a WPP. In particular, it implies to inject in a very short time (200 ms) a large power proportional to the "severity"[2] of the disturbance [101].

Hydro-Québec TransÉnergie recently researched the inertia emulation needs [45]. The analysis quantifies the impact on frequency performance and stability of the inclusion of new 2000 MW of wind power into the Hydro-Québec transmission system. Simulation results show that in order to maintain system frequency within its operating limits under a low frequency disturbance (58.5 Hz) and thus avoiding automatic load shedding, wind farms have to participate in frequency regulation with their inertia emulation. This statement is consistent with results of [123], which determines that the inertial response by wind turbines can help to avoid the activation of underfrequency automatic load shedding as higher frequency nadir are registered during a frequency disturbance. Going back to the discussion of Hydro-Québec TransÉnergie's work [45], it can be noted that inertia emulation parameters were quantified in terms of deadband for their activation, duration, active power contribution and recovery characteristics following that contribution. It is worth highlighting that the minimum duration of active power contribution for inertia emulation is set to 10 seconds (considering 6% of active power increase) in order to expand the contribution beyond the frequency nadir.

According to [102], there are two technical solutions under development for providing inertial response: providing a fast power injection proportional to the rate of change of frequency; and delivering fast frequency response (according to a power/frequency droop characteristic) with very short time response and time delay. Both strategies are discussed in Section 3.2 according to a literature review.

6.3 Participation methods of WPPs for primary frequency control and inertial response

6.3.1 Deloading methods of wind turbines for primary frequency control

Conventionally, wind turbines are operated at maximum aerodynamic efficiency, so that they can maximize the power extracted from the wind. At partial-load region, the speed of the turbine is controlled by the regulation of the aerodynamic torque [159], leading the so-called optimal torque rotor-

[2]This requirement is not defined in further detail in the Grid Code [101]

speed curve. In particular, the optimal aerodynamic torque is computed by

$$T^* = K_{cp}(\beta) \cdot \omega_t^2, \tag{6.4}$$

where ω_t is the speed of the turbine, K_{cp} is the so-called optimal aerodynamic torque coefficient and depends on the aerodynamics of the turbine and the pitch angle β.

For maximum power generation, β is maintained constant to zero degrees in partial-load operation of the turbine. The pitch angle is only regulated in full-load operating region. Usually, pitch control techniques are used to limit the power captured from wind in wind turbines in order not to exceed the rated power [272], [96], [40]. In this regard, the turbine's power is limited at wind speeds above the rated wind speed by applying a PI controller governed by the difference between the rated power of the wind turbine and the actual measurement of it [297]. Controlling the rotor speed at constant torque can be also a possibility for driving this PI controller.

As noted in Section 6.2, WPPs are required to participate in primary frequency control by ramping up and down their output according to a power - frequency droop characteristic and during a certain period of time. This means that wind turbines either have to be operated in a deloaded mode, or a suitable energy storage device has to be available. This chapter focuses on solutions for the first method. Different approaches can be found in the literature regarding deloading methods of wind turbines. They can be classified in two main categories: pitching techniques and overspeeding techniques [312].

Both methods are based on the idea of achieving a non-optimal working point in the power (or torque) rotor-speed curve of a wind turbine. As it can be noted in Figure 6.7, frequency control is then realised by using C (overspeeding the turbine) or B (pitching the blades) as standard operating points and switching between point A and additional deloaded points.

While applying pitching techniques, the rotating speed of the turbine is kept constant (point B). Conversely, while applying overspeeding techniques, the turbine is operated at a higher rotor speed, while keeping the pitch angle constant (point C). One main difference between these two strategies is the fact that overspeeding can only be applied in variable speed wind turbines (i.e. DFIG-based and full-converter-based wind turbines).

Underspeeding techniques are not preferably applicable as for increasing the power margin (i.e. reducing the generation level), the generated electric power first increases due to the kinetic energy delivered to the grid due to the deceleration of the rotor of the turbine. Small signal stability could be

also endangered (unlike with respect to pitching techniques) [152].

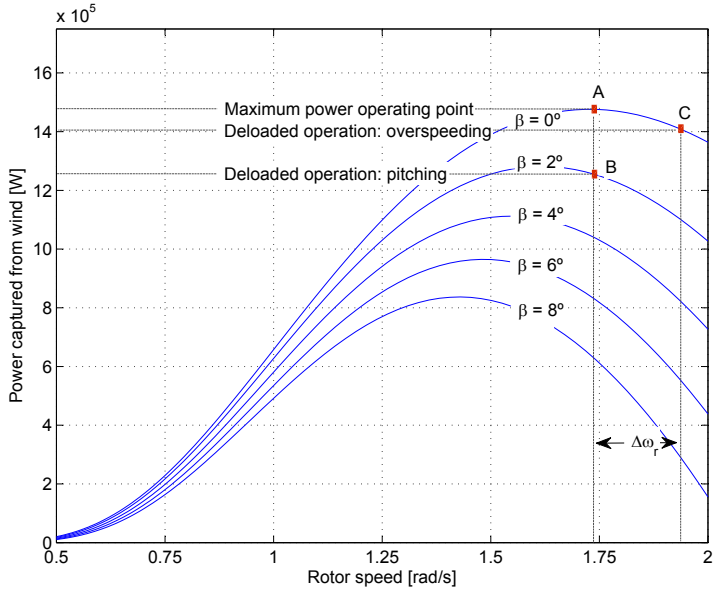

Figure 6.7: Power rotor-speed curves for different values of pitch angle and deloaded options for a 1.5 MW wind turbine (wind speed: 10m/s)

Depending on the wind speed level, one or the other method (pitching or overspeeding) is advantageous. Three different operating regions for wind turbines can be considered in this sense: low, medium and high wind speed ranges. In low wind speed range, wind turbines operate at partial load. Thus, the rotating speed of the turbine does not reach at any time its rated value, allowing the application of overspeeding techniques. In medium wind speed range wind turbines mostly operate at partial load but they can transiently achieve their rated rotational speed, and thus the pitch controller may be activated. In this region, a combination of overspeeding and pitching techniques may be a good option for deloading the wind turbine. And finally, in high wind speed range pitch control becomes a key factor for both limiting the power extracted from the wind in order not to exceed the ratings of the generator and for applying deloading strategies. Overspeeding strategies generally do not fit well in this region. Apart from the limitations regarding wind speed for applying the above mentioned deloading strategies, further related considerations can be found in the literature that must be taken into account. A brief summary of some of them is presented in Table 6.2.

Table 6.2: Considerations regarding deloading strategies of wind turbines

Overspeeding techniques
• Method preferably applied to below rated wind speed levels [192]. • Wind speed measurements are usually required for determining the maximum power that a wind turbine could extract from wind while applying the deloaded power - rotor speed curves. Accuracy and reliability of this wind speed measurement is crucial [73]. • Considering DFIG, the percentage of power transmitted through the set of back-to-back power converters becomes greater with greater values of slip. This limits the overspeeding of the wind turbine in order not to overcome the ratings of the power converters [192, 206]. • Danger of excessive mechanical stress in the rotor shaft due to the fast deloading through the fast torque control for speed regulation. Need of limitations of rate of change of torque [152]. • Rotor speed regulation is only possible in variable speed wind turbines. • Due to the inertia of the rotor, the power ramping is not linear.
Pitching techniques
• Method preferably applied to above rated wind speed [192]. • Excessive pitch control actions may lead to tear and wear of the mechanism [152, 300]. Moreover, pitch angle regulation could affect fatigue life of the blades as it affects their dynamic loads [51, 52]. • Larger time responses than in overspeeding techniques due to pitch servo time delays [206]. • Usually, no wind speed measurements are required [205].

The following subsections deal with a literature review regarding the application of each of the above mentioned strategies.

Control basis of overspeeding and pitching techniques for the deloaded operation of wind turbines: an example

Since deloaded operation is now considered, the input of the PI controller that drives the pitch actuator can be computed by the difference between the measurement of the generation level and the deloaded power reference. The control strategy is presented in Figure 6.8.

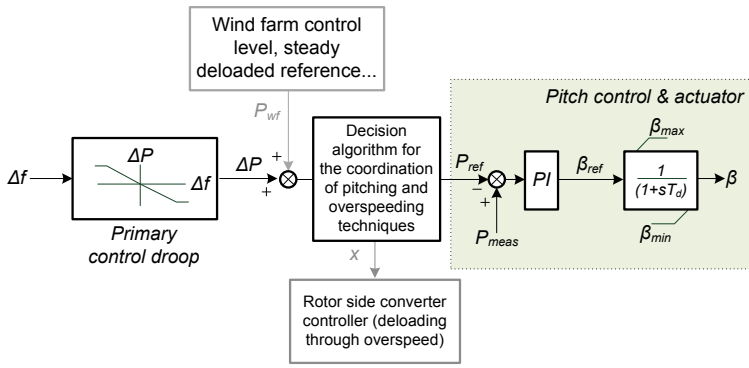

Figure 6.8: Pitch control scheme and primary frequency control droop of a wind turbine for deloaded operation. Scheme adopted and adapted from [140] and [280]

As shown, the deloaded power reference P_{ref} can be obtained from the sum of a signal from a WPP controller, P_{wf}, and the output of a primary frequency control droop ΔP. The control signal from the WPP controller can be determined considering the required deloading level for the WPP. However, this is not so trivial as the available power of the WPP has to be estimated continuously. It is worth noting that the update rate of this signal is much lower than the other control signals within the local controllers of the wind turbine.

Considering low wind speeds and rotor speeds below rated, deloaded operation is preferable carried out by means of overspeeding techniques. For wind speeds near or above nominal, when maximum rotor speed is reached, the required power reserve of a wind turbine is affected by the control of the pitch angle. In [73], overspeeding is achieved operating the wind turbines not following optimum $P - \omega$ curves as indicated by a MPT algorithm for extracting the maximum available power from the wind, but their active

power references are obtained from the so-called deloaded optimum power curves instead. This concept is also adopted in [74], [320], [319], [241] and [322]. The active power set-point of the wind turbine $P_{del_{opt}}$ obtained following this operating mode is dependent on the corresponding power reference that would be carried out following a MPT algorithm, P_{opt}, and also on the required reserve level

$$P_{del_{opt}} = P_{opt}(1 - x), \tag{6.5}$$

where x is the required power margin. Provided the desired level power $P_{del_{opt}}$ and wind speed measurement, the corresponding sub-optimal power coefficient $C_{p_{del}}$ can be computed as

$$C_{p_{del}}(v_w, \omega_r, \beta) = \frac{P_{del_{opt}}}{0.5\rho A v_w^3}. \tag{6.6}$$

Given the wind speed and $P_{del_{opt}}$, the value of $C_{p_{del}}(v_w, \omega_t, \beta)$ can be computed from equation (6.6). The power coefficient is a function of pitch angle, wind and rotor speed. Then, for a given pitch angle and wind speed, the corresponding rotor speed can be determined. By means of these operations a family of deloaded optimum $P - \omega$ curves can be defined, as plotted in Figure 6.9.

As can be noted, given a desired power margin x and the rotor speed, it is possible to access to the corresponding deloaded optimum power curve and determine the active power reference for the low level control of the generator. The torque reference can be also computed instead of the active power reference.

An example of a control scheme for providing primary reserves using overspeeding technologies based on the above depicted deloaded optimum power curves is detailed in Figure 6.10. As can be noted, the required power margin x is obtained, as in pitching techniques, from the WPP controller, P_{wf}, and the primary frequency control droop ΔP.

Overspeeding and pitching techniques for deloaded operation of wind turbines

Reference [320] proposes overspeeding techniques to below rated wind speed region (i.e. below rated rotor speeds) but the control scheme also combines pitching techniques near or above nominal wind speed in order to avoid rotor speeds beyond nominal. In [152] and [241], a look-up table is used to determine the deloaded power set-point which drives the low level active power control system of the rotor side converter of the generator. This look-up

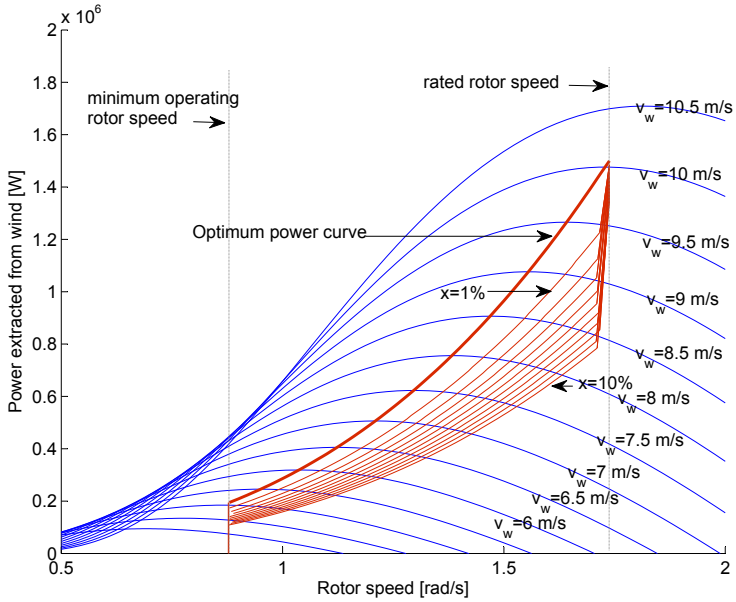

Figure 6.9: Deloaded optimum power curves for deloaded operation of a 1.5 MW DFIG-based wind turbine

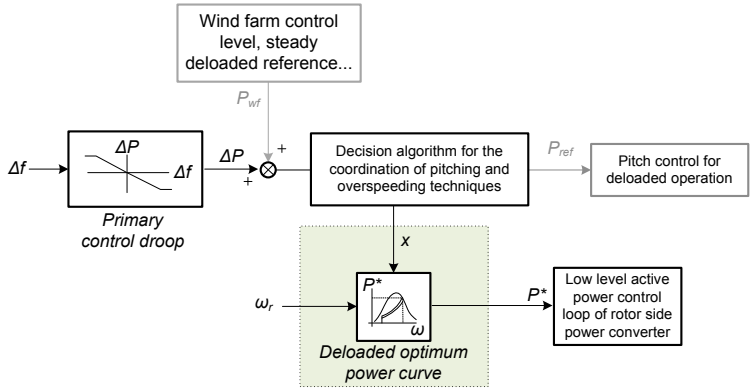

Figure 6.10: Rotor speed control scheme for deloaded operation

table takes as inputs the required power margin and the rotor speed measurement. No wind speed measurements are required. The determination of the power set-point in above rated wind speed region is carried out by means of a second look up table, which takes into account the required power margin and the pitch angle measurement. The output of this look up table is

the required deloaded power generation setpoint of the wind turbine. Also, it takes into account cubic interpolation between different but close pitch angles due to their large influence in the aerodynamic behaviour of wind turbine. Finally, it is remarkable that overspeeding and pitching actions are not carried out at the same time, but overspeeding only applies when pitch angle is set to zero.

Approaches which take wind speed measurement as input can also be found in the literature. For instance, in [73] it is proposed to access to the optimum power curve using wind speed as input, and determine the optimum power reference P_{opt} and its corresponding optimum rotor speed ω_{opt}. From these signals and the required power margin x, one can determine the deloaded optimum generating point.

In this way, accuracy and reliability of wind speed measurements become key issues for the implementation of the proposed control strategy. In fact, wind speed measurement on top of the nacelle is not really reliable when it comes to representing free wind speed due to influences by the rotor. The adopted reserve margin allows the wind turbine to increment its power output in response of a frequency drop.

Finally, it can be noted that the authors in [73] also propose to affect the active power set-points of wind turbines according to the inputs received from a wind farm central controller. The dispatch function of wind farm central controller is based on the solution of an optimization problem, which sets adjustments of active and reactive power set-points for each wind turbine so that to optimize the power flow within the wind park, i.e. to minimize active power losses while fulfilling the requirements of the system operator.

Another approach for combining rotor speed and pitch angle regulations but in this case at the same time in below rated rotor speed range is proposed in [320]. The idea is to control the above mentioned parameters in order to maintain a required deloaded level of the wind turbine. Thus, when a frequency drop occurs, wind turbine shifts the pitch angle and rotor speed references towards their optimal values (i.e., shifts pitch angle to a minimum value and rotor speed according to the optimal power curve of the wind turbine.) It is worth pointing out how the set-points of rotor speed and pitch angle are determined in order to provide the required power reserve. Given a required deloaded power level, the deloaded aerodynamic power coeficient $C_{p_{del}}(v_w, \omega_t, \beta)$ can be determined applying equation (6.6). For each wind speed, $C_{p_{del}}(v_w, \omega_t, \beta)$ is influenced by the selected combination of ω_t and β, and there is more than one possible combination. The authors research on the definition of an optimization procedure for determining the proper combination of ω_t and β so that the ω_t is maximized and thus it

is also maximized the kinetic energy stored in the rotating masses of the wind turbine. This optimization procedure is complex and time spending. Therefore, the offline obtained results were extrapolated to a suitable online strategy. It is worth highlighting that wind speed measurements are required for implementing this control algorithm. When a frequency drop occurs, and due to high initial rotor speed, the speed regulation of the wind turbine deals a large amount of kinetic energy injected to the grid in the first seconds of the frequency excursion. The above mentioned strategy only applies to below rated rotor speed range. For near or above rated wind speed levels, in order to avoid exceeding the rated rotor speed level, pitch control is responsible of carrying out the deloaded operation of the wind turbine. As a result of the maximization of the kinetic energy injected in the first seconds of the frequency disturbance, the frequency nadir is delayed in time and its value is higher than in the case of applying a deloaded strategy without this kinetic energy support. However, it is worth noting that the fast power regulation means large loads on the shaft of the turbine.

The idea of taking advantage of the kinetic energy stored in the rotating parts of a wind turbine while in deloaded operation is further investigated by the authors of [320] in [319]. Here, new control algorithms for both pitch angle and rotor speed that allow the maximization of the stored kinetic energy in the rotating parts of a wind turbine in order to improve the frequency control support are presented. It is worth noting that both articles conclude that using the kinetic energy stored in the wind turbine reduces the need of deloaded operation while still providing the required amount of power reserve for a short time frame. This time frame is considered to be the maximum deployment time of 100% of primary reserves according to the ENTSO-E [103], i.e, 30 seconds.

Deloaded operation of wind turbines taking also into account the interaction with wind farm central controllers are regarded in [253], [3] and [73]. In regard with communications within the park for this purpose, it is worth noting that reliable and fast SCADA systems with sampling rate of 1-3 s for frequency measurements should be adequate, considering the desired reaction time of wind turbines [152]. In [253], it is considered a wind farm active and reactive control system, which provides power set-points for each wind turbine. The active power set-point of a wind turbine is achieved varying the pitch angle, which in turns varies the rotor speed simultaneously.

Once local control of a wind turbine receives the active power set-point, two situations may happen. It could happen that wind speed is high enough, and therefore, it is possible to achieve the required generation level. Then, a PI controller is driven by the error between the active power set-point

and the measured power signal. The output of this PI is the required pitch angle. Therefore, the turbine is always operated at the maximums of the pitch angle curves of Figure 6.7, while the PI controller chooses the pitch angle curve. It is worth pointing out that the article does not analyze the stability issues derived from the interaction between the PI controller for pitching the turbine and the central control system of the WPP that sets out the active power reference for the wind turbines.

At the same time of computing the pitch angle, a MPT algorithm inputs the measured generation level of the wind turbine and outputs a speed reference. Since the output power is being reduced by the pitch controller, the MPT algorithm outputs a speed reference below its optimal value, dealing reduced values of tip speed ratio and C_p power coefficients and then, helping wind turbine to reduce its generation level. On the other hand, if wind speed is not high enough to achieve the required generation level, the pitch angle results saturated at its minimum value maximizing the power extracted from the wind. It is deduced that deloaded operation can be also be carried out with control techniques presented in this article.

The following paragraphs focus on the description of pitching techniques according to a literature review. A pitching technique for deloaded operation is presented in [140]. Pitch regulation is defined for two regions: region A (above rated power output), and region B (below rated power output). In region A, usually the active power output to the turbine is limited to its rated value by setting a non-minimum pitch angle. However, the turbine is deloaded in this case through a further pitch angle increment. In this manner, it is possible to ramp up and down the output of the wind turbine for frequency regulation. This output power ramping is commanded by a frequency - power droop characteristic. In region B, active power control scheme of the rotor side converter controller is commonly commanded by a MPT algorithm [159] (considering variable speed wind turbines). In this region the pitch angle is usually set to its minimum value in order to extract the maximum power from the wind. However, in this article the minimum pitch angle is also proportionally regulated to the change in frequency in a narrow band of ± 2 degrees for enabling the deloaded operation of the wind turbine in this region. Therefore, it is applied a frequency-pitch angle droop characteristic. It is pointed out that this narrow pitch angle regulation band deals up to 400 kW of power spill for a 2 MW DFIG-based wind turbine.

In [205], the proposed deloaded technique is applied to DFIG and PMSG-based wind turbines. As the power extracted from the wind is linear dependent on the power coefficient C_p, a defined percentage reduction of power generation can be achieved reducing in the same proportion C_p. The wind

turbine is always operated with an optimal tip speed ratio λ_{opt} (and thus with an optimal C_p when no deloaded operation is commanded). This means that a reduction in C_p from its optimal value can be achieved by determining a non-minimum pitch angle β. This pitch angle is mathematically computed from the following expression,

$$C_p(\lambda_{opt}, \beta) = (100 - x)\% \cdot C_{p,opt}(\lambda_{opt}, \beta_{min}). \tag{6.7}$$

Knowing the desired load percentage reduction x, λ_{opt} and $C_{p,opt}$, the desired value of $C_p(\lambda_{opt}, \beta)$ is determined and from it, the required pitch angle β. Deloaded operation is then achieved by the above mentioned strategy considering below rated wind speed. Above rated wind speed level, the output of a pitch angle PI controller, which is in charge of limiting the rotor speed to its rated level, is added to the previously and mathematically computed angle β for deloaded operation.

Finally, it is appropriate to note that the contribution of offshore wind farms to main grid frequency control support is also investigated. For instance, [129] considers an offshore wind farm connected to the grid via a VSC-HVDC link. The WPP is composed by full converter wind turbines. The objective is to regulate the output of the wind farm in response to main grid frequency variations. The power output of the wind turbines is governed by the offshore side VSC of the HVDC transmission and this converter does not receive any measurement of the main grid frequency. The frequency deviation is estimated by the offshore installation through the measurement of the dc voltage fluctuations of the HVDC transmission. The voltage level of the HVDC transmission is ramped up and down proportionally to the main grid frequency deviation. This voltage ramping is carried out by the main grid side VSC terminal. Results show an improvement in grid frequency control support during grid disturbances. The used deloading method of the wind turbines is not discussed though.

6.3.2 Inertial response

As discussed in Section 6.2.4, in order to promote high penetration levels of wind power into the grid without compromising frequency stability, WPPs may be required in future to provide an emulated inertial response [102]. Inertial response can be achieved proposing additional control schemes that affect the generated active power of wind turbines in the presence of frequency deviations, in order to allow them to behave similar to synchronized generating units in these situations.

According to [204] and [164], typical wind turbine's inertia constant is between 4 and 6 seconds. These values are comparable with the normalized inertia constant of conventional generating units (between 2 and 9 seconds depending on the type of generator). Using the fact that the rotor speed of variable speed wind turbines is not coupled to the grid frequency, the deceleration of the rotor can be chosen by the controller. This allows to choose the provided power or the duration. Since generator speed of a wind turbine can drop to 0.7 pu, while the speed of conventional synchronized generating units only normally drops to 0.95 pu (assuming that frequency variations stay within 47.5 to 52.5 Hz), wind turbines would have more than 4 times the capacity of regulation of the kinetic energy of conventional synchronized generating units [312].

The initial loading of wind turbines has great influence on their provision of inertial response as it depends on the square of the rotational speed (see equation (6.3)). Also, the ratings of the converters of the turbine [163] have to be taken into account for the evacuation of the kinetic energy through these power electronics.

Following the conventional torque control strategy (which has been shortly explained in Section 6.3.1), wind turbines basically does not react to changes in system frequency. Thus, proper design of inertial response control system should allow wind turbines to behave by approximation as synchronized generating units in this sense and thus to provide instantaneous power reserves.

In [241], an inertial response control system is proposed. Figure 6.11 depicts its topology. As shown, the loop L1 is in charge of providing a torque signal proportional to the ROCOF, e.g. a decelerating torque signal if the frequency drops down its nominal value. This decelerating torque signal lasts until the frequency stabilizes. Then, without the support of any additional control action, the turbine would be accelerated as the torque reference T^*_{elec} is determined from just the MPT algorithm. This acceleration transiently reduces the power injected to the grid as the turbine is gaining kinetic energy and this could reduce further the frequency level during the network disturbance.

In order to avoid the consequent acceleration of the turbine for the recuperation of the optimal rotational speed as soon as the frequency achieves the new steady state, the inertial response control system also includes, in this case, a second loop L2. It is worth noting that this is not commonly found in the literature though. This is in charge of providing an additional torque signal proportional to the frequency deviation not to the ROCOF, so its output lasts until the nominal frequency level is recovered.

Reference [67] adopts the previously presented inertial response control

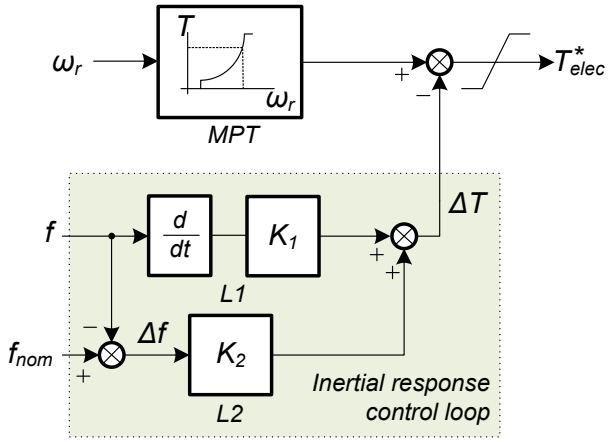

Figure 6.11: Determination of the electromagnetic torque set-point from a MPT algorithm and additional control loop for inertial response. Plot adopted and adapted from [241]

system. It is noticed, talking in terms of Figure 6.11, that both K_1 and K_2 are varied regarding the loading level of the wind turbine. It is done because, as discussed in the article, inadequate control parameters can cause unstable operation of the wind turbine. For instance, excessive value of proportional parameter K_2 under low wind conditions can cause wind turbine to stall because excessive extraction of kinetic energy. The control scheme also considers a recovering strategy for the wind turbines to their initial operating point. The recovering strategy on the WPP central controller is based on instructing each wind turbine to switch off their frequency support at different times.

Two different control methods for inertial response are proposed in [129]. The first method is composed by simply the control loop L1 in Figure 6.11. However, a low-pass filter is added after obtaining the frequency derivative signal. The aim of this filter is to avoid high rates of changes in the obtained torque set-point due to noise in frequency measurement. These undesirable excessive torque variations may affect the mechanical drive train and also may exceed the current limits of the power converters of the wind turbine. The second control method is based on the second loop L2 in Figure 6.11. This article is devoted to compare the performance of the above mentioned control methods under the event of a system frequency disturbance. It is concluded that the droop control of loop L2 deals lower increase in active power than the inertial response provided by loop L1. This results in lower

over-currents and mechanical stress for the wind turbine.

As previously noted, the additional loop L2 permanently affects the torque reference, even when the steady state is achieved. In order to overcome this effect the signal Δf is proposed to be affected by a high-pass filter in [241]. In this manner, loop L2 does not provide an additional torque signal at constant frequency levels.

A new inertial response approach is offered in [196]. This method relies on a conventional primary frequency control scheme, but performed in a transient manner. Therefore, the aim is not to let the wind turbine behave similar to a conventional generating unit but to take advantage of the capability of fast and transiently regulating the power of the wind turbine. To do that, a droop characteristic (in MW/Hz), is used to obtain a power reference signal, which is added to the output of the conventional MPT algorithm. In this article, Δf is affected by a wash-out filter (in order to reject the constant component of the signal), so the input of the power / frequency droop characteristic is zero as soon as the steady state is achieved.

It is worth pointing out that the article also considers the interaction of this fast and transient power regulation of wind turbines with their near conventional generating units. It is noticed that the fast response of wind turbines following a network power imbalance can slow down to some extent the response of conventional generators. This is because the additional and instantaneous power injection of wind turbines partly compensates the power network unbalance (affecting the network frequency). But their support lasts for a few seconds and then, conventional generators, which did not notice the real magnitude of the power unbalance from the beginning of the disturbance, are required to act to recover the network balance by full activation of their power reserves. In order to overcome this response delay of conventional generating units, a communication scheme between them and wind turbines is proposed.

Also, the article offers a comparison with the previously mentioned inertial response depicted in [241]. In regard with this comparison it is worth noting that care should be taken in setting the above mentioned proportional characteristic K_2 (see Figure 6.11), as higher values of this parameter can affect the oscillatory modes of an interconnected system. On the contrary, the implementation of the wash-out filter for the frequency in [196], favours the mitigation of these oscillatory modes.

Finally, in [164], the inertial response of a wind farm with variable speed wind turbines is depicted. It is worth noting that even though partial load conditions are considered for the analysis, the active power output of wind turbines is adjusted by the regulation of pitch angle. In the event of a

derivative of frequency, an increment in the active power set-point is directly commanded to the local controller of the power converters of each wind turbine. After 3 seconds from the activation of this power increase, a slow recovering process to the initial state of wind turbines is performed. This slow recovering process is carried out by delaying in time the particular recovering process of each wind turbine which would be commanded by the pitch control. Accordingly, each wind turbine is injecting an increased level of power for a specific time frame. This strategy smooths the net power injected by the wind farm during the recovering process which can last for up to 30 seconds. It is worth noticing that no aggregated model of the wind farm is used in order to allow individual recovering process to each wind turbine and also to take advantage of the spatial smoothing effect of wind farm. In fact, it is noticed that the total harmonic distortion of the power output of a WPP of N wind turbines is reduced by $1/\sqrt{N}$ that of a single wind turbine.

6.4 Chapter remarks

The following remarks are extracted from the contents of the chapter:

- Current Grid Codes of islanded European networks like UK and Ireland already considers the participation of WPPs in primary frequency control. In this sense, they require wind turbines to be operated not extracting the maximum available power from wind. They have to be operated in a deloaded mode instead, in order to be able to ramp up and down their output in the event of a frequency deviation.

- These above mentioned Grid Codes require to derate wind turbines up to 20% of the power they can extract from wind and for periods of time up to 30 minutes in the event of a frequency deviation. In case the frequency level is within the normal operating limits, wind turbines have to maintain a deloaded level up to 10% of the maximum power they can extract from wind.

- Future trends like the recent European Network Code developed by the ENTSO-E, indicates also the need of deloading wind turbines to participate in primary frequency control.

- Current regulations of strong electrical grids like the German grid, do not consider the operation of wind turbines in a deloaded mode in normal operating conditions. For instance, the German Grid Code

requires wind turbines to transiently reduce their power injection in the particular case of overfrequency.

- In the literature it can be found two major methods for deloading wind turbines: pitching methods and overspeeding methods. Both methods are based on the idea of achieving a nonoptimal working point in the power (or torque) - rotor speed characteristic of the wind turbine.

- Each of the above mentioned strategies fits best with different wind speed levels. For low and medium wind speed levels, considering that the rated rotor speed is not achieved, overspeeding techniques are preferable. Pitching techniques are best suited considering that the rated rotor speed is achieved.

- Among the consulted articles, it can be found approaches that consider the measurement of the wind speed for developing overspeeding techniques. This is intended as a major drawback. Also, some considerations have to take into account while applying overspeeding and pitching techniques like the tear and wear of the pitch actuator, reliability of control signals and high mechanical stress from the speed regulation of the wind turbines.

- Wind power plants may be required in the future to provide synthetic inertia. The idea is to equip wind turbines with control schemes to mimic both the dynamics and the dependency on frequency of synchronized generating units. The provision of synthetic inertia by wind turbines contributes to reduce the rate of change of frequency under a network disturbance, thus enhancing network frequency stability and the promotion of high penetration levels of wind power into the grid.

7

Coordinated operation of wind turbines and flywheel storage for primary frequency control support

Summary.- This chapter assesses the participation of wind power plants in primary frequency control support. To participate in frequency control-related tasks, the WPPs have to maintain a certain level of power reserves. In this chapter, the WPP is equipped with a flywheel-based storage system to fulfil the power reserve requirements set by the network operator. The chapter focuses on two main aspects: the definition of the control strategy to derate the wind turbines to provide part of the required power reserves; and the coordinated regulation of the power reserves of the wind turbines and the flywheels while participating in primary frequency control. This coordinated regulation enables the WPP to maintain the net level of power reserves set by the network operator while alleviating the need of deloading the wind turbines. The performance of the proposed control schemes are shown by simulation.

7.1 Introduction

More stringent requirements are gradually developed by system operators for the grid integration of WPPs [212, 95, 101]. These regulations require WPPs to behave in several aspects as conventional synchronized generating units. Among other requirements, it is set the participation of WPPs in system frequency control-related tasks (as indicated, for instance, by the Irish operator [95]).

Wind turbines are capable of providing system frequency control support [163, 312, 177, 240, 278]. In [163] it is proposed an analysis on the effects of the displacement of the conventional generating units in a power system with high penetration of WPPs. It is found the necessity of WPPs to participate in frequency control as the synchronized inertia of the system is lowered from the decoupling of the rotor inertia of the wind turbines by fast controlled power electronics. Frequency stability may be compromised with reduced levels of synchronized inertia if high rates of change of frequency are registered.

For ensuring the constancy and stability of the frequency of the electrical network, a certain level of active power reserves is required. These reserves are continuously regulated to match the power consumption and generation in the network, but also in presence of power disturbances such as sudden trips of generating units. Wind turbines have to be operated not extracting the maximum available power from the wind but maintaining a certain power margin in order to participate in primary frequency control.

But maintaining a power margin is a major drawback from the point of view of the operators of WPPs, as they are losing revenues from not selling up to 10% of the available power that can be captured from wind in normal and continuous operation. In addition, the primary frequency support WPPs can provide depends on the wind level and the control techniques used for governing the ramp up and down of the output of the wind turbines in response of a network power unbalance.

From the above mentioned considerations, it could be interesting to the owner of a WPP to connect an ESS in the point of common coupling of the generating facility with the external grid. In this case the wind turbines could be operated extracting the maximum available power from the wind. The ESS would provide the required power reserves for the participation of the WPP in primary frequency control therefore. The economic viability of the project would be determined by a cost-benefit analysis considering the cost of the storage system against the alternative of operating the wind turbines in a deloaded mode in a continuous basis.

Of course, from the point of view of the network operation, the inclusion of an ESS in the point of connection of a generation facility could not be the better allocation. It could be preferable the installation of the storage facility near the network loads in order to reduce transmission losses. However, it is also interesting to study the allocation of the storage system in the point of connection of a WPP for several reasons: i) The exploitation of the high-ramp power rates and short time responses of an adequate storage technology could lead to a great system primary frequency support from the point of common coupling of the wind facility to the grid; ii) To install a storage facility could help the WPP to fulfil the gradually increasing requirements of the Grid Codes regarding the grid integration of renewable-based power plants [83].

Several energy storage devices suitable for frequency control - related tasks can be found. Among them, the literature considers the application of large scale storage systems like pumped-hydro, compressed-air and hydrogen-based systems. Also, it is worth noting that batteries, flow batteries and those storage devices with very high ramp power rates and short time responses like SMES and flywheels are specially well-suited for this application [83].

This chapter considers the inclusion of a flywheel-based storage plant in the point of common coupling of a WPP with the external grid. The flywheels are considered to be part of the WPP and provide part of the power reserves indicated by the system operator to the WPP. This way, the WPP participates in primary frequency control. Wind turbines are required to operate to some extent in a deloaded mode depending on the level of power reserves of the flywheels, i.e. depending on their State of Charge (SoC). Thus, the required power reserves by the system operator to the wind facility can be computed by the sum of the power reserves of the flywheels and the power reserves provided by the wind turbines. The latter can be deduced from the capability of the wind turbines to increase their generation level up to the maximum available power that can be extracted from the wind. Conceptually, the scope of the chapter responds to Figure 7.1. It can be pointed out two contributions from the present work:

- The design of the central control system of the WPP and the local controllers of the wind turbines and the flywheels. These control systems are in charge of regulating the power reserves maintained by the wind turbines and the flywheels under network disturbances and also in normal operating conditions. In case of a network disturbance, i.e. of a system frequency deviation from its set-point, the power reserves

of the wind turbines and the flywheels are immediately activated by their local controllers. This activation though, is supervised by the central control system of the WPP, and this is the main contribution of the chapter.

- The determination of the control method to allow the wind turbines to maintain a certain power margin from the maximum available power that can be extracted from the wind. This control method is included in the local controller of the wind turbines. It is adopted and adapted from that presented in [206]. This is intended as a minor contribution of the chapter.

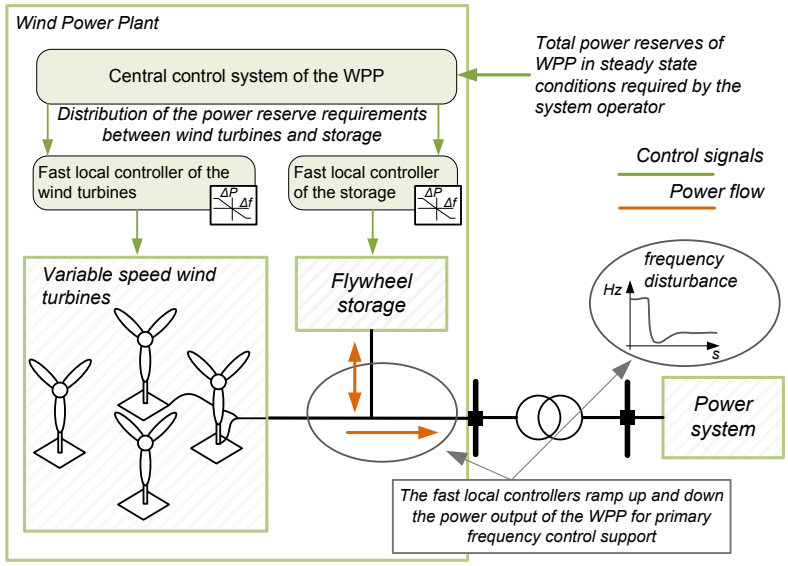

Figure 7.1: Conceptual diagram of the scope of the chapter

7.2 Proposed control schemes for the WPP

In regard of the main contributions of the chapter, this section deals with the presentation of control techniques for enabling a wind turbine to operate maintaining a power margin from the maximum available power that can be extracted from the wind. Also, the proposed central control system of the WPP to manage the power reserves of the wind turbines and the flywheels is detailed.

7.2.1 Deloaded operation of wind turbines

State of the art

As presented in Chapter 6, there are two options for enabling a wind turbine to maintain a certain level of power reserves and thus to participate in frequency control-related tasks. These options are overspeeding and pitching techniques of wind turbines for deloaded operation. Both are based on operating the wind turbines not extracting the maximum available power from wind. Overspeeding techniques are carried out applying the so-called deloaded optimum torque (or power) - omega curves $\Gamma - \omega$ [74, 320, 319, 241, 322]. These curves impose operating points out of the $\Gamma - \omega$ curve indicated by a maximum power tracking algorithm. The deloaded optimum $\Gamma - \omega$ curves are defined up to the rated speed of the turbine as presented in Figure 7.2. As it can be noted, following these operating curves the rated speed of the turbine is reached for wind speeds much lower than nominal.

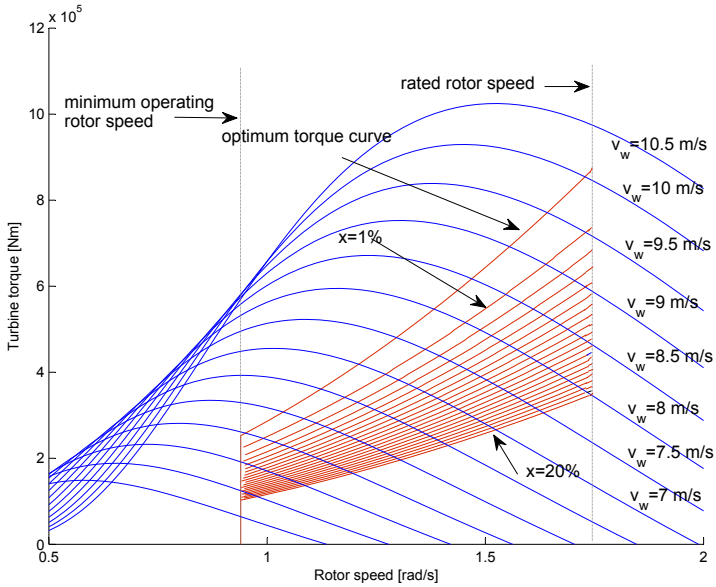

Figure 7.2: Deloaded optimum $\Gamma - \omega$ curves for a DFIG-based wind turbine of 1.5MW of rated power for power margins up to 20%. Rated wind speed 10.1 m/s

As an example, following the deloaded optimum $\Gamma - \omega$ curve for the power margin $x = 20\%$, the wind turbine achieves its rated rotational speed for wind speeds around 7.5 m/s. Note that, at maximum efficiency, the rated

wind speed for the turbine is around 10.1 m/s. Then, once the wind turbine reaches its rated speed combined regulations between the electrical torque and the pitch angle are needed in order to maintain the desired power margin level. Otherwise the wind turbine would overcome its speed ratings.

In the literature different approaches to the definition of the deloaded operating curves can be found. In [206] a strategy to ensure the required power margin at all operating ranges of a wind turbine is proposed. For wind speeds near and above nominal, when the rated rotor speed is reached, a three dimensional look-up-table which inputs the pitch angle and the required power margin is applied. The look-up-table provides the electrical power setpoint of the wind turbine. For the computation of this three dimensional look-up-table, and to the best of the knowledge of the authors of the present work, the power margin is defined in this article from the ratio between the developed electrical power and the rated power of the turbine.

In the present chapter, the power margin x is defined from the ratio between the generated electrical power $P_{opt_{del}}$ and the maximum power that can be extracted from the wind. Mathematically, this can be formulated as

$$(1-x) = \begin{cases} \frac{P_{opt_{del}}}{P_{opt}} & \text{if} \quad v_w \leq v_{w_{rated}} \\ \frac{P_{opt_{del}}}{P_{rated}} & \text{if} \quad v_w > v_{w_{rated}} \end{cases} \tag{7.1}$$

Proposed control method

The present chapter proposes an strategy for ensuring the required power margin at all operating ranges of a wind turbine. Overspeeding techniques are implemented for rotor speeds below the rated speed. In this operating range, the wind turbine is governed by the deloaded $\Gamma - \omega$ curves of Figure 7.2. Pitch angle is zero in this operating range. Once the rated speed of the turbine has been reached, the electrical torque reference is determined by a second look-up-table. As in [206], this look-up-table inputs the pitch angle, which is non-zero, and the required power margin. As a difference with [206], the output of the look up table is not the electrical power setpoint, but the electrical torque. Moreover, this magnitude is determined from the definition of the power margin presented in (7.1). Once the electrical torque reference is computed, it is sent to the low level control algorithm of the rotor-side power converter of the wind turbine.

The computation of this second look-up-table is presented as follows. Given a power margin x, the wind turbine achieves its rated speed at a wind speed below rated $v_{w_{min}}$. From this wind speed on (up to the rated wind speed for the wind turbine $v_{w_{rated}}$), the required power margin is achieved

with a proper combination of the pitch angle β and the electrical torque. Mathematically, the complementary of the power margin $(1-x)$ can be expressed as

$$\begin{aligned}\frac{P_{opt_{del}}}{P_{opt}} &= \frac{0.5\rho A v_w^3 C_{p_{del}}(v_w, \omega_{t_{rated}}, \beta)}{0.5\rho A v_w^3 C_{p_{opt}}(v_w, \omega_{t_{opt}}, 0)} \\ &= \frac{C_{p_{del}}(v_w, \omega_{t_{rated}}, \beta)}{C_{p_{opt}}(v_w, \omega_{t_{opt}}, 0)} = (1-x),\end{aligned} \tag{7.2}$$

where $v_w \epsilon [v_{w_{lim}}, v_{w_{rated}}]$ and there is one $v_{w_{lim}}$ for each power margin x. Therefore, solving this equation for each wind speed v_w and power margin x, the required pitch angle for each case can be calculated. Then, for each combination (v_w, β), it is possible to find the required deloaded optimum torque as

$$T_{opt_{del}} = \frac{0.5\rho A v_w^3 C_{p_{del}}(v_w, \omega_{t_{rated}}, \beta)}{\omega_{t_{rated}}}. \tag{7.3}$$

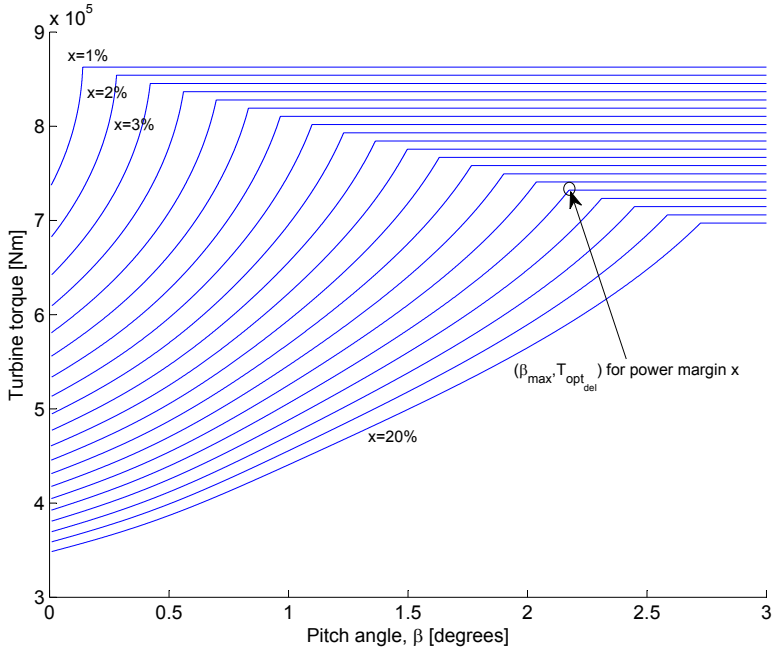

Figure 7.3: Proposed torque curves depending on the pitch angle and the power margin x

Applying this procedure, the torque curves of Figure 7.3 can be drawn. Note that for each power margin x, there is a pitch angle that corresponds

to the deloaded operating point at rated wind speed, denoted as β_{max}. From this pitch angle on, the electrical torque for the required deloaded operation becomes constant, as it is simply calculated as

$$T_{opt_{del|\beta \geq \beta_{max}}} = \frac{P_{rated}(1-x)}{\omega_{t_{rated}}}. \tag{7.4}$$

The proposed strategy for the determination of the torque reference at all operating ranges leads the control scheme for deloaded operation of the wind turbine of Figure 7.4.

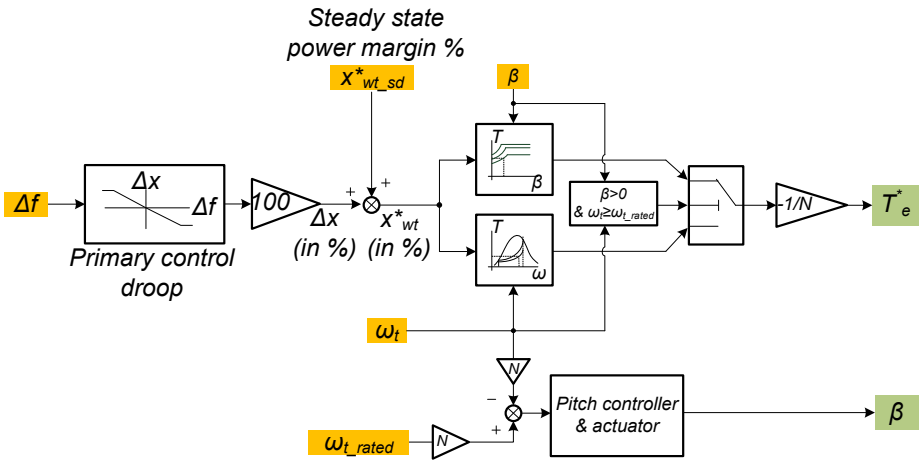

Figure 7.4: Control scheme for deloaded operation of a variable speed wind turbine for its participation in primary frequency control

As presented, the control system inputs five signals: the frequency deviation Δf from its nominal value, the power margin reference in steady state conditions $x^*_{wt\_sd}$, the rated rotational speed of the turbine ω_{t_rated}, and the measurement of the rotational speed of the turbine ω_t and the pitch angle β.

Given a frequency deviation Δf, the power / frequency droop characteristic for the primary frequency control outputs an increment or decrement in the desired power margin of the wind turbine in per unit values Δx. Then, this variation Δx is expressed in per cent and added to the required steady state power margin $x^*_{wt\_sd}$, given the total power margin reference x^*_{wt}. The steady state power margin reference can be determined by a high level control algorithm, e.g. the central controller of the WPP.

Considering that the rotational speed of the wind turbine is lower than the rated, the electrical torque reference T^*_e is obtained accessing to the

$\Gamma - \omega$ curve (Figure 7.2). This torque reference inputs the low level control algorithm of the rotor-side power converter of the wind turbine.

Once the rated speed of the wind turbine is reached, the regulation of the pitch angle comes into play. The pitch angle is regulated so that the rated speed of the turbine is not exceeded. In the case of a change in the deloaded conditions, a combined regulation of the electrical torque reference and the pitch angle is required. The electrical torque reference is obtained from the $\Gamma - \beta$ curves of Figure 7.3.

The pitch control system includes a PI controller. The tuning of this lineal controller has been carried out so that no greater gradients than ± 10 degrees per second in the pitch angle are reached. Also, the controller leads a second order type temporal response on a step-profiled reference, with a damping around 0.6-0.7. The maximum pitch angle is limited to 30 degrees.

7.2.2 Management of the power reserves of the wind turbines and the flywheels for frequency control support

The central control system of the WPP determines the power reserves of the wind turbines in steady state conditions function of the power reserves that the flywheels are capable of providing. Since part of the total power reserves required to the WPP is provided by the flywheels, the need of deloading the wind turbines so that they can maintain a certain power margin from the maximum available power they can extract from the wind is alleviating. The central control system does not govern the ramping up and down of the power of the wind turbines and the flywheels in the event of a frequency deviation. The fast local controllers of these elements are responsible of doing that instead.

The central control scheme of the WPP is presented in Figure 7.5, where it is also depicted the local control system of the flywheels and the wind turbines.

As it can be noted, the central control system of the WPP takes four input signals: the steady state power margin reference for the WPP (considering the wind turbines and the flywheels) x^*_{sd}; the total power margin reference for the wind turbines x^*_{wt}; the power output of the wind turbines at the point of common coupling of the WPP with the network P_{wt}; and the rotational speed of the flywheels ω_{fw}. It is considered that all flywheel units rotate at the same speed as they receive the same control references.

From these inputs, the central controller provides five output signals: the steady state power margin reference for the wind turbines $x^*_{wt\_sd}$, as well as the signals P_{cap+}, P_{cap-}, x_{cap+} and x_{cap-}. These four output signals are

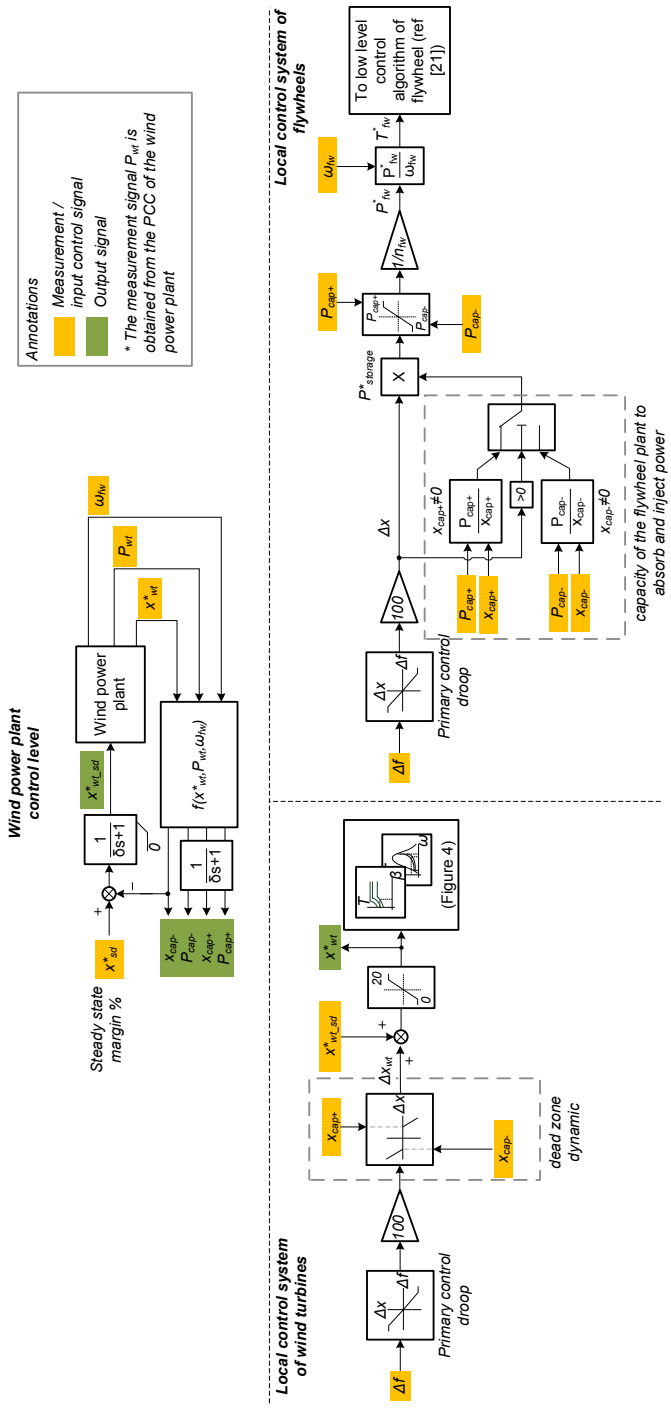

Figure 7.5: Central control system and local controllers of the wind turbines and the flywheels

needed to inform the local controllers of the wind turbines about the power margin that the flywheels can handle and thus, to limit their fast power output ramping up and down in the event of a frequency deviation.

The action of the central control system of the WPP should be so that it does not counteract with the fast control actions of the local controllers. Fast control actions of the central control system may affect the stability of the WPP as they would compete with the fast actuation of the local controllers of the flywheels and wind turbines. For that reason, the outputs of the central control system are affected by a first order type filter with a time constant of δ 5 seconds. This time constant is chosen taking into account that the time constant of the pitch actuator is in the order of 2 seconds, and the time constant of the response of the storage units are in the order of milliseconds.

Following contents detail the processes carried out by the central control system to provide the previously mentioned output signals.

As it can be noted in Figure 7.5, the input signals P_{wt}, x^*_{wt} and ω_{fw} serve to compute the function $f(P_{wt}, x^*_{wt}, \omega_{fw})$. This function determines the capacity of the flywheels to continuously inject or absorb power for up to 30 minutes. This is the period of time indicated in the ENTSO-E's recommendations [101] for the definition of the processes involving primary frequency control in the event of a frequency deviation.

The power (in MW) that the flywheels can continuously absorb for up to 30 minutes is denoted as P_{cap+}. The expression of this value in per cent of the maximum available power that the wind turbines can capture from wind is denoted as x_{cap+}. Similarly, the power (in MW) that the flywheels can inject continuously for up to 30 minutes is named P_{cap-}, and in percentage x_{cap-}. The signals P_{cap-} and P_{cap+} are computed as

$$P_{cap-} = \frac{n_{fw}}{2}\left(\frac{J_{fw}(\omega_{fw}^2 - \omega_{min}^2) - T_{loss}(\omega_{fw} - \omega_{min})t}{t}\right), \tag{7.5}$$

$$P_{cap+} = \frac{n_{fw}}{2}\left(\frac{J_{fw}(\omega_{fw}^2 - \omega_{max}^2) - T_{loss}(\omega_{fw} - \omega_{max})t}{t}\right), \tag{7.6}$$

where J_{fw} is the inertia of a flywheel unit in kgm^2, ω_{fw} is the speed in rad/s, ω_{min} and ω_{max} are the operating limits, T_{loss} is the torque losses, n_{fw} is the number of flywheel units of the storage plant and t is the time in seconds that the flywheels would be required to inject or absorb power continuously. This value is 30 minutes in normal operating conditions, but it

also represents the remaining time that the flywheels must exchange power from the event of a system frequency deviation.

To compute x_{cap+} and x_{cap-}, it is necessary to estimate the maximum power that wind turbines, as a global, could capture from wind at maximum efficiency, P_{wt_max} (in MW). This is carried out from the measurement of the power generated by the wind turbines at the point of common coupling of the WPP with the external grid and their total power margin reference x^*_{wt},

$$P_{wt\_max} = \frac{P_{wt}(1 + P_{loss_{wt}})}{1 - \frac{x^*_{wt}}{100}}. \tag{7.7}$$

To compute P_{wt_max}, it is necessary to estimate the power losses within the WPP. The power losses are represented by the magnitude $P_{loss_{wt}}$. It is assumed that its value is a percentage of the power measured in the point of common coupling with the external grid, e.g. of about 3%.

The ratio between P_{cap+} and P_{wt_max} leads x_{cap+},

$$x_{cap+} = \frac{P_{cap+}}{P_{wt\_max}} 100. \tag{7.8}$$

Analogously,

$$x_{cap-} = \frac{P_{cap-}}{P_{wt\_max}} 100. \tag{7.9}$$

The subtraction between the steady state power margin reference of the WPP x^*_{sd} and the power margin that the flywheels can handle x_{cap-} is the power margin that the wind turbines have to provide in steady state,

$$x^*_{wt\_sd} = x^*_{sd} - x_{cap-}. \tag{7.10}$$

It is important to note that $x^*_{wt\_sd}$ is bounded to 0% for consistency. Negative values of $x^*_{wt\_sd}$ would not have sense.

As previously noted, the outputs of the central control system P_{cap+}, x_{cap+}, P_{cap-} and x_{cap-} are used by the local controllers of the wind turbines and the flywheels to limit the ramping up and down of the power injected into the grid by these elements in the event of a frequency deviation (Figure 7.5). The local controllers are equipped with a primary control droop which translates the detected frequency deviation to a certain decrement (or increment) in the total power margin reference.

Considering a negative frequency deviation, i.e. a frequency level above 50 Hz, the WPP is required to ramp down its power injection into the grid incrementing the total power margin Δx. From the point of view of the

flywheels, this means to absorb power. In this case, the fraction of the total power margin increment (expressed in MW) set by the primary control droop that the flywheels can handle is

$$P^*_{storage|(>50Hz)} = \Delta x \frac{P_{cap+}}{x_{cap+}}. \tag{7.11}$$

Similarly, considering a frequency level under 50 Hz, the flywheels would be required to inject power to the grid, handling the power margin increment (in MW) expressed by

$$P^*_{storage|(<50Hz)} = \Delta x \frac{P_{cap-}}{x_{cap-}}. \tag{7.12}$$

$P^*_{storage}$ is bounded by the power capacity of the flywheels P_{cap-} and P_{cap+}. Then, the torque reference of each flywheel unit is computed by dividing the above-computed power reference by the rotating speed ω_{fw} and the number of flywheel units n_{fw}.

In the event of a frequency deviation, the primary control droop of the local control system of the wind turbines output the power margin increment Δx, as the local control system of the storage facility does. However, the local control systems of the wind turbines apply a dynamic dead zone to the signal Δx, in which the limits of the dead zone are x_{cap-} and x_{cap+}. This block outputs zero for inputs within dead zone. Also, it offsets inputs signals by either the negative or positive limits of the dead zone when outside of it. The output of this dynamic dead zone is the actual power margin increment required to the wind turbines Δx_{wt}. For instance, for an input $\Delta x = 7\%$, and $x_{cap+} = 5\%$, Δx_{wt} results $\Delta x_{wt} = 7\% - 5\% = 2\%$. By applying this strategy, the regulation of the power margin of the wind turbines comes into play just to handle the power margin increment that the storage facility cannot satisfy.

Once the power margin increment of the wind turbines is obtained, it is added to the steady state power margin set by the central control system of the WPP. The obtained power margin set point x^*_{wt} is then transmitted to the deloaded optimum torque omega curves of the wind turbines (see Figure 7.5) in order to develop the adequate electrical torque to fulfill the power margin requirements.

7.3 Simulation results

7.3.1 Network topology and configuration

Figure 7.6 shows the network topology. The network comprises a non-reheat steam turbine-based conventional power plant, a WPP and a load. The WPP is equipped with a flywheel-based storage facility.

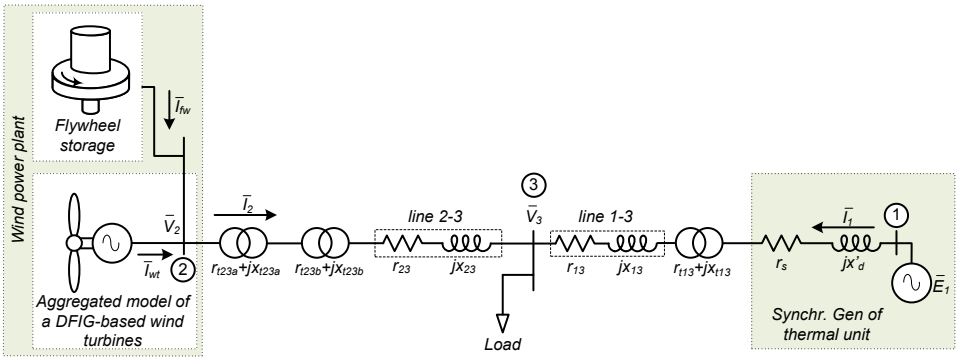

Figure 7.6: Network topology. The WPP is equipped with a flywheel-based storage system

The model of the conventional generating unit includes a third order type model of a synchronous generator, coupled to a non-reheat steam turbine. The electrical model of the generator is detailed extensively in [224], while the model of the steam turbine is explained in [173]. The power generation of the steam turbine is governed by a primary controller as detailed also in [173].

The model of the DFIG-based wind turbines including the electrical and mechanical models, as well as the low level control algorithms of the power converters are fully explained in [159].

Regarding the storage plant, it is worth noting that flywheels are commonly made up of a permanent magnet synchronous machine, mechanically coupled to a rotating disk. The power exchange with the external grid is through a set of back-to-back power converters. The model of a flywheel unit as well as the low level control algorithm of its power converters can be found in [84].

The present chapter considers a storage plant comprised by several flywheel units in parallel so that it can achieve the required power and energy capacity for participating in primary frequency control. High-speed flywheels commonly regulate hundreds of kilowatts for a few minutes. There-

fore, it is needed to dispose several flywheels to regulate tens of megawatts for up to 30 minutes.

According to the Irish network operators EirGrid and Soni, on their publication "All Island TSO Facilitation of Renewables Studies" [94], the Irish network has set the highest binding electricity target in the EU from renewable sources by 2020. In particular, 40% of electricity to come from renewables has been accorded. Some of the assumptions made in this study from the Irish network operators will be used in the current chapter for defining a realistic network with high penetration of wind power.

In the above mentioned work, it has been defined the so-called "operational metric 1". This magnitude defines the ratio of wind generation plus import and system load plus export. It could be intended as "inertialess penetration". Upper levels of this ratio than 60-80% are intended to be only technically viable with major adaptations of the power system. These adaptations refer, among others, to the change of the threshold levels of the rate of change of frequency for the relays at distribution level of more than the actual level of ±0.6Hz/s.

Considering an "inertialess penetration" of 50%, the expected ratio between the synchronized kinetic energy of the system E_k (in MWs) and the load level P_{load} (in MW) is around 6 seconds. This is the inertia constant of the conventional synchronized generation therefore. For a $P_{load} = 1000$ MW, the installed capacity of wind facilities becomes P_{wpp}=50%·P_{load}=500 MW. Taking into account that each wind turbine has a rated power of 1.5 MW, 333 wind turbines configure the total installed capacity of wind power.

Finally, the largest severity of the power imbalance in the network has to be determined for the analysis performed in the present study. For doing that, and according to [94], the so-called "operational metric 2" is defined. This magnitude is the ratio of kinetic energy stored in conventional generators plus load and the largest severity of the power imbalance. This ratio can be intended as an indicator of frequency stability. Stable operation of the 2020 scenario in the Irish network is considered with an "operational metric 2" greater than 20-30 MWs/MW. Considering that the kinetic energy stored in conventional generators is $E_k = 1000MW{\cdot}6s = 6000$ MWs, the largest severity of power imbalance is $P_{imb} = 6000MWs/30MWs \cdot MW^{-1} = 200$ MW.

The flywheel-based storage system is sized so that it has twice the power and energy capacity of a storage plant the manufacturer of flywheels Beacon Power has commissioned for frequency regulation [179]. This system is able to continuously regulate 20 MW for 15 minutes at full load, extending its operation for lesser loads. The storage plant proposed in the present chapter

is composed by 400 flywheel small units. Each unit can continuously regulate 100 kW for 15 minutes. Operated at partial load, one can come up with a storage plant that can continuously regulate 20 MW for 30 minutes. All units are connected in parallel, as in the above mentioned commercial solution. A summary of the parameters for the network configuration is presented in Table 7.1. The characteristic parameters of the particular model of each component of the system are presented in the Appendix.

Table 7.1: Parameters for the study case

Parameter	Value	Units
Rated power of conventional generation	1000	MVA
Primary control droop of conv. generation R	0.05	pu
Inertia constant of conventional generation H	6.0	s
Largest power imbalance in the network	200.0	MVA
Rated power of WPP	500.0	MVA
Primary control droop of WPP R_{wpp}	0.1	pu
Limits of Δx of primary control of WPP	0.1	pu
Steady state power margin of WPP x^*_{sd}	10	%
Ratings of flywheel-based storage plant	20-30	MW-min
Number of flywheel units n_{fw}	400	pu

7.3.2 Regulation of the deloading level of wind turbines

The following paragraphs evaluate the performance of the proposed control scheme for governing the deloaded level of the wind turbines (Section 7.2.1). Three different scenarios have been proposed: i) the wind speed is low, much lower than the rated level for the wind turbine, and therefore the pitch angle is zero at all times; ii) the wind speed is higher than in the previous case, but still lower than the rated wind speed level for the wind turbine. The pitch angle could be different from zero depending on the required power margin; iii) the wind speed is very high, higher than the rated wind speed of the wind turbine, and a non-minimum pitch angle is therefore required regardless the required power margin.

In the first scenario, the desired power margin of the wind turbine x^*_{wt} can be achieved just overspeeding the wind turbine. Figure 7.7 plots the response of the turbine on a step-profiled power margin increment from $x^*_{wt} = 10\%$ to $x^*_{wt} = 15\%$. The wind speed is maintained constant at 7.5 m/s. As shown, since the wind speed is low, the rated rotor speed is not achieved even while

derating the turbine. Therefore, the pitch angle is zero at all times and the torque reference is obtained from the $\Gamma - \omega$ curves of Figure 7.2.

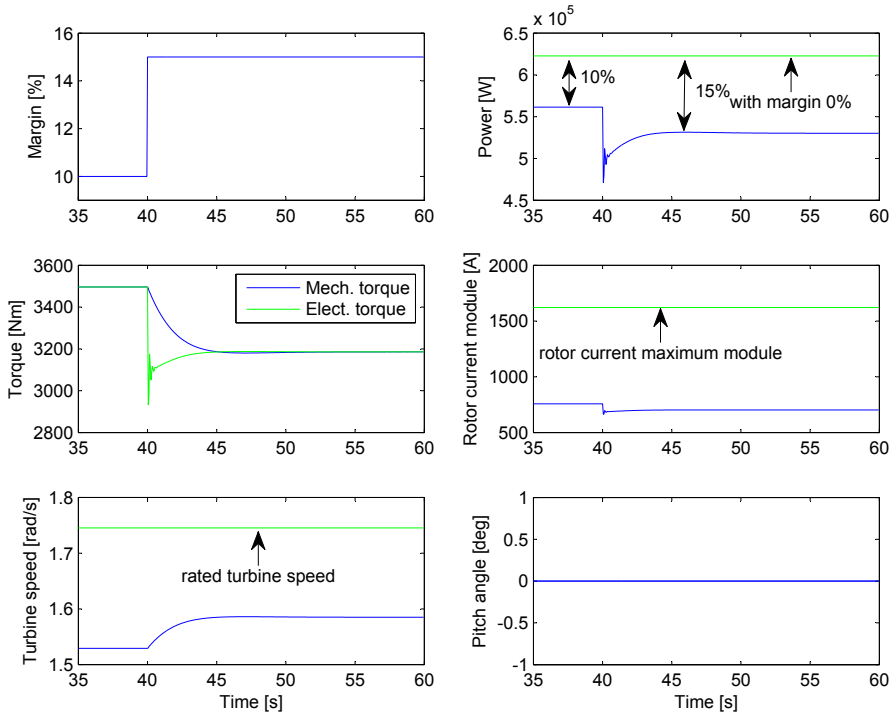

Figure 7.7: Performance evaluation of the proposed control system for deloaded operation. The power margin reference x^*_{wt} is incremented from 10% to 15%. The wind turbine is subjected to a low wind speed of 7.5 m/s

Figure 7.8 plots the response of the turbine on a step-profiled power margin increment from $x^*_{wt} = 10\%$ to $x^*_{wt} = 15\%$. The wind speed is maintained constant at 8.5 m/s. The wind speed is lower than the rated wind speed for the turbine at maximum efficiency (10.1 m/s). However, the rated rotor speed of the turbine is achieved for a power margin x^*_{wt} of 15%. From this point on the pitch angle is not zero and the torque reference is obtained from the second look-up-table (see Figure 7.3), which inputs the pitch angle and the required power margin. It is worth noting that the turbine speed is maintained within its operating limits due to the combined regulations of the electrical torque and the pitch angle. The temporal response of the speed of the turbine presents just a little overshot between 40 and 41 seconds. The peak value of the rotor speed during this overshot overpasses in just 0.4% the rated rotor speed.

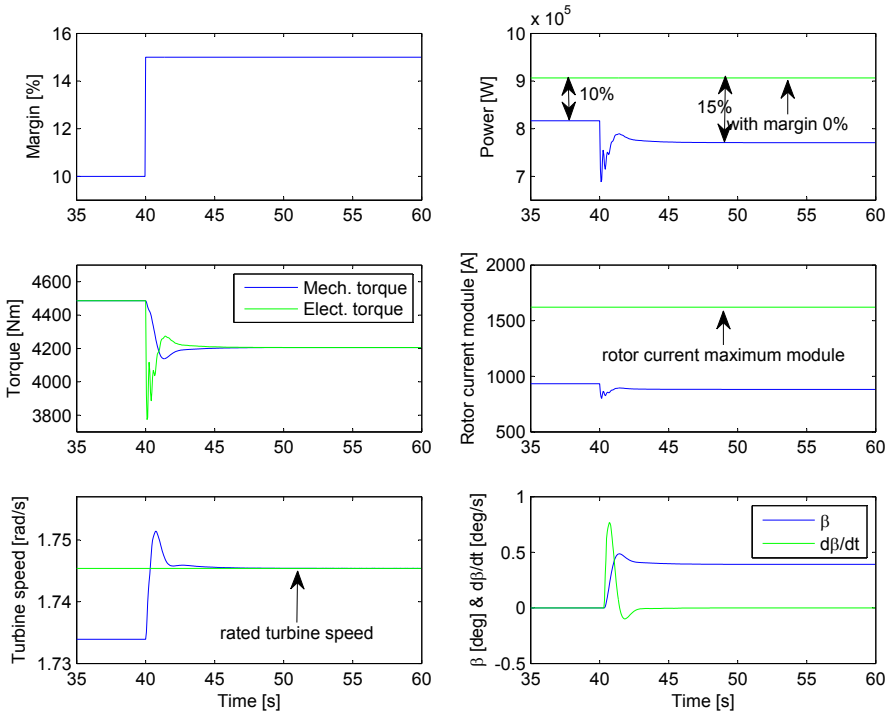

Figure 7.8: Performance evaluation of the proposed control system for deloaded operation. The power margin reference x^*_{wt} is incremented from 10% to 15%. The wind turbine is subjected to a low wind speed of 8.5 m/s

The primary frequency control support that the wind turbines can provide is evaluated in Figure 7.9. Nor the flywheels, neither other control schemes apart from the control scheme for deloading the wind turbines (Figure 7.4) are affecting the power margin reference of the wind turbines. As it can be noted, the maximum rate of change of frequency (registered at the beginning of the disturbance) is the same in all cases as the synchronized inertia of the system does not vary. Considering wind speeds below the rated (7.5 m/s and 8.5 m/s), both the frequency nadir and the steady state level of the frequency after the disturbance are improved with the participation of wind turbines in primary frequency support. In this region, the regulation of the power margin maintained by the wind turbines is mainly carried out by overspeeding the turbines. As previously noted in Figure 7.7 and Figure 7.8 this regulation is very fast and also implies the exchange of kinetic energy of the rotor of the turbines with the network. These aspects favours the provided primary frequency support to the network.

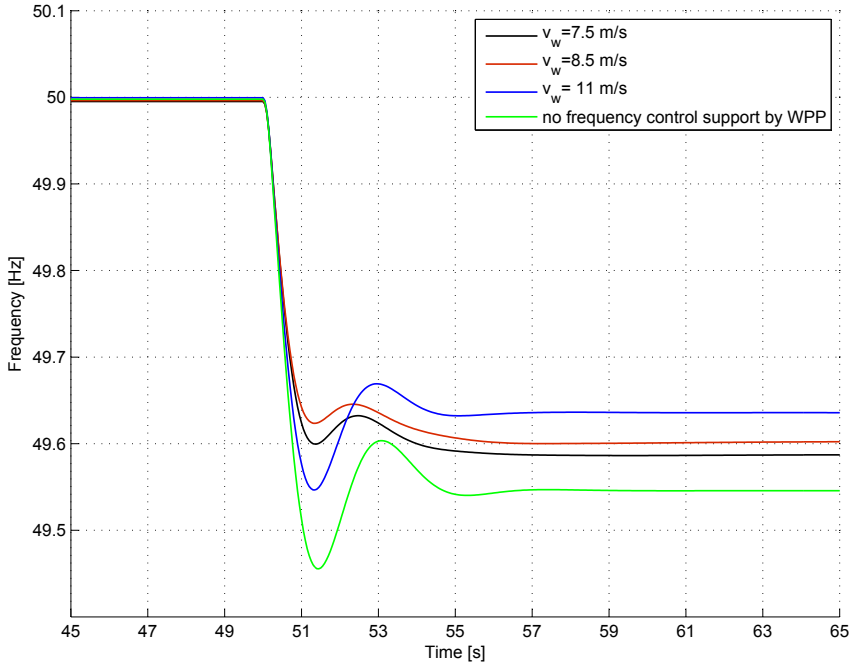

Figure 7.9: Network frequency excursion due to a sudden change in the load level of 200 MW. Wind turbines participate in primary frequency control under different load conditions. The flywheels are not involved

Considering wind speeds above rated (blue line in Figure 7.9), the power

regulation of the wind turbines is influenced by the dynamics of the pitch control. These dynamics are much slower than those involved in overspeeding techniques. Also, since the rotational speed of the turbines is kept constant, there is no kinetic energy of the rotor of the turbines exchanged with the network. These aspects lead a lower frequency nadir than applying overspeeding techniques. On the other hand, since a variation in the power margin reference of the turbines Δx implies the regulation of high power, the new steady state frequency level achieved after the network disturbance is much higher than in the case of considering low wind speed levels.

7.3.3 Coordinated activation of the power reserves of the wind turbines and the flywheels under a network disturbance

The following set of simulations concerns the coordinated regulation of the power margin developed by the components within the WPP, i.e. the wind turbines and the flywheels, so that it can fulfil the power margin requirements set by the network operator in steady state conditions and also during a network disturbance.

This coordinated regulation of the power margin developed by the components of the WPP is carried out by the central control system of the WPP and the local controllers of the wind turbines and the flywheels (Figure 7.5).

In order to evaluate the performance of the proposed control systems under different load conditions of the wind turbines, two wind speed levels have been considered. Firstly, it is considered a wind speed level low enough to permit the wind turbines to fulfil their power margin reference x^*_{wt} by just applying overspeeding techniques. Secondly, it is considered a wind speed level above the rated so the required power margin of the wind turbines is affected by their pitch control.

Although, in practice, the setpoint for each wind turbine is different, as the wind speed can be quite different from one wind turbine to the other, the same wind speed level is considered for all wind turbines as an average. This simplification has been considered as the aim of the study at this point is to evaluate the support that the wind power plant could provide as a global in primary frequency control. Moreover, it is worth noting that the designed wind power plant controller does not consider any control signal from an individual wind turbine, but it considers the net power generated by all wind turbines as a global. Notwithstanding, further studies considering different wind speed levels for each wind turbine would complement the performance evaluation of the proposed controller and the support of wind power plants in primary frequency control.

Low wind speed level

As in the previous simulations, it is considered a sudden power imbalance in the network that the generating units of the system (both the conventional generating unit and the WPP) have to compensate through their primary frequency controllers.

Figure 7.10 plots the total power margin developed by the WPP. As a reminder, the total power margin for the WPP is determined from the sum of the steady state power margin reference for the WPP x^*_{sd} and the power margin increment or decrement set by the primary control droop Δx. As it can be noted in Figure 7.10, at 60 seconds simulation time it is considered a sudden system load increase. This provokes the system frequency to drop to a level below 50 Hz, and therefore the WPP is required to reduce the developed power margin, i.e. to increase its power injection to the grid. The steady state power margin reference for the WPP is set to $x^*_{sd} = 10\%$ with respect to the maximum available power that could be extracted from wind.

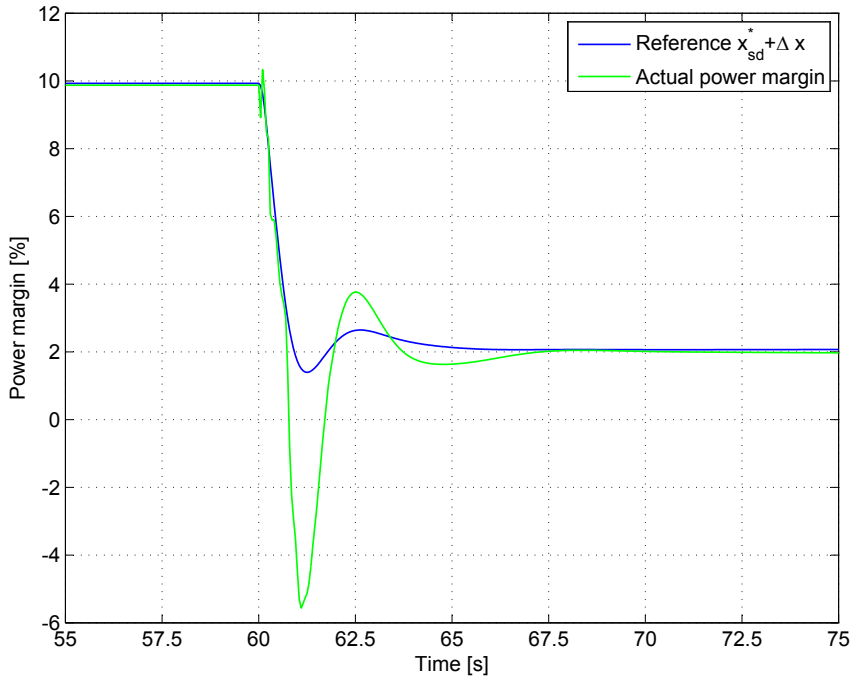

Figure 7.10: Power margin developed by the WPP. At time t=60 seconds there is a sudden increase of the system load level. The wind turbines are exposed to a wind speed of 8.5 m/s

The required power margin is provided by the power reserves of the wind turbines and the energy stored in the flywheels. The variation of the power margin of the wind turbines is carried out as soon as the primary control droop of the local controllers of the wind turbines output an increment or decrement power margin variation Δx greater than the power margin the storage facility can handle. This can be appreciated in Figure 7.11.

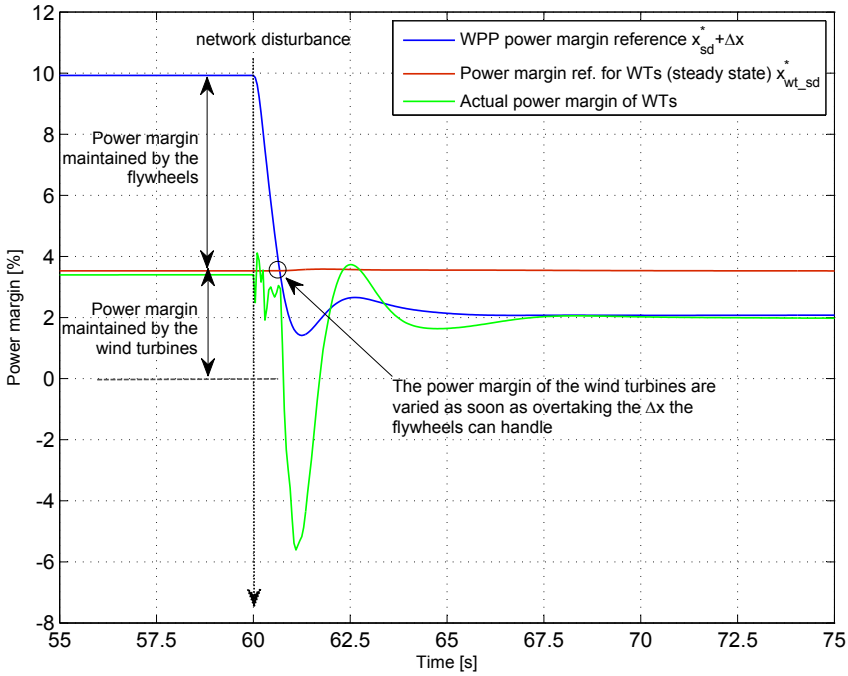

Figure 7.11: Power margin developed by the WPP. Detail of the power margin developed by the wind turbines and the flywheels. At 60 seconds simulation time there is a network disturbance. The wind turbines are exposed to a wind speed of 8.5 m/s

As it can be observed, the developed power margin by the wind turbines previous to the network disturbance is about $x_{wt} = 3.4\%$. The total power margin required by the system operator is $x^*_{sd} = 10\%$. Thus, the storage facility, which SoC is 100%, is in charge of handling a power margin $x_{fw} = 10\% - 3.4\% = 6.6\%$. The network disturbance provokes that the primary control droops of the local controllers of the flywheels and the wind turbines output a decrement in the developed power margin Δx. Then, the total power margin reference for the WPP becomes $x^*_{sd} + \Delta x$. The regulation of the power reserves of the wind turbines is carried out as soon as the frequency

deviation requires a decrement in the developed power margin greater than the maximum power margin the storage facility can handle x_{cap-}.

As presented in Figure 7.11, the actual power margin developed by wind turbines does not follow the power margin reference $x^*_{sd} + \Delta x$ during the transient state provoked by the network disturbance, until achieving the new steady state. This is due to the fact that since the operating points of the wind turbines require applying just overspeeding techniques, there is kinetic energy released to the network from the speed regulation of the wind turbines. This surplus of energy released during the transient state is intended to be a benefit from the point of view of the network, as it complements the primary frequency support provided by the WPP.

To evaluate the provided frequency control support, Figure 7.12 plots the frequency excursion of the network. Red line plots the case of no frequency control support by the WPP. Only conventional synchronized generating units are in charge of developing this task therefore. With the participation of the WPP (the flywheels are fully charged), the frequency profile depicted by the blue line can be obtained. As it can be noted, higher frequency nadir and also higher frequency level at the new steady state after the disturbance can be obtained in this case.

As it can be observed in Figure 7.12, the contribution of the WPP in primary frequency control depends on the SoC of the flywheels. Considering the flywheels discharged, i.e. leaving the wind turbines alone for carrying out the task, a higher frequency nadir than in the case the flywheels are also participating can be obtained. This is due to the fact that in this case, the power margin of the wind turbines is regulated by just applying overspeeding techniques. Thus, some kinetic energy of the rotor of the turbines is exchanged with the network from the variation of their rotational speeds. As previously noted in the chapter, this surplus of energy injected to the grid improves the performance of the provided primary frequency support. Therefore, if the flywheels are discharged, the wind turbines have to satisfy the net variation of the power margin requirements, and then they are speeded down in a higher extent than in the case the required power margin decrement is satisfied also by the flywheels, leading a higher kinetic energy exchanged with the network.

Wind speed above rated

This section deals with the evaluation of the performance of the proposed controllers for the WPP while having wind speeds above the rated wind speed of the wind turbines. The wind speed level is set to 11 m/s (the

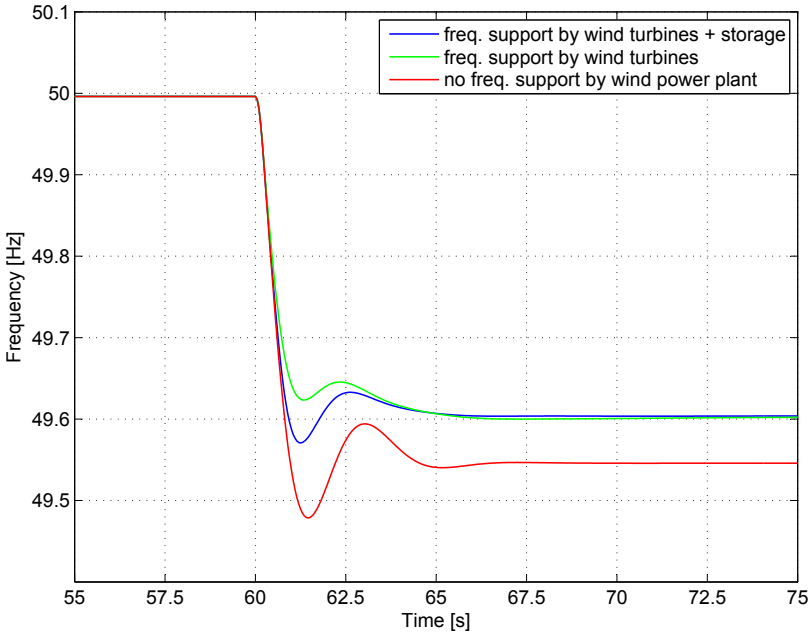

Figure 7.12: Frequency deviation caused by a sudden load increase. Red line plots the case of no frequency support by the WPP. Blue line shows the obtained performance from the support of the WPP (wind turbines and flywheels). Green line presents the obtained result considering the flywheels discharged. The wind turbines are exposed to a wind speed of 8.5 m/s

rated wind speed is 10.1 m/s) and the flywheels are fully charged. Figure 7.13 plots the power margin developed by the WPP while having a network disturbance.

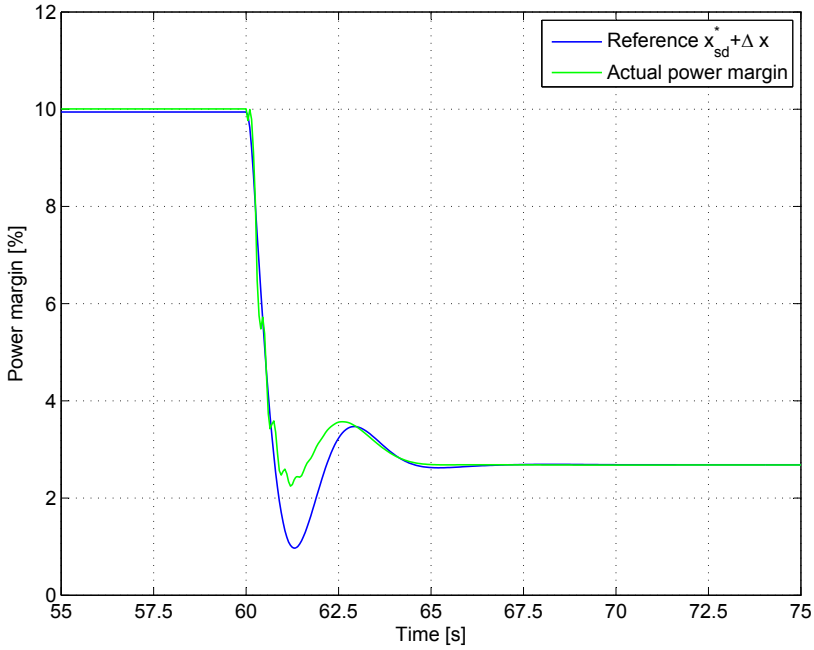

Figure 7.13: Actual power margin developed by the WPP and its reference value $x^*_{sd} + \Delta x$. The wind speed is 11 m/s

As it can be noted in Figure 7.13, the developed power margin by the WPP follows the reference $x^*_{sd} + \Delta x$ to a large degree. From a certain point the developed power margin is transiently different that the reference level. At the beginning of the frequency deviation, the flywheel storage activates very fast its power reserves, so the developed power margin matches with the reference. This occurs until the regulation of the power margin of the wind turbines comes into play. Since the regulation of the power margin of the wind turbines depends, in this case, on the slow dynamics of their pitch actuator, the regulation of the power margin is not fast enough to follow the reference during the transient state.

The dynamics of the pitch actuator of a wind turbine are shown in Figure 7.14 (bottom left corner). Figure 7.14 also plots the speed and torque of the turbine. As shown the turbine speed is varied in a very little extent. In the top left corner the SoC of a flywheel is presented. As shown, flywheel units

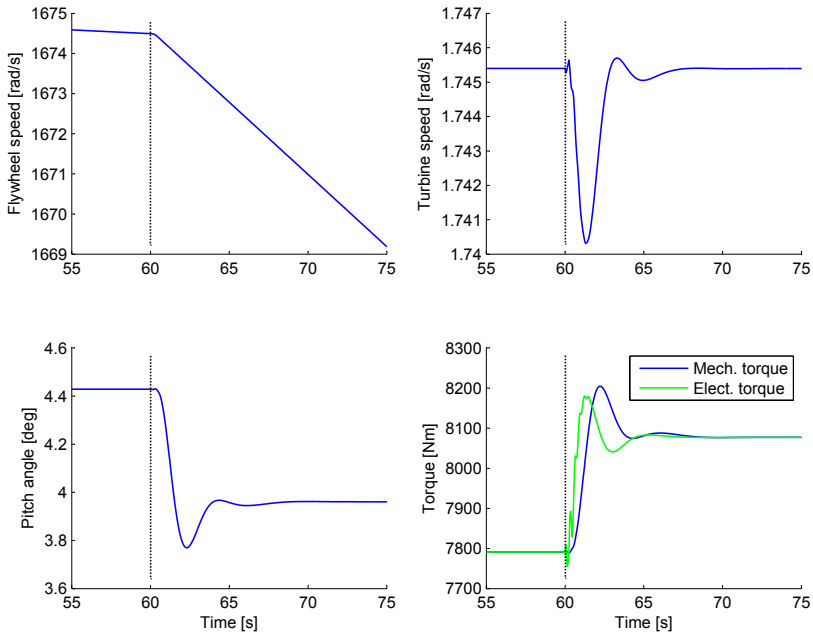

Figure 7.14: Flywheel speed before and after detecting the network disturbance at time 60 seconds. Also, it is shown the speed, the pitch angle and the mechanical and electrical torque developed by wind turbines. The wind turbines are exposed to a wind speed of 11 m/s

become continuous (but slowly) discharged due to the standing losses. At 60 seconds simulation time, the primary control droop of its local control system detects the frequency deviation and the flywheel starts injecting power into the grid. As shown, there are no fast changes in the speed of the flywheel. This favours the slow dynamics of the control signals x_{cap-}, x_{cap+}, P_{cap-} and P_{cap+}.

Figure 7.15 plots the frequency excursion due to the network disturbance at 60 seconds simulation time. Red line plots the case of no frequency control support by the WPP. Only conventional generating units are in charge of this task in this case. With the participation in primary frequency control of the WPP (the flywheels are charged) it is obtained the frequency excursion depicted by the blue line. As it can be noted, the contribution of the wind turbines and the flywheels improve the obtained frequency nadir and also the new steady state after the disturbance.

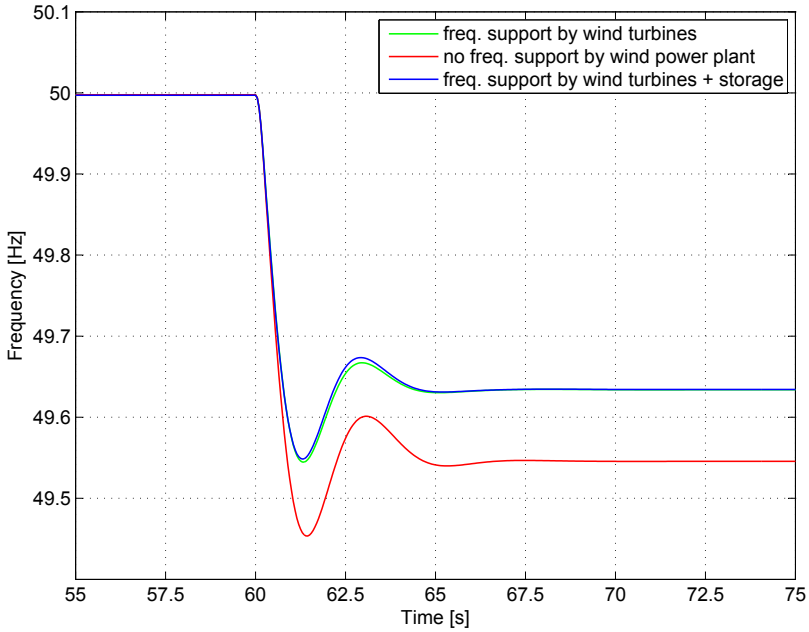

Figure 7.15: Frequency deviation caused network disturbance. Red line plots the case of no frequency support by the WPP. Blue line shows the obtained performance from the contribution of the WPP (wind turbines and flywheels). Green line presents the result considering the flywheels discharged. The wind turbines are exposed to a wind speed of 11 m/s

Figure 7.15 also plots the case of considering the flywheels discharged.

Table 7.2: Power reserve allocation between wind turbines and flywheels (fully charged)

	Wind speed (m/s)				
	7.0	8.0	9.0	10.0	11.0
	Required power reserve to the WPP in (MW)				
	16.7	25.3	35.9	49.2	50.7
	Power reserve allocation				
W. turbines (MW)	0.0	5.3	15.9	29.3	30.7
Flywheels (MW)	20.0	20.0	20.0	20.0	20.0
Flywheels share (%)	120.0	79.3	55.7	40.7	39.5

The primary frequency control support the wind turbines can provide in this case (their power margin is affected by the dynamics of the pitch actuator) is as good as the support provided by the WPP when considering the fast actuation of the flywheels. This is due to the fact that despite the flywheels responds in the range of milliseconds to a power request, its power injection is governed by the slow dynamics imposed by the output of the primary control droop of its local control system, i.e. the slow dynamics of the frequency excursion.

From the analysis performed in this Section 7.3.3, it is worth to remark that the main advantage of including the flywheels in the WPP is the reduction of the power margin that the wind turbines have to maintain during network disturbances and also in steady state conditions. In this regard, Table 7.2 depicts the assignment of the required power reserve to the WPP between the flywheels and the wind turbines. As it can be noted, the flywheels, while being fully charged, are capable of providing up to the net level of power reserves of the WPP depending on the wind speed, enabling the wind turbines to operate at maximum efficiency in a continuous basis (as for 7.0 m/s wind speed).

7.4 Chapter remarks

The final remarks of the presented chapter are outlined as follows:

- A control method for derating variable-speed wind turbines has been developed. This control method combines overspeeding techniques and pitching techniques. From the application of the designed method, the

wind turbines can be operated so that they maintain a power margin from the maximum available power that can be extracted from wind. The method is applicable to all wind speed ranges of variable speed wind turbines; both above and below the rated wind speed level.

- The frequency control support that the wind turbines can provide permits to improve the frequency nadir and the steady state level of the frequency due to a network disturbance. The contribution of the wind turbines though, is subjected to the applied control techniques. For instance, in case of governing the power margin through overspeeding techniques, the frequency control support they can provide is augmented by the kinetic energy of the rotor of the turbine exchanged with the network due to the variation of their rotating speed.

- Looking at the contribution of the WPP to primary frequency control, it is worth noting that the application of the designed central control system of the WPP and the local controllers of the wind turbines and the flywheels, allow the management of the level of reserves maintained by the wind turbines in function of the SoC of a flywheels. The inclusion of the flywheels in the WPP reduces the need of operating the wind turbines in a deloaded mode, enabling them to operate extracting the maximum available power from the wind and thus maximizing the revenues of the WPP operator while still providing the primary frequency control support to the network.

8 Conclusions

This thesis focuses on the research on the applications in wind power of energy storage systems in general, and of flywheel-based energy storage systems in particular. This Chapter covers the general conclusions of the work. Particular remarks on the topic of each chapter can be found in dedicated sections.

The thesis has covered literature review, simulation-based and experimental works using laboratory equipments. The main contributions of the thesis are listed as follows:

- An introduction to several energy storage systems and the identification of their potential uses in wind power plants.
- The setting up of a scale-lab flywheel-based energy storage system for the experimental validation of some of the developed control methods throughout the thesis.
- The definition of an optimization criteria for the operation of the flywheel for the power smoothing of wind turbines. This covers the formulation and deterministic solution of an optimization problem.
- The design and the experimental validation of a novel energy management algorithm of a flywheel for the power smoothing of wind power plants. The designed control algorithm takes into account the previously defined optimization criteria for the operation of the flywheel and it is based on feedback control techniques.
- The literature review on control methods of wind power plants and grid codes requirements for system frequency control.

- The design of a control method for variable speed wind turbines for enabling their participation in system frequency control.

- The design of a control system for wind power plants considering the support of energy storage devices for primary frequency control. The control system manages the power reserves of the wind turbines and the storage devices within the plant (flywheel-based in this case) for the participation of the wind power plant in primary frequency control.

From the results of the thesis, it is concluded that flywheels can be used to enhance the grid integration of wind power. For instance, the high-ramp power rates and short time responses define flywheels as well suited for reducing the variability of the power generated by wind turbines, and thus for improving the quality of the power injected to the grid by wind power plants. Also, since flywheels can exchange power during several minutes at full power, they can also help wind power plants to provide the mandatory ancillary services set by the network operators in their grid codes such as system frequency control support. Besides, it is worth highlighting the following conclusions from the thesis:

- The solution of the optimization problem proposed in Chapter 4, leads that in order to maximize the wind power smoothing, it is convenient to adjust the average state of charge of the storage device to the expected magnitude of the fluctuating components of wind power to be compensated. As a result, it is found that the higher average wind power, the higher optimum average state of charge of the flywheel. Simulation results for an illustrative example show that the optimum average state of charge of the flywheel varies between 89 to 93% of its maximum energy capacity depending on the considered generation levels of the wind turbine. Also, following the proposed optimization criteria, simulation results show that an attenuation of up to 97.1% of the fluctuating components of wind power from a cutoff frequency of 0.4 Hz can be achieved. The power fluctuating components from this cut off frequency include the power disturbances associated to the rotating sampling effect of the wind turbine.

- The control algorithm for the flywheel for wind power smoothing designed and experimentally validated in Chapter 5 permits to adjust the average state of charge of the flywheel as a function of the average wind power. Also, it is worth noting that the control of the indicated average rotational speed of the flywheel avoids the progressive

discharge of the storage device in its operation due to the losses of the system, while permitting the fast accelerations of the flywheel for wind power smoothing. Experimental results show that most of the fluctuating components of the power of the wind turbine due to the rotating sampling effect can be compensated by the flywheel, supporting the simulation results obtained in Chapter 4. Also, it is depicted the convenience of varying the average state of charge of the flywheel with the magnitude of wind power to be compensated. In particular, it is found an attenuation of the fluctuating components of wind power of up to 85% while the flywheel test bench is rotating at 120 rad/s in average, and an increased attenuation to 92% considering 220 rad/s as the average rotational speed of the flywheel test bench.

- Finally, and regarding the results of Chapter 7, it is worth noting that the inclusion of flywheels in wind power plants reduces the need of operating the wind turbines in a deloaded mode for primary frequency control support, enabling them to operate extracting the maximum available power from the wind. Since the wind turbines are operated at maximum efficiency, the revenues of the wind power plant operator can be maximized. In particular, it is found that a flywheel-based storage plant with rated power 20 MW and energy capacity of 10 MWh provides enough power reserves to fulfil the reserve requirements of 500 MW of installed capacity of wind power for primary frequency control support.

8.1 Further related work

From the conclusions of the thesis, there is no doubt that energy storage systems can benefit the grid integration of wind power. This assertion is mainly based on technical arguments such as the possibility of improving the controllability of the power output of wind power plants. Major barriers for the installation of energy storage devices have to do with economical aspects. In this sense, it is proposed to evaluate the inclusion (looking at the location, sizing and operation) of the storage devices for enhancing an optimal operation of the electrical network while considering high penetration rates of wind power plants.

Moreover, there is a wide research field on the support that wind power plants (equipped or not with storage devices) can provide to system frequency control related tasks. Some proposals regarding further work in this direction are depicted in the following:

- To propose further control methods of wind power plants for their participation in system frequency control related task. For instance, aspects such as different control architectures and the recovering process of the power reserves of the wind power plant required by the network operator after a network disturbance should be investigated.

- To improve the primary frequency control support that wind power plants could provide by evaluating the inertial response capability of wind turbines. This inertial response could be provided by acting on either the local controllers of the wind turbines, but also it can be provided by storage devices with high ramp power rates and short time responses included in the wind power plant.

- In the views of the network frequency stability, it is proposed to study the effect of the fast regulation of the power output of the wind power plants while participating in primary frequency control.

- To perform a cost-benefit analysis evaluating the installation of storage devices against the alternative of operating the wind turbines in a deloaded mode in a continuous basis. As explained in the thesis, to operate the wind turbines in a deloaded mode is needed for the provision of the required power reserves for their participation in system frequency control.

Finally, it is proposed to compare flywheel systems with other short-term storage devices such as ultracapacitors or SMES for evaluating also their suitability in wind power applications.

Bibliography

[1] A123 Systems website, http://www.a123systems.com/ [accessed 07.05.2013] 23, 25

[2] Abbey, C. and Joos, G. Supercapacitor energy storage for wind energy applications. IEEE Transactions on Industry Applications 2007;43:769-8 33, 35

[3] Abdelkafi, A., Krichen, L. New strategy of pitch angle control for energy management of a wind farm. Energy 2011;36:1470-1479 154

[4] Ackermann, T. Wind power in power systems. John Wiley & Sons, Ltd; 2005 3, 86, 135, 234

[5] Active Power website, http://www.activepower.com/ [07.05.2013] 25

[6] Adachi, K., Tajima, H. and Hashimoto, T. Development of 16 kWh power storage system applying Li-ion batteries. Journal of Power Sources 2003;119-121:897-5 15, 24, 25

[7] Agbossou, K., Kolhe, M., Hamelin, J. and Bose, T.K. Performance of a stand-alone renewable energy system based on energy storage as hydrogen. IEEE Transactions on Energy Conversion 2004;19:633-8 32, 39

[8] Ahmad-Lone, S.A. and Mufti, M.-u-D. Integrating a redox flow battery system with a wind-diesel power system. In: International Conference on Power Electronics, Drives and Energy Systems. 2006 32

[9] Aifantis, K.E., Hackney, S.A. and Vasant-Kumar, R. High energy density lithium batteries. WILEY-VCH Verlag GmbH & Co. KGaA; 2010 25

[10] Akagi, H., Watanabe, E.H. and Aredes, M. Instantaneous power theory and applications to power conditioning. New Jersey: John Wiley & Sons, Inc.; 2007 62

[11] Alaska Energy Authority. Energy Storage Review, `http://www.aidea.org/aea/` [accessed 07.05.2013] 23, 32, 33

[12] Alcad website, `http://www.alcad.com/` [07.05.2013] 25

[13] Ali, M.H., Minwon Park, In-Keun Yu, Murata, T. and Tamura, J. Improvement of wind generator stability by fuzzy logic-controlled SMES. IEEE Transactions on Industry Applications 2009;45:1045-7 33, 35

[14] Ali, M.H. and Wu, B. Comparison of stabilization methods for fixed-speed wind generator systems. IEEE Transactions on Power Delivery 2010;25:323-9 33

[15] Ali, M.H., Wu, B. and Dougal, R.A. An overview of SMES applications in power and energy systems. IEEE Transactions on Sustainable Energy 2010;1:38-10 25, 26

[16] American Superconductor Corporation website, `http://www.amsc.com/` [accessed 07.05.2013] 25

[17] Anagnostopoulos, J.S. and Papantonis, D.E. Simulation and size optimization of a pumped-storage power plant for the recovery of wind-farms rejected energy. Renewable Energy 2008;33:1685-10 32, 41

[18] Aström, K.J. and Murray, R.M. Feedback systems: An introduction for scientists and engineers. Princeton University Press; 2008 58, 64, 71, 89

[19] Arrouf, M. and Bouguechal, N. Vector control of an induction motor fed by a photovoltaic generator. Applied Energy 2003;74:159-167 49

[20] Arsoy, A.B., Liu, Y., Ribeiro, P.F. and Wang, F. Static-synchronous compensators and superconducting magnetic energy storage systems in controlling power system dynamics. IEEE Industry Applications Magazine 2003;21-8 33

[21] Ashby, M.F. Materials selection in mechanical design. Elsevier Butterworth-Heinemann; 2005 22

[22] Baker, J. New technology and possible advances in energy storage. Energy Policy 2008;36:4368-6 24

[23] Bakhoum, E.G. New mega-farad ultracapacitors. IEEE Transactions on Ultrasonics, Ferroelectrics, and Frequency Control 2009;56:14-8 27

[24] Balducci, A., Dugas, R., Taberna, P.L., Simon, P., Plée, D., Mastragostino, M., and Passerini, S. High temperature carbon-carbon supercapacitor using ionic liquid as electrolyte. Journal of Power Sources 2007;165:922-6 27

[25] Barin, A., Canha, L.N., Magnago, K. and da-Rosa-Abaide, A. Fuzzy multi-sets and multi-rules: Analysis of hybrid systems concerning renewable sources with conventional and flow batteries. In: 15th International Conference on Intelligent System Applications to Power Systems. 2009 23

[26] Barker, P.P. Ultracapacitors for use in power quality and distributed resource applications. In: IEEE Power Engineering Society Summer Meeting. 2002 25, 27, 33

[27] Barote, L. and Marinescu, C. A new control method for VRB SOC estimation in stand-alone wind energy systems. In: International Conference on Clean Electrical Power. 2009 32, 39

[28] Barote, L., Weissbach, R., Teodorescu, R., Marinescu, C. and Cirstea, M. Stand-alone wind system with Vanadium Redox Battery energy storage. In: 11th International Conference on Optimization of Electrical and Electronic Equipment. 2008 24, 32, 39

[29] Baroudi, J.A., Dinavahi, V. and Knight, A.M. A review of power converter topologies for wind generators. Renewable Energy 2007;32:2369-17 36

[30] Barrado, J.A., Griñó, R. and Valderrama-Blavi, H. Power-quality improvement of a stand-alone induction generator using a STATCOM with battery energy storage system. IEEE Transactions on Power Delivery 2010;25:2734-8 33, 36

[31] Barton, J.P. and Infield, D.G. Energy storage and its use with intermittent renewable energy. IEEE Transactions on Energy Conversion 2004;19:441-8 25, 31, 38

[32] Baumann, L., Boggasch, E., Rylatt, M. and Wright, A. Energy flow management of a hybrid renewable energy system with hydrogen. In: IEEE Conference on Innovative Technologies for an Efficient and Reliable Electricity Supply (CITRES). 2010 32

[33] Bayod-Rújula, A.A. Future development of the electricity systems with distributed generation. Energy 2009;34:377-7 31

[34] Beacon Power Corporation website `http://www.beaconpower.com` [accessed 07.05.2013] 23, 24, 25, 74

[35] Beaudin, M., Zareipour, H., Schellenberglabe, A. and Rosehart, W. Energy storage for mitigating the variability of renewable electricity sources: An updated review. Energy for Sustainable Development 2010;14:302-13 9, 23, 25, 27, 31

[36] Beck, F. and Ruëtschi, P. Rechargeable batteries with aqueous electrolytes. Electrochimica Acta 2000;45:2467-16 17, 24

[37] Benitez, L. E., Benitez, P. C. and Cornelis Van Kooten, G. The economics of wind power with energy storage. Energy Economics 2008;30:1973-17 25, 32, 41

[38] Bernal-Agustín, J.L. and Dufo-López, R. Hourly energy management for grid-connected wind-hydrogen systems. International Journal of Hydrogen Energy 2008;33:6401-13 32, 40

[39] Bhatia, R.S., Jain, S.P., Jain, D.K. and Singh, B. Battery energy storage system for power conditioning of renewable energy sources. In: International Conference on Power Electronics and Drives Systems 2005;501-6 33

[40] Bianchi, F.D., De Batista, H. and Mantz, R.J. Wind turbine control systems. Principles, modeling and gain scheduling design. Springer; 2007 81, 82, 84, 85, 147

[41] Bito, A. Overview of the sodium-sulfur battery for the IEEE Stationary Battery Committee. In: IEEE Power Engineering Society General Meeting. 2005 15, 25, 33

[42] Bolund, B., Bernhoff, H. and Leijon, M. Flywheel energy and power storage systems. Renewable & Sustainable Energy Reviews 2007;11:235-24 21, 22

[43] Boukettaya, G., Krichen, L. and Ouali, A. A comparative study of three different sensorless vector control strategies for a Flywheel Energy Storage System. Energy 2010;35:132-8 33, 34, 49, 81

[44] Brekken, T.K.A., Yokochi, A., von-Jouanne, A., Yen, Z.Z., Hapke, H.M. and Halamay, D.A. Optimal energy storage sizing and control for wind power applications. IEEE Transactions on Sustainable Energy 2011;2:69-9 32, 39

[45] Brisebois, J. and Aubut, N. Wind farm inertia emulation to fulfill Hydro-Québec's specific need. In: IEEE Power and Energy Society General Meeting. 2011 146

[46] Broussely, M. and Pistoia G. Industrial applications of batteries. From cars to aerospace and energy storage. Elsevier B.V.; 2007 13, 14, 24, 25

[47] Brown, P.D., Peças Lopes, J.A. and Matos, M.A. Optimization of pumped storage capacity in an isolated power system with large renewable penetration. IEEE Transactions on Power Systems 2008;23:523-9 32, 40, 41, 42

[48] Bruce, P.G. Energy storage beyond the horizon: Rechargeable lithium batteries. Solid State Ionics 2008;179:752-9 15

[49] Bueno, C. and Carta, J.A. Wind powered pumped hydro storage systems, a means of increasing the penetration of renewable energy in the Canary Islands. Renewable and Sustainable Energy Reviews 2006;10:312-29 32

[50] Butler, P.C., Cole, J.F. and Taylor, P.A. Test profiles for stationary energy-storage applications. Journal of Power Sources 1999;78:176-6 33

[51] Camblong, H. Digital robust control of a variable speed pitch regulated wind turbine for above rated wind speeds. Control Engineering Practice 2008;16:946-958 149

[52] Camblong, H., Nourdine, S., Vechiu, I. and Tapia, G. Comparison of an island wind turbine collective and individual pitch LQG controllers designed to alleviate fatigue loads. IET Renewable Power Generation 2012;6:267-275 149

[53] Caralis, G. and Zervos, A. Value of wind energy on the reliability of autonomous power systems. IET Renewable Power Generation 2010;4:186-12 32

[54] Cárdenas, R., Peña, R., Asher, G. and Clare, J. Control strategies for enhanced power smoothing in wind energy systems using a flywheel driven by a vector-controlled induction machine. IEEE Transactions on Industrial Electronics 2001;48:625-11 33, 34, 49, 81, 109

[55] Cárdenas, R., Peña, R., Asher, G., Clare, J. and Blasco-Giménez, R. Control strategies for power smoothing using a flywheel driven by a sensorless vector-controlled induction machine operating in a wide speed range. IEEE Transactions on Industrial Electronics 2004;51:603-12 33, 34, 49, 56, 81

[56] Cárdenas, R., Peña, R., Pérez, M., Clare, J., Asher, G. and Wheeler, P. Power smoothing using a flywheel driven by a switched reluctance machine. IEEE Transactions on Industrial Electronics 2006;53:1086-8 33, 34, 81

[57] Carton, J.G. and Olabi, A.G. Wind/hydrogen hybrid systems: Opportunity for Ireland's wind resource to provide consistent sustainable energy supply. Energy 2010;35:4536-9 19, 20, 32, 41

[58] Castronuovo, E.D. and Lopes, J.A.P. On the optimization of the daily operation of a wind-hydro power plant. IEEE Transactions on Power Systems 2004;19:1599-8 32

[59] Cavallo, A. Controllable and affordable utility-scale electricity from intermittent wind resources and compressed air energy storage (CAES). Energy 2007;32:120-8 32, 39

[60] Cericola, D., Ruch, P.W., Kötz, R., Novák, P. and Wokaun, A. Simulation of a supercapacitor/Li-ion battery hybrid for pulsed applications. Journal of Power Sources 2010;195:2731-6 24, 28

[61] Chang, Y., Mao, X., Zhao, Y., Feng, S., Chen, H. and Finlow, D. Lead-acid battery use in the development of renewable energy systems in China. Journal of Power Sources 2009;191:176-7 33

[62] Chen, G.Z, Liu, D.Y., Wang, F. and Ou C.Q. Determination of installed capacity of pumped storage station in WSP hybrid power supply system. In: International Conference on Sustainable Power Generation and Supply. 2009 32

[63] Cimuca, G.O., Saudemont, C., Robyns, B. and Radulescu, M.M. Control and performance evaluation of a flywheel energy-storage system associated to a variable-speed wind generator. IEEE Transactions on Industrial Electronics 2006;53:1074-1085 49, 81, 109, 110

[64] Cinergia website, `http://www.cinergia.coop/` [accessed 07.05.2013] 66

[65] Clark, N.H. and Doughty, D.H. Development and testing of 100 kW / 1 min Li-ion battery systems for energy storage applications. Journal of Power Sources 2005;146:798-6 23, 25, 33

[66] Colet-Subirachs, A., Ruiz-Álvarez, A., Gomis-Bellmunt, O., Alvarez-Cuevas-Figuerola, F. and Sudria-Andreu, A. Centralized and distributed active and reactive power control of a utility connected microgrid using IEC61850. IEEE Systems Journal 2012;6:58-67 50

[67] Conroy, J. and Watson R. Frequency response capability of full converter wind turbine generators in comparison to conventional generation. IEEE Transactions on Power Systems 2008;23:649-656 157

[68] Conte, M., Iacobazzi, A., Ronchetti, M. and Vellone, R. Hydrogen economy for a sustainable development: state-of-the-art and technological perspectives. Journal of Power Sources 2001;100:171-17 19

[69] Control Techniques website, `http://www.controltechniques.coop/` [accessed 06.05.2013] 52, 66

[70] Corey, G.P. An assessment of the state of the zinc-bromine battery development effort, `http://www.redflow.com` [accessed 07.05.2013] 23

[71] Dai, X., Deng, Z., Liu, G., Tang, X., Zhang, F. and Deng, Z. Review on advanced flywheel energy storage system with large scale. Transactions of China Electrotechnical Society 2011;26:133-140

[72] Daneshi, H., Daneshi, A., Tabari, N.M. and Jahromi, A.N. Security-constrained unit commitment in a system with wind generation and compressed air energy storage. In: 6th International Conference on the European Energy Market. 2009 32, 42

[73] de Almeida, R., Castronuovo, E. and Peças-Lopes J. Optimum generation control in wind parks when carrying out system operator requests. IEEE Transactions on Power Systems 2006;21:718-725 149, 150, 153, 154

[74] de Almeida, R. and Peças-Lopes, J. Participations of doubly fed induction wind generators in system frequency regulation. IEEE Transactions on power systems 2007;22:944-950 151, 168

[75] de Prada-Gil, M., Gomis-Bellmunt, O., Sumper, A. and Bergas-Jané, J. Power generation efficiency analysis of offshore wind farms connected to a SLPC (single large power converter) operated with variable frequencies considering wake effects. Energy 2012;37:455-468 84

[76] Deane, J.P., Ó Gallachóir, B.P. and McKeogh, E.J. Techno-economic review of existing and new pumped hydro energy storage plant. Renewable and Sustainable Energy Reviews 2010;14:1293-10 32

[77] de-Boer, P. and Raadschelders, J. Flow batteries. Leonardo Energy, briefing paper, `http://www.leonardo-energy.org/webfm_send/164` [accessed 07.05.2013] 23, 25

[78] Dehkordi, B.M., Kiyoumarsi, A., Hamedani, P. and Lucas, C. A comparative study of various intelligent based controllers for speed control of IPMSM drives in the field-weakening region. Expert Systems with Applications 2011;38:12643-11

[79] Dell, R.M. and Rand, D.A.J. Energy storage - a key technology for global energy sustainability. Journal of Power Sources 2001;100:2-16 14, 24, 31

[80] Denholm, P. and Kulcinski, G. L. Life cycle energy requirements and greenhouse gas emissions from large scale energy storage systems. Energy Conversion and Management 2004;45:2153-20 11, 24, 25

[81] Denholm, P. and Sioshansi, R. The value of compressed air energy storage with wind in transmission-constrained electric power systems. Energy Policy 2009;37:3149-10 32, 41

[82] Díaz-González, F., Sumper, A., Gomis-Bellmunt, O. and Bianchi F.D. Energy management of flywheel-based energy storage device for wind power smoothing. Applied Energy 2013;110:207-219 109, 110, 113, 122, 125

[83] Díaz-González, F., Sumper, A., Gomis-Bellmunt, O. and Villafáfila-Robles, R. A review of energy storage technologies for wind power applications. Renewable and Sustainable Energy Reviews 2012;16:2154-2171 81, 88, 109, 131, 166

[84] Díaz-González, F., Sumper, A., Gomis-Bellmunt, O. and Villafáfila-Robles, R. Modeling, control and experimental validation of a flywheel-based energy storage device. Journal of European Power Electronics 2013;23:1-21 116, 123, 177

[85] Divya, K.C. and Ostergaard, J. Battery energy storage technology for power systems - An overview. Electric Power Systems Research 2009;79:511-10 12, 18, 23, 24

[86] Domínguez-García, J.L., Gomis-Bellmunt, O., Trilla-Romero, L. and Junyent-Ferré, A. Indirect vector control of a squirrel cage induction generator wind turbine. Computers & Mathematics with Applications 2012;64:102-114 62

[87] Dong, Z., Kennedy, S.J. and Wu, Y. Electrospinning materials for energy-related applications and devices. Journal of Power Sources 2011;196:4886-4904 27

[88] Dresser-Rand website, `http://www.dresser-rand.com/` [accessed 07.05.2013] 25

[89] Du, W., Wang, H.F., Cheng, S., Wen, J.Y., and Dunn, R. Robustness of damping control implemented by Energy Storage Systems installed in power systems. Electrical Power and Energy Systems 2011;33:35-8 33, 37

[90] Du-Pasquier, A., Plitz, I., Menocal, S. and Amatucci, G. A comparative study of Li-ion battery, supercapacitor and nonaqueous asymmetric hybrid devices for automotive applications. Journal of Power Sources 2003;115:171-8 24, 28

[91] Dufo-López, R., Bernal-Agustín, J.L. and Domínguez-Navarro, J.A. Generation management using batteries in wind farms: Economical and technical analysis for Spain. Energy Policy 2009;37:126-14 32, 33, 40

[92] Dursun, B. and Alboyaci, B. The contribution of wind-hydro pumped storage systems in meeting Turkey's electric energy demand. Renewable and Sustainable Energy Reviews 2010;14:1979-10 10, 32, 41

[93] EA Technology. Review of electrical energy storage technologies and systems and of their potential for the UK (2004), `http://www.wearemichigan.com/JobsAndEnergy/documents/file15185.pdf` [accessed 07.05.2013] 24

[94] EirGrid and System Operator for Northern Ireland (SONI). All island tso facilitation of renewables studies, http://www.eirgrid.com [accessed 26.04.2013] 131, 135, 178

[95] EirGrid. Eirgrid grid code version 4.0, http://www.eirgrid.com [accessed 26.04.2013] XVI, 132, 138, 139, 140, 141, 165

[96] El-Tous, Y. Pitch angle control of variable speed wind turbine. Americal Journal of Engineering and Applied Sciences 2008;1:118-120 147

[97] Electricity Storage Association website, http://www.electricitystorage.org/ [accessed 07.05.2013] 18, 23, 24

[98] Elias-Alcega, A., Roman-Barri, M., Ruiz-Álvarez, A., Cairo-Molins, I., Sumper, A. and Gomis-Bellmunt, O. Implementation of a test microgrid in Barcelona. In: 21st International Conference and Exhibition on Electricity Distribution, Frankfurt, Germany, 2011 50

[99] Emerging electric technologies whitepaper. Parcon website, http://www.parcon.uci.edu/ [accessed 07.05.2013] 24

[100] Enis Windgen, Renewable Energy Systems Llc, http://www.eniswindgen.com/ [accessed 07.05.2013] 25

[101] ENTSO-E. Entso-e network code for requirements for grid connection applicable to all generators, https://www.entsoe.eu/ [accessed 26.04.2013] XVI, 132, 143, 145, 146, 165, 174

[102] ENTSO-E. Network code for requirements for grid connection applicable to all generators. Frequently asked questions (2012), https://www.entsoe.eu/ [accessed 26.04.2013] 146, 156

[103] ENTSO-E. Operational handbook; policies; load-frequency control and performance (2009), https://www.entsoe.eu/ [accessed 26.04.2013] XVI, 133, 134, 136, 137, 138, 140, 154

[104] ENTSO-E. Operational reserve ad hoc team report. final version (2012), https://www.entsoe.eu/ [accessed 26.04.2013] XVI, 133, 139, 140

[105] EPCOS AG website, http://www.epcos.com/ [accessed 07.05.2013] 25

[106] EPRI. EPRI-DOE handbook supplement of energy storage for grid connected wind generation applications (2004), http://www.epri.com/abstracts/Pages/ProductAbstract.aspx?ProductId=000000000001008703 [accessed 07.05.2013] 23, 31, 32, 36

[107] Erlich, I., Winter. W and Dittrich, A. Advanced grid requirements for the integration of wind turbines into the German transmission system. In: IEEE Power Engineering Society General Meeting. 2006 137

[108] Esmaili, A. and Nasiri, A. Energy storage for short-term and long-term wind energy support. In: 36th Annual Conference on IEEE Industrial Electronics Society. 2010 18, 24, 32

[109] Exide Technologies website, http://www.exide.com/ [accessed 07.05.2013] 25

[110] Faias, S., Santos, P., Sousa, J. and Castro, R. An overview on short and long-term response energy storage devices for power systems applications. In: International Conference on Renewable Energies and Power Quality. 2008 23

[111] Fergus, J.W. Recent developments in cathode materials for lithium ion batteries. Journal of Power Sources 2010;195:939-16 15

[112] First Hydro Company website, http://www.fhc.co.uk/pumped_storage.htm [accessed 07.05.2013] 10, 25

[113] Fuel Cell Energy Inc. website, http://www.fuelcellenergy.com/ [accessed 07.05.2013] 23, 25

[114] GAMS website, http://www.gams.com/ [accessed 08.05.2012] 91

[115] Georgilakis, P.S. Technical challenges associated with the integration of wind power into power systems. Renewable and Sustainable Energy Reviews 2008;12:852-12 31

[116] Ghedamsi, K. and Aouzellag, D. Improvement of the performances for wind energy conversions systems. Electrical Power and Energy Systems 2010;32:936-945 81

[117] Ghedamsi, K., Aouzellag, D. and Berkouk, E.M. Control of wind generator associated to a flywheel energy storage system. Renewable Energy 2008;33:2145-12 33

[118] Goel, P.K., Singh, B., Murthy, S.S. and Kishore, N. Isolated wind-hydro hybrid system using cage generators and battery storage. IEEE Transactions on Industrial Electronics 2011;58:1141-13 32

[119] Gomis-Bellmunt, O., Junyent-Ferré, A., Sumper, A. and Bergas-Jane, J. Permanent magnet synchronous generator offshore wind farms connected to a single power converter. In: IEEE Power and Energy Society General Meeting. 2010 62, 87

[120] Gomis-Bellmunt, O., Junyent-Ferre, A., Sumper, A. and Bergas-Jane, J. Ride-through control of a doubly fed induction generator under unbalanced voltage sags. IEEE Transactions on Energy Conversion 2008;23:1036-11 34

[121] Gomis-Bellmunt, O., Liang, J., Ekanayake, J. and Jenkins, N. Voltage - current characteristics of multiterminal HVDC-VSC for offshore wind farms. Electric Power Systems Research 2011;81:440-11 34, 50

[122] González, A., McKeogh, E. and Gallachoóir, B.Ó. The role of hydrogen in high wind energy penetration electricity systems: The Irish case. Renewable Energy 2003;29:471-19 32, 41

[123] Gonzalez-Longatt, F. Impact of synthetic inertia from wind power on the protection/control schemes of future power systems: simulation study. In: 11th IET International Conference on Developments in Power Systems Protection. 2012 146

[124] Goswami, D.Y., Kreith, F. Energy conversion. New York: Taylor & Francis Group; 2008

[125] Grant-Wilson, I.A., McGregor, P.G. and Hall, P.J. Energy storage in the UK electrical network: Estimation of the scale and review of technology options. Energy Policy 2010;38:4099-8 32

[126] Greenblatt, J.B., Succar, S., Denkenberger, D.C., Williams, R.H. and Socolow, R.H. Baseload wind energy: modeling the competition between gas turbines and compressed air energy storage for supplemental generation. Energy Policy 2007;35:1474-19 13

[127] Gualous, H., Bouquain, D., Berthon, A. and Kauffmann, J.M. Experimental study of supercapacitor serial resistance and capacitance variations with temperature. Journal of Power Sources 2003;123:86-8 27

[128] Hadjipaschalis, I., Poullikkas, A. and Efthimiou, V. Overview of current and future energy storage technologies for electric power applications. Renewable and Sustainable Energy Reviews 2009;13:1513-10 13, 16, 19, 22, 23, 24, 25

[129] Haileselassie, T., Torres-Olguin, R., Vrana, T. and Uhlen, K. Main grid frequency support strategy for VSC-HVDC connected wind farms with variable speed wind turbines. In: IEEE Trondheim PowerTech. 2011 156, 158

[130] Hall, P. J. and Bain, E. J. Energy-storage technologies and electricity generation. Energy Policy 2008;36:4352-4 16, 18, 23, 24, 25

[131] Harding Energy Inc. website, `http://www.hardingenergy.com/` [accessed 07.05.2013] 24, 25

[132] Hassenzahl, W.V., Hazelton, D.W., Johnson, B.K., Komarek, P., Noe, M. and Reis, C.T. Electric power applications of superconductivity. Proceedings of the IEEE 2004;92:1655-20 23

[133] Hayashi, H., Hatabe, Y., Nagafuchi, T., Taguchi, A., Terazono, K., Ishii, T. and Taniguchi, S. Test results of power system control by experimental SMES. IEEE Transactions on Applied Superconductivity 2006;16:598-4 26, 33, 36

[134] Hee-Yeol Jung, A-Rong Kim, Jae-Ho Kim, Minwon Park, In-Keun Yu, Seok-Ho Kim, Kideok Sim, Hae-Jong Kim, Ki-Chul Seong, Asao, T. and Tamura, J. A Study on the operating characteristics of SMES for the dispersed power generation system. IEEE Transactions on Applied Superconductivity 2009;19:2028-4 33, 34

[135] Hennessy, T. Overcoming transmission constraints: energy storage and wyoming wind power, `http://www.sandia.gov/ess/docs/pr_conferences/2006/farber.pdf` [accessed 07.05.2013] 32

[136] Helwig, A. and Ahfock, T. Ultra-capacitor assisted battery storage for remote area power supplies: A case study. In: 19th Australasian Universities Power Engineering Conference: Sustainable Energy Technologies and Systems. 2009 25, 28, 33

[137] Hessami, M.-A. and Bowly, D.R. Economic feasibility and optimisation of an energy storage system for Portland Wind Farm (Victoria, Australia). Applied Energy 2011;88:2755-2763 81

[138] Hida, Y., Yokoyama, R., Shimizukawa, J., Iba, K., Tanaka, K. and Seki, T. Load following operation of NAS battery by setting statistic margins to avoid risks. In: IEEE Power and Energy Society General Meeting. 2010 33, 39

[139] Hirabayashi, S., Tomita, Y. and Iwamoto, S. Enhancement of transient stability ATC using NAS battery systems. In: IEEE/PES Transmission and Distribution Conference and Exposition. 2008 33

[140] Holdsworth, L., Ekanayake, J., Jenkins, N. Power system frequency response from a fixed speed and double fed induction generator-based wind turbines. Wind Energy 2004;7:21-35 XVII, 133, 150, 155

[141] Holm, S.R., Polinder, H. and Ferreira, J.A. Analitycal modeling of a permanent-magnet synchronous machine in a flywheel. IEEE Transactions on Magnetics 2007;43:1955-13 22

[142] Hu, W., Chen, Z. and Bak-Jensen, B. Optimal operation strategy of battery energy storage system to real-time electricity price in Denmark. In: IEEE Power and Energy Society General Meeting. 2010 32

[143] Hu, W., Chen, Z., Wang, Y. and Wang, Z. Flicker mitigation by active power control of variable-speed wind turbines with full-scale back-to-back power converters. IEEE Transactions on Energy Conversion 2009;24:640-649 81

[144] Huang, K-L., Li, X-G., Liu, S-Q., Tan, N. and Chen L-Q. Research progress of vanadium redox flow battery for energy storage in China. Renewable Energy 2008;33:186-7 17, 24, 25

[145] Ibrahim, H., Ilinca, A. and Perron, J. Energy storage systems - characteristics and comparisons. Renewable and Sustainable Energy Reviews 2008;12:1221-30 9, 10, 11, 21, 23, 24, 25, 32

[146] IEEE Power & Energy Society. IEEE Recommended practice for the characterization and evaluation of emerging energy storage technologies in stationary applications. IEEE Std 1679-2010. 2010 13, 75

[147] Iijima, Y., Sakanaka, Y., Kawakami, N., Fukuhara, M., Ogawa, K., Bando, M. and Matsuda, T. Development and field experiences of NAS battery inverter for power stabilization of a 51 MW wind farm. In: International Power Electronics Conference. 2010 33, 39

[148] Ipsakis, D., Voutetakis, S., Seferlis, P., Stergiopoulos, F. and Elmasides, C. Power management strategies for a stand-alone power system using renewable energy sources and hydrogen storage. International Journal of Hydrogen Energy 2009;34:7081-15 32, 39

[149] Iqbal, M.T. Modeling and control of a wind fuel cell hybrid energy system. Renewable Energy 2003;28:223-15 32

[150] Ise, T., Kita, M. and Taguchi, A. A hybrid energy storage with a SMES and secondary battery. IEEE Transactions on Applied Superconductivity 2005;15:1915-4 33

[151] Jalal Kazempour, S., Parsa Moghaddam, M., Haghifam, M. R. and Yousefi, G. R. Electric energy storage systems in a market-based economy: Comparison of emerging and traditional technologies. Renewable Energy 2009;34:2630-10 15, 23, 24, 25

[152] Janssens, N., Lambin, G. and Bragard, N. Active power control strategies of dfig wind turbines. In: IEEE Laussane Power Tech. 2007 148, 149, 151, 154

[153] Jerbi, L., Krichen, L. and Ouali, A. A fuzzy logic supervisor for active and reactive power control of a variable speed wind energy conversion system associated to a flywheel storage system. Electric Power Systems Research 2009;79:919-925 81, 109

[154] Jiancheng, Z., Lipei, H., Zhiye, C. and Su, W. Research on flywheel energy storage system for power quality. In: Proceedings of International Conference on Power System Technology, POWERCON. 2002 22

[155] Jiancheng, Z. Research on flywheel energy storage system using in power network. In: International Conference on Power Electronics and Drives Systems 2005;1344-1347

[156] Joerissen, L., Garche, J., Fabjan, Ch. and Tomazic, G. Possible use of vanadium redox-flow batteries for energy storage in small grids and stand-alone photovoltaic systems. Journal of Power Sources 2004;127:98-7 32

[157] JSC ESMA website, `http://www.esma-cap.com/` [accessed 07.05.2013] 25

[158] Jun-Keun, J. DSP-based self-tuning IP speed controller with load torque compensation for rolling mill DC drive. IEEE Transactions on Industrial Electronics 1995;42:282-386 109

[159] Junyent-Ferré, A., Gomis-Bellmunt, O., Sumper, A., Sala, M. and Mata, M. Modeling and control of the doubly fed induction generator wind turbine. Simulation Modeling Practice and Theory 2010;18:1365-1381 34, 62, 87, 146, 155, 177

[160] Kaldellis, J. K. and Zafirakis, D. Optimum energy storage techniques for the improvement of renewable energy sources-based electricity generation economic efficiency. Energy 2007;32:2295-11 10, 23, 24, 25

[161] Kapsali, M. and Kaldellis, J.K. Combining hydro and variable wind power generation by means of pumped-storage under economically viable terms. Applied Energy 2010;87:3475-11 32, 40

[162] Kawakami, N., Iijima, Y., Sakanaka, Y., Fukuhara, M., Ogawa, K., Bando, M. and Matsuda, T. Development and field experiences of stabilization system using 34MW NAS batteries for a 51MW wind farm. In: IEEE International Symposium on Industrial Electronics (ISIE). 2010 23

[163] Kayikci, M., Milanovic, J. Dynamic contribution of DFIG-based wind plants to system frequency disturbances. IEEE Transactions on Power Systems 2009;24:859-867 131, 135, 136, 157, 165

[164] Keung, P.-K., Li, P., Banakar, H. and Ooi, B. Kinetic energy of wind-turbine generators for system frequency support. IEEE Transactions on Power Systems 2009;24:279-287 157, 159

[165] Kim, A.-R., Seo, H.-R., Kim, G.H., Park, M., Yu, I.-K., Otsuki, Y. and Tamura, J. Operating characteristic analysis of HTS SMES for frequency stabilization of dispersed power generation system. IEEE Transactions on Applied Superconductivity 2010;20:1334-5 26, 33, 34

[166] Kim, H.J., Seong, K.C., Cho, J.W., Bae, J.H., Sim, K.D., Kim, S., Lee, E.Y., Ryu, K. and Kim, S.H. 3 MJ / 750 kVA SMES system for improving power quality. IEEE Transactions on Applied Superconductivity 2006;16:574-4 33

[167] Kinjo, T., Senjyu, T., Urasaki, N. and Fujita, H. Terminal-voltage and output-power regulation of wind-turbine generator by series and par-

allel compensation using SMES. IEEE Proceedings Generation, Transmission and Distribution 2006;153:276-7 33, 35

[168] Kondoh, J., Ishii, I., Yamaguchi, H., Murata, A., Otani, K., Sakuta, K., Higuchi, N., Sekine, S. and Kamimoto, M. Electrical energy storage systems for energy networks. Energy Conversion & Management 2000;41:1863-12 25, 28, 33

[169] Korpas, M. and Greiner, C.J. Opportunities for hydrogen production in connection with wind power in weak grids. Renewable Energy 2008;33:1199-10 32, 41, 43

[170] Kotz, R. and Carlen, M. Principles and applications of electrochemical capacitors. Electrochimica Acta 2000;45:2483-17 25

[171] Krause, P.C., Wasynczuk, O., Sudhoff, S.D. Analysis of electric machinery and drive systems. USA: John Wiley & Sons, Inc.; 2002 49, 52, 55, 56, 88, 118

[172] Krishnan, R. Control and operation of PM synchronous motor drives in the field-weakening region. In: International Conference on Industrial Electronics, Control and Instrumentation. 1993 56

[173] Kundur, P. Power system stability and control. Mc Grau-Hill Inc., 1993 177, 233, 234

[174] Kuperman, A. and Aharon, I. Battery-ultracapacitor hybrids for pulsed current loads: A review. Renewable and Sustainable Energy Reviews 2011;15:981-12 33

[175] Kusko, A. and Dedad, J. Short-term and long-term energy storage methods for standby electric power systems. IEEE Industry Applications Magazine 2007;66-7 23, 28

[176] Gonçalves-Lacerda, V., Barbosa-Mageste, A., Boggione-Santos, I.J. and Henrique-Mendes, L. Separation of Cd and Ni from NiCd batteries by an environmentally safe methodology employing aqueous two-phase systems. Journal of Power Sources 2009;193:908-6 14

[177] Lalor, G., Mullane, A. and O'Malley, M. Frequency control and wind turbine technologies. IEEE Transactions on Power Systems 2005;20:1905-1913 131, 135, 136, 165

[178] Lazarewicz, M.L. and Rojas, A. Grid frequency regulation by recycling electrical energy in flywheels. In: IEEE Power Engineering Society General Meeting. 2004. p. 2038-5 33

[179] Lazarewicz, M. Status of flywheel storage operation of first frequency regulation plants. Beacon Power Corporation, 2011. 123, 178, 234

[180] Leclercq, L., Robyns, B. and Grave, J.-M. Control based on fuzzy logic of a flywheel energy storage system associated with wind and diesel generators. Mathematics and Computers in Simulation 2003;63:271-280 33, 82, 109

[181] Lee, T.-Y. Operating schedule of battery energy storage system in a time-of-use rate industrial user with wind turbine generators: A multipass iteration particle swarm optimization approach. IEEE Transactions on Energy Conversion 2007;22:774-9 33

[182] Lee, D.-J. and Wang, L. Small-signal stability analysis of an autonomous hybrid renewable energy power generation/energy storage system part I: Time-domain simulations. IEEE Transactions on Energy Conversion 2008;23:311-10 32, 33, 38

[183] Lex, P. and Jonshagen, B. The zinc bromine battery system for utility and remote area applications. Power Engineering Journal 1999;13:142-7 18, 32

[184] Li, P. Energy storage is the core of renewable energy technologies. IEEE Nanotechnology Magazine 2008;2:13-6 21, 25

[185] Li-Tec Battery GmbH. website, `http://www.li-tec.de/en/` [accessed 07.05.2013] 25

[186] Little, M., Thomson, M. and Infield, D. Electrical integration of renewable energy into stand-alone power supplies incorporating hydrogen storage. International Journal of Hydrogen Energy 2007;32:1582-7 32, 39, 43

[187] Liu, D.B., Shi, L.J., Xu, Q., Du, W.J. and Wang, H.F. Selection of installing locations of flywheel energy storage system in multimachine power systems by modal analysis. In: International Conference on Sustainable Power Generation and Supply. 2009 33, 37

[188] Liu, F., Mei, S., Xia, D., Ma, Y., Jiang, X. and Lu, Q. Experimental evaluation of nonlinear robust control for SMES to improve the transient stability of power systems. IEEE Transactions on Energy Conversion 2004;19:774-9 33, 37

[189] Liu, H. and Jiang, J. Flywheel energy storage - an upswing technology for energy sustainability. Energy and Buildings 2007;39:599-6 21, 22, 24

[190] Liu, Q., Nayfeh, N.H., Yau, S.-T. Supercapacitor electrodes based on polyaniline-silicon nanoparticle composite. Journal of Power Sources 2010;195:3956-4 24

[191] Loisel, R., Mercier, A., Gatzen, C., Elms, N. and Petric, H. Valuation framework for large scale electricity storage in a case with wind curtailment. Energy Policy 2010;38:7323-15 32, 41

[192] Loukarakis, E., Margaris, I., Moutis, P. Frequency control support and participation methods provided by wind generation. In: IEEE Electrical Power and Energy Conference (EPEC). 2009 149

[193] Lund, H. and Salgi, G. The role of compressed air energy storage (CAES) in future sustainable energy systems. Energy Conversion and Management 2009;50:1172-8 24, 25, 39

[194] Lund, H., Salgi, G., Elmegaard, B. and Andersen, A.N. Optimal operation strategies of compressed air energy storage (CAES) on electricity spot markets with fluctuating prices. Applied Thermal Engineering 2009;29:799-8 32

[195] Majima, M., Ujiie, S., Yagasaki, E., Koyama, K. and Inazawa, S. Development of long life lithium ion battery for power storage. Journal of Power Sources 2001;101:53-7 15

[196] Mauricio, J., Marano, A., Gomez-Exposito, A. and Martinez-Ramos, J. Frequency regulation contribution through variable-speed wind energy conversion systems. IEEE Transactions on Power Systems 2009;24:173-180 159

[197] Maxwell technologies Inc. website, `http://www.maxwell.com/` [accessed 07.05.2013] 24, 25, 27

[198] McDowall, J. Integrating energy storage with wind power in weak electricity grids. Journal of Power Sources 2006;162:959-6 13, 23, 24

[199] Mercier, P., Cherkaoui, R. and Oudalov, A. Optimizing a battery energy storage system for frequency control application in an isolated power system. IEEE Transactions on Power Systems 2009;24:1469-9 33, 38

[200] Miyake, S. and Tokuda, N. Vanadium redox-flow battery for a variety of applications. In: IEEE Power Engineering Society Summer Meeting. 2001 32

[201] Mohamed, Y.A.-R.I. Adaptive self-tuning speed control for permanent-magnet synchronous motor drive with dead time. IEEE Transactions on Energy Conversion 2006;21:855-862 109

[202] Moreno-Muñoz, A., González de la Rosa, J.J., Flores-Arias, J.M., Bellido-Outerino, F.J. and Gil-de-Castro, A. Energy efficiency criteria in uninterruptible power supply selection. Applied Energy 2011;88:1312-1321 81

[203] Moriokaa, Y., Narukawab, S. and Itou, T. State-of-the-art of alkaline rechargeable batteries. Journal of Power Sources 2001;100:107-10 13

[204] Morren, J., Pierik, J. and de Haan, S. Inertial response of variable speed wind turbines. Electric Power Systems Research 2006;76:980-987 157

[205] Moutis, P., Loukarakis, E., Papathanasiou, S. and Hatziargyriou, N. Primary load-frequency control from pitch-controlled wind turbines. In: IEEE Power Tech. 2009 149, 155

[206] Moutis, P., Papathanassiou, S., Hatziargyriou, N. Improved load-frequency control contribution of variable speed variable pitch wind generators. Renewable Energy 2012;48:514-523 149, 167, 169

[207] Mufti, M., Lone, S.A., Iqbal, S.J., Ahmad, M. and Ismail, M. Supercapacitor based energy storage system for improved load frequency control. Electric Power Systems Research 2009;79:226-8 27, 33

[208] Muljadi, E., Butterfield, C.P., Chacon, J. and Romanowitz, H. Power quality aspects in a wind power plant. In: IEEE Power Engineering Society General Meeting. 2006 31, 81

[209] Muyeen, S.M., Hasan-Ali, M., Takahashi, R., Murata, T. and Tamura, J. Damping of blade-shaft torsional oscillations of wind turbine gener-

ator system. Electric Power Components and Systems 2008;36:195-17 33

[210] MWH Global Inc. website, http://www.mwhglobal.com/, . Access date: 20/04/2011 25

[211] Nakken, T., Strand, L.R., Frantzen, E., Rohden, R., Eide, P.O. The Utsira wind hydrogen system - Operational Experience. Proceedings of the EWEC. 2006, http://www.ewec2006proceedings.info/ [accessed 07.05.2013] 32

[212] National Grid plc. The grid code, issue 4 revision 13 (2012), http://www.nationalgrid.com/uk/ [accessed 26.04.2013] XVI, 138, 142, 143, 144, 165

[213] NEC TOKIN Corp. website, http://www.nec-tokin.com/ [accessed 07.05.2013] 25

[214] Neef, H.-J. International overview of hydrogen and fuel cell research. Energy 2009;34:327-7 20

[215] Ngamroo, I., Cuk-Supriyadi, A.N., Dechanupaprittha, S. and Mitani, Y. Power oscillation suppression by robust SMES in power system with large wind power penetration. Physica C 2009;469:44-8 33, 37

[216] NGK Insulators Ltd. website, http://www.ngk.co.jp/english/ [accessed 07.05.2013] 15

[217] Nichita, C., Luca, D., Dayko, B. and Ceanga, E. Large band simulation of the wind speed for real time wind turbine simulators. IEEE Transactions on Energy Conversion 2002;17:523-529 82

[218] Nielsen, K.E., and Molinas, M. Superconducting Magnetic Energy Storage (SMES) in power systems with renewable energy sources. In: IEEE International Symposium on Industrial Electronics. 2010. p. 2487-6 22, 24, 25, 26, 33

[219] Nomura, S., Ohata, Y., Hagita, T., Tsutsui, H., Tsuji-Iio, S. and Shimada, R. Wind farms linked by SMES systems. IEEE Transactions on Applied Superconductivity 2005;15:1951-4 33, 34

[220] Nyamdash, B., Denny, E. and Malley, M.O. The viability of balancing wind generation with large scale energy storage. Enery Policy 2010;38:7200-9 32, 42

[221] Okuyama, R. and Nomura, E. Relationship between the total energy efficiency of a sodium-sulfur battery system and the heat dissipation of the battery case. Journal of Power Sources 1999;77:164-6 14

[222] Onar, O.C., Uzunoglu, M. and Alam, M.S. Dynamic modeling, design and simulation of a wind/fuel cell/ultra-capacitor-based hybrid power generation system. Journal of Power Sources 2006;161:707-16 32

[223] Onar, O.C., Uzunoglu, M. and Alam, M.S. Modeling, control and simulation of an autonomous wind turbine/photovoltaic/fuel cell/ultra-capacitor hybrid power system. Journal of Power Sources 2008;185:1273-11 28

[224] Ong, C.-M. Dynamic simulation of electric machinery using Matlab / Simulink. Prentice Hall PTR, 1997 177

[225] Padimiti, D.S. and Chowdhury, B.H. Superconducting Magnetic Energy Storage System (SMES) for improved dynamic system performance. In: IEEE Power Engineering Society General Meeting. 2007 33, 37

[226] Papaefthimiou, S., Karamanou, E., Papathanassiou, S. and Papadopoulos, M. A wind-hydro-pumped storage station leading to high RES penetration in the autonomous island system of Ikaria. IEEE Transactions on Sustainable Energy 2010;1:163-10

[227] Papaefthimiou, S., Karamanou, E., Papathanassiou, S. and Papadopoulos, M. Operating policies for wind-pumped storage hybrid power stations in island grids. IET Renewable Power Generation 2009;3:293-11 32, 40

[228] Parker, C.D. Lead-acid battery energy-storage systems for electricity supply networks. Journal of Power Sources 2001;100:18-11 12, 33

[229] Payman, A., Pierfederici, S. and Meibody-Tabar, F. Energy control of supercapacitor/fuel cell hybrid power source. Energy Conversion and Management 2008;49:1637-8 28

[230] Petru, T. Modeling of wind turbines for power system studies. Chalmers University of Technology; 2001 82

[231] Pickard W. F., Shen, Q. A. and Hansing, N. J. Parking the power: Strategies and physical limitations for bulk energy storage in supply-

demand matching on a grid whose input power is provided by intermittent sources. Renewable and Sustainable Energy Reviews 2009;13:1934-12 9, 11, 16, 25, 26, 27

[232] Piller Power Systems website, http://www.piller.com [accessed 07.05.2013] 22, 23, 25

[233] Ponce-de-León, C., Frías-Ferrer, A., González-García, J., Szánto, D.A. and Walsh, F.C. Redox flow cells for energy conversion. Journal of Power Sources 2006;160:716-17 17, 18, 19, 23, 24, 25

[234] Premium Power Corp. website, http://www.premiumpower.com/ [accessed 07.05.2013] 23, 25

[235] Price, A. Technologies for energy storage - present and future: Flow batteries. In: IEEE Power Engineering Society Summer Meeting. 2000 19

[236] Proton Energy Systems website, http://www.protonenergy.com/ [accessed 07.05.2013] 19

[237] Prudent Energy Corp. website, http://www.pdenergy.com/ [accessed 07.05.2013] 23, 24, 25

[238] Qu, L. and Qiao, W. Constant power control of DFIG wind turbines with supercapacitor energy storage. IEEE Transactions on Industry Applications 2011;47:359-9 31, 33

[239] Rafik, F., Gualous, H., Gallay, R., Crausaz, A. and Berthon, A. Frequency, thermal and voltage supercapacitor characterization and modeling. Journal of Power Sources 2007;165:928-7 24, 27

[240] Rahmat-Ullah, T., Thiringer, N. and Karlsson, D. Temporary primary frequency control support by variable speed wind turbines - potential and applications. IEEE Transactions on Power Systems 2008;23:601-612 165

[241] Ramtharan, J., Ekanayake, G. and Jenkins, N. Frequency support from doubly fed induction generator wind turbines. IET Renewable Power Generation 2007;1:3-9 XVII, 151, 157, 158, 159, 168

[242] Ran, L., Xiang, D. and Kirtley, J. Analysis of electromechanical interactions in a flywheel system with a doubly-fed induction machine. IEEE Transactions on Industry Applications 2011;47:1498-1506 33

[243] Ray, P.K., Mohanty, S.R. and Kishor, N. Proportional-integral controller based small-signal analysis of hybrid distributed generation systems. Energy Conversion and Management 2011;52:1943-12 33, 34

[244] Rebours, Y. and Kirschen, D. What is spinning reserve?. The University of Manchester, http://www.eee.manchester.ac.uk/research/groups/eeps/publications/reportstheses-/aoe/rebours%20et%20al_tech%20rep_2005A.pdf [accessed 07.05.2013] 37

[245] Red Eléctrica de España. P.O 7.1 servicio complementario de regulación primaria. Resolución de 30.07.1998, boe 18.08.1998, http://www.ree.es [accessed 26.04.2013] 138

[246] Red Eléctrica de España. P.O. 7.2 regulación secundaria. Resolución de 18.05.2009, boe 28.05.2009, http://www.ree.es [accessed 26.04.2013] 138

[247] Redflow Technologies Ltd. website, http://www.redflow.com.au/ [accessed 07.05.2013] 18, 25

[248] Regenesys Technologies website, http://www.regenesys.com [accessed 07.05.2013] 25

[249] Ribeiro, P.F., Johnson, B.K., Crow, M.L., Arsoy, A. and Liu, Y. Energy storage systems for advanced power applications. Proceedings of the IEEE 2001;89:1744-13 22, 23, 24, 26, 33, 81, 109

[250] Ridge Energy Storage & Grid Services L.P. The economic impact of CAES on wind in TX, OK, and NM. http://www.ridgeenergystorage.com/re_wind_projects-compressed2005.pdf [accessed 07.05.2013] 23

[251] Ries, G. and Neumueller, H.-W. Comparison of energy storage in flywheels and SMES. Physica C 2001;357-360:1306-5 24

[252] Roberts, B.P. Sodium-Sulfur (NaS) batteries for utility energy storage applications. In: IEEE Power and Energy Society General Meeting - Conversion and Delivery of Electrical Energy in the 21st Century. 2008 33, 40

[253] Rodriguez-Amenedo, J., Arnalte, S., Burgos, J. Automatic generation control of a wind farm with variable speed wind turbines. IEEE Transactions on Energy Conversion 2002; 17:279-284 154

[254] Ruiz-Álvarez, A., Colet-Subirachs, A., Álvarez-Cuevas, F., Gomis-Bellmunt, O. and Sudria-Andreu, A. Operation of a utility connected microgrid using an IEC 61850-based multi-level management system. IEEE Transactions on Smart Grid 2012;3:858-865 50, 118

[255] Rydh, C.J. and Sandén, B.A. Energy analysis of batteries in photovoltaic systems. Part II: Energy return factors and overall battery efficiencies. Energy Conversion and Management 2005;46:1980-21 17, 24, 25

[256] Rydh, C.J. Environmental assessment of vanadium redox and lead-acid batteries for stationary energy storage. Journal of Power Sources 1999;80:21-9 17, 24, 25

[257] Saft Batteries website, `http://www.saftbatteries.com/` [accessed 07.05.2013] 23, 25

[258] Sannomiya, T., Hayashi, H., Ishii, T. and Ikeda, R. Test results of compensation for load fluctuation under a fuzzy control by a 1 kWh / 1 MW SMES. IEEE Transactions on Applied Superconductivity 2001;11:1908-4 23, 26

[259] Sasaki, T., Kadoya, T. and Enomoto, K. Study on load frequency control using redox flow batteries. IEEE Transactions on Power Systems 2004;19:660-8 32, 38

[260] Scamman, D.P., Gavin, W.R and Roberts, E.P.L. Numerical modelling of a bromide-polysulphide redox flow battery. Part 1: Modelling approach and validation for a pilot-scale system. Journal of Power Sources 2009;189:1220-11 16, 18

[261] Schwab A. Elektroenergiesysteme, 2. Auflage, Springer, 2009 133

[262] Sebastián, R. and Peña-Alzola, R. Effective active power control of a high penetration wind diesel system with a Ni-Cd battery energy storage. Renewable Energy 2010;35:952-14 33

[263] Sebastián, R. and Peña Alzola, R. Flywheel energy storage systems: Review and simulation for an isolated wind power system. Renewable and Sustainable Energy Reviews 2012;16:6803-6813

[264] Sebastian, R. Modelling and simulation of a high penetration wind diesel system with battery energy storage. Electrical Power and Energy Systems 2011;33:767-774 33

[265] Seong, K.C., Kim, H.J., Kim, S.W., Cho, J.W., Kwon, Y.K., Hahn, S.R., Jeon, H.J. and Yu, I.K. Design and test of a 1-MJ SMES system. IEEE Transactions on Applied Superconductivity 2002;12:391-4 26

[266] Sharma, P. and Bhatti, T.S. A review on electrochemical double-layer capacitors. Energy Conversion and Management 2010;51:2901-12 27, 28, 33

[267] Sherif, S.A., Barbir, F. and Veziroglu, T.N. Wind energy and the hydrogen economy - review of the technology. Solar Energy 2005;78:647-14 19, 32

[268] Shi, G., Cao, Y.F., Li, Z. and Cai, X. Impact of wind-battery hybrid generation on isolated power system stability. In: International Symposium on Power Electronics, Electrical Drives, Automation and Motion. 2010. p. 757-5 33

[269] Shi, J., Tang, Y.J., Ren, L., Li, J.D. and Chen, S.J. Application of SMES in wind farm to improve voltage stability. Physica C 2008;468:2100-4 33, 35

[270] Shikimachi, K., Moriguchi, H., Hirano, N., Nagaya, S., Ito, T., Inagaki, J., Hanai, S., Takahashi, M. and Kurusu, T. Development of MVA class HTS SMES system for bridging instantaneous voltage dips. IEEE Transactions on Applied Superconductivity 2005;15:1931-4 26

[271] Skogestad, S. and Postlethwaite I. Multivariable feedback control, analysis and design. Chichester, John Wiley and Sons Ltd., 2007 115

[272] Slootweg, J., Polinder, H. and Kling, W. Representing wind turbine electrical generating systems in fundamental frequency simulations. IEEE Transactions on Energy Conversion 2003;18:516-525 147

[273] Smith, S.C. and Sen, P.K. Ultracapacitors and energy storage: Applications in electrical power system. In: 40th North American Power Symposium. 2008 24

[274] Smith, W. The role of fuel cells in energy storage. Journal of Power Sources 2000;86:74-10 19, 21, 24

[275] Song, Z., Xia, C., Shi, T. Assessing transient response of DFIG based wind turbines during voltage dips regarding main flux saturation and rotor deep-bar effect. Applied Energy 2010;87:3283-3293 87

[276] Sørensen, P., Hansen, A.D. and Carvalho-Rosas, P.A. Wind models for simulation of power fluctuations from wind farms. Journal of Wind Engineering and Industrial Aerodynamics 2002;90:1381-1402 81, 85

[277] Stulrajter, M., Hrabovcová, V., Franko, M. Permanent magnets synchronous motor control theory. Journal of Electrical Engineering 2007;58:79-84 55, 88

[278] Sumper, A., Gomis-Bellmunt, O., Sudria-Andreu, A., Villafafila-Robles, R. and Rull-Duran, J. Response of fixed speed wind turbines to system frequency disturbances. IEEE Transactions on Power Systems 2009;24:181-192 136, 165

[279] Sun, X.D., Koh, K.H., Yu, B.G., Matsui, M. Fuzzy-logic-based V/f control of an induction motor for a DC grid power-leveling system using flywheel energy storage equipment. IEEE Transactions on Industrial Electronics 2009;56:3161-3168 49

[280] Sun, Y.-Z., Zhang, Z.-S., Li, G.-J., Lin, J. Review on frequency control of power systems with wind power penetration. In: IEEE International Conference on Power System Technology. 2010 XVII, 135, 150

[281] Superconductor Technologies Inc. website, `http://www.suptech.com/home.htm` [accessed 07.05.2013] 25

[282] Suvire, G.O. and Mercado, P.E. DSTATCOM with Flywheel Energy Storage System for wind energy applications: Control design and simulation. Electric Power Systems Research 2010;80:345-9 33, 36, 88

[283] Swider, D.J. Compressed air energy storage in an electricity system with significant wind power generation. IEEE Transactions on Energy Conversion 2007;22:95-8 32, 39

[284] Świerzyński, M., Teodorescu, R., Rasmussen, C.N., Rodriguez, P. and Vikelgaard, H. Storage possibilities for enabling higher wind energy penetration. In: EPE Wind Power Symposium. 2010 31

[285] Tascikaraoglu, A., Uzunoglu, M. and Vural B. The assessment of the contribution of short-term wind power predictions to the efficiency of stand-alone hybrid systems. Applied Energy 2012;94:156-165 81

[286] Tascikaraoglu, A., Uzunoglu, M., Vural, B. and Erdinc, O. Power quality assessment of wind turbines and comparison with conventional legal

regulations: A case study in Turkey. Applied Energy 2011;88:1864-1872 81

[287] Ter-Garzarian, A. Energy storage for power systems. Peter Peregrinus Ltd.; 1994 11

[288] Terorde, G. Electrical drives and control techniques. 1st ed. Leuven: Acco; 2004 49, 55, 88, 118

[289] The European Wind Energy Association website, http://www.ewea.org/ [accessed 07.05.2013] 3

[290] The Scottish Government website, http://www.scotland.gov.uk/Publications/2010/10/28091356/4 [accessed 07.05.2013] 11

[291] The University of New South Wales website, http://www.ceic.unsw.edu.au/centers/vrb/Index.html [accessed 07.05.2013] 17

[292] Tomoo Yamamura, T., Wu, X., Ohta, S., Shirasaki, K., Sakuraba, H., Satoh, I. and Shikama, T. Vanadium solid-salt battery: Solid state with two redox couples. Journal of Power Sources 2011;196:4003-9 18, 24

[293] Ton, D.T., Hanley, C.J., Peek, G.H. and Boyes, J.D. Solar energy grid integration systems - energy storage (SEGIS-ES), http://prod.sandia.gov/techlib/access-control.cgi/2008/084247.pdf [accessed 07.05.2013] 23

[294] Tsai, M.-T., Lin, C.-E., Tsai, W.-I. and Huang, C.-L. Design and implementation of a demand-side multifunction battery energy storage system. IEEE Transactions on Industrial Electronics 1995;42:642-11 33

[295] Tsili, M. and Papathanassiou, S. A review of grid code technical requirements for wind farms. IET Renewable Power Generation 2009;3:308-24

[296] U.S. Department of Energy, Energy Efficiency & Renewable Energy website, http://www1.eere.energy.gov/hydrogenandfuelcells/fuelcells/ [accessed 07.05.2013] 20

[297] Valsera-Naranjo, E., Sumper, A., Gomis-Bellmunt, O., Junyent-Ferré, A. and Martínez-Rojas, M. Pitch control system design to improve frequency response capability of fixed-speed wind turbine systems. European Transactions on Electrical Power 2010;21:1984-2006 147

[298] Van-der-Linden, S. Bulk energy storage potential in the USA, current developments and future prospects. Energy 2006;31:3446-12 23, 32, 33

[299] Varkaraki, E., Lymberopoulos, N., Zoulias, E., Guichardot, D. and Poli, G. Hydrogen-based uninterruptible power supply. International Journal of Hydrogen Energy 2007;32:1589-8 19

[300] Venne, P. and Guillaud, X. Impact of wind turbine controller strategy on deloaded operation. In: CIGRE/IEEE PES Joint Symposium Integration of Wide-Scale Renewable Resources Into the Power Delivery System. 2009 149

[301] Verband der Netzbetreiber - VDN - e.V. beim VDEW. Transmissioncode 2007. Network and system rules of the German transmission system operators (2007), `http://www.vde.com` [accessed 26.04.2013] 137, 138

[302] Virulkar, V., Aware, M. and Kolhe, M. Integrated battery controller for distributed energy system. Energy 2011; article in press 33

[303] Wagner, R. Large lead/acid batteries for frequency regulation, load levelling and solar power applications. Journal of Power Sources 1997;67:163-10 33

[304] Wakihara, M. Recent developments in lithium ion batteries. Materials Science and Engineering 2001;33:109-26 15

[305] Wang, L., Chen, S.-S., Lee, W.-J. and Chen, Z. Dynamic stability enhancement and power flow control of a hybrid wind and marine-current farm using SMES. IEEE Transactions on Energy Conversion 2009;24:626-14 33, 37

[306] Wang, W., Ge, B., Bi, D. and Sun, D. Grid-connected wind farm power control using VRB-based energy storage system. In: IEEE Energy Conversion Congress and Exposition. 2010 32

[307] Wang, X.Y., Vilathgamuwa, D.M. and Choi, S.S. Buffer scheme with battery energy storage capability for enhancement of network transient stability and load ride-through. Journal of Power Sources 2008;179:819-11 33

[308] Wang, W., Ge, B., Bi, D., Qin, M. and Liu, W. Energy storage based LVRT and stabilizing power control for direct-drive wind power system. In: International Conference on Power System Technology. 2010 32, 35

[309] Wen, Z., Cao, J., Gu, Z., Xu, X., Zhang, F. and Lin, Z. Research on sodium sulfur battery for energy storage. Solid State Ionics 2008;179:1697-5 14, 23, 24, 25, 33

[310] Winter, C-J. Hydrogen energy - Abundant, efficient, clean: A debate over the energy-system-of-change. International Journal of Hydrogen Energy 2009;34:1-52 19, 20, 21

[311] Wu, B., Lang, Y., Zargari, N. and Kouro S. Power conversion and control of wind energy systems. John Wiley & Sons Inc; 2011 233

[312] Yingcheng, X., Nengling, T. Review of contribution to frequency control through variable speed wind turbine. Renewable Energy 2011;11:1671-1677 131, 147, 157, 165

[313] Yogi-Goswami, D. and Kreith, F. Energy conversion. CRC Press Taylor & Francis Group; 2007 14, 16, 18, 19, 21, 22

[314] Yoshimoto, K., Nanahara, T. and Koshimizu, G. Analysis of data obtained in demonstration test about battery energy storage system to mitigate output fluctuation of wind farm. In: CIGRE/IEEE PES Joint Symposium Integration of Wide-Scale Renewable Resources Into the Power Delivery System. 2009 32, 38

[315] Zafirakis, D., Chalvatzis, K.J., Baiocchi, G. and Daskalakis, G. Modeling of financial incentives for investments in energy storage systems that promote the large-scale integration of wind energy. Applied Energy 2013;105:138-154 81, 109

[316] Zafirakis, D. and Kaldellis, J.K. Economic evaluation of the dual mode CAES solution for increased wind energy contribution in autonomous island networks. Energy Policy 2009;37:1958-10 32, 41

[317] Zaghib, K., Dontignya, M., Guerfi, A., Charest, P., Rodrigues, I., Mauger, A., Julien, C.M. Safe and fast-charging Li-ion battery with long shelf life for power applications. Journal of Power Sources 2011;196:3949-6 15, 16

[318] ZBB Energy Corporation website, `http://www.zbbenergy.com/` [accessed 07.05.2013] 18, 25

[319] Zertek, G., Verbic, A. and Pantos M. A novel strategy for variable-speed wind turbines' participation in primary frequency control. IEEE Transactions on Sustainable Energy 2012;3:791-799 151, 154, 168

[320] Zertek, G., Verbic, A. and Pantos M. Optimised control approach for frequency-control contribution of variable speed wind turbines. IET Renewable Power Generation 2012;6:17-23 151, 153, 154, 168

[321] Zhang, J. Research on flywheel energy storage system using in power network. In: International Conference on Power Electronics and Drives Systems. 2005 21

[322] Zhang, Z.-S., Sun, Y., Lin, J. and Li, G.-J. Coordinated frequency regulation by doubly fed induction generation-based wind power plants. IET Renewable Power Generation 2012;6:38-47 151, 168

[323] Zhong, Y., Zhang, J., Li, G. and Chen, Z. Research on restraining low frequency oscillation with flywheel energy storage system. In: International Conference on Power System Technology. 2006 33, 37

A List of Publications

This Chapter lists the publications in peer-reviewed journals, non peer-reviewed journals, conferences papers as well as other relevant publications derived from the development of the thesis.

A.1 Peer-reviewed journal articles

- Díaz-González, F., Sumper, A., Gomis-Bellmunt, O. and Villafáfila-Robles, R. A review of energy storage technologies for wind power applications. Renewable and Sustainable Energy Reviews 2012;16:2154-2171
- Díaz-González, F., Sumper, A., Gomis-Bellmunt, O. and Villafáfila-Robles, R. Modeling, control and experimental validation of a flywheel-based energy storage device. Journal of European Power Electronics 2013;23:1-21
- Díaz-González, F., Sumper, A., Gomis-Bellmunt, O. and Bianchi, F.D. Energy management of flywheel-based energy storage device for wind power smoothing. Applied Energy 2013;110:207-219
- Díaz-González, F., Bianchi, F.D., Sumper, A. and Gomis-Bellmunt, O. Design and experimental validation of a novel control strategy for a flywheel energy storage device for power smoothing of wind power plants. Submitted to IEEE Transactions on Energy Conversion
- Díaz-González, F., Hau, M., Sumper, A. and Gomis-Bellmunt, O. Participation of wind power plants in system frequency control: Review of

grid code requirements and control methods. Submitted to Renewable and Sustainable Energy Reviews

- Díaz-González, F., Hau, M., Sumper, A. and Gomis-Bellmunt, O. Coordinated operation of wind turbines and flywheel storage for primary frequency control support. Submitted to IEEE Transactions on Power Systems

A.2 Conference papers

- Díaz-González, F., Sumper, A. and Gomis-Bellmunt, O. and Martínez-Rojas, M. Power smoothing of DFIG wind turbines with flywheel. In: European Wind Energy Association (EWEA '11), Brussels, Belgium

- Díaz-González, F., Sumper, A., Gomis-Bellmunt, O. and Villafáfila-Robles, R. Modeling and validation of a flywheel energy storage labsetup. In: 3rd IEEE PES Innovative Smart Grid Technologies (ISGT) Europe Conference (2012), Berlin, Germany

A.3 Other publications

Other relevant publications in non peer-reviewed journals or not directly related to the thesis are listed in this section.

- Díaz-González, F., Martínez-Rojas, M., Sumper, A., Gomis-Bellmunt, O. and Trilla, L. Strategies for reactive power control in wind farms with STATCOM. In: Third EPE Wind Energy Chapter seminar (2010), Stafford, UK

- Díaz-González, F., Martínez-Rojas, M., Sumper, A. and Gomis Bellmunt, O. Strategies for reactive power control in wind farms with STATCOM. In: 9th International Wind Power Integration Workshop (2010), Quebec, Canada

- Díaz-González, F. and Gomis-Bellmunt, O. Volantes de inercia: un complemento para impulsar las energías renovables. Automática e Instrumentación 2012;43:1-5 (non peer-reviewed journal)

- Girbau-Llistuella, F., Sumper, A. and Díaz-González, F. Flicker mitigation by reactive power on wind farm with doubly fed induction generators. Submitted to International Journal of Electrical Power and Energy Systems

B Appendix

This Appendix summarizes those parameters which, for the sake of clarity, have not been previously included and are needed for developing the models presented in previous chapters of the thesis, as well as those characteristics of the experimental setup in Chapter 5.

B.1 Parameters of the system for the purposes of Chapter 4

Table B.1 depicts the parameters of the models of the wind and wind turbine, the flywheel and the optimization problem presented in Chapter 4.

B.2 Parameters for the purposes of Chapter 5

B.2.1 Parameters of the experimental setup

Table B.2 presents the parameters of the experimental setup that was performed for the purposes of Chapter 5.

B.2.2 High-pass filter for obtaining the fluctuating components of the power of the wind turbine

The fluctuating components of the wind turbine power profile P_{fluc} are identified through the application of a third order high pass filter (Butterworth type) to the wind power profile P_{wt}.

Table B.1: Parameters of the system

System	Parameter	Value
Wind turbine	P_{rated} (MW)	1.5
	R (m)	41.7
	N (p.u.)	105
	J_t (kg·m^2)	$1.6{\cdot}10^6$
	J_g (kg·m^2)	100
	D (Nms/rad)	$7.5{\cdot}10^5$
	k (Nm/rad)	$12{\cdot}10^7$
Wind model	L_V (m)	180
	a_1 (pu)	0.4
	a_2 (pu)	0.25
	P (-)	3
	σ_v (pu)	0.16
	ω_{sf} (rad/s)	10
	d (pu)	0.14
Storage device	P_{rated}(kW)	100
	ω_{max}(krpm)	31.0
	ω_{min}(krpm)	15.5
	$T_{acc_{max}}$(Nm)	31.2
	$T_{acc_{min}}$(Nm)	-31.2
	J(kg·m^2)	0.72
PMSM	ψ_m(Wb)	0.052
	L_d & L_q(mH)	0.1
	R_s(mΩ)	8
	p	2
PMSM control	K_{psqd}	0.0767
	K_{isqd}	6.1359
Opt. problem	k_2	0.36 kgm^2
	c_1	$9{\cdot}10^{-5}$ Ws^2/rad^2
	c_2	0.175 Ws/rad

Table B.2: Parameters of the experimental setup

System	Parameter	Value
Wind turbine emulator	2 3-phase IGBT bridge in back-to-back	
	S_{rated} (kVA)	4.0
	$U_{ACrated}$ (V)	400.0
	$U_{DCrated}$ (V)	750.0
	I_{max} (A)	16.0
	C (μF)	0.0050
Flywheel	Ratings	3.0 kW @ 30 kWs
	Efficiency	73%
	ω_{max} (rpm)	3000.0
	ω_{min} (rpm)	1000.0
	T_{rated} (Nm)	12.2
	J (kg·m^2)	0.868
Flywheel (PMSM)	ψ_m (Wb)	0.2465
	L_d & L_q (mH)	$2.88{\cdot}10^{-3}$
	R_s (Ω)	0.44
	pole pairs	2
Flywheel (power electronics)	(same as emulator)	

The cutoff frequency of the filter is 0.4 Hz and its mathematical expression, in Laplace domain, is

$$F(s) = \frac{s^3}{s^3 + 5.03s^2 + 12.63s + 15.88}. \tag{B.1}$$

B.3 Parameters for the purposes of Chapter 7

The characteristic parameters of the synchronous generator of the conventional power plant are extracted from [173] (in p.u. stator base): rated power 1000 MVA, rated stator line-to-line voltage 18 kV, $r_s = 0.0033$, $x_d = 1.65$, $x_q = 1.57$, $x_{ls} = 0.15$, $x'_d = x'_q = 0.275$, $T'_{d0} = 6.5$ s, $T'_{q0} = 1.25$ s. The parameters of its speed governor are [173] (in p.u. stator base): $R = 0.05$, $T_G = 0.2$ s. The parameter of the non-reheat turbine is [173]: $T_{CH} = 0.3$ s.

The characteristic parameters of the DFIG are [311]: rated mechanical power 1.5 MW, rated stator line-to-line voltage 690 V, rated rotor speed 1750 rpm, $r_s = 2.65$ mΩ, $r'_r = 2.63$ mΩ, $x_{ls} = 0.053\Omega$, $x'_{lr} = 0.042\Omega$, $x_m = 1.72$, poles $P = 4$, inertia $J_g = 100$ kg·m^2. The characteristic parameters of the turbine are: $R = 41.7$ m, inertia $J_t = 3 \cdot 10^6$ kg·m^2, damping coefficient

$D = 7.5{\cdot}10^5$ Nms/rad, stiffness $k = 12{\cdot}10^7$ Nm/rad, gear-box ratio $N = 105$, rated wind speed $v_w = 10.1$ m/s. The aerodynamic parameters are [4]: $c_1 = 0.73$, $c_2 = 151$, $c_3 = 0.58$, $c_4 = 0.0002$, $c_5 = 2.14$, $c_6 = 13.2$, $c_7 = 18.4$, $c_8 = -0.02$, $c_9 = -0.003$.

The characteristic parameters of a flywheel unit are [179]: rated power 100 kW, operating speed limits $16 - 8$ krpm, torque losses $T_{loss} = 1.19$ Nm, inertia $J_{fw} = 86.4$ kg$\cdot$ m^2.

The characteristic parameters (in per unit) of the power transformers of the system are [173]: copper losses 0.1% of rated power, short-circuit voltage $\varepsilon = 0.15$ pu, leakage reactance 0.1 pu. The particular ratings of each transformer are: ratings of the step-up power transformer for the voltage of the conventional generating unit 1000 MVA - 220 kV / 18 kV; ratings of the step-up transformers for the voltage of the wind power plant 500 MVA - 220 kV / 30 kV and 500 MVA - 30 kV / 690 V.

The characteristic parameters of the lines are: $r_{13} = r_{23} = 0.0212\Omega$/km, $x_{13} = x_{23} = 0.116\Omega$/km (50 km).